Cranfield University

B. Cho

Control of A Hybrid Electric Vehicle with Predictive Journey Estimation

School of Engineering

PhD

Cranfield University

School of Engineering

PhD THESIS

2008

B. Cho

Control of A Hybrid Electric Vehicle with Predictive Journey Estimation

Supervisor: Prof. N. D. Vaughan

Academic Year 2007 to 2008

This thesis is submitted in partial fulfilment of the requirements for the degree of PhD

© Cranfield University, 2008. All rights reserved. No part of this publication may be reproduced without the written permission of the copyright holder.

ABSTRACT

Battery energy management plays a crucial role in fuel economy improvement of charge-sustaining parallel hybrid electric vehicles. Currently available control strategies consider battery state of charge (SOC) and driver's request through the pedal input in decision-making. This method does not achieve an optimal performance for saving fuel or maintaining appropriate SOC level, especially during the operation in extreme driving conditions or hilly terrain. The objective of this thesis is to develop a control algorithm using forthcoming traffic condition and road elevation, which could be fed from navigation systems. This would enable the controller to predict potential of regenerative charging to capture cost-free energy and intentionally depleting battery energy to assist an engine at high power demand.

The starting point for this research is the modelling of a small sport-utility vehicle by the analysis of the vehicles currently available in the market. The result of the analysis is used in order to establish a generic mild hybrid powertrain model, which is subsequently examined to compare the performance of controllers. A baseline is established with a conventional powertrain equipped with a spark ignition direct injection engine and a continuously variable transmission. Hybridisation of this vehicle with an integrated starter alternator and a traditional rule-based control strategy is presented. Parameter optimisation in four standard driving cycles is explained, followed by a detailed energy flow analysis.

An additional potential improvement is presented by dynamic programming (DP), which shows a benefit of a predictive control. Based on these results, a predictive control algorithm using fuzzy logic is introduced. The main tools of the controller design are the DP, adaptive-network-based fuzzy inference system with subtractive clustering and design of experiment. Using a quasi-static backward simulation model, the performance of the controller is compared with the result from the instantaneous control and the DP. The focus is fuel saving and SOC control at the end of journeys, especially in aggressive driving conditions and a hilly road. The controller shows a good potential to improve fuel economy and tight SOC control in long journey and hilly terrain. Fuel economy improvement and SOC correction are close to the optimal

solution by the DP, especially in long trips on steep road where there is a large gap between the baseline controller and the DP. However, there is little benefit in short trips and flat road. It is caused by the low improvement margin of the mild hybrid powertrain and the limited future journey information.

To provide a further step to implementation, a software-in-the-loop simulation model is developed. A fully dynamic model of the powertrain and the control algorithm are implemented in AMESim-Simulink co-simulation environment. This shows small deterioration of the control performance by driver's pedal action, powertrain dynamics and limited computational precision on the controller performance.

Keywords: Fuel economy, Online predictive control, Dynamic programming, Adaptive-network-based fuzzy inference system, Software-in-the-loop co-simulation

ACKNOWLEDGEMENTS

I would like to say a big thank-you to Prof. Nick Vaughan for his care and encouragement, not only as an academic supervisor but also as a mentor over the challenging period so far. I would also like to thank everybody in Cranfield who gave me a warm welcome and kind support.

I am very grateful to my mates, Enrico and Baptiste, for the invaluable discussions, sparkling jokes and honest friendship. Thanks also go to the gents next door, Andreas, Christian, and Eudoxios, for their friendly chat.

I wish to acknowledge providing AMESim software and technical support of Imagine SA, and appreciate the valuable information and data of IVT from Torotrak Ltd.

Thank you to all family, especially parents and parents-in-law for their love and support. Most of all, I feel very special heart to my wife Hojeong for her endless love throughout this entire journey, which I could not complete without her encouragement and patience. My heart is also full of love to my little chaps Jaehoon and Jaeseok always making a smile on my face.

CONTENTS

LIST OF FIGURES

LIST OF TABLES

ACRONYMS

2WD	2-Wheel Drive
4WD	4-Wheel Drive
AMT	Automated Manual Transmission
ANFIS	Adaptive-Network-based Fuzzy Inference System
AT	Automatic Transmission
BCU	Brake Control Unit
BMEP	Brake Mean Effective Pressure
BSA	Belt Starter Alternator
CNG	Compressed Natural Gas
CO_2	Carbon Dioxide
CVT	Continuously Variable Transmission
DOE	Design Of Experiment
DP	Dynamic Programming
ECU	Engine Control Unit
EM	Electric Machine
EV	Electric Vehicle
FCV	Fuel Cell Vehicle
FIS	Fuzzy Inference System
FMEP	Friction Mean Effective Pressure
FTP	Federal Test Procedure
FWD	Front Wheel Drive
GFR	Gas-Fuel Ratio
GPS	Global Positioning System
HEV	Hybrid Electric Vehicle
HWFET	Highway Fuel Economy Test
ICE	Internal Combustion Engine
IMA	Integrated Motor Assist
IMEP	Indicated Mean Effective Pressure
IOL	Ideal Operating Line
IOS	Ideal Operating Surface

ISA	Integrated Starter Alternator
IVT	Infinitely Variable Transmission
LP	Linear Programming
LMI	Linear Matrix Inequality
MCU	Motor Control Unit
MPC	Model Predictive Control
MPI	Multi Point Injection
MT	Manual Transmission
NEDC	New European Driving Cycle
NN	Neural Network
NYCC	New York City Cycle
OCV	Open Circuit Voltage
PMEP	Pumping Mean Effective Pressure
RMS	Root Mean Squared
RWD	Rear Wheel Drive
SCU	Supervisory Control Unit
SI	Spark Ignition
SIDI	Spark Ignition Direct Injection
SIL	Software-In-the-Loop
SOC	State Of Charge
SULEV	Super Ultra Low Emission Vehicle
SUV	Sport-Utility Vehicle
TCU	Transmission Control Unit
THS	Toyota Hybrid System
TPBVP	Two-Point Boundary Value Problem
VCM	Variable Cylinder Management
VVT	Variable Valve Timing
WOT	Wide-Open Throttle

NOMENCLATURE

A_d	Frontal area
AFR	Air/fuel ratio by mass
$amep$	Accessory mean effective pressure
$bsfc$	Break specific fuel consumption
B	Diameter of cylinder bore
$bmep$	Brake mean effective pressure
C_1	Indicated mean effective pressure correction factor
C_{BAT}	Battery capacity
C_d	Discharge coefficient
c_{exh}	Flow resistance coefficient of exhaust system
C_{th}	Thermal efficiency correction factor
C_v	Cylinder volumetric efficiency correction factor
$cfmep$	Crankshaft friction mean effective pressure
E_{BAT}	Battery energy
E_{FUEL}	Fuel energy
EGR	Exhaust gas recirculation ratio by mass
F_{AERO}	Aero-dynamic resistance force
F_{GRAD}	Force by road gradient
F_{ROLL}	Rolling resistance force
f_{roll}	Rolling resistance coefficient
$fmep$	Friction mean effective pressure
GFR	Gas/fuel ratio by mass
g	Gravitational acceleration
i_{BAT}	Battery output current
$imep_g$	Gross indicated mean effective pressure
$imep_{g,ideal}$	Ideal gross indicated mean effective pressure

J_{EM}	Electric machine inertia
J_{ENG}	Engine inertia
J_{FW}	Flywheel inertia
J_{IOS}	Cost function of ideal operating surface
J_{TXin}	Transmission inertia at input side
J_{TXout}	Transmission inertia at output side
J_{WHL}	Wheel inertia
M_{BAT}	Battery mass
M_{VEH}	Vehicle mass
$\dot{m}_a$	Mass flow rate of induced air
$\dot{m}_e$	Mass flow rate of exhausted gas
$\dot{m}_f$	Mass flow rate of fuel
n	Number of cylinders
n_{ev}	Number of exhaust valves per cylinder
n_{iv}	Number of inlet valves per cylinder
P_a	Ambient pressure
$P_{ACC,elec}$	Electrical accessory power
$P_{ACC,mech}$	Mechanical accessory power
P_{BAT}	Battery output power
P_e	Exhaust manifold pressure
$P_{EM,loss}$	Electric machine power loss
P_i	Inlet manifold pressure
P_{VEH}	Vehicle power
$pmep$	Pumping mean effective pressure
$pmep_v$	Pumping mean effective pressure by valves
Q_{LHV}	Lower heating value of fuel
R	Specific gas constant

R_{BAT}	Battery internal resistance
R_{FD}	Final drive ratio
R_{TX}	Transmission ratio
r_{WHL}	Wheel radius
r_c	Compression ratio
r_e	Radius of exhaust valve
r_i	Radius of inlet valve
$rfmep$	Reciprocating friction mean effective pressure
$rfmep_{gas}$	Reciprocating friction mean effective pressure by gas loading effect
S	Stroke of cylinder
S_p	Mean piston speed
SOC	Battery state of charge
SOC_{HI}	High limit of battery state of charge
SOC_{LO}	Low limit of battery state of charge
SOC_{req}	Required battery state of charge
$T_{ACC,mech}$	Mechanical accessory torque
T_{BRK}	Brake torque
T_{CRANK}	Torque at crankshaft
$T_{CRANK,req}$	Required torque at crankshaft
T_{EM}	Electric machine torque
$T_{EM,GEN}$	Generating torque limit of electric machine
$T_{EM,MOT}$	Motoring torque limit of electric machine
$T_{EM,req}$	Required electric machine torque
T_{ENG}	Engine torque
$T_{ENG,CTT}$	Engine closed throttle torque
$T_{ENG,req}$	Required engine torque
$T_{ENG,WOT}$	Engine wide open throttle torque

T_e	Temperature of gas in the exhaust manifold
T_i	Temperature of gas in the exhaust manifold
$T_{IOL,HIGH}$	Engine torque on upper ideal operating line
$T_{IOL,LOW}$	Engine torque on lower ideal operating line
T_{TXclu}	Transmission clutch torque
T_{TXin}	Transmission input torque
$T_{TXin,loss}$	Transmission loss torque at input side
T_{TXout}	Transmission output torque
$\overline{T}_{TXout}$	Normalised transmission output torque
$T_{TXout,\max}$	Transmission maximum output torque
T_{WHL}	Wheel torque
$T_{WHL,predict}$	Predicted wheel torque
tmfmep	Total mechanical friction mean effective pressure
V_{BAT}	Battery voltage
V_{BAToc}	Battery open circuit voltage
V_s	Cylinder swept volume
v_{VEH}	Vehicle velocity
$v_{VEH,predict}$	Predicted vehicle velocity
vfmep	Valvetrain friction mean effective pressure
x_b	Burned gas fraction by mass
x_r	Residual gas fraction by mass
γ	Specific heat ratio
η_c	Combustion efficiency
η_{ENG}	Engine efficiency
η_{FD}	Final drive efficiency
η_{otto}	Thermal efficiency of ideal Otto cycle
η_{th}	Thermal efficiency

η_v	Cylinder volumetric efficiency
$\eta_{v,ideal}$	Ideal cylinder volumetric efficiency
$\overline{\eta}_{ENG}$	Normalised engine efficiency
θ_{grad}	Road gradient angle
ω_{EM}	Electric machine speed
ω_{ENG}	Engine speed
ω_{TXin}	Transmission input speed
ω_{TXout}	Transmission output speed
ω_{WHL}	Wheel speed

1 INTRODUCTION

1.1 BACKGROUND

The environmental impact of automobiles is increasingly one of the most important social issues of today, which has led to the implementation of the Kyoto protocol [1]. To meet the required carbon dioxide (CO_2) reduction target, many kinds of new technologies in the transportation sector have been suggested in order to reduce fuel consumption and the amount of harmful emissions.

In the conventional vehicle, the internal combustion engine (ICE) burns fuel to generate the mechanical power, which is transferred to the wheels through the transmission. The wheels consume the delivered power in order to overcome the rolling and the aerodynamic resistance and accelerate the vehicle. Therefore, the improvement of the tank-to-wheel efficiency is crucial in reducing the vehicle's fuel consumption. To achieve better efficiency, advanced powertrain technologies including a spark ignition direct injection (SIDI) engine and a continuously variable transmission (CVT) have been introduced. At the same time, alternative clean vehicles such as electric vehicles (EVs), hybrid electric vehicles (HEVs) and fuel cell vehicles (FCVs) have been developed. However, considering the technical and infrastructural limitations, the HEV is currently seen as a ready-to-use solution.

The HEV uses two or more prime movers as sources of power. Theoretically, the HEV powertrain configurations are almost infinite, but can be classified as the series, the parallel or the power split that is the combination of series and parallel, according to the power mixing structure. The series HEV has great fuel saving potential when used with an ideal power plant such as a homogeneous charge compression ignition engine or a fuel cell, but the cost and the technical challenges are major obstacles for their use in passenger cars at this moment. Consequently, the parallel mild hybrids and the power split hybrids are the only available variants in the commercial market.

The physical configuration is the important factor from the mechanical point of view, but the impact of the optimised control strategy on the fuel consumption is significant, too. The mechanical design depends not only on the technical considerations but also on

the non-technical aspects such as the production cost. On the other hand, the control strategy can be more generalised, and many research activities have been reported from both the industrial and the academic areas.

1.2 OBJECTIVE OF THESIS

The aim of this research is to develop a control algorithm of an HEV, in particular the potential for predictive journey estimation focussing on the fuel economy benefit.

The main objectives are as follows:

- To investigate the HEV technologies which are currently available and their control strategies
- To construct a generic hybrid powertrain simulation model
- To design a realtime control strategy using predictive journey estimation to maximise fuel economy
- To demonstrate the fuel economy benefit of the online predictive control strategy through offline and software-in-the-loop (SIL) computer simulation

1.3 THESIS OUTLINE

This thesis consists of 8 chapters.

Chapter 2 presents an extensive literature survey on HEV technologies and their control strategies.

Chapter 3 introduces the baseline powertrain and the vehicle model. The mathematical representation of the engine, the transmission and the vehicle are presented. Descriptions are also given of the quasi-static backward simulation model and the fuel economy figure over the standard driving cycles.

The hybridisation of the vehicle is covered in Chapter 4. It shows the methodology to find an appropriate electric machine (EM) size, and the mathematical model of the EM and the battery is integrated into the baseline model. The root causes of the fuel saving of the HEV are revealed through analysis of the simulation results.

Chapter 5 presents the fuel economy potential of the HEV using the dynamic programming (DP). The optimal solution to minimise the fuel consumption is

demonstrated on the different kinds of driving cycles with the road gradient. This work leads to the necessity of a new control strategy using future journey estimation.

Chapter 6 shows the torque distribution and the energy management of the hybrid powertrain. The DP is applied to the various operating conditions, and the optimal engine operating strategy is presented, followed by the development of a fuzzy controller using predictive journey estimation. The new control algorithm is tuned by the optimal dataset generated from the DP. A structure of the information provided from the navigation system is optimised by the design of experiment (DOE). The effect of the optimisation on the different road conditions is also demonstrated.

Chapter 7 describes a forward dynamic model of the powertrain developed in the AMESim-Simulink co-simulation environment. The SIL simulation is demonstrated, and the effect of dynamics on the performance of the controller is discussed.

Chapter 8 covers conclusions of the work conducted and areas for further research.

2 LITERATURE REVIEW

2.1 HYBRID ELECTRIC VEHICLE TECHNOLOGIES

2.1.1 ALTERNATIVE POWERTRAINS

The ICE has been widely used as a prime mover of automobiles for more than a century. Gasoline and diesel have higher specific energy than the alternatives such as alcohol, hydrogen, and electric batteries. In addition, the ICE-based vehicle has good well-to-wheel energy efficiency, but still has significant room for fuel economy improvement. Therefore, it is expected that the ICE still has a long life ahead of it [2]. However, petroleum is not a renewable resource and the oil industries anticipate that it will last for only a few more decades.

Hydrogen is the most likely long-term alternative to petroleum. The scenario from petroleum to hydrogen [3] illustrates that the FCV could be commercialized between 2020 and 2030 and that the HEV is the main stopgap solution on the route to hydrogen powered vehicles. Ng et al. [4] forecast that parallel HEVs equipped with gasoline engines would be top selling HEVs in 2005, and FCVs will occupy more than 50 % of the whole hybrid market in 2020. However, HEV market still stays in low volume even though more players are entering the competition, and the mass production of FCVs is not expected in the near future. This disappointing penetration mainly results from high cost of energy storage, lack of infrastructure and customers' perception of new powertrain technologies.

The analysis for the North American market by Conley and Taylor [5] emphasises the importance of thermal efficiency improvements and the benefit of the full hybrid system. In order to meet an aggressive 36 mpg target of fuel economy, they suggest the diesel, the hybrid, and the fuel cell technology as candidates. In the prediction of the North American market by Gott et al. [6], it is expected that over half of all light vehicles will have some degree of hybridisation by 2020. It includes the 42V micro hybrid with the stop-start and the mild hybrid with the launch assist function. They also say that the diesel will remain as the most efficient ICE through 2020 and that the SIDI is promising

to enable future fuel efficiency mandates but that the FCV will not be commercialised by 2020.

Ronning and Grant [7] indicate that Sweden and the UK are large potential markets of the HEV due to the potential energy savings and also California by the exceptionally high incentives. West [8] says that the use of HEVs depends on the legislation which either increases the fuel cost or mandates high fuel economy. As a result, France and the UK are good potential markets because of the high fuel price.

2.1.2 FUEL ECONOMY POTENTIAL

It is not easy to estimate the fuel economy potential of the HEV because it relies on too many factors with complex interactions. Furthermore, if the economic factors such as the fuel cost and the incentive programs are involved, it will be hard to predict it precisely. In spite of these difficulties, many research activities have been carried out into various aspects of the work.

Cuddy and Wipke [9] show that the parallel hybrid can achieve 24% better fuel economy than the conventional diesel vehicle, and 18 % in the case of the series. An et al. [10] claim that the fuel economy improvements by the HEV over the corporate average fuel economy cycle for a high performance vehicle are 27-41% according to the hybridisation level, but the benefits are reduced to 21-23% for a low performance vehicle. In the following research [11], they conclude that the moderate package using an improved spark ignition (SI) engine, a CVT or 5-speed automatic transmission (AT) and an integrated starter alternator (ISA), enables 37-70% improvements in powertrain efficiency within 4.3-6.6% cost increment. In the case of the more advanced package adopting a SIDI and a 6-speed AT, the fuel economy benefit is increased up to 98% with less than 8% of cost.

One of the advantages of the HEV is that more electrical energy is available on board. In the study of Lukic and Emadi [12], the 42V electric system with the electrically assisted HEV propulsion option increases fuel economy up to 27.3% by means of the electrification of the ancillaries such as the throttle actuation, power steering, air conditioning, active suspension and the electrically heated catalyst.

Louis [13] concludes that the HEV using diesel or compressed natural gas (CNG) produces the same amount of greenhouse gas as the best fuel cell options running on the CNG or compressed hydrogen, with the assumption that fuels are produced from either crude oil or natural gas. From the primary energy efficiency point of view, Ahman [14] shows that given the uncertainties, the EV, the HEV, and the FCV have approximately the same primary energy efficiency when supplied with fossil or biomass fuel. Moghbelli et al. [15, 16] say that the difference between the HEV and the FCV is not large when considering the well-to-wheel efficiency and the fuel economy of the diesel HEV is competitive with the direct hydrogen FCV. Additionally, the potential for the hybridisation of the FCV studied by Atwood et al. [17] shows that some degree of hybridisation can improve the energy efficiency of the FCV, because the storage works as a buffer to capture the regenerative braking energy and the fuel cell system may benefit from downsizing somewhat to prevent excessive operation under a light load. From the oil preservation point of view [18], if the HEVs replace the all ICE vehicle within 10 years, the expected life of the oil reserves can be extended by at least, another decade, compared with only 3 years by introducing the FCV into the market in 2020.

There are still different opinions as to whether the HEV is worth introducing or not [19, 20], and most of these arguments revolve around the relative fuel benefits to the incremental cost. In general, the potential fuel bill saving is same or less than the optional cost of hybridisation at this moment. However, continuing technological improvement is cutting the cost of advanced powertrain and its components. On the contrary, oil price is going up and not likely to be down in the long term. Moreover, limited reserve of fossil fuel and global warming by greenhouse gas are making governments initiate various incentive programs such as tax return, redemption of congestion charges, and free parking. Other dominant factors, for example the emission legislation and the customers' expectations of the new technologies, also exist.

2.1.3 CURRENT HYBRID ELECTRIC VEHICLES

Toyota Prius, the world's first mass produced HEV, was introduced to the Japanese domestic market in 1997. It shows a new HEV configuration with an electric CVT, classified as the power split hybrid [21]. It recorded a remarkable 52 mpg in city driving and 45 mpg in motorway, and met the California super ultra low emission vehicle

(SULEV) standard in emission at the time of launching in North America and Europe in 2000 [22, 23]. The engine and motor power were upgraded to 53kW and 33kW respectively. In 2003, the remodelled Prius was introduced with a more powerful 57kW engine and a 50kW electric motor to eliminate the lack of power complaint from the users. [24, 25] They call this system the Toyota Hybrid System II (THS-II) to distinguish it from the former. After the successful launching of the Prius, Toyota introduced two different concepts in 2001. One of them is a mild hybrid that adopts a belt starter alternator (BSA) device and a 42V system [26-28], and the other is the 4-wheel drive (4WD) hybrid with a CVT [29-33]. However, the availability of both is limited to the Japanese domestic market. In 2005, Toyota applied the THS-II to the two sport-utility vehicle (SUV) models, Lexus RX400h and Highlander [34, 35]. They use the combination of a 155kW 3.3L V6 engine and a 123kW motor and an optional 50kW motor at the rear wheel for the electric 4WD system. Toyota claims that this system achieved both the V8 engine power performance and a compact class fuel economy.

In 1999, Honda developed Insight [36] using the ISA device, which they call an Integrated Motor Assist (IMA) system. This 2-seater passenger car adopts the 1L variable valve timing (VVT) gasoline engine with a 5-speed manual transmission (MT) or a CVT and a permanent magnetic motor. The CVT version achieves 57 mpg in the city and 56 mpg on motorway fuel economy and meets the SULEV emission standard [37]. The Insight uses a different approach from the Toyota Prius but both present remarkable fuel economy improvements and emission reductions, and they are frequently used for benchmarking [38-40] or comparative targets for new concept HEVs [41, 42]. Honda has expanded the application to the compact and med-size sedan. They introduced Civic hybrid in 2002 based on the mass production conventional vehicle [43]. In 2005, Accord hybrid was launched on the market [44]. It incorporated new technologies, including the variable cylinder management (VCM) that turns off the three cylinders of the V6 engine under the low load and the IMA system, which improves the driveability during the transient of the cylinder deactivation control.

Nissan Tino [45] has a similar configuration as the IMA, except for the engine disconnecting clutch between the EM and the engine, and the separate generator. This configuration has the advantage of more regenerative braking as engine friction can be

eliminated, but it has the drawback of an expensive two-motor solution. It adopts a 1.8 litre gasoline engine with a motor integrated CVT.

GM launched two full size hybrid pickup truck models, Sierra and Silverado, in 2004 [46, 47]. These are a kind of mild hybrids with start-stop and minimal electric assist. They use the ISA installed in bell housing together with the torque converter of the AT and a 42V battery system. GM plans an additional type, the two-mode power split. The two mode power split is conceptually related to the power split full hybrids. GM has some patents [48, 49] of the two mode system, and claims that it can reduce the EM size with the same performance using a combination of clutches and brakes [50]. A similar system is also being investigated by the others parties [51].

Ford contributed to the hybrid market with a small SUV, Escape, in 2004. They licensed the power split hybrid system from Toyota [52]. The structure of the hybrid transmission is the same as the RX400h or Highlander but the motor power is 65kW, which is about half of the Toyota's. Mercury Mariner has also introduced its hybrid variants in 2005 and it shares the same powertrain as the Escape.

Most of the major automotive manufacturers have been developing many types of HEVs. Additionally, independent research companies and universities are participating in this new challenging area. There is no clear evidence whether HEVs can occupy a rich market or only a niche market in near future. However, they are being considered as only available clean vehicle technology at this moment.

2.2 CONTROL STRATEGIES OF HYBRID ELECTRIC VEHICLES

The control strategy is one of the most important parts of the HEV technologies. HEVs have two or more power sources and complex power transfer paths [53]. Because of these complexities, it is necessary to use a high level controller, the so-called vehicle system controller [54, 55] or supervisory controller [56, 57], positioned at the top of the hierarchical structure of the controllers. The main role of the supervisory controller is to determine the torque or power demand of the engine, the EM, and the brake according to the driver's pedal input.

The supervisory control algorithms can be classified into the following 5 categories.

- Nonlinear optimal control methods to find global optimal operation during a given entire journey
- Rule based intelligent control for instantaneous optimal operation of the powertrain using the information of current states
- Offline predictive techniques to estimate the road conditions and forecast other future parameters based on the stored database
- Online predictive control to identify the road terrain and traffic information, using on-board information from the navigation devices
- Other approaches

Each of these categories is reviewed throughout the following subsections.

2.2.1 OPTIMAL CONTROL

The nonlinear optimal control is one of the classical methods for the control problems of the plant expressed by nonlinear differential equations. There are two kinds of approaches. One is the DP developed by Bellman [58] and the other is the variational approach using the Pontryagin's minimum principle.

Kleimaier and Schroder [59] use a numerical optimal control problem solver to find the global optimal control trajectory of an HEV using a CVT. Because of the heavy computation load, the result is limited to the offline simulation. In the other work [60], they suggest a real time control law based on the global optimal operating line calculated by the previous study. The key idea is to minimise the total power dissipation at the current state. It shows quite good results in the Economic Commission for Europe cycle and New European Driving Cycle (NEDC), but does not examine the result over the real world cycle. This approach might be effective on the simple driving conditions with the pre-calculated global optimal control trajectory, but not likely to be effective in arbitrary and dynamic real road situations.

Lin et al. [61] solve the minimum fuel optimal control problem for a hybrid electric truck by the DP, and then extract a simple rule-based real-time controller through the analysis of the optimisation result. The calculation load of the DP is increased exponentially with the number of states and the resolution of the quantisation, so that

pre calculated maps are used in order to reduce the processing time. The results show that the optimal gear shifting, the charge and discharge schedule, and relieving the engine load through more efficient motor assist make important contributions to the fuel economy. This study presents a global optimal solution, but the suggested rule based real time controller is not easily generalised because it is extracted from and verified with the same operating cycle. In a later study [62], they consider the exhaust emissions and the robustness of the controller with different driving cycles.

Paganelli et al. [63-65] study the optimal control strategy for parallel torque addition HEVs using static simulation models. In this work, the equivalent consumption minimisation strategy, which considers the battery as an auxiliary reversible fuel tank, is suggested. The result of this instantaneous optimal control strategy is also compared with the global optimal solution based on the simulated annealing method. In the other publication [66], they convert the electrical power flow into the equivalent fuel cost based on the average cost of the electricity through the various power paths. The weakness of these works is that the calculation process of the equivalent fuel amount or the cost of the electric energy is highly dependent on the assumptions of the production cost of the electricity and the efficiency of the electric energy transfer. Additionally, the optimal operation point found by the simulated annealing method is not always a true optimal but one of the local optimal solutions.

Delprat et al. [67, 68] point out the above problem of the simulated annealing method and suggest a global optimisation algorithm using the variational approach. To avoid the difficult two-point boundary value problem, the reformulation to an initial value problem with only one state variable and the iterative methods to put the final value within an error boundary are used. Their investigation includes the engine shutdown control and it shows good improvement of fuel economy. The recent study [69] suggests the online control algorithm based on the previous works. It is quite simple and realisable in real time but may not be effective because the estimation algorithm of the future states is not reliable and robust.

Kirschbaum et al.[70] suggest a modified DP solution for a HEV fuel optimal control. This iterative DP variant deals with a third order system with three inputs as a system having four variables, which is the sum of the states and the inputs. This methodology is

suitable in cases where the road slope and the vehicle speed is given, which is a very general assumption in the computer simulation environment. This algorithm can reduce a substantial amount of the calculation time usually required by the conventional DP. However, it remains in the offline application category because of the causality and the computation load.

Yoon and Lee [71] solve the numerical optimisation problem for a given driving cycle. They calculate the optimal motor assisted map for the minimum fuel consumption, and investigate the design parameters for the control aspects. This result can approach the global optimal for the given cycle, but cannot be generalised for real arbitrary driving environments.

The optimal control finds the global optimal route of energy consumption minimisation but it is hard to be realised in real-time because of the non-causal attribute, which requires the future state and the heavy calculation load. However, it shows the maximum benefit of the hybrid vehicle, so that can be used as an index to compare the performance of the other controllers.

2.2.2 INTELLIGENT CONTROL

Rule based intelligent control is another field that many researchers have studied for the HEV. From the simple intuitive rule based controllers, the fuzzy and the neural net approaches are the main fields to be investigated these days.

One of the simplest algorithms to control the HEV powertrain is the switching logic control [72]. To achieve a more effective result, the operating condition of the vehicle powertrain is divided into three regions according to the required torque level. For each level, the controller determines the torque distributions of the engine, the EM, and the brake with the different control schemes to maximise the state of charge (SOC) of the battery. This controller always tries to maintain the SOC at a certain level. Consequently, the charging occurs too frequently, regardless of the engine operating conditions, and it is not efficient in the sense of fuel consumption minimisation.

Another simple rule based control algorithm is to maintain the operating point on the static optimal condition line. Bowles et al. [73] propose this type of control scheme for a CVT based HEV. The engine and the CVT are controlled to be operated along the pre

calculated optimal operating line, which is similar to that used in the conventional CVT powertrain control. The SOC level and the idle stop are separately controlled within a set of given threshold levels. This approach is a convenient way to hybridise a conventional CVT vehicle because much of the control algorithm is reusable. However, it cannot get the full benefits of hybridisation because the control action to maintain the SOC also limits the engine operating condition.

Koo et al. [74] present a general fuzzy logic approach to control a hybrid bus powertrain. It optimises not only the fuel consumption but also the emission reduction. Additionally, the driver's intention as well as the power balance is considered when designing the controller. Lee and Sul [75] also show similar results with the same approach. However, the target system in these works is a shuttle service bus, so the driving route is simple, repeatable, and easily predictable. This aspect may play a role in overestimating the benefit.

Brahma et al. [76] suggest a scalable and reconfigurable simulation technique and a fuzzy controller to control the power flow in a hybrid SUV with a CVT. In the following series of research [77, 78], the fuzzy controller uses 3 inputs, the driver's intention, SOC, and EM torque, and controls the ICE operating point in an optimal sense. The concept of the degree of hybridisation to decide the rough boundary of the EM size for a given powertrain and vehicle is also presented. In spite of the comprehensive works, all efforts are placed only on the optimisation of the ICE, and the efficiencies of the other parts are not considered. Moreover, the fuel-use strategy, one of the control schemes studied in these papers, limits the power to get an optimal solution, regardless of the user's driving intention. It means that the vehicle cannot meet the given driving condition in some instances. It is not sensible for the real implementation in practice even though the fuel saving potential is great.

Salman et al. [79] and Schouten et al. [80, 81] study the fuzzy control logic for a parallel HEV to optimise the power output of the EM and the engine simultaneously. The driver's commands, the SOC, and the EM speed are selected as inputs. Other separate controllers optimise the braking and the gear shifting. The simulation result over a standard driving cycle shows about a 7.7% improvement over the result of the control strategy that only optimises the engine efficiency. In the recent work, Kheir et al. [82]

demonstrate the same control scheme for both the emissions reduction and the fuel economy improvement.

Piccolo et al. [83] define the control of the hybrid powertrain as a classical optimal control problem and apply the genetic algorithm to assist the designer for the tuning of the control logic. Through the case studies, it is demonstrated that this algorithm effectively finds the optimal solution for a given driving condition. It also considers the weighting functions for the various emission controls. The proposed controller requires less real-time computing power than the conventional gradient-based algorithm, but it is still hard to apply it to a real-time application. Moreover, it needs the calculation of the optimal parameters for each driving cycle because it cannot guarantee the optimality for arbitrary driving situations.

The rule-based intelligent approaches are intuitive, relatively simple to design, and easily implemented in modern digital real time controllers. However, they cannot find the global optimal point and gain the maximum benefits of the HEVs. In addition, most of the research is concentrated on the instantaneous optimal operation, so the SOC control does not consider the future possibilities by charging the battery or discharging it to assist the engine.

2.2.3 OFFLINE PREDICTIVE CONTROL

It is obvious that a great fuel saving benefit can be realised if future driving conditions can be predicted. This fact explains the reason why the optimal controls can get the best fuel economy, whereas the instantaneous control schemes cannot. One of the solutions to this problem is predictive control, based on the offline data.

The early study [84] is a fuzzy decision making use of everyday driving patterns. A method to predict the everyday driving habits of people and a decision-making strategy using fuzzy logic are suggested. The base control algorithm starts with a simple fuzzy decision making to balance the two propelling sources presented in the previous study [85]. In these works, the controller estimates the journey distance and the duration based on the information of the departure time and whether it occurs on a weekday or at a weekend. The estimation performance depends on the dataset gathered from the driving pattern of a certain group of drivers, and consequently, it is not easy to generalise the

result. However, it is one of the good examples to study in order to predict the future journey pattern.

Won and Langari [86] suggest a torque distribution control algorithm based on the fuzzy logic for a parallel HEV. In a series of successive papers [87-90], they propose a sophisticated predictive control structure, which consists of several small sub-modules. This is a very systematic and well-organised approach to design the predictive controller. However, all the identification functions are basically dependent on the database, so the performance is limited by the quality of the data and the level of matching with the driving situation in the real world.

Jeon et al. [91] propose a methodology to recognise the driving pattern. Six standard driving patterns are defined and an algorithm to assign the current driving pattern to one of those six representatives by the neural network (NN) is developed. Finally, they develop a multi mode driving control algorithm, which periodically adapts the driving control strategy to a current driving pattern by the driving pattern recognition algorithm. To avoid overload on the processor, the control algorithm stores data every 1 second and updates the control algorithm every 300 seconds. It may be effective if the driving condition is well matched to one of the pre-defined patterns. However, the predicted performance depends on the quality of the pre-defined patterns and the long update period might show a poor performance when it meets an abrupt change in the driving conditions.

Ippolito et al. [92] introduce a quite different approach. It finds the global optimal operating conditions for some given driving cycles in the offline simulation, and keeps all the operating conditions and states as a database. In a real situation, the fuzzy controller compares the current states and the data in the database to find a similar situation and applies the optimal control input. The performance of the controller still depends on the quality of the database, but the response against the condition change is faster than in the previous research.

The research by Ichikawa et al.[93] point out two important practical considerations. The first point is that they concentrate on the commuting route from home to work, because this is more repeatable and occupies most of the driving distance. The other point is that the entire database is distance-based rather than time-based. The time-based

data is easy to deal with but less consistent than the distance-based data. The study shows a comparison of both and how the distance based data is more reliable to make the database on the commute route. It suggests a process to cluster each section of the route and to integrate it into the database. However, this study concentrates on design methodology and does not present a proposal to match current driving conditions with the database, which significantly affects the performance of the controller.

The offline predictive control algorithms are based on the database gathered from the real road statistically and experimentally. Therefore, the performance of these controllers is highly dependent on the quality of the database and the driving cycles from which the database is made. Additionally, the algorithms to identify the proper dataset to match with the current driving condition are not easy to implement in real time within the short control loop time.

2.2.4 ONLINE PREDICTIVE CONTROL

In spite of the possibilities of a great fuel saving potential, the future journey prediction is not easy. One of the feasible solutions is the online prediction of the future state using modern navigation devices. Jackson [94] suggests that the advanced control technology allows the vehicle to be more efficient by knowing what lies ahead via the global positioning system (GPS) and the digital map. In the recent report of Owen and Gordon [95], the advance control technology using knowledge of the forthcoming road conditions including the road type, topography, the traffic and the junctions can enable improvements in aspects of the powertrain control such as the energy management strategy as well as the diagnostic systems. It says that the near to midterm studies are likely to use the information from on-board devices like the GPS and the map on the optical storages, and vehicle-to-vehicle communication could add to the functionality of this technology as a long term research theme. It claims that this technology could bring the CO_2 reduction down to less than 10%.

The online predictive control has been used in the automatic transmission control [96, 97], and the extensive research activities focus on the driver assistant system [98-100], the adaptive cruise control [101], and the conventional powertrain control to save fuel[102]. The recent patents show the possibility of online prediction applications in the HEV powertrain control. One of them uses the journey route information selected

by the user on the navigation system and determines the usage of two power plants of the HEV in the optimal sense [103]. A more advanced concept [104] suggests the trajectory optimisation based on the future operating conditions from the navigation information integrated in the vehicle system controller.

Rajagopalan and Washington [105] are developing a predictive control strategy of the HEV using the GPS information. They assume that the traffic and elevation information from the GPS over the entire trip are known, and use an adaptive fuzzy logic controller. An instantaneous control strategy for a parallel HEV with discrete ratio gearbox is continuously modified based on future driving conditions. This controller considers not only fuel economy but also emission reduction, and the simulation results show a good compromise between them. This research puts forward the possibility of an online predictive control, but the optimisation methodology of the control parameters is left for future work. In addition, it assumes that the road information is given at regular time intervals, but this is very unlikely because traffic sensors are evenly spaced along the road and the individual vehicle speed is variable.

Back et al. [106-108] present a predictive powertrain control of an HEV in the route-domain. They suggest some ideas on how to use the DP for solving the optimisation problem in the model predictive control (MPC) approach in the receding horizon. The information from the telematic device is used in order to predict the future torque request profile. The main effort concentrates on the reduction of the calculation time of the DP, which usually requires a heavy calculation load. It is found that an accurate vehicle speed prediction is the basis for an effective working MPC algorithm, but the effect of the traffic situation should be included as well.

The research by Sciarretta et al. [109] investigate the hybrid powertrain control based on a real-time minimisation of the equivalent fuel consumption. The ratio of the recuperated electrical energy and the delivered positive mechanical energy is a key parameter to optimise the control operation. The paper proposes an online estimation of the ratio, which is obtained by the offline estimation from the given load conditions in their previous work [110]. The algorithm estimates an updated value whenever the on-board telemetry system provides any new information during the journey with the defined points. The information provided from the telemetry system is moving or fixed

obstacles and the algorithm sequentially estimates the vehicle velocity profile, the energy contribution, and the electric energy ratio. It is very efficient from the external information interaction point of view, but a series of multiple estimation processes cannot guarantee the accuracy of the final key parameter.

Jackson et al.[111] present an idea for using the information from the telematic device to optimise the energy flow of diesel hybrid powertrain. The greatest benefit can be achieved from the electric drive and the electrified ancillary systems. Furthermore, they demonstrate the possibility of reducing the fuel consumption by the electrified diesel particulate filter heater. It indicates a new potential area of the hybrid combined with the diesel powertrain.

Deguchi et al [112] propose an idea for optimising the charging level of the battery according to the predicted engine efficiency on the forthcoming route. The navigation system feeds the information of the road profile and the congestion level, and the controller classifies the operating condition into the six pre-defined road types and the four congestion levels. Compared with the existing HEV control strategy, a 0.5~7.8% fuel economy improvement is claimed. Even though this approach uses the online traffic information, the performance of the controller depends on the clustering of the road type and the traffic situation. In conclusion, it can be positioned between the offline and online predictive control.

The research of the predictive control based on the information supplied by the vehicle navigation system by Johannesson et al.[113] examine three optimal controllers, each with a different level of information accesses to the driven route. The results indicate that, for an urban route with varying topography, the use of predictive control can significantly reduce fuel consumption. There are two important conclusions in this work. Firstly, the topography plays an essential part of the savings in the fuel consumption due to the long term planning of the SOC. The second point is that only general aspects of the velocity need to be predicted so that the real-time implementation of the predictive controller with close to the optimal performance should be possible.

Modern navigation technologies are being developed rapidly, and will be standard for passenger cars in the near future. If the HEV controller is combined with these modern technologies, they will show a great synergy effect. Even though some research results

have been published in this challenging field, many remaining areas still require further investigation in order to evaluate the status of the real application.

2.2.5 OTHER APPROACHES

The unified modelling of the EM as an ICE is one of the interesting approaches [114]. In this study, the whole electrical system is modelled as an equivalent mechanical system, and the effective specific fuel consumption is applied for the two virtual mechanical power sources. Then, optimal operating condition maps are generated and used for the control of power load distribution. It is a kind of the classical map based instantaneous controls, which are widely used in conventional vehicles.

Jeon et al. [115] apply a linear quadratic penalty function in the form of linear matrix inequality (LMI), without considering the gear shifting, to find the optimal gear change schedule in the receding horizon. The receding horizon control uses only a finite set of the future information, so can overcome the drawback of the intensive calculation load generally required in the infinite horizon. If the information of the future journey can be supplied in real time, it could be a good candidate for an optimal controller.

Soltis and Chen [116] apply the game theory generally used in the social science field to the powertrain control application. In this study, two players, an ICE and an EM play the game to maximise the payoff to minimise fuel consumption. Because the game theory can only deal with the discrete decision making problems, it requires the heavy iterative computation if the digitised resolution of the control signal are very fine.

Pisu et al. [117] show the result of the model based linear robust control. They formulate the hybrid powertrain control as a linear optimal control problem with a set of the LMI constraints. To formulate the control as the LMI form, the plant model should be linearised at the operating point, but the powertrain model is highly nonlinear and not able to be linearised with a reasonable error margin.

2.3 RESEARCH DIRECTION

A HEV is a foremost off-the-shelf solution among alternative powertrain technologies. It has a good fuel economy potential, which is directly affected by the control of an on-board bidirectional energy storage such as a battery. As reviewed in the previous section, the traditional optimal control is not feasible for real-time application, and the

intelligent control is limited to the instantaneous optimal solution. Therefore, only the predictive control methods are able to consider the forthcoming energy saving potential. This study focuses on the design of an online predictive control algorithm, which is a new challenging area in HEV energy management combined with modern navigation and the GPS technologies.

3 BASELINE VEHICLE

In this chapter, the baseline vehicle model is introduced, which will be used in the following chapters to demonstrate the benefit of a control algorithm. The mathematical representation of the powertrain and its backward simulation model are described, followed by the fuel economy simulation results.

3.1 VEHICLE CONFIGURATION

3.1.1 SPORT UTILITY VEHICLE

The vehicle type is one of the important parameters of fuel economy, because the weight, body shape, and tyre resistance affect the total energy consumption of the vehicle. Table 3-1 shows the broad spectrum of HEVs in the North American market [118]. All of these are parallel mild hybrids or power split full hybrids, and midsize cars and SUVs are the majority of them. In this study, the SUV is chosen as a target vehicle because it is more effective to hybridise the SUV rather than a passenger car taking account of relatively poor efficiency, low extra cost, and easy packaging. Seven models among the nine SUVs in the table are compact SUVs based on the passenger car platforms. The specification of those vehicles is summarised in Table 3-2. Some of them provide multiple choices for the engine, in which case the largest engine variant is selected. The average fuel economy is 8.3 and 10.6 km/L in the US city and the highway cycle respectively. These values are relatively lower than the passenger cars equipped with similar size engines due to the heavy weight, the wide tyres, the large frontal area, and the high aerodynamic drag. These vehicles are used as the reference vehicles to configure a generic SUV model in the next subsection.

3.1.2 ENGINE SIZE

Two comparative studies of the hybrid powertrains [42, 119] show the strong relationship between the vehicle kerb weight and the engine peak power. This approach can suggest a general guideline to determine an appropriate engine size for a given vehicle weight. However, the vehicles in the studies are only a few HEVs. Therefore, the resulting values represent the average of the limited number of vehicles in the different segments. Applying this methodology, more data on the available SUVs

should be gathered and analysed. It is not easy to classify a vehicle as an SUV because the definition is not unique and clear. In this study, the 2006 model SUVs on the Environmental Protection Agency fuel economy guide [120] are investigated.

The total 86 SUV models with the 127 engine variants are listed in Table 3-3. To remove the exceptional cases, those powered by diesel engine, the alternative fuel engine such as natural gas or alcohol, and the turbo or supercharged engine are not considered. If there are more than one driveline options, the 2-wheel drive (2WD) standard configuration is selected. The data of the engine power and the vehicle kerb weight are shown together. A few data are old or not available but it may not affect the statistical results very much.

Figure 3-1 depicts the relationship between the engine peak power and the vehicle kerb weight. The kerb weight is distributed in the range from 1402kg to 2637kg, and the peak engine power is between 104kW and 317kW. The trend line gives the average value of 94.2kW/1000kg. The selected reference vehicles listed in Table 3-2 are clearly positioned in the low power and weight area. The average kerb weight of them is 1590kg, so the appropriate engine power is 150kW. This is just 4% deviation from the average value of the reference vehicles, 156kW.

To estimate the appropriate engine size, the specific engine power is examined. The engine sizes of the SUVs are widely spread from 2.0 to 6.1L. From Figure 3-2, the average specific engine power is 46.2kW/L. As a result, the estimated engine size to produce 150kW at peak is 3.2L. It is well matched with the average value of the reference vehicle engines.

3.1.3 SPARK IGNITION DIRECT INJECTION ENGINE

It is said that an advanced diesel engine is the best prime mover from a fuel economy point of view[121]. However, even though the diesel engine is more efficient than the gasoline engine, both of them will share the market because the gasoline and the diesel are extracted from the same source, the crude oil, and cannot be converted to each other. Furthermore, California's decision to submit the diesel engine to the same emissions criteria as the SI engines undermines the expectation in the North American market [122]. For luxury cars or SUVs, the gasoline engine will be more likely to be used

because of the comfort in noise, vibration and harshness and the less emission such as no particulate. In this sense, the SIDI engine has a good potential for the conventional and the HEV application.

Morita [123] mentions in the study of the future automotive power sources that among the next generation vehicle candidates only the HEV can be presently regarded as the alternative energy vehicle that has the potential to rank alongside conventional vehicles in terms of cost and convenience. This paper indicates that the SIDI engine has the significant potential as a next generation engine because its heat efficiency approaches that of the direct injection diesel engine under the low load condition. Additionally, since the SIDI engine starts up quickly and smoothly by minimising the cranking time and amount of vibration, it is compatible with the engine shutdown system used in HEVs. In the study of Salber et al. [124], the SIDI engine shows a 10-14% fuel saving potential over the conventional multi point injection(MPI) engine. Combined with the fully VVT technology, it can be increased up to 18%, and a maximum of 23% with the VCM. It should be emphasised that all of these individual technologies are ready to use. Shayler et al. [125-127] study the fuel economy and emissions of stratified charge SIDI engines. They derive generic functions to predict the fuel economy and use the NN to calibrate the spark and injection timing for the emissions reduction. The final results show that the SIDI can achieve around 20% fuel economy benefit over the port injection engine and reduce the oxides of nitrogen significantly without large fuel economy penalty. From these results, Horn [128] suggests that hybridisation with the ISA can increase the fuel economy potential of the SIDI by up to 29.1%.

A stratified charge SIDI engine is chosen as a base powerplant because it has good efficiency in the low power region, which is frequently used in normal driving conditions. In addition, its low friction loss can reduce the cranking time from the idle stop and maximise the energy absorption by the regenerative braking in the HEV. A small number of SIDI engines have been commercialised but it is hard to find a 3.2L stratified charge type and access the experimental data of the fuel consumption. To generate the engine fuel map, the algorithm suggested by Horn et al. [125-128] is adopted for this research. The data grids used in the computer simulation are

200rev/min of the speed and 0.5bar of the brake mean effective pressure (BMEP). The detailed calculation procedure is explained in Appendix A.

The mass fuel flow rate is shown in Figure 3-3. The graph has discontinuities at around 3200 rev/min, which indicates the change in the operation modes between the stratified and the homogeneous charge. The maximum BMEP is less than 10 bar, which is slightly lower than the typical value because the rich fuel injection to increase the output torque at the high throttle is not accounted for. The rich fuelling with modified injection and spark timing is difficult to predict in this sort of model. It may affect the vehicle performances such as the top speed and the maximum acceleration but there is little effect on the fuel economy study in the standard driving cycles. The minimum torque at the closed throttle is also an important factor of the HEV because it acts as an additional loss for the regenerative braking. To absorb the kinetic energy of the vehicle using the ISA, the friction loss of the engine should be minimised or an additional clutch should be installed between the engine and the ISA. However, most of the mild hybrids do not adopt the latter option because of the mechanical complexity and limited space. The full VVT can be an alternative option because it reduces the pumping loss by closing the valves and shutting off the fuel during the regenerative braking. This study assumes this version, so the closed throttle torque is calculated excluding the pumping loss.

Figure 3-4 shows the result of the engine efficiency map. The maximum efficiency is 31% and it is the typical value for this size of gasoline engine. The conventional MPI engines show the best efficiency at around the wide-open throttle (WOT) line, but there is another peak efficiency island in the low power region in the case of the SIDI. It is the beneficial point of the SIDI engine and plays an important role in the fuel savings, as explained in the following sections.

3.1.4 CONTINUOUSLY VARIABLE TRANSMISSION

Since the late 1990s, many new technologies have been introduced in the transmission field, and these make it difficult to anticipate the future market. The automated manual transmission (AMT) has been considered as an alternative for the conventional AT due to its good transfer efficiency. However, it has only been adopted for compact cars because of the poor shift feeling and the dynamic performance. Dual clutch transmission was introduced [129] to overcome the torque interruption during the

shifting of the AMT, but it is not still popular. In the AT market, ZF introduced the world's first rear wheel drive (RWD) 6-speed AT [130]. The ratio span is 6.0, which is much wider than those of 4 or 5-speed ATs, and good ratio steps are delivered. It licenses Lepelletier's concept[131] that uses only the 5 friction elements, and it is 12 % lighter than the 5-speed. The first model 6HP26 is able to deliver 440 Nm, 230kW and is installed in the BMW 7 series. Using the same architecture, 6 and 7-speed ATs for the front wheel drive (FWD) as well as the RWD have been introduced in the market recently [132-134].

Theoretically, the CVT is the ideal transmission for the ICE. It makes the engine run at the optimal operating conditions, but the application has been limited in small engines because of the low torque capacity and the relatively poor transfer efficiency [135]. Wagner [136] forecasts that 5 or 6-speed MT and AT will occupy the majority and the CVT will be able to share only the longitudinal and transverse driveline market under 360Nm input capacity. Kluger and Long [137] suggest the best achievable overall efficiencies for MT and AT are 96.7% and 86.7% respectively, while the CVT is expected to be 88.4% and 91% for the belt and the toroidal type.

The mainstream of the CVT is the metal push belt type. The highest torque capacity of this type reaches 350Nm [138], but it is not sufficient to cover the large gasoline or the diesel engines. To overcome the limited torque capacity and poor efficiency, power split mechanisms have been studied for a long time. Fussner and Singh study the single stage [139] and the dual stage [140] input coupled power split transmission and conclude that the single stage cannot be better for the wide ratio span or the high power application than the dual stage in spite of the simple structure and clutchless mode change.

Another option is the toroidal CVT. Nissan is the only manufacturer of the toroidal CVT equipped vehicles, which use a 3.0 litre engine[141]. This CVT adopts the torque converter as a starting device and the dual cavity half toroidal traction drive system. The torque capacity is 390 Nm and it shows quick response and stability for the driveability requirement [142]. NSK developed and supplies the toroidal unit of the CVT [143]. In their comparative study [144], it is said that the efficiency of the half toroidal is basically better than that of the full toroidal because there is no spin effect. NSK is also developing the power split system [145] and the three roller design for the high power

application [146]. The additional advantage of the power split mechanism is the geared neutral function. Vahabzadeh et al. [147, 148] investigate the mechanism of the power split geared neutral transmission and develop a detailed simulation model and the control strategy. It offers good fuel economy, large torque multiplication for the vehicle launching, and elimination of the starting device. Torotrak is developing an infinitely variable transmission (IVT), which is the power split geared neutral, full toroidal CVT, from the FWD application [149] to the new design for a RWD large SUV [150]. It has a good potential for the medium to large power range engines with the wider ratio spread than the conventional CVTs. Additionally, the geared neutral function can omit the torque converter, which is the most inefficient part of the conventional ATs or CVTs.

The IVT illustrated in Figure 3-5 is used in this research because of the good fuel economy potential and high capacity. The CVT generally suffers from the drivability issue because it tends to operate the engine near to the full throttle line where the efficiency is good. As a result, the torque margin is smaller than the stepped gearbox, so the engine speed should be increased when the vehicle requires more power. Increasing the speed takes longer than increasing the torque because the engine has to accelerate the rotating inertia including the flywheel or the torque converter. If the CVT is combined with the SIDI engine, it is possible to operate the engine in relatively low torque and overcome this drawback.

The detailed dynamics of the IVT are quite complex due to the torque transfer mechanism of the full toroidal variator [151, 152]. An additional difficulty in modelling the IVT is the control of the variator. In the case of the belt type CVT, the ratio of the hydraulic pressure on the two pulleys determines the speed ratio, but the pressure on the pistons of the rollers in the toroidal variator produces the torque in the input and the output side. Consequently, the speed ratio is not controlled directly by the pressure and the time-consuming iterative calculation is needed to match the torques on both sides to obtain the desired speed ratio [153]. To avoid the complexities and accelerate the simulation speed, it is modelled as three parts, the input loss that represents all internal losses, an ideal lossless CVT and a disconnecting clutch on the output side.

The loss torque of the IVT mainly depends on the torque and the transmission ratio, but the influence of the speed is relatively small. To describe this characteristic simply, the

map of the loss torque including the pump driving torque is generated as a function of the output torque and the transmission ratio. The loss torque tends to be proportional to the output torque normalised by the maximum value at a given speed ratio. To increase the accuracy of the loss torque model, the grid of the loss torque map is based on the ratio and the normalised output torque calculated as the following equations.

$$T_{TXin,loss} = f\left(R_{TX}, \overline{T}_{TXout}\right) \tag{3-1}$$

$$\overline{T}_{TXout} \equiv \frac{T_{TXout}}{T_{TXout,\max}} \tag{3-2}$$

The torque loss and the maximum output torque are calculated from IVT System Design Tool, which is the in-house software provided by Torotrak. The result is illustrated in Figure 3-6. Only the forward ratio from the neutral to the maximum overdrive is considered. Due to the two regime configuration, there is a discontinuous point at the synchronising ratio where the regime changes. As for the belt CVTs, the loss increases when the ratio is towards extreme values and the torque is higher. The variator capacity and the pump pressure limit the maximum output torque of the IVT, but it is the function of the speed ratio only when the hardware design is fixed.

3.2 SIMULATION MODEL

The vehicle modelling techniques used in the fuel economy study can be divided into two categories according to the direction of the power flow calculation. One is backward, which calculates the required power from the wheel to the engine, and the other is forward, which calculates the power from the engine to the wheel. ADVISOR [154] and PSAT [155] are widely used public domain simulation software using backward and forward facing respectively. The main difference is that the forward simulation model requires a driver model and there is an error in the vehicle speed between the reference cycle and the real simulation result. For the fuel economy study, the backward simulation can provide faster and more accurate result.

A quasi-static backward simulation model is developed. The detailed dynamics of the sensors and the actuators is eliminated, and the vehicle mass and the large rotating inertia are considered. From the vehicle dynamics point of view, only the longitudinal motion is considered because the effect of the other dimensions is not significant for the

fuel economy study. In addition, the rolling resistance is assumed as a constant, since the higher order terms do not have a significant effect at the low vehicle speed. Then, the required wheel torque and speed can be calculated from the given vehicle speed and the road gradient as follows:

$$\omega_{WHL} = \frac{v_{VEH}}{r_{WHL}} \tag{3-3}$$

$$F_{AERO} = \frac{1}{2} C_d \rho_{air} A_d v_{VEH}^2 \tag{3-4}$$

$$F_{ROLL} = M_{VEH} g f_{roll} \tag{3-5}$$

$$F_{GRAD} = M_{VEH} g \sin\theta_{grad} \tag{3-6}$$

$$\frac{T_{WHL} - 4J_{WHL}\dot{\omega}_{WHL}}{r_{WHL}} = F_{AERO} + F_{ROLL} + F_{GRAD} + M_{VEH}\dot{v}_{VEH} \tag{3-7}$$

From the wheel torque and the brake torque, the transmission output torque can be calculated with the fixed ratio and efficiency of the final drive.

$$\omega_{TXout} R_{FD} = \omega_{WHL} \tag{3-8}$$

$$\frac{T_{TXout}}{R_{FD}} \eta_{FD} - T_{BRK} = T_{WHL} \tag{3-9}$$

The rotating inertia of the transmission is lumped at the input and the output. It is assumed that the output disconnecting clutch is positioned between the output of the ideal CVT and the output inertia. The equivalent loss torque at the transmission input reflects all the internal losses.

$$\omega_{TXin} R_{TX} = \omega_{TXout} \tag{3-10}$$

$$T_{TXclu} - J_{TXout}\dot{\omega}_{TXout} = T_{TXout} \tag{3-11}$$

$$\frac{T_{TXin} - J_{TXin}\dot{\omega}_{TXin} - T_{TXin,loss}}{R_{TX}} = T_{TXclu} \tag{3-12}$$

Finally, the engine speed and torque can be expressed as the follows. It is assumed that the engine accessories consume constant power during the operation.

$$\omega_{ENG} = \omega_{TXin} \tag{3-13}$$

$$T_{ENG} - \left(J_{ENG} + J_{FW}\right)\dot{\omega}_{ENG} - \frac{P_{ACCmech}}{\omega_{ENG}} = T_{TXin} \tag{3-14}$$

All the parameters are summarised in Table 3-4. Most of the vehicle parameters are set as the average values of the seven reference SUVs. The inertia of the CVT and the flywheel is simply scaled from the IVT developed for the large SUV, and the final drive ratio is carried over from the IVT, which applied to a midsize passenger car. The general value of the engine rotating inertia is 0.05kgm^2/L, in consequence, 0.16 kgm^2 is used for this 3.2L engine.

3.3 CONTROL STRATEGY

3.3.1 OPERATING MODE

The control strategy should vary according to the required vehicle status. In this research, three different control modes, the idling, the braking, and the propelling, are defined by the vehicle speed and the wheel torque.

When the required vehicle speed is zero, then the mode is idling. In this case, the engine runs at 800rpm, which is usually expected in common gasoline engines. The CVT ratio becomes zero, and the output clutch is disengaged. Therefore, the engine spends the fuel to maintain the idle speed. The required torque is to drive the mechanical accessory and balance the CVT loss.

If the vehicle speed is non-zero and the required wheel torque is positive, the mode is propelling. In the propelling mode, the transmission clutch is engaged and the ratio is controlled in the optimal sense, which will be explained in the next subsection. The required engine torque is obviously calculated from the wheel torque and the speed.

The mode becomes braking if the required wheel torque is negative. Entering to the braking mode, the transmission ratio is fixed at the previous state. If the vehicle speed is reduced to the point that makes the engine speed below the idle speed, the ratio is decreased to maintain the engine idle. In the braking mode, the maximum engine brake torque at the wheel is calculated and compared with the required wheel torque. If the required braking torque is larger than the engine friction torque at the wheel, then the

mechanical brake is activated. The CVT output clutch is disengaged when the required ratio is under a certain level, at which the required input torque is positive even though the output is negative. This characteristic of the IVT is caused by the singularity of the power split structure and it is useful for cruising downhill at a very low speed but not appropriate for improving fuel economy. If the clutch is disengaged, the engine status is the same as the idle, and the required wheel torque is covered by the mechanical brake. The threshold ratio of the clutch disengagement is set as 0.3 in the simulation.

3.3.2 TRANSMISSION RATIO CONTROL

For the vehicles equipped with the step transmissions, the engine speed is directly related to the vehicle speed. As a result, there is no control parameter in the backward-facing simulation. The gear selection schedule is generally related to the vehicle speed and the accelerator pedal position. On the other hand, the CVT provides a degree of freedom to isolate the engine speed from the vehicle speed. This is the reason why the CVT potentially operates the engine more efficiently and the controller is more complex.

Most of the CVT control algorithms proposed in many previous studies are based on the ideal operating line (IOL), which is a set of the most efficient points on the iso-power lines from the viewpoint of the engine output [156-158]. It is effective and easy to get from the efficiency map, but not always a true optimal. For example, under the low vehicle speed and the high power requirement, the IOL requires a very low transmission ratio to meet the speed relationship between the wheel and the engine. In this case, the transmission efficiency drops sharply, so the overall efficiency from the engine to the wheel drops. To be precise, the important factor of the speed ratio control is not the engine efficiency but the overall powertrain efficiency.

The concept of the ideal operating surface (IOS) is suggested in this study. IOS consists of the points of the speed ratio and the engine torque to minimise the fuel consumption at a given vehicle speed and power demand. The cost function is to minimise the fuel flow rate with the transmission ratio as below,

$$J_{IOS} = \min_{R_{TX}} \dot{m}_f \left(T_{ENG}, \omega_{ENG} \right) \tag{3-15}$$

$$\omega_{ENG} = \frac{v_{VEH}}{r_{WHL} R_{TX} R_{FD}} \tag{3-16}$$

$$T_{ENG} = T_{TXout} R_{TX} + T_{TXin,loss}\left(R_{TX}, T_{TXout}\right) + T_{ACC,mech}\left(\omega_{ENG}\right) \quad (3\text{-}17)$$

$$T_{TXout} = \frac{P_{VEH} r_{WHL}}{v_{VEH}} \frac{R_{FD}}{\eta_{FD}} \quad (3\text{-}18)$$

The calculation result of the transmission ratio is shown in Figure 3-7. The black line on the top indicates the maximum available power at the wheel. The trend is clear and sensible. When the vehicle speed at a given power is increased, the ratio is increased and the engine torque is decreased, which means that the overall powertrain efficiency is higher for a low engine speed. There is a large gap in the ratio between 0.8 and 0.9 because the CVT efficiency reaches maximum at the synchronisation ratio between the two regimes.

The tank-to-wheel efficiency can be seen in Figure 3-8, in which the peak value is 26.4%. Recalling 31% of the maximum engine efficiency, the overall efficiency from the engine output to the wheel, including the accessory loss, is about 85%. The important point is that the quite broad high efficiency area is positioned in the mid-power range, and this advantage comes from the combination of the SIDI engine and the CVT. Figure 3-9 illustrates the improvement of the tank-to-wheel efficiency by the IOS against the traditional IOL. Compared with Figure 3-8, the IOS shows the advantage in the efficient CVT ratio 0.8~0.9, and more than a 5% improvement in the low speed and mid to high torque region. It implies that the transmission efficiency is more important than the engine efficiency in this area.

Figure 3-10 and Figure 3-11 show the optimal engine torque and the speed, which are used in the controller. The IOS is derived from the steady state efficiency of the driveline components but the required engine torque includes a dynamic load to accelerate or decelerate the engine and the transmission input side inertia by changing the gear ratio in transient. The dynamic torque is hard to predict in advance in the offline calculation of the IOS. As a result, the engine operating points can be on the IOS only if in the steady state condition.

3.4 FUEL ECONOMY SIMULATION

A quasi-static backward simulation program is developed in Matlab. Matlab provides a convenient programming environment and it has been widely accepted in modelling and control engineering.

3.4.1 SIMULATION TIME STEP

The effect of the simulation time-step on the fuel economy study is not small. Even though the detailed dynamics are omitted in the quasi-static mode, the rotating inertia still affects the operating state. The finer time-step would be expected to produce a more accurate result, but requires more computing power. Therefore, there should be a compromise between the two contradictory aspects.

The simulation error is plotted against the time-step over the four standard driving cycles in Figure 3-12. These cycles are the NEDC, Federal Teat Procedure-75 (FTP-75), Highway Fuel Economy Test (HWFET), and Japanese 10-15, which are officially used in order to measure fuel economy in Europe, US, and Japan. The modern electronic powertrain controllers usually use a few milliseconds as a loop-time. It is assumed that the simulation with a 10msec resolution is accurate enough to predict the fuel consumption. As shown in the figure, the longer time-step resulting a larger error in most of the cycle, usually to the negative, which means underestimation of the fuel consumption. To keep the error amount within 0.5% in all the cases, a 0.2sec time-step is chosen for the simulation.

The histograms of the engine and the CVT operating efficiency in the FTP-75 cycle are drawn in Figure 3-13 and Figure 3-14, to investigate the cause of the error due to the large time-step. It is obvious that the distortion of the operating efficiency is large in the case of the 0.5 and 1.0sec resolution. In the case of the 0.2sec, it is fairly close to the 10msec case. Consequently, for this case, 0.2sec is the largest limit for predicting the fuel consumption accurately.

3.4.2 FUEL ECONOMY

Four standard driving cycles are used in order to demonstrate the fuel economy of the baseline vehicle. Table 3-5 shows the calculation result. The worst case is 9.3km/L in the 10-15 mode, which has the long idling time and low vehicle speed. In the HWFET,

the fuel economy is 13.0km/L, the best value, due to the high power operation and no stop during the cycle. The other two cycles represent the combination of the urban and the extra-urban driving conditions, and the results are very similar to each other. Basically, the simulation result of the baseline vehicle shows much better fuel economy than the reference vehicles which is shown in Table 3-2. Disregarding the fact that the cold start might partly affect the result in the FTP-75 cycle, it can be seen that use of the SIDI engine and the CVT has a good potential for fuel economy improvement.

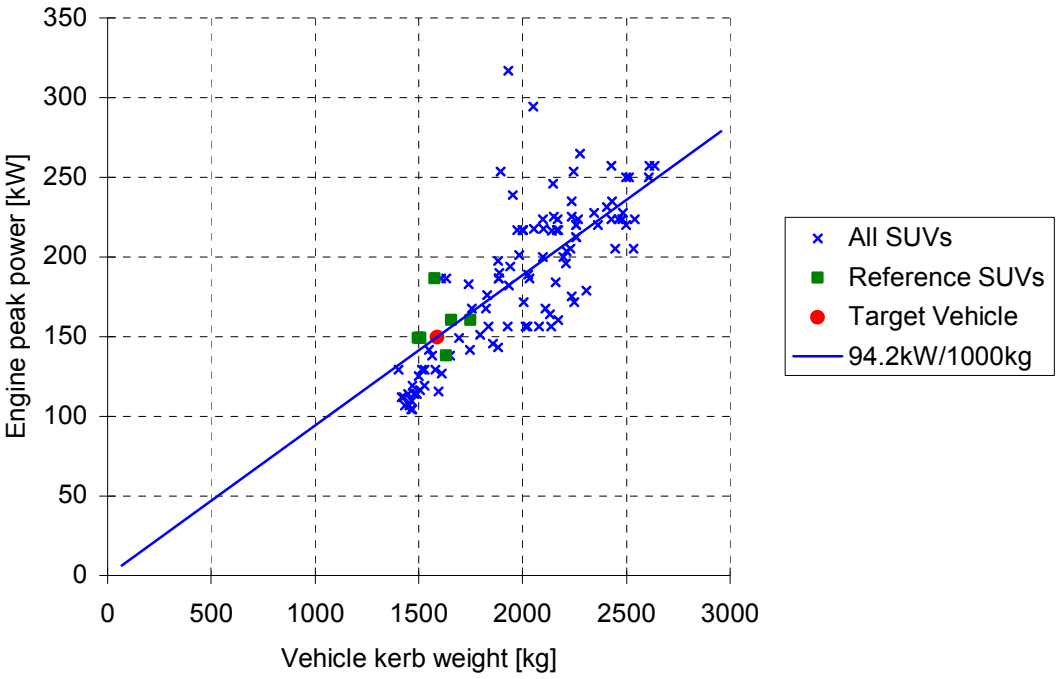

Figure 3-1 Relationship between vehicle kerb weight and engine peak power

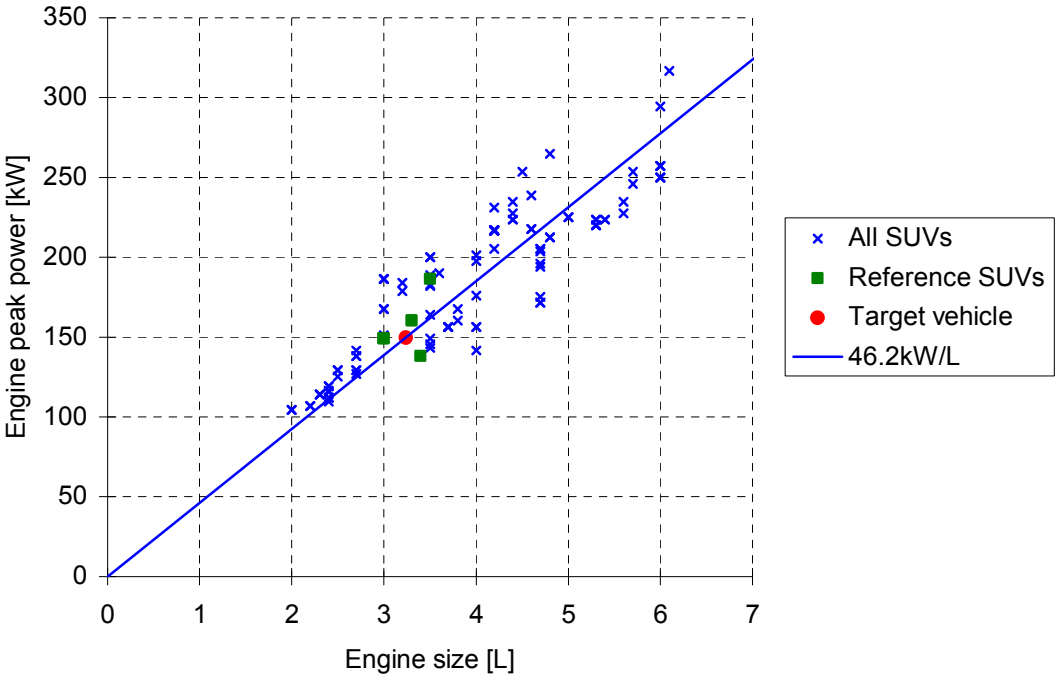

Figure 3-2 Relationship between engine peak power and engine size

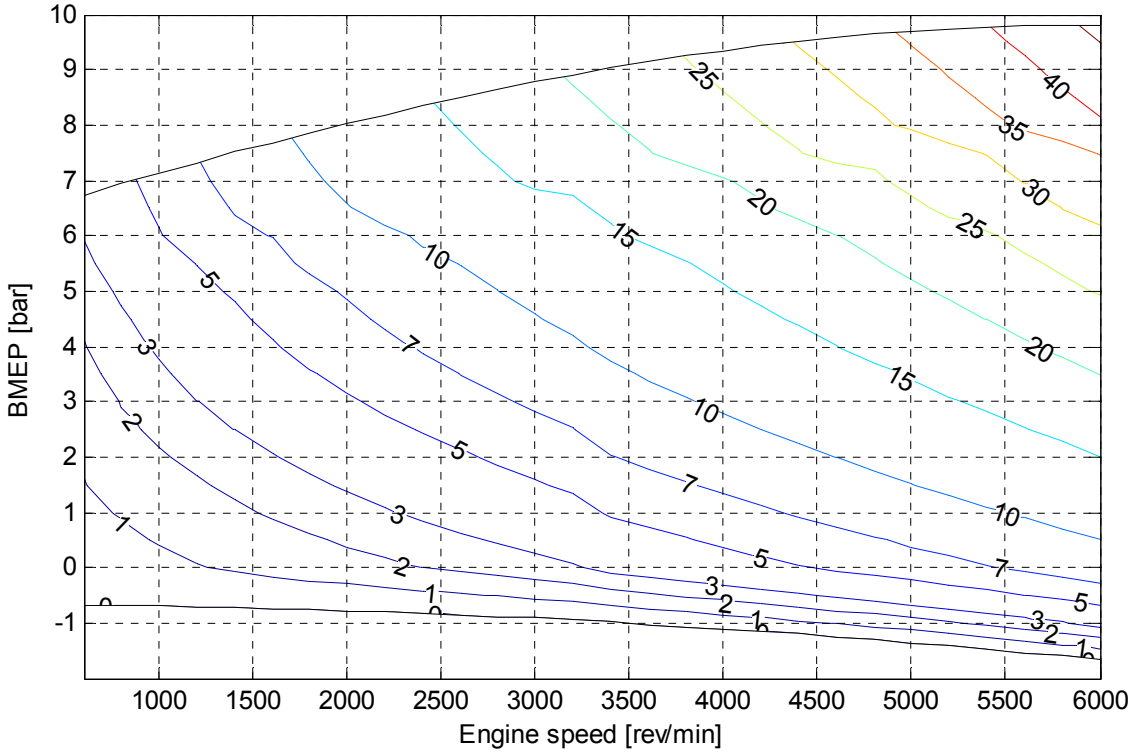

Figure 3-3 Engine mass fuel flow rate [kg/h]

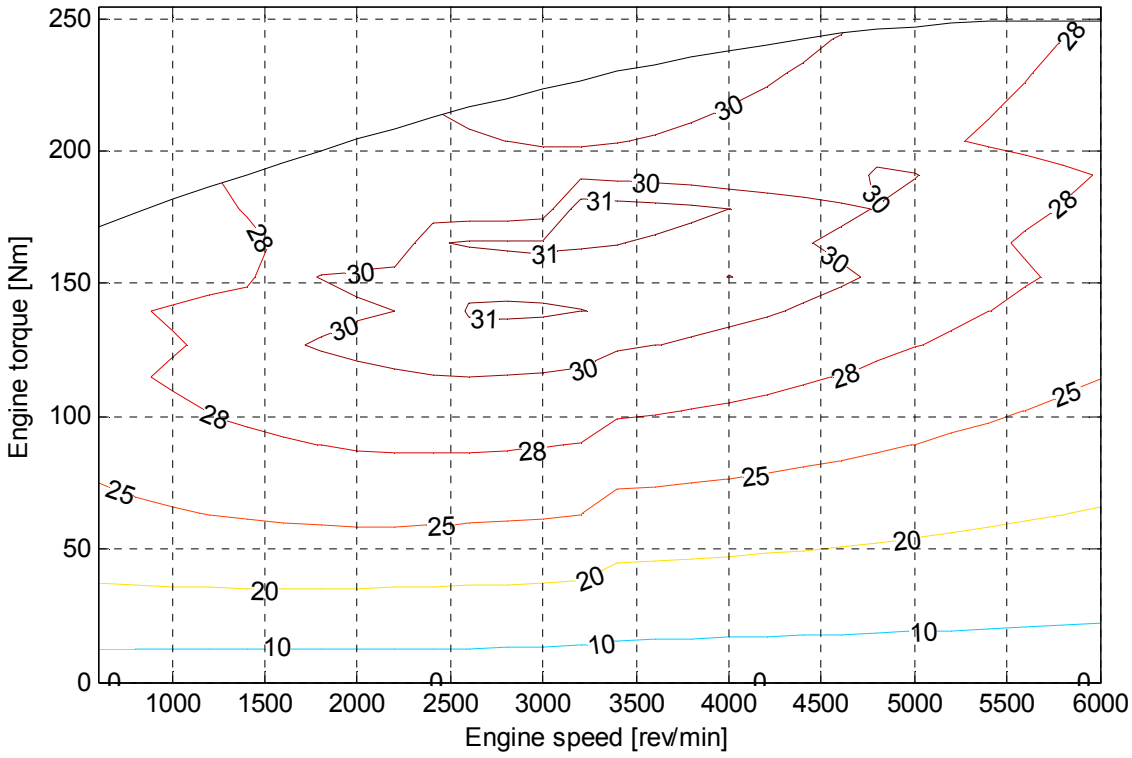

Figure 3-4 Engine efficiency [%]

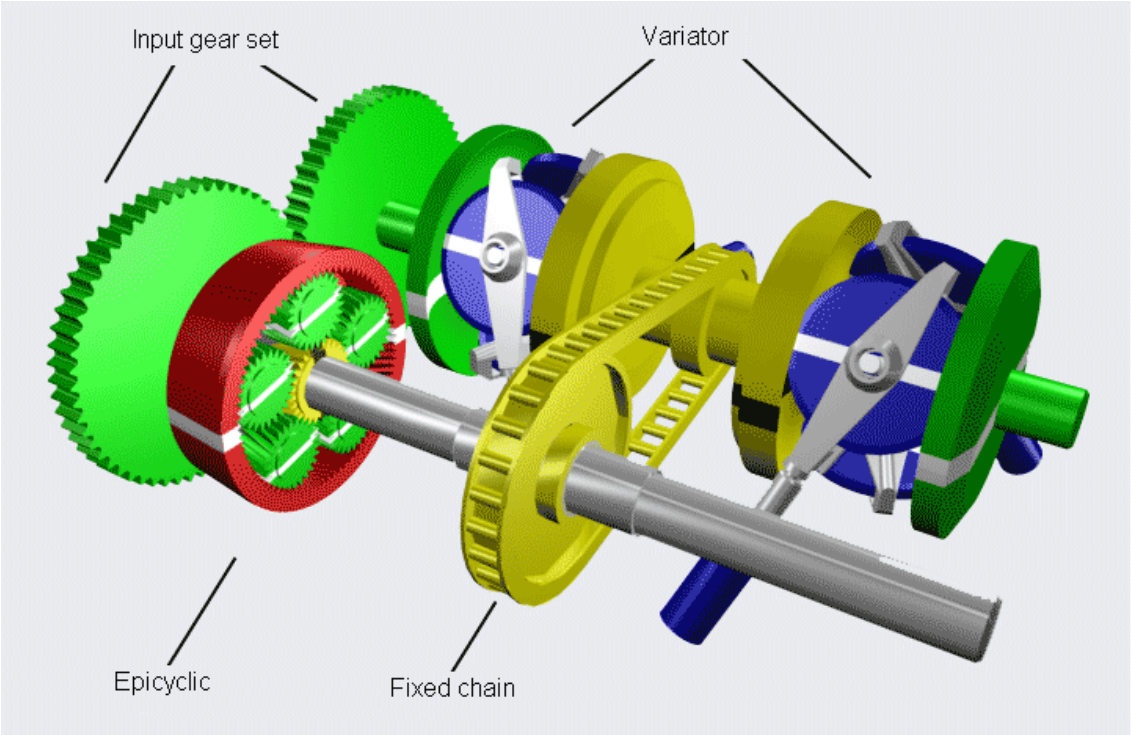

Figure 3-5 IVT schematic [159]

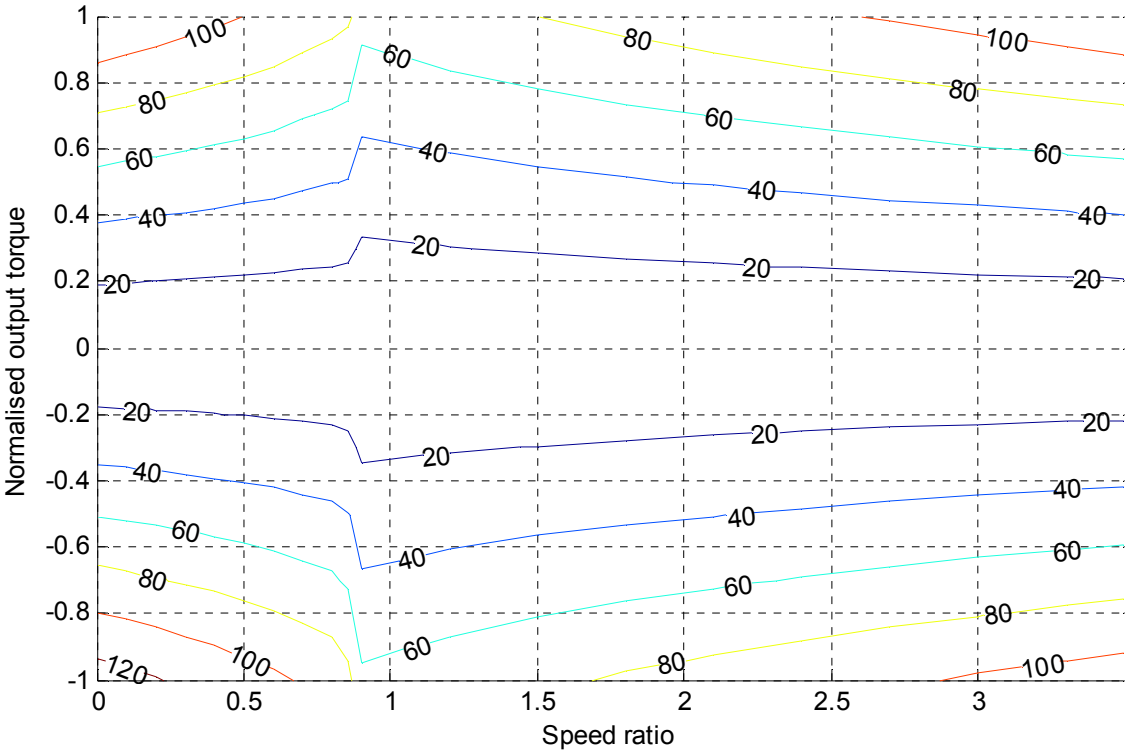

Figure 3-6 Transmission loss torque [Nm]

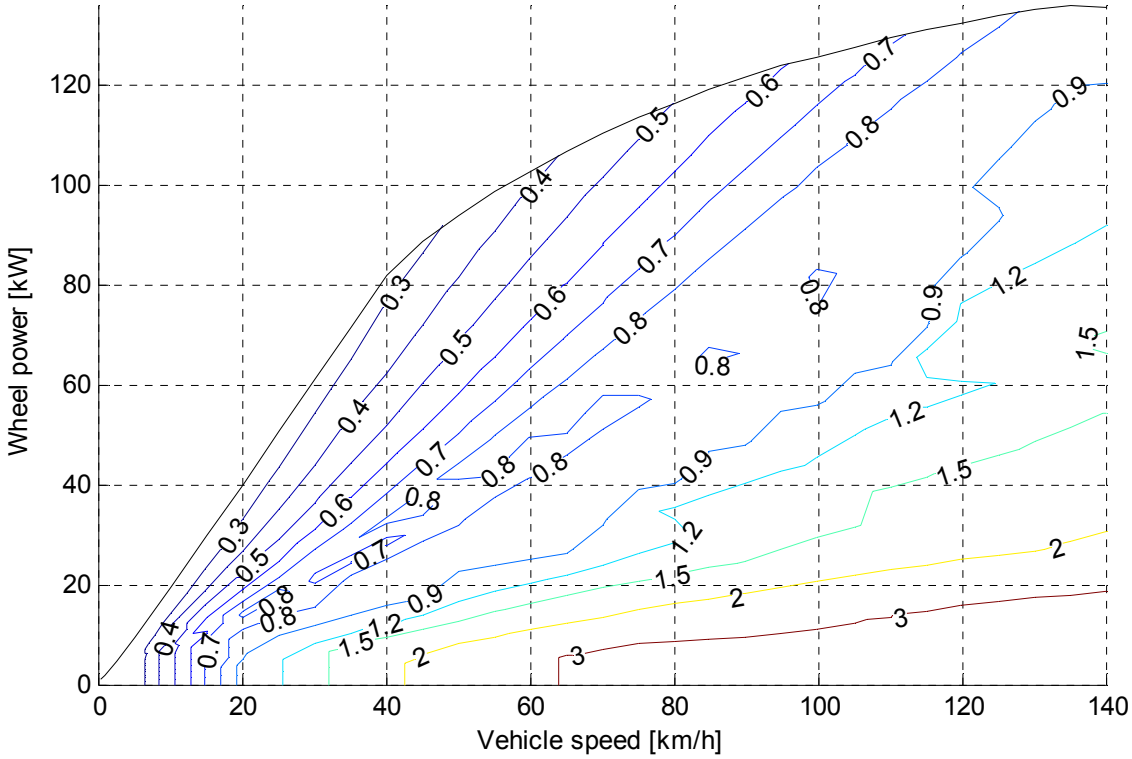

Figure 3-7 Optimal transmission speed ratio

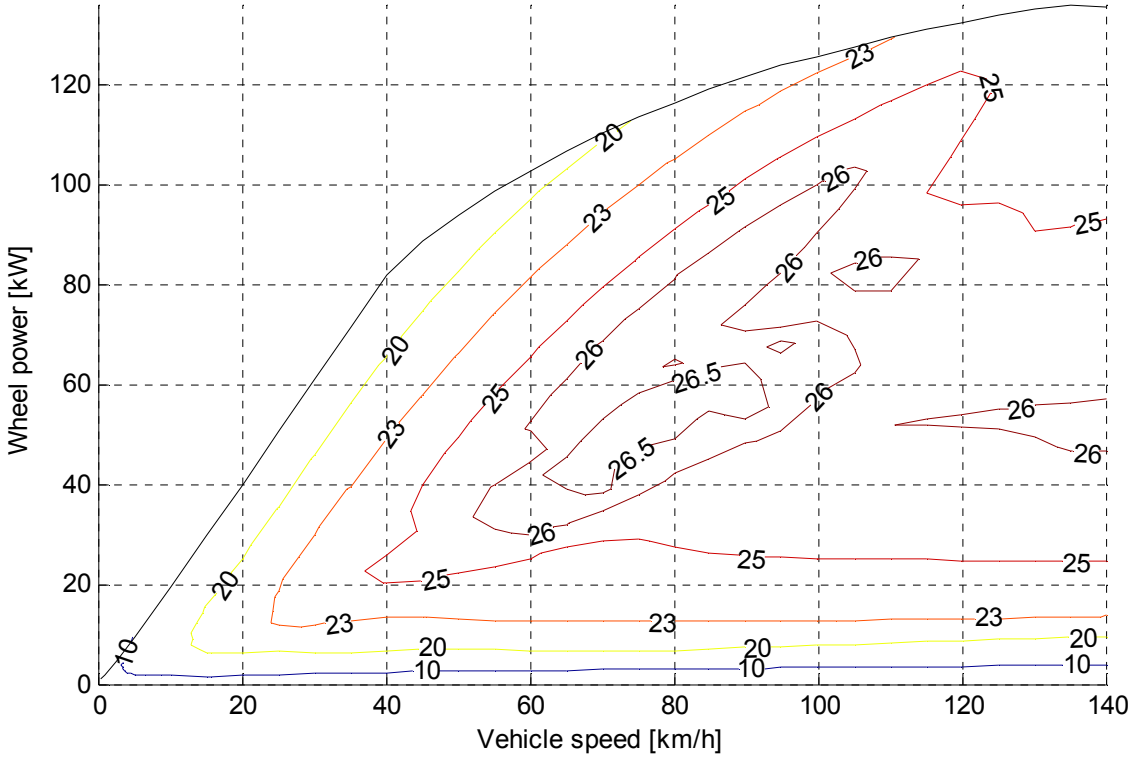

Figure 3-8 Tank-to-wheel efficiency [%]

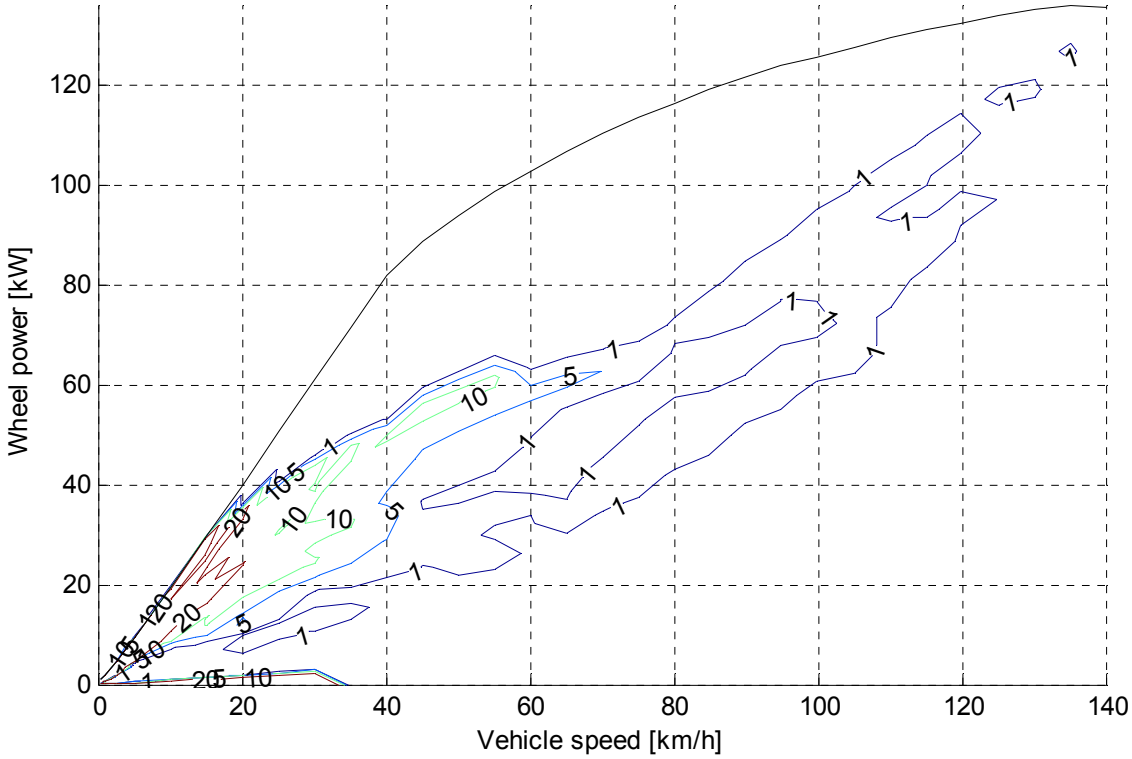

Figure 3-9 Efficiency improvement of IOS vs IOL [%]

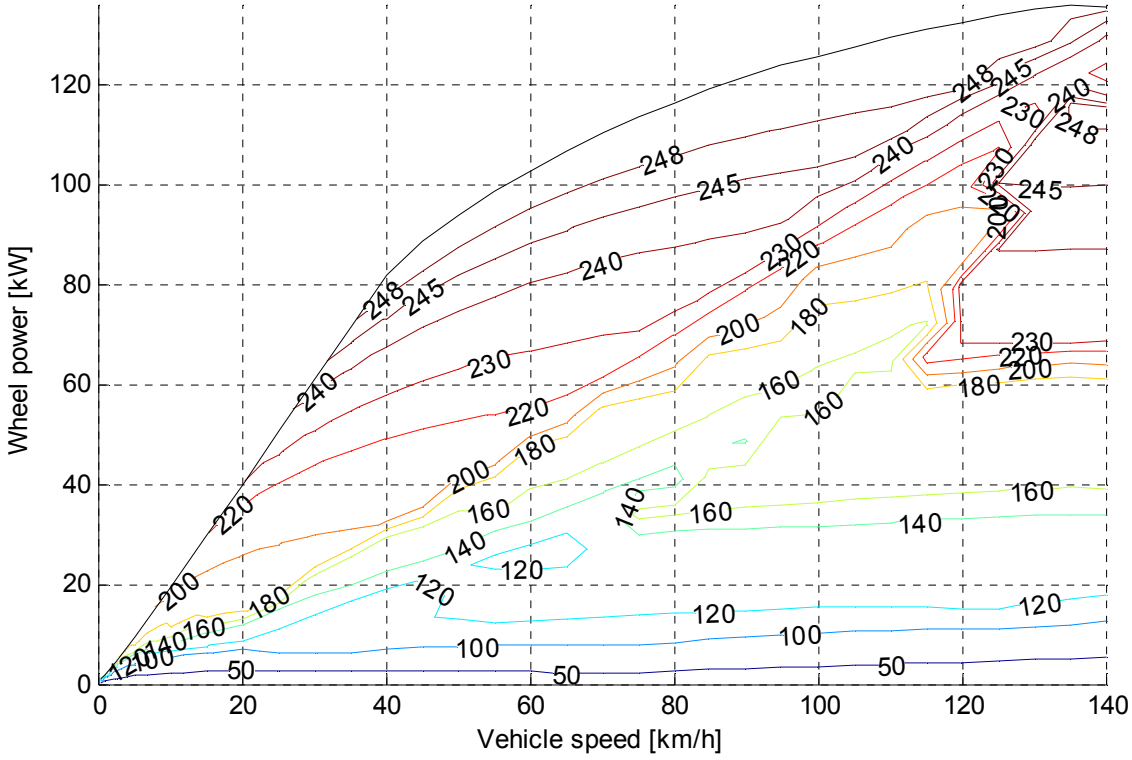

Figure 3-10 Optimal engine torque [Nm]

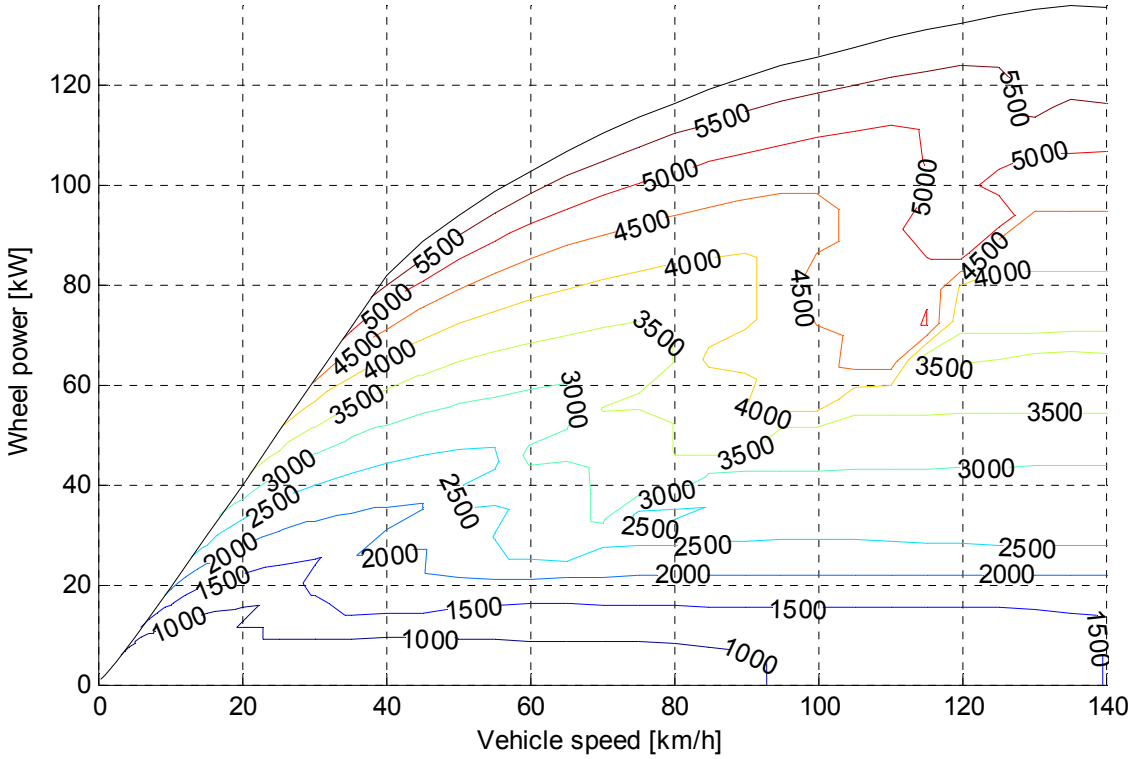

Figure 3-11 Optimal engine speed [rev/min]

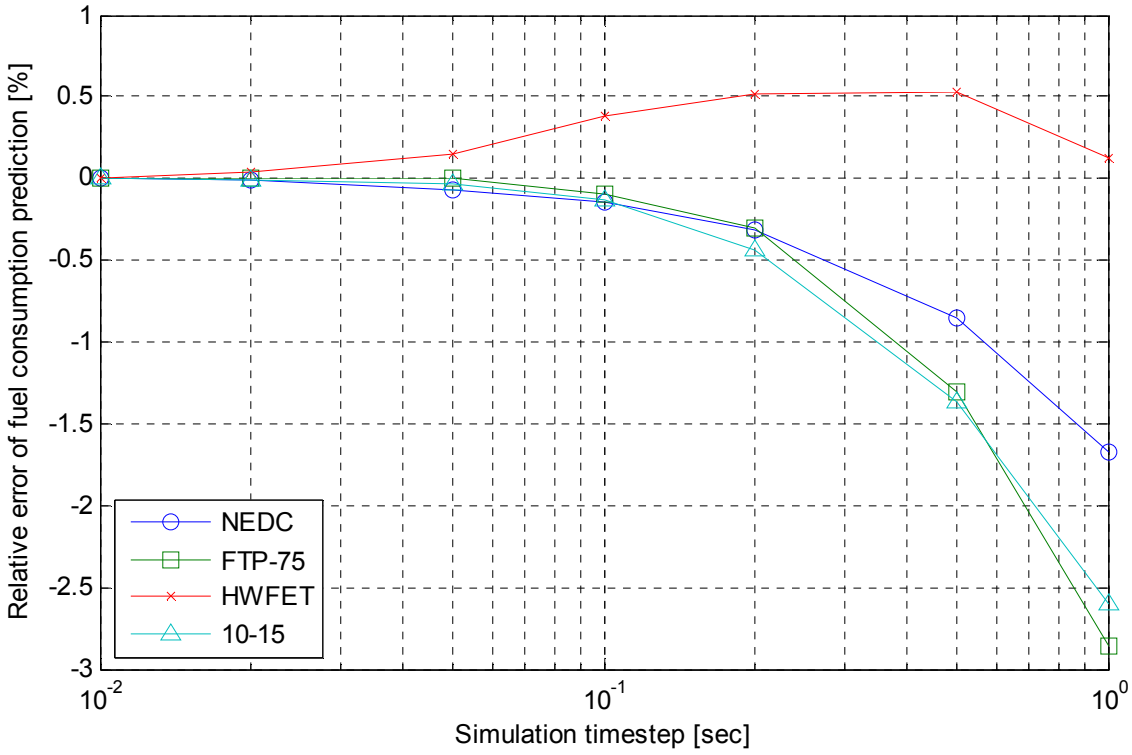

Figure 3-12 Effect of simulation time step on fuel economy prediction

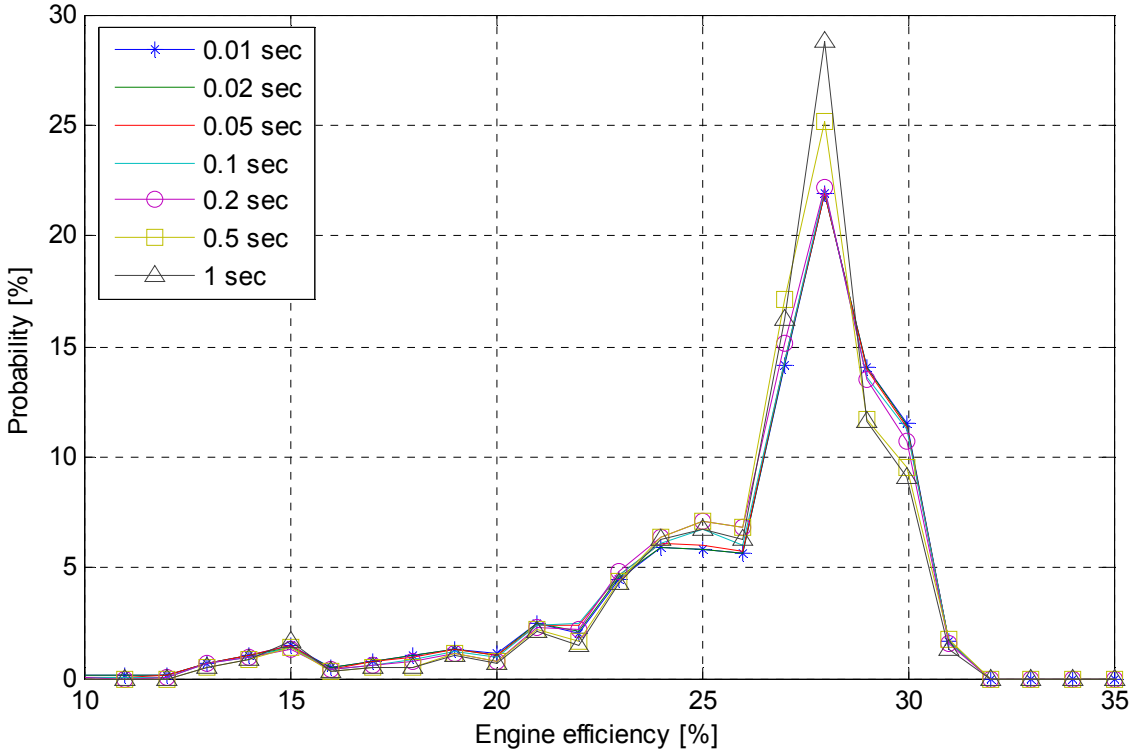

Figure 3-13 Engine operating efficiency in FTP-75 cycle

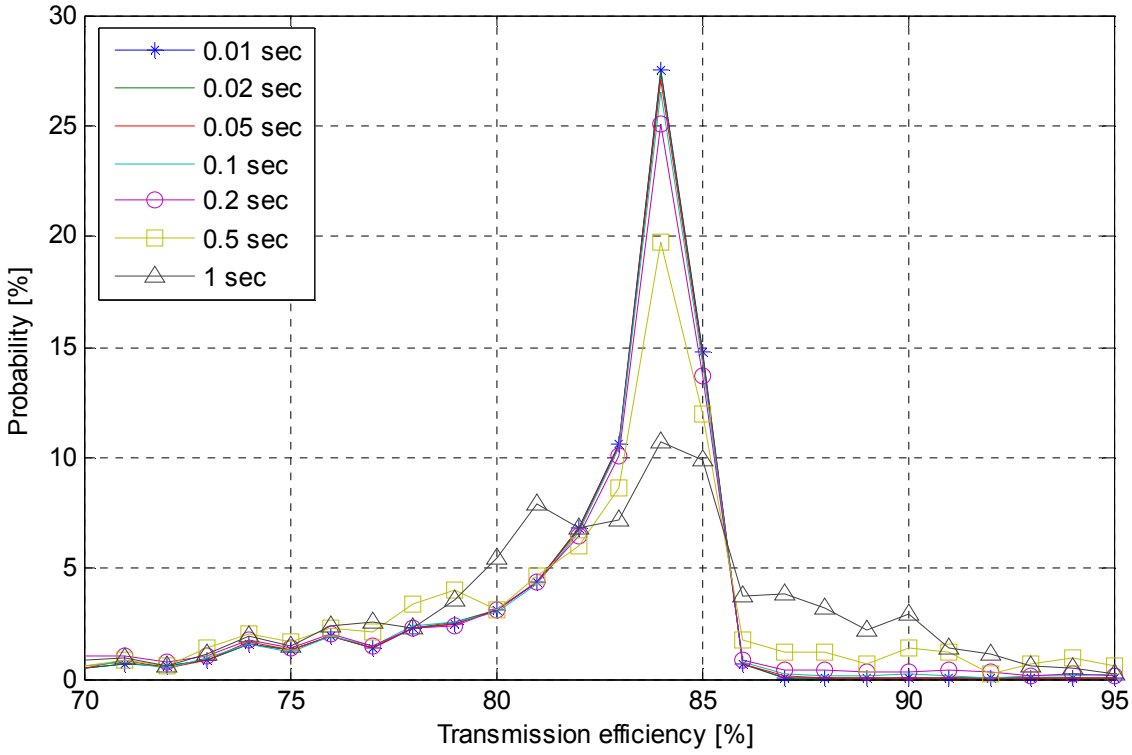

Figure 3-14 Transmission operating efficiency in FTP-75 cycle

Table 3-1 HEVs in North American market [118]

Year	Maker	Model	Vehicle type	Hybrid type
~2005	Chevrolet	Silverado	Pickup Truck	ISA
	Ford	Escape	SUV	Power Split
	GMC	Sierra	Pickup Truck	ISA
	Honda	Accord	Midsize Car	ISA
		Civic	Compact Car	ISA
		Insight	2 Seater	ISA
	Lexus	RX 400h	SUV	Power Split
	Mazda	Tribute	SUV	Power Split
	Mercury	Mariner	SUV	Power Split
	Toyota	Highlander	SUV	Power Split
		Prius	Midsize Car	Power Split
2006	Lexus	GS 450h	Midsize Car	Power Split
	Nissan	Altima	Midsize Car	Power Split
	Saturn	VUE	SUV	ISA (BSA)
	Toyota	Camry	Midsize Car	Power Split
2007	Chevrolet	Equinox	SUV	ISA (BSA)
		Malibu	Midsize Car	ISA (BSA)
		Tahoe	SUV	Power Split (Two mode)
	GMC	Yukon	SUV	Power Split (Two mode)
2008	Chevrolet	Silverado	Pickup Truck	Power Split (Two mode)
	Ford	Fusion	Midsize Car	Power Split
	GMC	Sierra	Pickup Truck	Power Split (Two mode)
	Mercury	Milan	Midsize Car	Power Split

Table 3-2 Specification of reference SUVs [120, 160]

Make	Engine		Fuel economy [km/L]		Weight [kg]		Tire	Drag Area* [m^2]	Drag Coef.
	Size [L]	Power [kW]	City	High way	Kerb	Gross			
Equinox	3.4	138	8.1	10.2	1634	2300	235/65 R16	2.71	NA
Escape	3.0	149	8.5	10.2	1498	2041	235/70 R16	2.68	NA
RX 330	3.3	160	8.1	10.6	1751	2379	225/65 R17	2.63	0.35
Tribute	3.0	149	8.5	10.2	1505	1987	235/70 R16	2.76	0.39
Mariner	3.0	149	8.5	10.2	1510	2041	235/70 R16	2.68	NA
VUE	3.5	186	8.5	11.9	1578	2220	235/65 R16	2.61	0.40
Highlander	3.3	160	8.1	10.6	1656	2431	225/70 R16	2.68	0.34
Average	3.2	156	8.3	10.6	1590	2200	235/70 R16	2.68	0.37

* Estimated from 85% of width x height

Table 3-3 2006 model year SUVs in North American market [120, 160]

Maker	Model	Driveline		Engine		Kerb Weight [kg]
				Size [L]	Power [kW]	
ACURA	MDX	4WD	5AT	3.5	189	2028
BMW	X3	4WD	6MT	3.0	168	1825
	X5	4WD	6MT	3.0	168	2110
			6AT	4.4	235	2235
	X5 4.8IS	4WD	6AT	4.8	265	2275
BUICK	Ranier	2WD	4AT	4.2	217	2004
				5.3	NA	
	Rendezvous	2WD	4AT	3.5	145	1858
				3.6	NA	
CADILLAC	Escalade	2WD	4AT	6.0	257	2428
	Escalade ESV	4WD	4AT	6.0	257	2613
	Escalade EXT	4WD	4AT	6.0	257	2637
	SRX	2WD	5AT	3.6	190	1889
				4.6	239	1951
CHEVROLET	C1500 Tahoe	2WD	4AT	4.8	213	2258
				5.3	220	2258
	Equinox	2WD	5AT	3.4	138	1634
	HHR	2WD	5MT	2.2	107	1431
			4AT	2.4	NA	

	K1500 Suburban	4WD	4AT	5.3	220	2497
				6.0	250	2497
	Trailblazer	2WD	4AT	4.2	217	1976
				5.3	NA	
	Trailblazer	4WD	4AT	6.0	295	2052
	Trailblazer EXT	2WD	4AT	4.2	217	2164
				5.3	NA	
CHRYSLER	Pacifica	2WD	4AT	3.5	186	2033
				3.8	NA	
	PT Cruiser	2WD	5MT	2.4	112	1427
	PT Cruiser Convertible	2WD	5MT	2.4	112	1416
DODGE	Durango	2WD	4AT	3.7	157	2138
			5AT	4.7	172	2248
				5.7	NA	
	Magnum	2WD	4AT	2.7	142	1745
		4WD	5AT	3.5	186	1886
		2WD	5AT	5.7	254	1896
				6.1	317	1932
FORD	Escape	2WD	5MT	2.3	114	1479
			4AT	3.0	149	1498
	Expedition	2WD	4AT	5.4	224	2428
	Explorer	2WD	5AT	4.0	157	2014
			6AT	4.6	218	2055
	Freestyle	2WD	CVT	3.0	151	1796
GMC	C1500 Yukon	2WD	4AT	4.8	213	2258
				5.3	220	2258
	Envoy	2WD	4AT	4.2	217	1998
				5.3	224	2098
	Envoy XL	2WD	4AT	4.2	217	2170
				5.3	224	2268
	Envoy XUV	2WD	4AT	4.2	(205)	(2230)
	K1500 Yukon	4WD	4AT	5.3	220	2363
				6.0	250	2512
	K1500 Yukon XL	4WD	4AT	6.0	250	2610
HONDA	CR-V	2WD	5AT	2.4	116	1505
	Element	2WD	5MT	2.4	(119)	(1529)

	Pilot	2WD	5AT	3.5	182	1934
HUMMER	H3	4WD	5MT	3.5	164	2132
HYUNDAI	SantaFe	2WD	4AT	2.4	NA	
				2.7	127	1610
			5AT	3.5	149	1695
	Tucson	2WD	5MT	2.0	104	1470
			4AT	2.7	129	1529
INFINITI	QX56	2WD	5AT	5.6	235	2431
ISUZU	Ascender 5-Passenger	2WD	4AT	4.2	217	2004
	Ascender 7-Passenger	2WD	4AT	4.2	217	2165
				5.3	NA	
JEEP	Commander	2WD	5AT	3.7	157	2078
				4.7	175	2236
				5.7	NA	
	Grand Cherokee	2WD	5AT	3.7	157	1930
				4.7	172	2005
		4WD	5AT	5.7	246	2148
	Liberty/Cherokee	2WD	6MT	3.7	157	1834
	Wrangler/TJ	4WD	6MT	2.4	110	1466
				4.0	142	1550
KIA	Sorento	2WD	5MT	3.5	143	1882
	Sportage	2WD	5MT	2.0	104	1463
			4AT	2.7	129	1517
LAND ROVER	LR3	4WD	6AT	4.0	NA	
				4.4	(224)	(2461)
	Range Rover	4WD	6AT	4.4	227	2483
	Range Rover Sport	4WD	6AT	4.4	224	2480
LEXUS	GX470	4WD	5AT	4.7	196	2209
	LX 470	4WD	5AT	4.7	205	2536
	RX 330	2WD	5AT	3.3	160	1751
LINCOLN	Navigator	2WD	6AT	5.4	224	2541
MAZDA	Tribute	2WD	5MT	2.3	114	1448
			4AT	3.0	149	1505
MERCEDES	ML350	4WD	7AT	3.5	200	2097
	ML500	4WD	7AT	5.0	225	2151
	R350	4WD	7AT	3.5	200	2196

	R500	4WD	7AT	5.0	225	2236
MERCURY	Mariner	2WD	4AT	2.3	114	1490
				3.0	149	1510
	Mountaineer	2WD	5AT	4.0	157	2023
			6AT	4.6	218	2101
MITSUBISHI	Endeavor	2WD	4AT	3.8	168	1755
	Montero	4WD	5AT	3.8	160	2171
	Outlander	2WD	5MT	2.4	119	1470
NISSAN	Armada	2WD	5AT	5.6	227	2344
	Murano	2WD	CVT	3.5	(183)	(1740)
	Pathfinder	2WD	5AT	4.0	201	1984
	Xterra	2WD	6MT	4.0	198	1882
PONTIAC	Torrent	2WD	5AT	3.4	138	1634
PORSCHE	Cayenne	4WD	5AT	3.2	184	2160
	Cayenne S	4WD	5AT	4.5	254	2245
SAAB	9-7X	4WD	4AT	4.2	216	2141
				5.3	224	2169
SATURN	VUE	2WD	5MT	2.2	107	1455
			5AT	3.5	186	1578
SUBARU	B9 Tribeca	4WD	5AT	3.0	186	1885
	Baja	4WD	5MT	2.5	129	1581
	Forester	4WD	5MT	2.5	129	1402
	Outback	4WD	5AT	3.0	186	1608
	Outback Wagon	4WD	5MT	2.5	125	1501
			5AT	3.0	186	1633
SUZUKI	Grand Vitara	2WD	5MT	2.7	138	1566
	Grand Vitara XL7	2WD	5AT	2.7	138	1650
TOYOTA	4Runner	2WD	5AT	4.0	176	1830
				4.7	194	1941
	Highlander	2WD	4AT	2.4	116	1597
			5AT	3.3	160	1656
	Land Cruiser Wagon	4WD	5AT	4.7	205	2445
	Sequoia	2WD	5AT	4.7	204	2211
VOLKSWAGEN	Touareg	4WD	6AT	3.2	179	2307
				4.2	231	2404
VOLVO	XC 90	4WD	6AT	4.4	232	2189

Table 3-4 Simulation parameters

Parameter	Unit	Value	Parameter	Unit	Value
A_d	[m^2]	2.68	J_{WHL}	[kg m^2]	0.50
C_d	-	0.37	M_{VEH}	[kg]	2200
f_{roll}	-	0.01	$P_{ACC,ENG}$	[kW]	1.0
J_{ENG}	[kg m^2]	0.16	R_{FD}	-	0.1923
J_{FW}	[kg m^2]	0.10	r_{WHL}	[m]	0.3677
J_{TXin}	[kg m^2]	0.20	η_{FD}	-	0.98
J_{TXout}	[kg m^2]	0.10			

Table 3-5 Fuel economy

Driving cycle	NEDC	FTP-75	HWFET	10-15
Fuel economy [km/L]	10.2	10.3	13.0	9.3

4 HYBRID VEHICLE

4.1 HYBRIDISATION

As illustrated in Table 3-1, there are two main paths of hybridisation, which are the mild hybrid with the ISA and the power split full hybrid. The power split hybrid can achieve better fuel economy by combining two large EMs, but it requires a greater engineering effort to hybridise the conventional vehicle and the larger battery capacity. In the mild hybrid, the ISA is connected to the engine crankshaft, and is used as a motor to assist the engine or as a generator to charge the battery. As a result, there are many complex compromises in the interactions between design and control methods, and the fuel saving potential is lower than the power split hybrid. However, the HEV has to compete with conventional vehicles not only in fuel economy but also in production cost. Furthermore, even though the Toyota Prius and Honda Insight succeeded in being launched on the market, these are purpose-built HEVs. They demonstrate remarkable fuel economy but it is not easy to cover the increasing cost from the manufacturers' point of view. Clearly, a less expensive hybrid system is more likely to appeal to a great number of mainstream customers, and this is one of the most notable advantages of the mild hybrid sharing the conventional vehicle platform. Considering the complexities and the additional cost, the mild hybrid is a good compromising solution available at this point. In this research, the mild hybrid is chosen to demonstrate the impact of the control strategy on fuel economy.

Besides the common functions and benefits of hybridisation, the ISA needs the additional space and layout change in conventional vehicles because it fits into the space normally taken up by the flywheel and starter motor in the transmission bell housing [161]. The additional loading on the shaft between the engine and the transmission by the high speed rotating part, the thermal effect to the EM by the engine, and the slim design fitted into a given space are the main technical difficulties of the ISA. For the first two problems, much effort has been made on the design optimisation of the crankshaft and bell housing through computer-aided engineering analysis [162, 163]. The axial flux permanent magnetic machine can be considered as a candidate to solve the last obstacle [164].

4.1.1 ELECTRIC MACHINE AND BATTERY

The performance of the EM can be represented with the maximum torque, power, and speed. Even though the required power is given, the torque and the speed limit and the rotating inertia of the EM depend on the applied technology and the dimensions. In this study, the parameters of the EM used in the Honda Accord hybrid are adopted with an appropriate scaling factor. According to Kabasawa [165], its maximum power is 12 kW for motoring and 14kW for generating, and the maximum torque is ±136 Nm. The rotating inertia of the rotor is assumed as 0.072 kg-m^2, which is the estimation from the diameter, the width and the average mass density of the rotor [166] as 240mm, 40mm, and 5500 kg/m^2 respectively.

The efficiency of the ISA gives more difficulties because there is no experimental data except for that of the Insight in ADVISOR. However, Honda's research shows the improvement of the efficiency from the Insight to the Civic [43] and the comparison between the Civic and the Accord [165]. According to these studies, the power loss of the ISA used in the Accord, including the power electronics, is around 30% less than that of the Insight. Figure 4-1 depicts the resulting efficiency map taking into consideration of the improvements. In the most commonly used region, the efficiency is over 90% and it is quite well matched with the efficiency map of the Accord.

The battery model is also carried over from the Insight. Like in the ISA, the battery has been significantly improved from the Insight to the Accord. The main improvement is the reduction of the internal resistance by the modification of the current collector [167]. Taking account of this, the internal resistance of the battery is set with 30% reduced value from the data of the Insight in ADVISOR. The open circuit voltage (OCV) and the internal resistance are shown in Figure 4-2. It is efficient to operate the battery at high voltage and low resistance. Therefore, the 50~70% of the SOC is the good area for normal operation.

4.1.2 MODIFIED SIMULATION MODEL

In the case of the hybrid, the total vehicle mass is increased and there are 2 power sources to produce the torque required at the transmission input. Therefore, the Equations (3-7), (3-13) and (3-14) are replaced with the following.

$$\frac{T_{WHL} - 4J_{WHL}\dot{\omega}_{WHL}}{r_{WHL}} = F_{AERO} + F_{ROLL} + F_{GRAD} + (M_{VEH} + M_{BAT})\dot{v}_{VEH} \quad (4\text{-}1)$$

$$\omega_{ENG} = \omega_{EM} = \omega_{TMin} \quad (4\text{-}2)$$

$$T_{ENG} - J_{ENG}\dot{\omega}_{ENG} + T_{EM} - J_{EM}\dot{\omega}_{EM} = T_{TMin} \quad (4\text{-}3)$$

Only the battery pack weight is added to the baseline vehicle because it is assumed that the weight of the ISA is equivalent to the flywheel, which is removed for the HEV. Additionally, the mechanical accessory load on the engine is substituted by the electric load on the battery as the same amount of power, which means a fully electrified accessory drive. The battery supplies the power to drive the EM and the electric accessories. Using Equations (4-4) ~ (4-6), the battery output current and the SOC are calculated from the total power extracted from the battery. In Equation (4-4), the power loss of the EM includes not only the mechanical loss but also the power electronics loss as a function of the EM speed and the torque. The loss due to the internal resistance of the battery was included, as seen in Equation (4-5).

$$P_{BAT} = T_{EM}\omega_{EM} + P_{EM.loss} + P_{ACC,ELEC} \quad (4\text{-}4)$$

$$P_{BAT} = V_{BATOc}i_{BAT} - R_{BAT\,\mathrm{int}}i_{BAT}^2 \quad (4\text{-}5)$$

$$SOC = \frac{1}{C_{BAT}}\int i_{BAT}\,dt \quad (4\text{-}6)$$

4.1.3 ELECTRIC MACHINE SIZE

A systematic way of EM sizing is suggested by Barnard and Jefferson[168] but it is hard to generalise for the variety of the HEVs. Using a mild hybrid SUV, Cho and Vaughan[169] claim that the stop-start and the electrical accessory load driven by the regenerative braking energy occupy the majority of the fuel economy improvement in the mild hybrid. Consequently, the capacity of the regenerative braking is the most important factor in the mild hybrid design.

The recoverable braking energy over a journey can be calculated by simulation with the different EM powers. The speed profiles over the driving cycles are achieved with the CVT control strategy used in the baseline vehicle. The results over the four standard

driving cycles are illustrated in Figure 4-3. The x-axis represents the maximum generating power capacity of the EM. The y-axis indicates the recuperated mechanical energy by the regenerative braking divided by the total available amount of braking energy at the crankshaft. Generally speaking, the larger EM can absorb the more kinetic energy of the vehicle, but raise the space and the weight issues for installing both the EM and the battery. In the 10-15 mode, the only 9kW EM can capture 90% of the total available regenerative braking energy. In the HWFET cycle, it requires 19kW to capture 80% of the kinetic energy. This fairly different figure is caused by the vehicle operating conditions represented by the speed and acceleration pattern. The 10-15 mode has a relatively low speed with mild acceleration but the HWFET represents the high speed and dynamic driving condition. The results of the NEDC and the FTP-75 cycles lie between the two extreme cases. In this study, the appropriate level of absorbing energy is set as 80% in the urban and 70% in the highway driving cycles. To achieve this target, the required power of the EM in the generation mode is 14 kW, which is the same value as the reference EM used in the Honda Accord. The specifications of the EM and the battery are summarised in Table 4-1.

Figure 4-4 depicts the scatter plots of the EM operating points through the driving cycles with the 14kW EM. The generating torque limit is represented as red lines. To capture more energy, the EM torque has to be increased at low speed, but it is not very useful at the high speed because most of the energy is distributed under 14kW.

4.2 CONTROL STRATEGY

To examine the hybridisation effect on the fuel economy, a control strategy should be developed. One of the well-known algorithms for the mild hybrid is the Honda IMA used in the Insight. The advantage of using this strategy is that the very detailed algorithm has been implemented in many pieces of public domain software, which have been based on extensive experimental work. However, the first Insight model uses the mechanical throttle control and the MT, so that the control of the ISA is tied to the driver's pedal input. Another candidate is the control algorithm for the parallel hybrid with CVT in ADVISOR [154]. It is widely used for the back-to-back benchmarking of the new parallel hybrid control strategy. In this chapter, its modified version is developed as a reference controller.

4.2.1 STOP-START

In real driving conditions, vehicles are frequently stopped in the ignition-on state, for example at traffic lights and pedestrian crossings, or in traffic jams. It is wasteful because fuel is consumed without any output at the wheel. However, it is unavoidable because the engine cannot be restarted rapidly and frequently without annoying the driver. To reflect these real situations in fuel economy, most urban driving cycles include frequent vehicle stop conditions. To save the fuel burnt during the engine idle, the HEV stops the engine when the vehicle is fully stopped. To restart the engine from the idle stop, the ISA is switched on when the mode is moved from idling to propelling. There is an electric idle control like the engine idle control to maintain the crankshaft speed at 600rev/min, which is the minimum speed to operate the CVT and the other accessories effectively and ignite the engine smoothly. This stop-start functionality provides a large part of the benefit of the HEV, especially in mild hybrids.

4.2.2 REGENERATIVE BRAKING

Unlike the ICE, the EM is a bidirectional energy converter. It is operated as a generator to produce electrical energy from mechanical energy, as well as a motor to convert the electrical energy to mechanical energy. The vehicle has kinetic energy depending on the mass and speed. When the brake works to reduce the speed, this kinetic energy is dissipated as heat. The HEV can save this energy to the battery by the EM, which is working as a generator. In fact, this is cost free energy and considerably increases the fuel economy of the HEV.

The maximum braking energy at the wheel by the regenerative braking is much higher than in the conventional vehicle because the regenerative braking torque is larger than the engine friction torque. Within this limit, the EM absorbs the kinetic energy of the vehicle. If the required braking torque is over the limit, the controller distributes the braking torque between the EM and the service brake. This study accounts for only the longitudinal motion of the vehicle, and the braking torque distribution between the front and the rear wheel is not considered. This assumption is quite reasonable in the case of the front wheel drive SUV with an active braking force distribution system, because the maximum deceleration in the standard driving cycles is around 0.4g and is achievable from only the front wheels without a problem for stability. According to the

regenerative braking study of a large SUV [170], this value of deceleration is possible by the front wheel with the friction coefficient of 0.4, which is much less than the standard value, 0.8, for typical road conditions.

4.2.3 TORQUE DISTRIBUTION

When the operating mode is idling or braking, the control decision is straightforward. However, in propelling mode, the controller should harmonise the two power sources to produce the torque required at the crankshaft. The main factors to decide the distribution of the torque to the engine and the EM are the engine efficiency and the battery SOC.

The torque distribution algorithm in the parallel hybrid control strategy of ADVISOR is quite simple.

- If the required power at the crankshaft is negative, then the EM absorbs the energy (regenerative braking)
- If the required power at the crankshaft is between 0 and 20% of the maximum engine power, then the vehicle is driven by motor (electric vehicle)
- If the required power at the crankshaft is between 20 and 80% of the maximum engine power, then the engine provides the power to drive the vehicle and charge the battery (charging)
- If the required power at the crankshaft is over 80% of the maximum engine power, then the EM provides the power to assist the engine (assist)

This algorithm is intuitive, but some modifications are needed for this research. Firstly, the electric vehicle mode is not suitable for the mild hybrid. The parallel hybrid control strategy was originally developed for the parallel full hybrid, whose EM power is more than 50% of the engine power. The other point is that the threshold of the mode change is not well matched with the SIDI engine, because the SIDI engine has the best efficiency point at a lower torque area than the typical MPI engine.

The key idea of the modification is to keep engine efficiency within a boundary. As shown in Figure 3-4, the engine efficiency is high in the middle of the engine operating area and decreases at the higher or the lower torque. If a desired level of efficiency is chosen, an upper and a lower limit of the torque can be calculated, which becomes an

assist and a charging torque level respectively. For numerical simplicity, the normalised engine efficiency defined as Equation (4-7) is used in order to decide the torque boundaries.

$$\overline{\eta}_{ENG} = \frac{\eta_{ENG}}{\max(\eta_{ENG})} \tag{4-7}$$

The control actions are modified as follows;

- If the required torque at the crankshaft is less than the engine friction torque, then the EM absorbs the energy (regenerative braking)
- If the required torque at the crankshaft is between the engine friction and the charging torque level, the engine produces the charging level torque to drive the wheel and charge the battery. (charging)
- If the required torque at the crankshaft is between the charging and the assist torque, then the engine drives the wheel (engine only)
- If the required torque at the crankshaft is over the assist torque level, then the EM provides the excessive torque to assist the engine (assist)

4.2.4 CHARGE BALANCE

The balance of the battery SOC is the important feature of the charge sustaining HEVs. The deep charging or discharging affects the battery life and performance. Therefore, the SOC of the battery should be maintained within an appropriate boundary. As shown in Figure 4-2, the minimum internal resistance of the battery is achieved at 50% of the SOC and the OCV is linear between 30 and 80% of the SOC. In this research, the target SOC is set at 60% and the high and low limits for the charge balance control boundary is +/- 10% from the target SOC. Additionally, the hardware limit of the battery is assumed as being between 20 and 80%.

If the assist and the charging torque levels are fixed according to the engine efficiency, the SOC cannot be maintained at an appropriate level over the driving conditions. Therefore, the assist and the charging torque level should be controlled in relation to the SOC. The mode change criteria and the charge balance control strategy are illustrated in Figure 4-5. As shown in the figure, the threshold of the normalised engine efficiency is

the only parameter that can be tuned. The higher threshold value means that the engine only operating area is reduced and the EM works more actively. If the SOC is lower than 50%, the engine is operated up to its most efficient torque to charge the battery as much as possible. In contrast, when the SOC is over 70%, the engine does not charge the battery and is responsible for the portion of the required torque over the most efficient point of the engine.

4.3 FUEL ECONOMY SIMULATION

4.3.1 PARAMETER TUNING

To decide the optimal threshold efficiency, the backward simulation of the HEV is performed for the same driving cycles with 10% steps of the normalised engine efficiency. The fuel economy and the final SOC are shown in Figure 4-6. The initial SOC is set at 60%, so the final SOC has to be as close as possible to 60%.

There is no standard criteria of the allowable charge difference, but one of the recommended guidelines [171] suggests the following equation.

$$\left|\frac{\Delta E_{BAT}}{E_{FUEL}}\right| = \left|\frac{\Delta SOC \times V_{BAT} \times C_{BAT}}{m_f \times Q_{LHV}}\right| \leq 1\% \tag{4-8}$$

This boundary is illustrated as a shadow in Figure 4-6. The allowable band is narrow in the 10-15 mode as it uses a small amount of the fuel. In the case of the FTP-75 and HWFET, the limit is over ±10%.

In all cycles, the trend is obvious; increasing the threshold decreases the fuel economy and increases the final SOC. In the NEDC, the fuel economy drops rapidly over the 60% of the normalised engine efficiency. There is no considerable change in the FTP-75 cycle, and the trend of the HWFET is similar to the NEDC. The 10-15 mode is the most sensitive and the final SOC is beyond the boundary from the 70% of the engine normalised efficiency.

The large difference between the initial and the final SOC implies that the fuel economy depends on the pre-stored electric energy. Therefore, it is preferable to maintain the difference as a minimum in the charge sustaining HEVs. To reconcile this fact with the

maximum fuel economy benefit, 50% of the normalised engine efficiency is selected as a threshold value for the controller.

4.3.2 FUEL ECONOMY

Table 4-2 shows the comparative fuel consumption of the baseline and the hybrid vehicle. Hybridisation improves the fuel economy considerably from the baseline. In the 10-15 mode the improvement is 26.8%, and 1.3% in the HWFET is the worst case. These differences arise from the characteristics of the driving cycles. In the NEDC and FTP-75, the improvements are 15.0% and 13.1% respectively, and these values are anticipated from other recent studies of the mild hybrid SUVs [172, 173].

The charge sustaining HEV has to maintain the SOC regardless of the driving conditions. It means that the control strategy should be designed to recover the SOC more actively if it is far from the target value. In the standard driving cycles, it is preferable that the final SOC is as close as possible to the initial value, because there are few clear methods to convert the difference of the energy stored in the battery to the equivalent fuel consumption. The SOC variation over the driving cycles is illustrated in Figure 4-7 along with the vehicle speed. The initial SOC level is set at the same target SOC, 60%. In all cases, the SOC is controlled within the normal operating boundaries, +/- 10%. The lowest point is 50% in the NEDC cycle, and the highest value is 65% in the FTP-75. The SOC is generally decreased when there is no energy flow to or from the EM because the electric accessory consumes the energy from the battery continuously. Additionally, hard acceleration during the vehicle launch requires a large amount of power instantaneously. All of these energy consumptions are recovered mainly and rapidly by the regenerative braking. Actually, the final deceleration of the vehicle at the end of the cycles can offer sufficient energy to recover the lost SOC. Over these 4 standard driving cycles, the charge sustaining control strategy is working as well as the intended design.

The stop-start function of the HEV provides the majority of the fuel saving as expected. In Table 4-3, the absolute amount of saved fuel is presented along with in percentage terms to the total consumption. The idle stop saves up to 16.3% of the fuel, while the fuel saving in the non-idling period is 1.2~4.9%.

The interesting fact is that there is little difference in engine efficiency between the baseline vehicle and the HEV. Table 4-4 shows that the engine efficiency of the HEV is higher than the overall engine efficiency of the baseline vehicle. However, comparing the non-idling efficiency, the baseline vehicle is slightly better than the HEV except for the HWFET cycle. This is caused by the fact that the baseline vehicle engine is usually operated in the more efficient high power region to drive the mechanical accessory. In addition, the SIDI engine and the CVT are already operated very efficiently, so there is little room to improve the powertrain efficiency by mild hybridisation. This means that mild hybridisation hardly moves the powertrain operating points into a more efficient area.

Most of the fuel saving of the HEV comes from the electric accessory driving. Table 4-5 shows the electric energy balance between the EM, the engine and the electric accessory. In the case of the NEDC cycle, the regenerative braking energy does not provide enough energy for the accessory. Therefore, the EM has to generate the electricity rather than assist the engine. In the FTP-75, the regenerative braking supplies the energy to drive the accessory, and the interactions between the engine and the EM are almost balanced. The situation of the 10-15 mode is more or less that of the FTP-75. The HWFET cycle shows a different figure. The sum of the accessory drive and the engine assist requires more than double the amount of the regenerative braking energy, and consequently the energy shortage results in a large amount of charging and a tiny fuel economy improvement.

In conclusion, the stop-start and the effective recuperation of the braking energy to drive the electric accessory are dominant factors of fuel economy improvement in the urban cycles, while the efficient interaction between the engine and the EM is more important in motorway driving conditions.

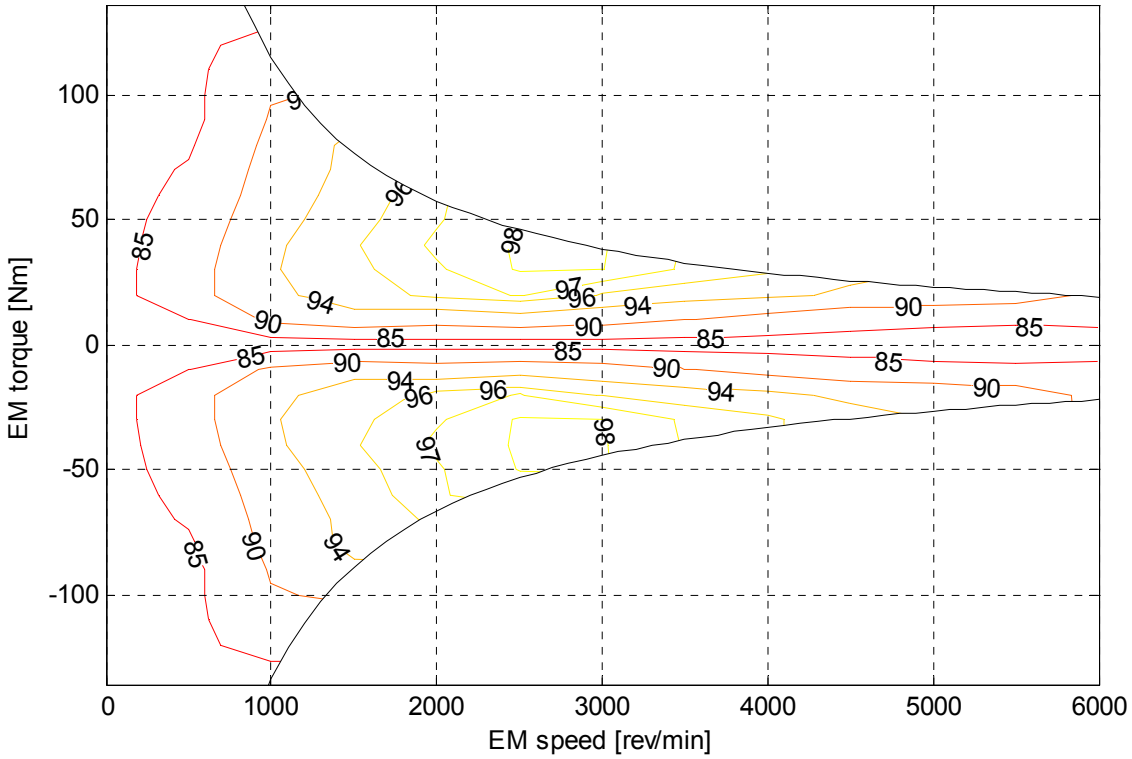

Figure 4-1 EM efficiency [%]

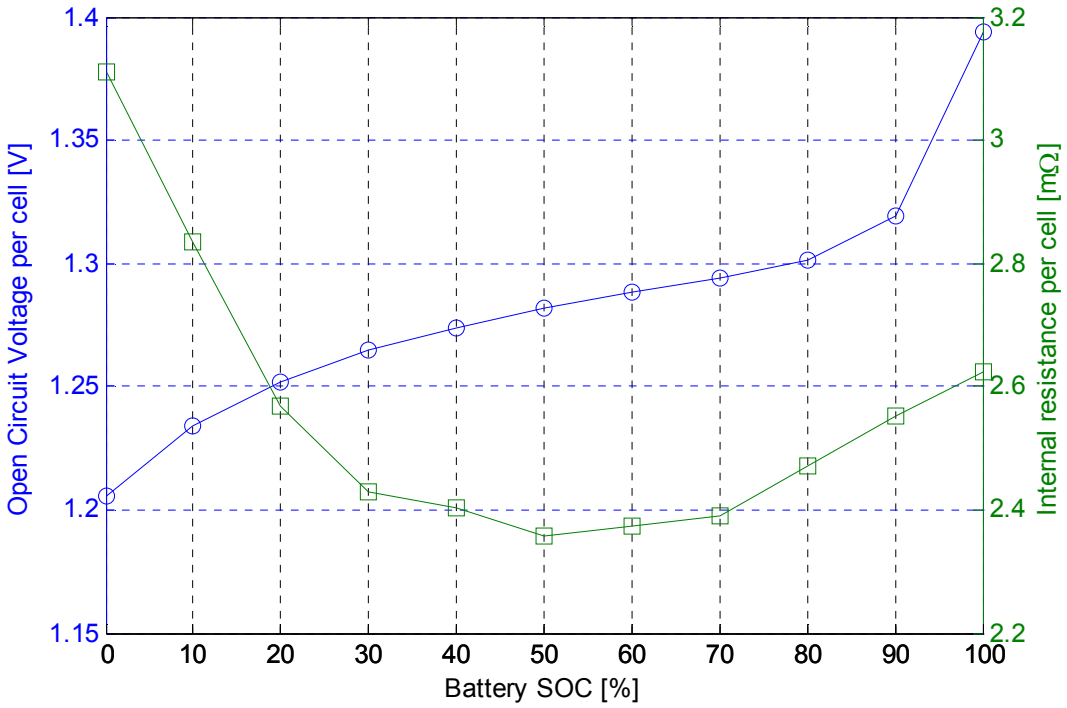

Figure 4-2 Battery properties

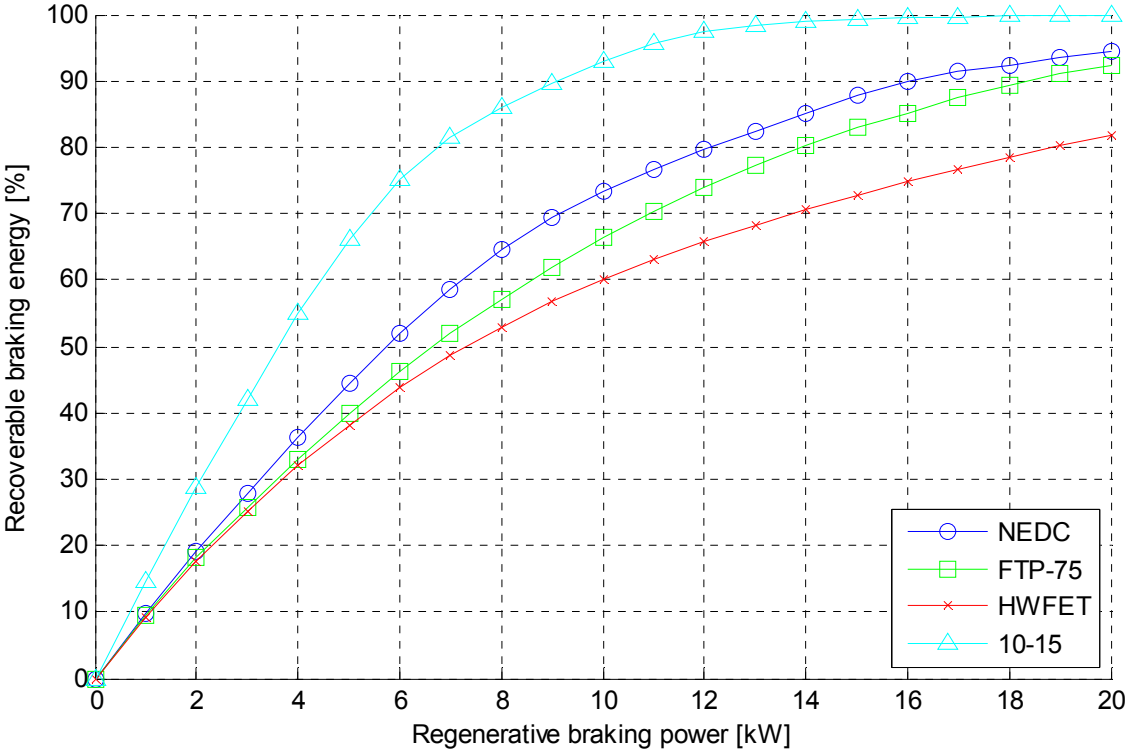

Figure 4-3 Energy recovery

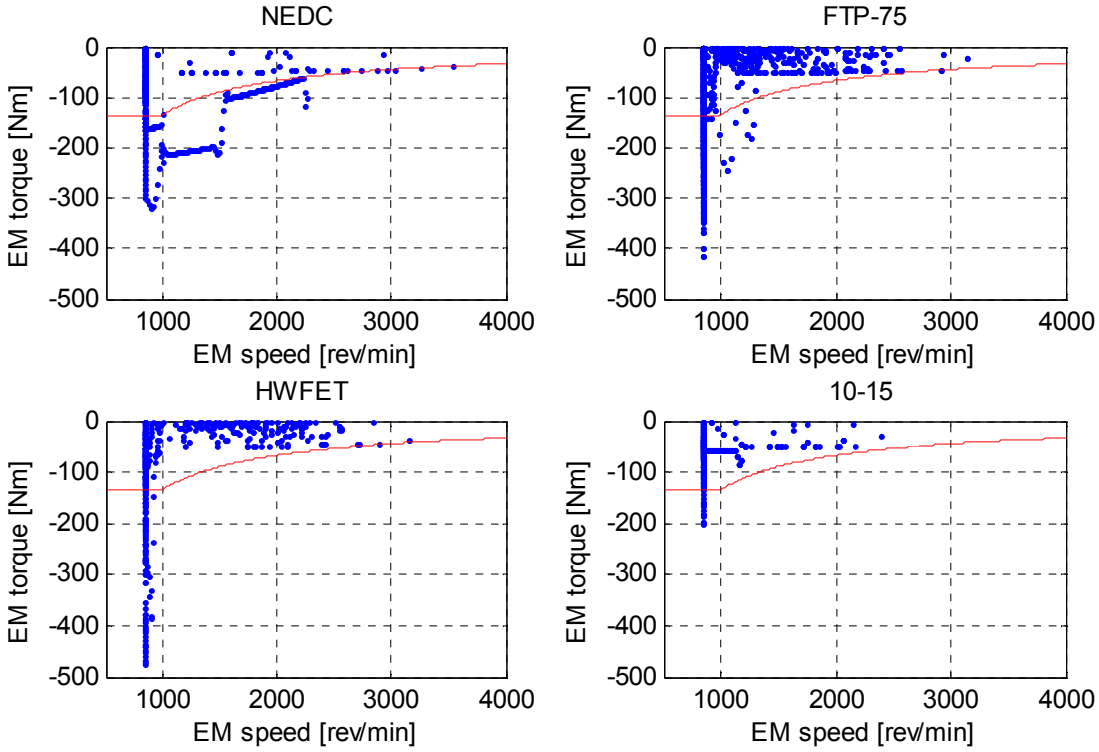

Figure 4-4 Energy recovery operating condition

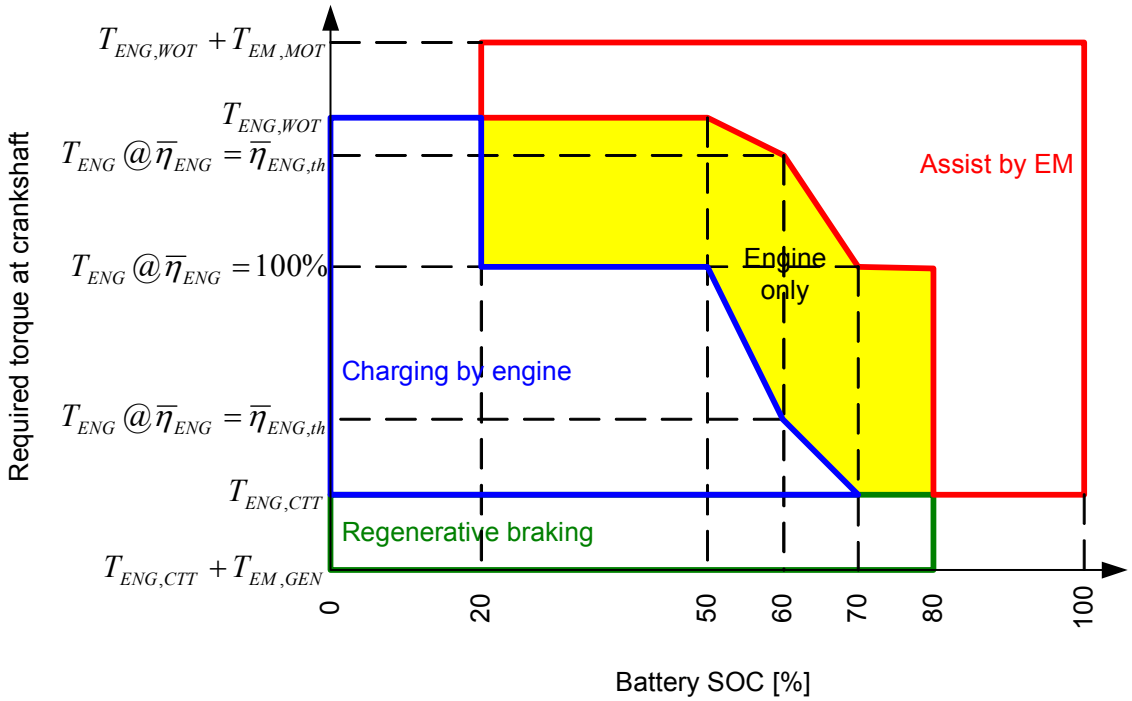

Figure 4-5 Reference control strategy

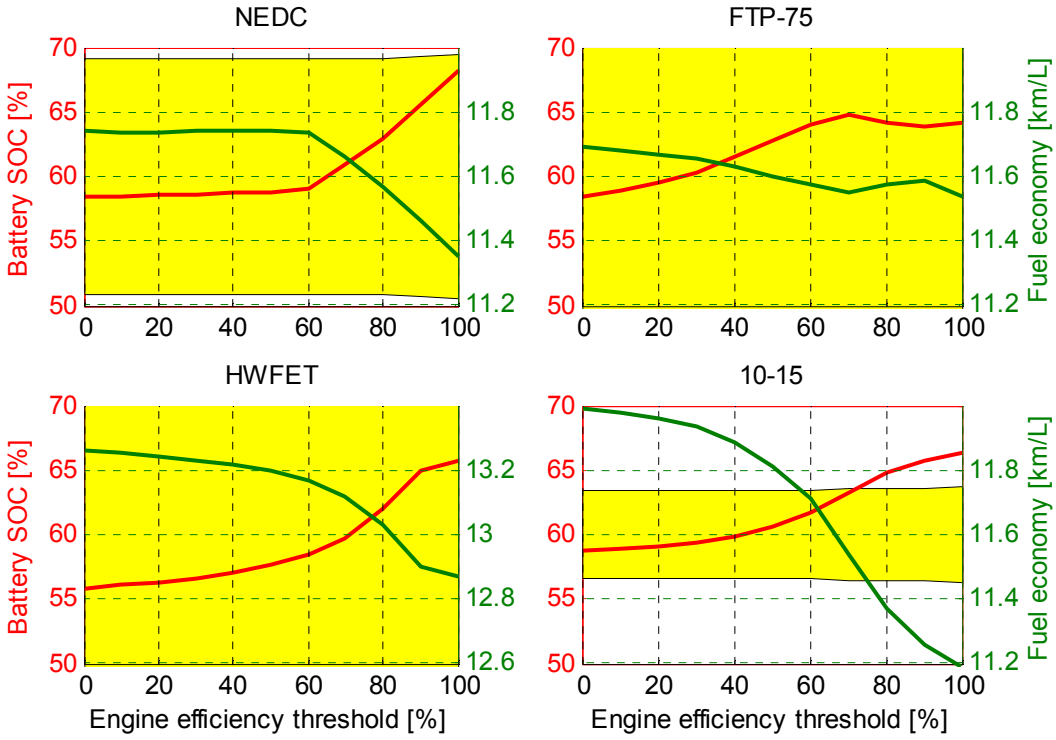

Figure 4-6 Control parameter tuning

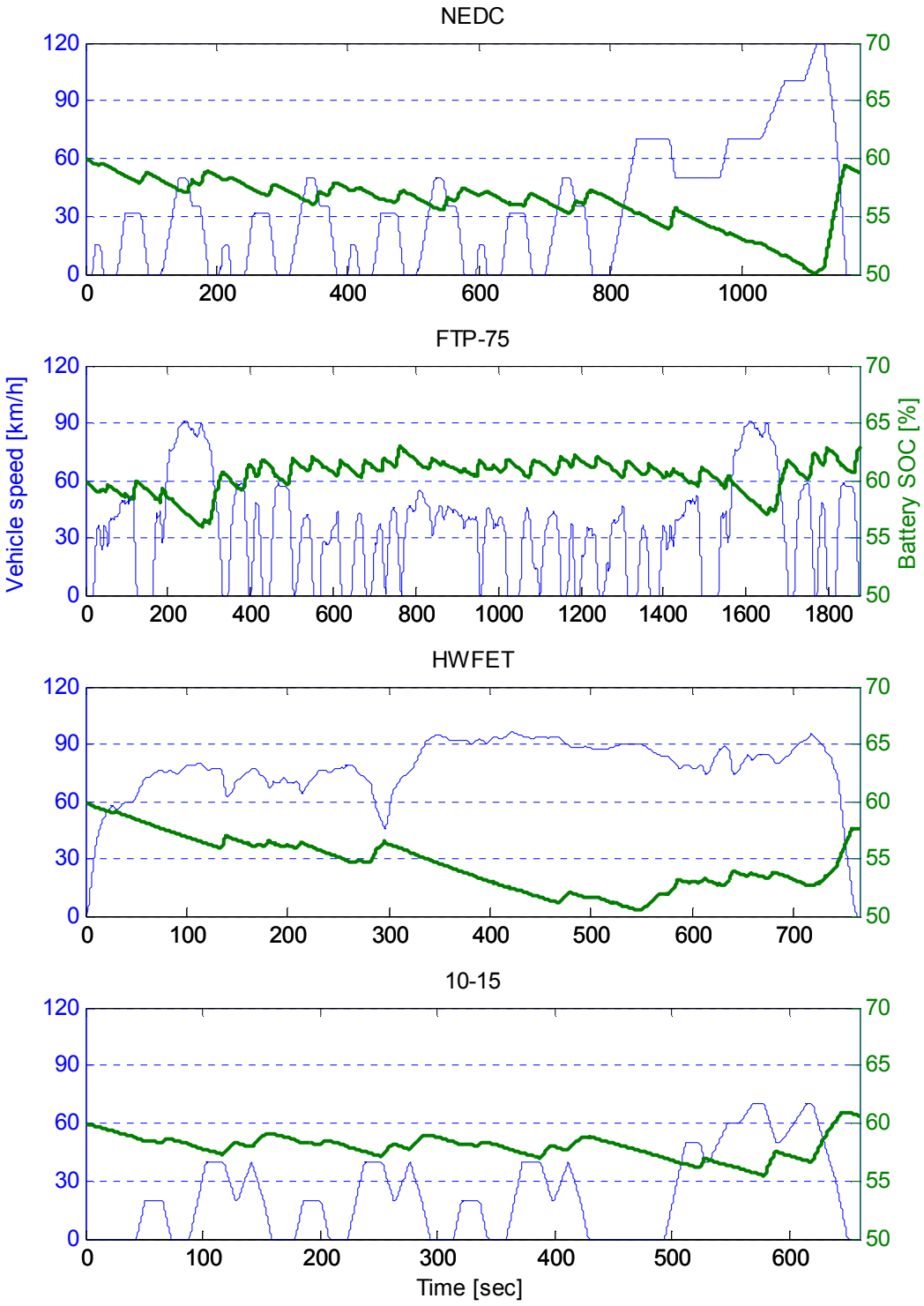

Figure 4-7 Battery SOC

Table 4-1 EM and battery parameters

	Parameter	Unit	Value
EM	Maximum motoring power	kW	12.0
	Maximum generating power	kW	14.0
	Maximum torque	Nm	±136
	Inertia	kgm^2	0.072
Battery	Capacity	Ah	6.5
	Nominal voltage per cell	V	1.2
	Number of cells per module	-	6
	Number of module in series	-	20
	Number of module in parallel	-	1
	Mass including power electronics	kg	35
	Electric accessory load	kW	1.0

Table 4-2 Fuel economy

	NEDC	FTP-75	HWFET	10-15
Baseline [km/L]	10.2	10.3	13.0	9.3
HEV [km/L]	11.7	11.6	13.2	11.8
Improvement [%]	15.0	13.1	1.3	26.8

Table 4-3 Consumed fuel

		NEDC	FTP-75	HWFET	10-15
Baseline [L]	Idling	0.099	0.118	0.001	0.073
	Non-idling	0.967	1.613	1.266	0.374
HEV [L]	Idling	0.000	0.000	0.000	0.000
	Non-idling	0.927	1.531	1.251	0.353
Fuel saving [L] (to total [%])	Idling	0.099 (9.2)	0.118 (6.8)	0.001 (0.1)	0.073 (16.3)
	Non-idling	0.040 (3.8)	0.082 (4.7)	0.015 (1.2)	0.022 (4.9)

Table 4-4 Engine efficiency

		NEDC	FTP-75	HWFET	10-15
Baseline [%]	Idling	13.5	13.5	13.5	13.5
	Non-idling	27.1	26.4	28.6	25.5
	Overall	25.8	25.5	28.6	23.5
HEV [%]		26.9	26.2	28.7	25.2

Table 4-5 Electric energy

		NEDC	FTP-75	HWFET	10-15
EM [MJ] (to regenerative braking [%])	Regenerative braking	1.080 (100.0)	2.193 (100.0)	0.404 (100.0)	0.689 (100.0)
	Charged by engine	0.232 (21.5)	0.254 (11.6)	0.440 (108.9)	0.072 (10.5)
	Assisting engine	-0.081 (-7.5)	-0.289 (-13.2)	-0.109 (-27.1)	-0.036 (-5.2)
Electric accessory consumption [MJ] (to regenerative braking [%])		1.180 (109.2)	1.874 (85.4)	0.765 (189.5)	0.660 (95.8)

5 FUEL ECONOMY POTENTIAL

As shown in Chapter 4, hybridisation delivers a considerable fuel economy benefit, and the rule-based control strategy manages battery SOC very well in four standard driving cycles. However, in general, a rule-based control does not provide a global optimal solution. It implies that there is a possibility to achieve better fuel economy. Another issue is that the controller was tuned in the same cycles, so the performance could not be guaranteed in different conditions. Therefore, the following questions are naturally raised.

- How much additional improvement can be achievable? In other words, how close is the fuel economy to the global optimal?
- Does it work well in different driving situations, for example, extremely congestive traffic or hilly terrain?

The above questions will be answered using the DP in this chapter.

5.1 DYNAMIC PROGRAMMING

Two methods of the optimisation in classical control are the variational approach based on the minimum principle of Pontryagin and the DP developed by Belman [58]. The variational method leads the optimisation to a nonlinear two-point boundary value problem (TPBVP). In general, the TPBVP does not guarantee a solution to exist nor the solution to be a global optimum. The DP is a powerful tool to find the optimal solution of nonlinear dynamic system for given boundary conditions. The advantage of the DP is that it is able to find the global optimal solution for any kind of system. However, non-causal nature and the requirement for intensive computing power make this useful tool difficult to apply to real-time applications.

To apply the DP in control, the problem can be divided into multiple time stages with a control action required at each stage. Each stage has a number of states associated with it. The control at one stage transforms one state into a state in the next stage. Given the current state, the optimal control for each of the remaining states does not depend on the

previous states or control. Bellman has called this property the principle of optimality [174]:

> "An optimal policy has the property that whatever the initial state and the initial decisions are, the remaining decisions must constitute an optimal policy with regard to the state resulting from the first decision"

There exists a recursive relationship that identifies the optimal control at time t, given that stage $t+\Delta t$ has already been solved, and the final stage must be solvable by itself. In a control problem, the recursive formula is a mathematical model of a plant, and the values at the final stage are usually given from boundary conditions.

In this research, the DP is used in order to find the maximum achievable fuel economy to compare the optimality between the controllers. Therefore, the application is limited to offline simulation.

5.2 STANDARD CYCLES

5.2.1 FORMULATION

Using the DP, the governing equations of the system should be rearranged and simplified for efficient calculation. Even though the HEV has two power sources, the transmission control strategy is not different from the conventional vehicle. In other words, required torque and speed at crankshaft is exactly same and can be calculated before using the DP. From Equation 4-2, the engine and EM speed are determined regardless of the torque distribution. From Equation 4-3, the required crankshaft torque, which should be supplied from the two power plants, is defined as below.

$$T_{CRANK} \equiv T_{ENG} + T_{EM} = T_{TMin} + J_{ENG}\dot{\omega}_{ENG} + J_{EM}\dot{\omega}_{EM} \tag{5-1}$$

Therefore, either the engine or EM torque can be a control variable, and the rest of them become dependent on the control decision. Intuitively, EM torque is the better candidate than engine torque because it is closely related to the behaviour of the electrical system that has a state variable, battery SOC. For a given set of the EM torque values, the battery SOC is calculated using Equations 4-4, 4-5 and 4-6.

The DP was developed for the digital computer application, so state and control variables should be quantised with appropriate resolution. Finer resolution of variables

can give more accurate result but requires longer calculation time. The chosen EM power capacity is +12kW/-14kW, so 1% of the full range is 260W. Considering the 0.2sec calculation time-step, the energy handled by the EM during one time-step is 52J, which is equivalent to 0.00154% battery SOC and 2.07Nm torque at 1200rev/min if the losses of the EM and battery are neglected. In this research, 0.002% of the SOC resolution and 2Nm EM torque increment are used for the DP calculation.

5.2.2 CALCULATION DOMAIN

As mentioned at the beginning of this chapter, the DP requires a heavy calculation load. Even though modern computer technologies have been improved rapidly and new efficient algorithms have been introduced, it is a time-consuming process to calculate all the combinations of the state and control variables. Furthermore, a long driving cycle with short time-step makes the situation worse. For time saving and efficient memory handling, the following ideas are involved.

- Battery SOC limits are considered. Theoretically, wider battery SOC usage gives a larger potential of fuel economy improvement but shortens battery life. In this research, it is assumed that the limit of battery operating range is between 20 and 80%. Therefore, the battery SOC, the state variable, outside this range should not be considered.
- The EM capability limits the state variable change rate. For example, if the initial SOC is 60%, then the SOC at the next step cannot be 80 or 20% because the EM cannot supply this amount of energy within a time-step. The same theory is applied to the final condition. As a result, the variation of the state variable should stay in a limited range for some initial and final time durations. In addition, the EM generation torque cannot be larger than the difference between the engine WOT torque and the required crankshaft torque. Similarly, the EM is able to assist the torque within the difference between the required torque and the engine friction torque.
- Control strategy is an additional constraint. When the vehicle is stationary, the optimal control turns off the engine to stop fueling. In addition, there is no choice when the required torque at the crankshaft is over the sum of the engine WOT

torque and the EM maximum motoring torque. The opposite case, which means that the required torque is under the sum of the engine friction and the EM generation torque, can be dealt in the same way.

These constraints are mathematically expressed as follows;

$$SOC_{LO} \le SOC \le SOC_{HI} \tag{5-2}$$

$$\min\left(T_{EM,GEN}, T_{CRANK} - T_{ENG,WOT}\right) \le T_{EM} \le \max\left(T_{EM,MOT}, T_{CRANK} - T_{ENG,CTT}\right) \tag{5-3}$$

$$T_{EM} = \begin{cases} T_{EM,MOT} & , T_{CRANK} \ge T_{EM,MOT} + T_{ENG,WOT} \\ 0 & , V_{VEH} = 0 \\ T_{EM,GEN} & , T_{CRANK} \le T_{EM,GEN} + T_{ENG,CTT} \end{cases} \tag{5-4}$$

Figure 5-1 displays the results in the standard driving cycles. Yellow shaded areas indicate the actual calculation domain, along with the speed profiles as blue thick lines. The area outside of the SOC limit is excluded from the domain. At the beginning and the end of the cycle, the SOC limits are converged to the initial and final target SOC values. This saves a significant portion of the calculation on the 10-15 cycle, which is the shortest among the four standard cycles. The control strategy also contributes calculation saving, especially in the 10-15 and NEDC cycles.

The number of calculation nodes is quantitatively illustrated in Table 5-1. In the FTP-75, which is the longest cycle, there are 468 million nodes of battery SOC if the DP conducts full domain. However, the battery SOC limits, the EM torque limits, and the control strategy eliminate 40%, 7.3%, and 12.6% of the nodes respectively. As a result, only 40% of the original nodes are carried out by the DP algorithm. In addition, the calculation time is approximately 6 hours using 2GHz Pentium-4 machine with 1GB memory. In the case of the 10-15 mode, the DP need to evaluate only 25% of the full nodes because of long idling periods and large effect of the initial and final condition constraints. The worst case is the HWFET cycle, which has few stop events and short decelerating phases. The overall calculation time saving is 50 to 75% depending on the characteristic of the driving conditions.

5.2.3 FUEL ECONOMY SIMULATION

Figure 5-2 shows the optimal battery SOC trajectory obtained by the DP compared with the results of baseline control strategy. As the time-backward characteristic of the DP, the final SOC is converged to 60%, which is exactly same as the initial condition for all driving conditions.

In the NEDC and 10-15 cycles, the main difference between the DP and the baseline control strategy is that the SOC changes during constant speed cruising. The DP result shows that the optimal control action maintains SOC during most cruising periods. In other words, the EM constantly supplies the electric energy requested by the electrical accessory like a conventional alternator. On the contrary, the baseline controller depletes the battery SOC with the same rate of idling. As a result, the DP allows the EM to supply more energy to assist the engine when the vehicle is accelerated.

In the FTP cycle, the two controllers show very similar behaviour up to 1100 seconds. Beyond this point, the DP control consumes more electric energy to assist the engine during the vehicle acceleration and reduce the battery SOC below 55%, which can be covered by the long regenerative braking around at 1700 second. The DP can consider the electric energy recovery opportunity during the whole journey, so it can meet the final SOC target exactly.

During the HWFET, the baseline controller spends too much electric energy to drive the accessory and have only a few chances to recover it by regenerative braking. It results the lower final SOC than the initial value. The DP controls the SOC in an appropriate level by generating electricity using the engine power. In moderate engine power region, small additional torque load does not require a significant amount of fuel and increase the engine efficiency.

Fuel economy improvement by the DP on the standard driving cycles are summarised in Table 5-2. The improvements are between 0.13 ~ 2.21%, which are not very considerable. This implies that the baseline controller has a good performance and it is well optimised in these driving cycles. In the NEDC and HEFET cycle, the improvements are relatively small because the DP uses more engine power to pull up the final battery SOC to the same level of the initial value. On the contrary, the fuel

saving is large in the FTP-75 and 10-15 because the DP can spend more electrical energy to meet the final SOC condition.

Table 5-3 shows the comparison of the engine operating efficiency in two controllers. There is no big improvement because the combination of the SIDI engine and the CVT is already highly optimised and there is only a little room for further improvement. In case of the FTP-75 and 10-15, the fuel economy improvements are larger than the engine efficiency increments. It supports the fact that the final battery SOC adjustments contribute to the fuel economy benefit. The NEDC and HWFET show contradictory results because of their opposite direction of the final SOC adjustment by the DP.

The mechanical energy flow at the crankshaft is shown in Table 5-4. The regenerative braking energy is nearly the same in the two controllers, because both use the same regenerative control strategy. The large difference between the controllers is the interactions between the engine and the EM. The baseline controller exchanges much less energy than the DP. The DP uses more than 6% of the energy produced by the engine to charge the battery, but the baseline controller does 2~4%. Consequently, the DP uses the EM to assist the engine much more than the baseline controller.

According to the trade-offs between fuel economy and the final SOC in Figure 4-6, the same level of fuel economy as the DP can be achievable when the threshold is around 20~40% with 2~4% final SOC penalty. The exceptional case is the FTP-75. Even though the threshold value goes to the extreme ends, the DP provides better fuel economy with exact final condition. Both the NEDC and 10-15 mode are synthetic cycles that consist in simple ramps and constant cruising, so they are not adequate to demonstrate the HEV fuel economy benefit. The HWFET is a real-world cycle like the FTP-75 but the HEV cannot give much benefit in the motorway driving conditions. These reasons result in only a small amount of fuel savings in standard driving cycles. Consequently, aggressive real-world driving cycles are appropriate to demonstrate the actual fuel economy benefit of the HEV, which will be investigated in the next section.

5.3 AGGRESSIVE DRIVING CONDITIONS

Standard driving cycles are used in legislation test to measure fuel consumption and emissions of vehicles in a precisely controlled condition. However, the traffic

conditions in major cities have become worse, and the vehicle performance has been rapidly improved. Consequently, normal drivers are adapting to these changes and their driving pattern is becoming aggressive.

Another argument against standard cycles is that they have been developed for conventional ICE based vehicles. Alternative powertrains such as HEVs use different types of power sources to propel or brake vehicle but the standard driving cycles have not been modified to account for these modern technologies. For example, deceleration phase does not affect the fuel economy of conventional vehicle very much because it just dissipates kinetic energy of the vehicle by mechanical brake. However, the regenerative braking provides cost-free energy to HEVs and very important role in fuel saving.

Finally, any standard cycle does not consider road gradient. In real driving situations, it is hard to find perfectly flat terrain over a long distance. Combined with aggressive driving pattern, this could give HEVs more opportunity to improve fuel economy.

5.3.1 DRIVING CYCLES

Speed-acceleration plots of the standard cycles are in the first row of Figure 5-3. Synthetic cycle such as the NEDC and 10-15 consists of repeated constant acceleration and cruising phases. Therefore, they have limited operating points in the plot. The top speed and the maximum acceleration of the NEDC are higher than the 10-15, which represent different average traffic situations between Europe and Japan. However, the acceleration rate of the NEDC is still far from the real-world driving conditions.[175] The FTP-75 and HWFET are real-world cycle but the acceleration rate is intentionally bounded as shown in the figure. As a result, regenerative braking and engine assist by EM are limited as well in these cycles.

The next row of Figure 5-3 shows four additional cycles, which are more aggressive than the above. SC03 and US06 are supplementary cycles of the US emissions test standard, and New York City Cycle (NYCC) and LA92 represent New York city driving and California urban and extra-urban driving conditions. SC03 is similar to the FTP-75 but slightly higher acceleration characteristic. US06 is very aggressive motorway cycle with highest top speed range and maximum acceleration is more than

double of the HWFET. The NYCC is positioned at the opposite extreme of US06, which means very slow speed with frequent stops to reflect congested city driving condition. LA92 covers a wide range of speed and acceleration to represent the combined driving situation.

Figure 5-4 illustrates the average speed and the root mean squared (RMS) acceleration of all eight cycles. The NYCC, LA92 and US06 form the highest level of acceleration over the whole speed range. SC03 has very similar properties to the FTP-75 as we can see in Figure 5-3 as well. The NEDC and 10-15 have low acceleration profile, and the average speed is between the NYCC and LA92. The HWFET cycle has the same average speed of US06 but the acceleration is less than half of US06.

Figure 5-5 depicts the distribution of speed and acceleration. Red lines in the boxes represent median and the both ends of the boxes mean lower and upper quartile values. The lines extending from each end of the boxes show the distribution of extreme quartiles. In the case of the NEDC, FTP-75 and 10-15, 50 percentile around the median is positioned below 50km/h. On the other hand, 50 percentile of the HWFET is around 80 km/h. It is very clear that the LA92, NYCC and US06 can cover whole range of the eight cycles with minimum overlapping in speed range. LA92 can be substituted by SC03, the FTP-75 or NEDC but these cycles have narrow distribution of acceleration. As a conclusion, in this section, the LA92, NYCC and US06 will be used in order to demonstrate the HEV fuel economy potential.

5.3.2 ROAD GRADIENT

Road gradient acts as an additional load to vehicles. Steep downhill could give HEVs more opportunity to recuperate the energy to top up battery SOC, and the saved energy in the battery can be used to assist the engine on uphill.

The detailed real road elevation can be found in digital maps but there is no standard driving cycles that have information of terrain data. However, a guideline of road construction from government authorities gives a boundary of road gradient. For example, the design manual for roads and bridges[176] suggests that the maximum desirable gradient is 3, 4, 6% for motorways, dual carriageways and single carriageways respectively. However, it also says that steeper gradient in hilly terrain will be

frequently required. Rajagopalan et al.[105] create a driving profile with real-world data from Denver to Vail along the motorway, which contains extensive change in elevation at high speed. The first 20km of the road profile is shown in Figure 5-6. The peak gradient is over 7% but usually lower than 6%. In this study, this profile is applied to the three aggressive driving cycles. The geographical data represents uphill, but the same profile in reverse direction is used in order to simulate downhill as well.

5.3.3 FUEL ECONOMY SIMULATION

In Table 5-5, fuel economy simulation results using the baseline controller and the DP are compared. There is a big difference in fuel economy improvement according to the road gradient as well as driving cycles. In the case of downhill, substantial amount of fuel saving is achieved by the DP. It should be emphasised that the improvement by the DP in the LA-92 is more than 5 times of the NYCC. In addition, there is a considerable improvement in motorway cycle, in which it is usually hard to get such amount of benefit in level road. The improvement potential at level road is the same level as standard driving cycles presented in the previous section. In the extreme case, the NYCC shows no improvement. Finally, in uphill, the DP shows better performance only in the LA-92 and spends more fuel in the city and motorway driving conditions.

Figure 5-7 gives comprehensive interpretation of the above results. Battery SOC traces show huge difference between the baseline and the DP, especially in the LA-92 downhill. The battery SOC controlled by the baseline controller increases up to the upper limit in the first 500 seconds, and then there is little room to capture the cost-free regenerative braking energy. On the contrary, the DP depletes the battery for a few hundreds seconds, and then fill the battery to 72%. This means the DP can save much fuel in the first a few hundred seconds by electric assist, then recover the battery SOC by regenerative braking. Obviously, these are possible only when controller has the knowledge of future driving conditions, which is long downhill road in this case. The fuel saving potential by the DP in US-06 cycle is less than LA92 but the trend of battery SOC control shows the same trend. This means the first portion of the cycle requires more torque demand at the crankshaft, so EM assist is more beneficial to save fuel. After the middle of the cycle in both cases, the DP controls SOC to 60% to meet the boundary condition. In the NYCC, the journey length is much shorter than the others, so

the DP tries to regulate SOC towards the end of the trip time as soon as it starts. The level road gives less fuel saving potential but the trend between cycles are not very different. It means longer journey time gives more fuel saving by the DP. The NYCC is the extreme case, which shows no more fuel benefit, but battery SOC is fully recovered by the DP using same amount of fuel. The third row represents uphill trip and there is no more fuel benefit. However, baseline controller depletes battery during the cycles, which is not preferable for the charge sustaining HEV case. The DP still works well to control SOC without much more fuel spending.

The battery SOC at the end of the trips is shown in Table 5-6. As mentioned above paragraph, performance of the baseline controller is not very good in case of the long trip such as the LA-92 and US06 at hilly terrain cases. It is clear that the final battery SOC deviation by the baseline controller and further improvement of fuel economy by the DP represented in Table 5-5 have strong relationship. More electric assist gives better fuel economy but lower final SOC resulting from depleting battery. Large deviation of the final SOC is harmful for the battery life even though it is finished at higher level than the starting point. Conversely speaking, if wider SOC swing is allowed by new battery technology, the DP gives a chance to reduce the battery capacity by appropriate energy management.

Table 5-7 compares engine operating efficiency. As same as in standard driving cycles, the DP does not improve engine efficiency significantly. In some downhill cases, the engine efficiency becomes worse. In the LA-92 and US-06 downhill, the DP makes engine run in inefficient low power region because of more electric assist. Therefore, engine efficiency is lower than baseline even though fuel economy improved significantly. In the other cases, improvement is positive but less than 1%. This tells a key fact. SIDI engine and CVT powertrain used in this study has good efficiency in wide operating area and the baseline controller already highly optimised at the engine operating point of view. Therefore, it is hard to improve engine efficiency by optimising controller. In other words, optimising battery energy control is more important for fuel economy, and the engine efficiency change resulted from the different SOC control strategy does not give significant impact on the fuel economy.

Table 5-8 supports the above claim. Except for the downhill LA-92 and US-06, the DP makes engine spend 5.44~20.69% of the load to generate electricity. In case of the baseline, these values are between 1.61~10.84%. Consequently, the engine assist is smaller than the DP and consumes more fuel to produce same amount of energy at the wheel. In the LA-92 and US-06 downhill, significant amount of energy is captured from regenerative braking and spent to engine assist by the DP. This is consistent with the fact that SOC is saturated at the upper limit during the cycle in baseline controller.

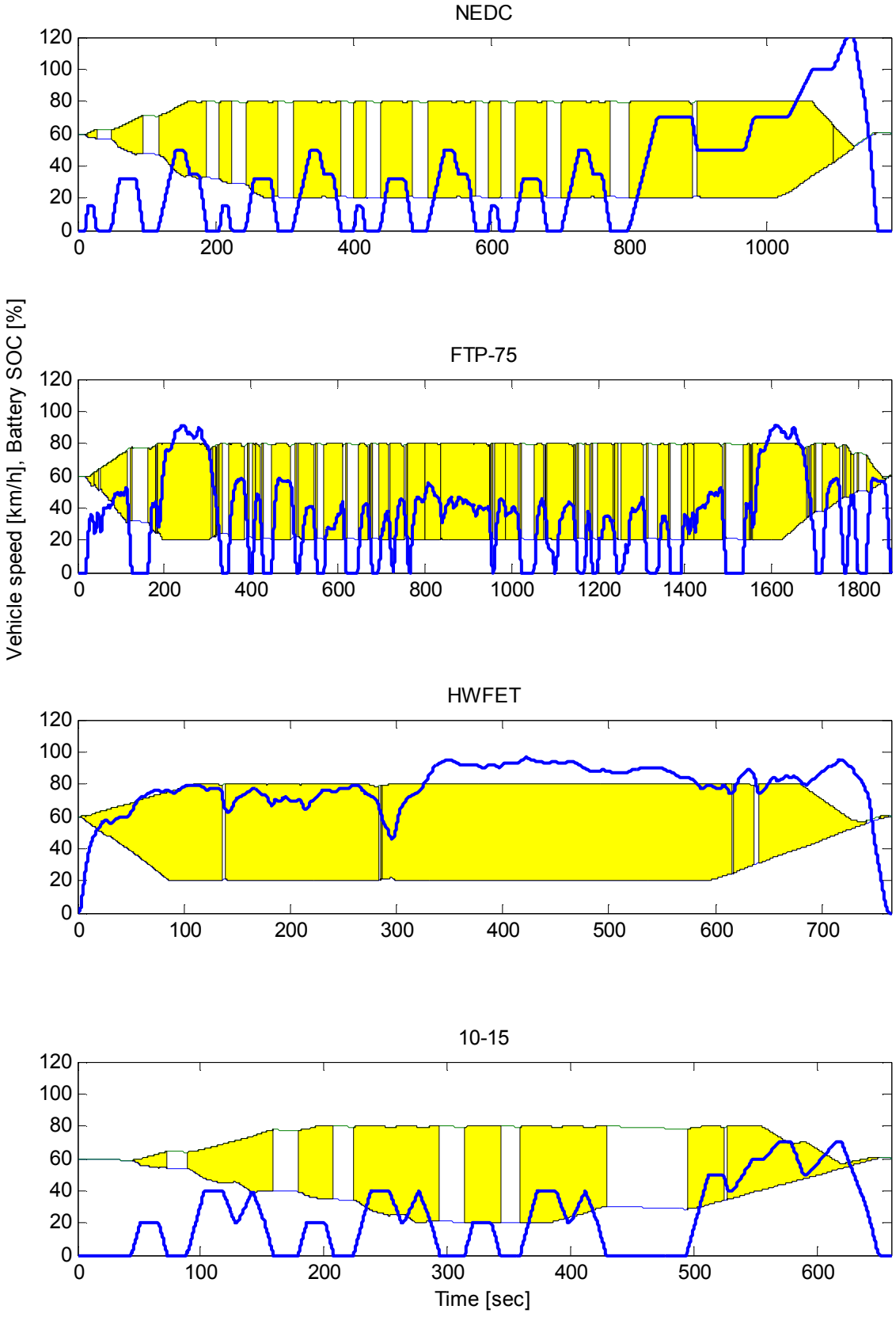

Figure 5-1 Calculation domain of dynamic programming

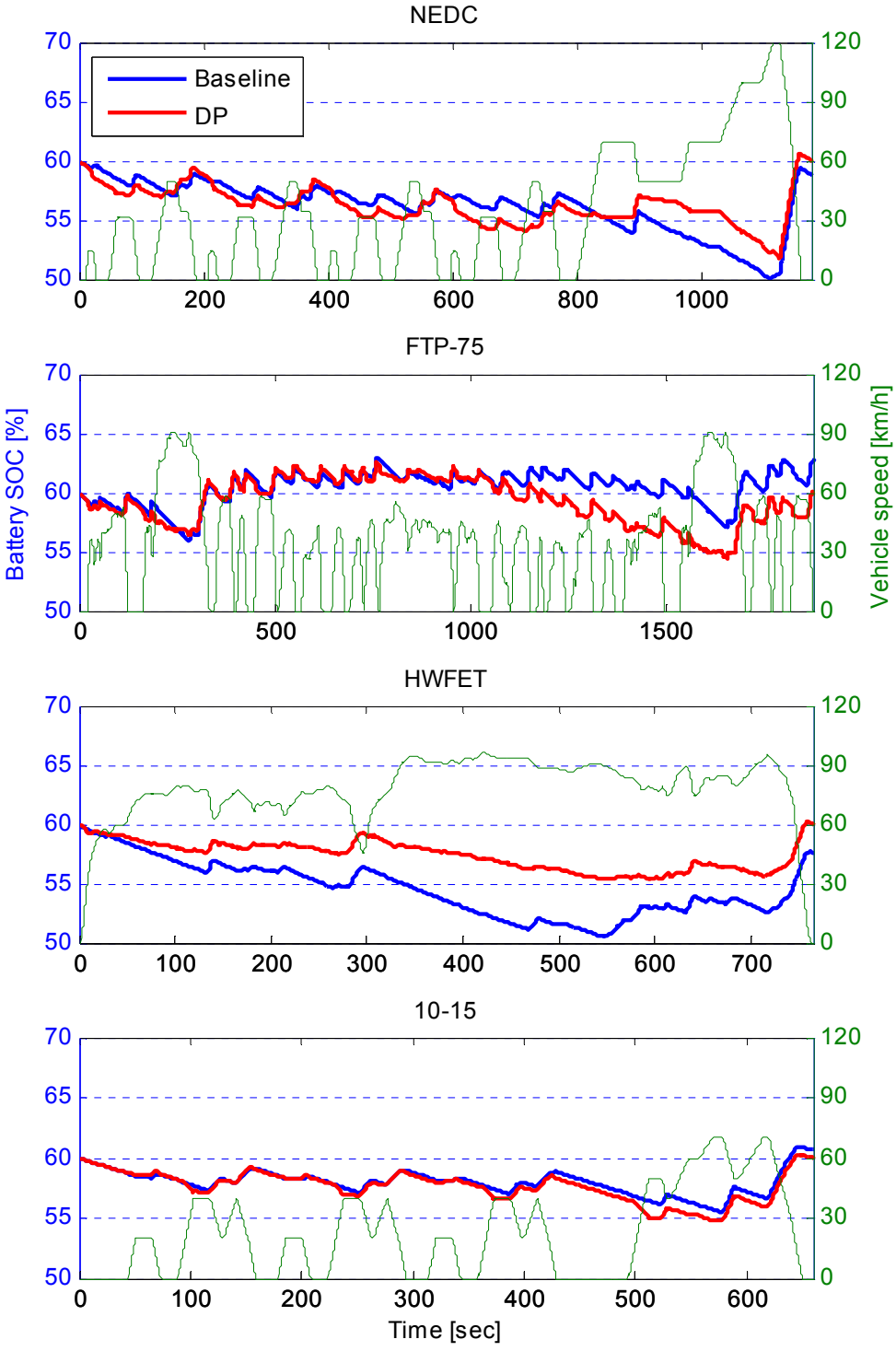

Figure 5-2 Battery SOC control

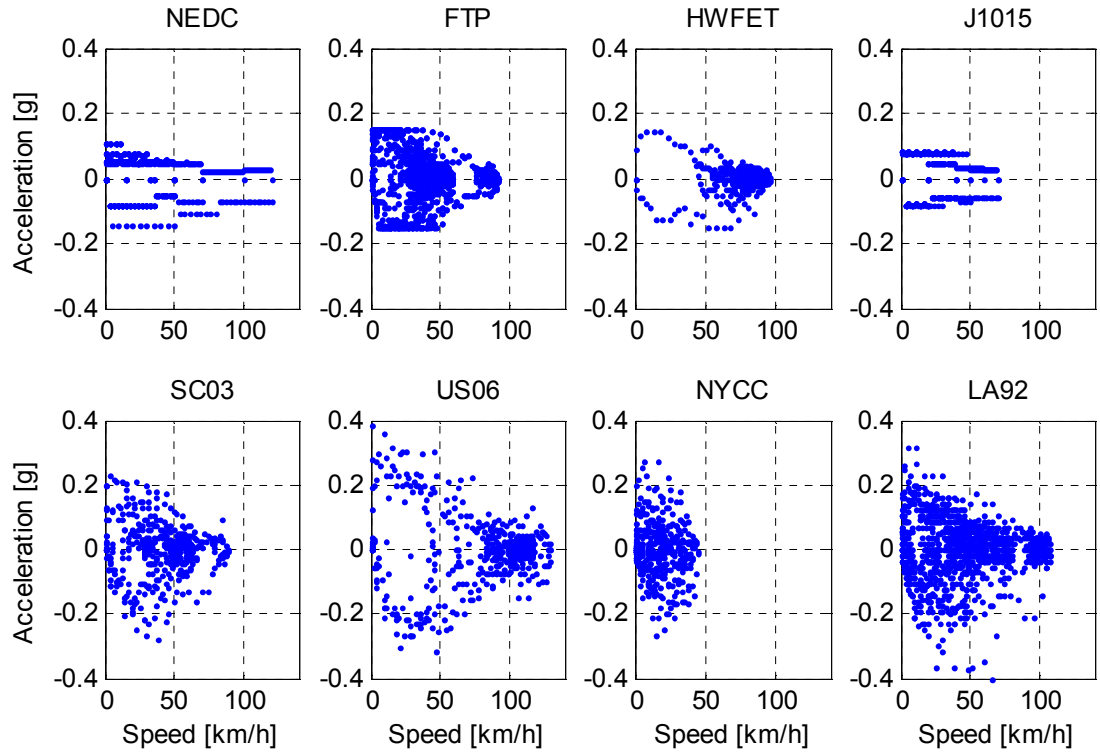

Figure 5-3 Speed-acceleration diagram

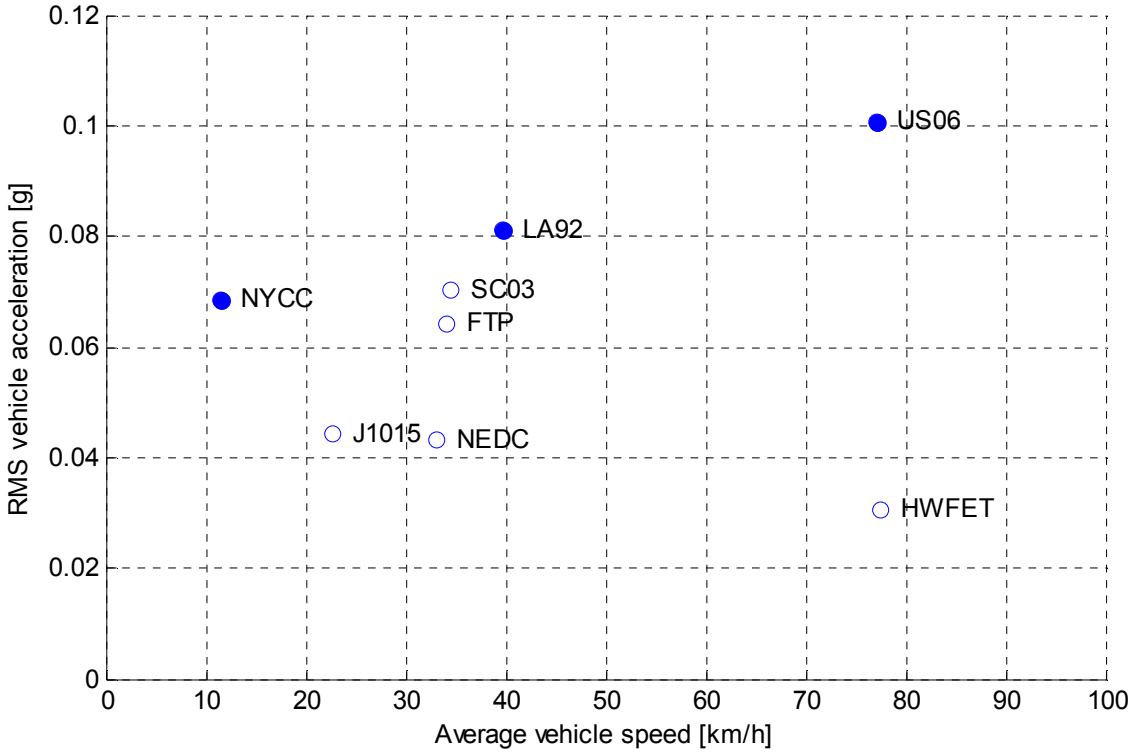

Figure 5-4 Characteristic of driving cycles

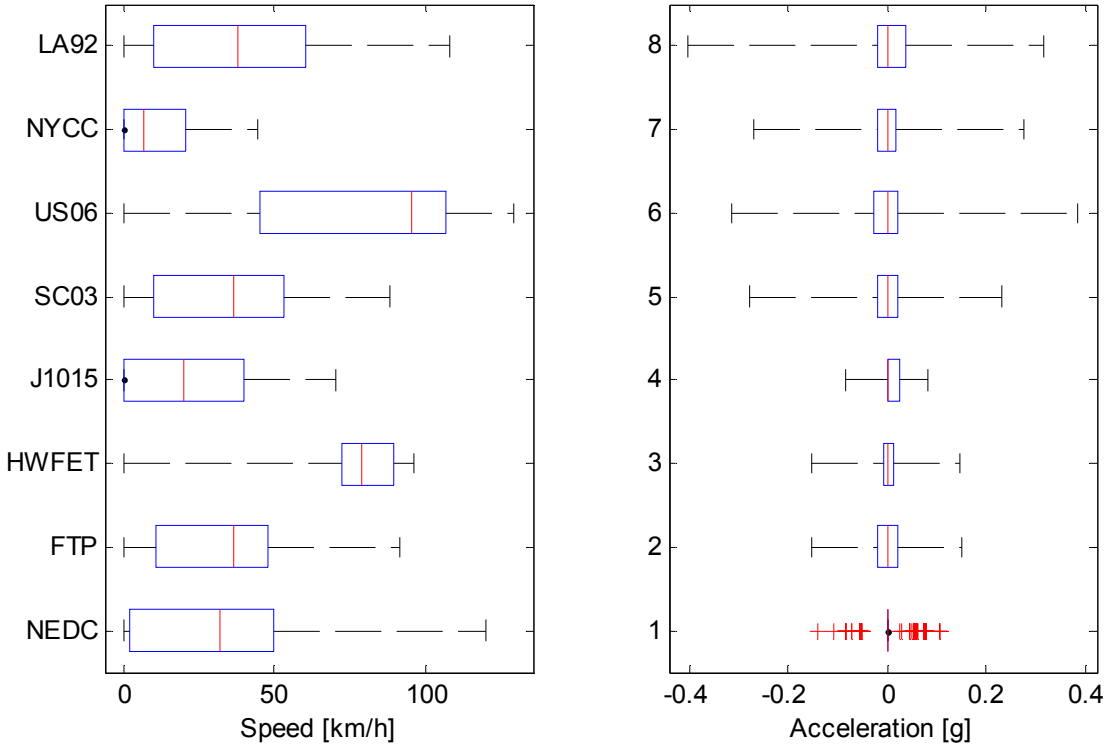

Figure 5-5 Speed and acceleration distribution

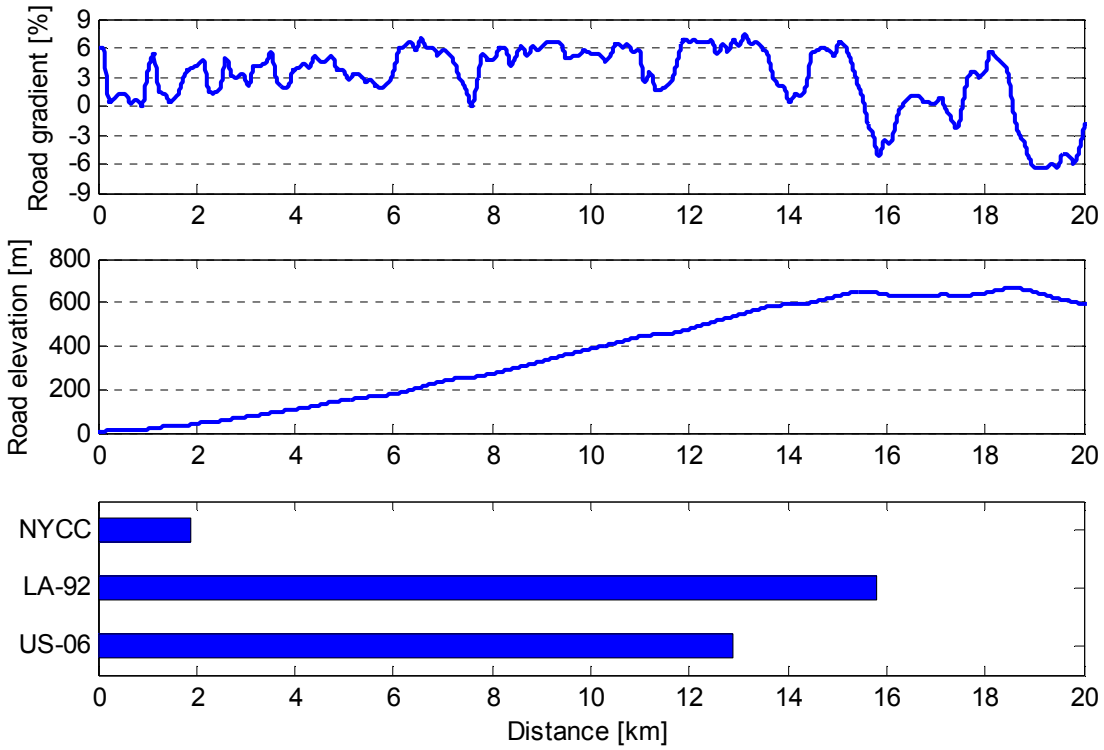

Figure 5-6 Road gradient

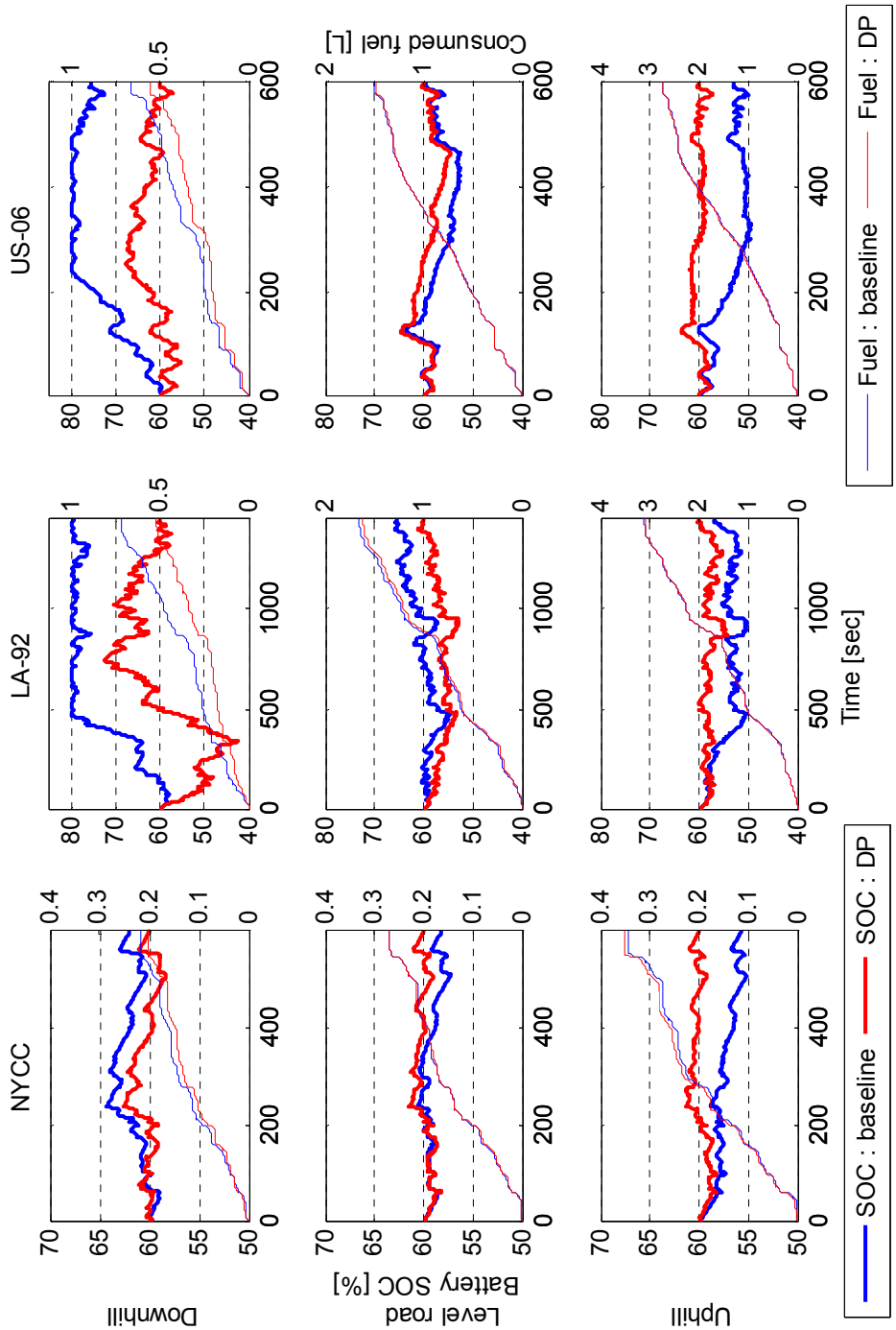

Figure 5-7 Energy usage

Table 5-1 Number of calculation node

		NEDC	FTP-75	HWFET	10-15
Total node [×10^6] ([%])		295.01 (100.0)	468.51 (100.0)	191.25 (100.0)	165.00 (100.0)
Eliminated node [×10^6] ([%])	Battery SOC limit	118.00 (40.0)	187.40 (40.0)	76.50 (40.0)	66.00 (40.0)
	EM torque limit	34.36 (11.6)	34.26 (7.3)	19.70 (10.3)	39.04 (23.7)
	Control strategy	33.06 (11.2)	59.10 (12.6)	1.32 (0.7)	18.11 (11.0)
Net node [×10^6] ([%])		109.59 (37.1)	187.75 (40.1)	93.73 (49.0)	41.85 (25.4)

Table 5-2 Fuel economy in standard cycles

	NEDC	FTP-75	HWFET	10-15
Baseline controller[km/L]	11.74	11.60	13.20	11.81
Dynamic programming [km/L]	11.76	11.84	13.21	11.97
Improvement [%]	+0.18	+2.21	+0.13	+1.37

Table 5-3 Engine efficiency in standard cycles

	NEDC	FTP-75	HWFET	10-15
Baseline controller[%]	26.91	26.24	28.68	25.22
DP [%]	27.08	26.70	28.92	25.37

Table 5-4 Mechanical energy exchange in standard cycles

			NEDC	FTP-75	HWFET	10-15
Baseline controller [MJ] (to Engine [%])	Engine		8.234	13.260	11.838	2.934
	EM	Regenerative braking	1.205 (14.64)	2.564 (19.33)	0.469 (3.96)	0.770 (26.24)
		Engine charging	0.261 (3.17)	0.277 (2.09)	0.478 (4.03)	0.080 (2.71)
		Engine assist	0.025 (0.30)	0.181 (1.37)	0.046 (0.38)	0.010 (0.35)
DP [MJ] (to Engine [%])	Engine		8.271	13.216	11.921	2.913
	EM	Regenerative braking	1.215 (14.69)	2.586 (19.57)	0.472 (3.96)	0.782 (26.85)
		Engine charging	0.564 (6.81)	0.950 (7.19)	0.728 (6.11)	0.213 (7.31)
		Engine assist	0.278 (3.36)	0.888 (6.72)	0.215 (1.80)	0.165 (5.67)

Table 5-5 Fuel economy

Driving cycle	Road gradient	Baseline controller [km/L]	Dynamic programming [km/L]	Improvement [%]
NYCC	Down	8.67	9.33	+7.61
	Level	7.07	7.07	0.00
	Up	5.53	5.38	-2.73
LA-92	Down	21.85	30.30	+38.69
	Level	9.52	9.77	+2.68
	Up	5.08	5.10	+0.43
US-06	Down	19.47	23.01	+18.19
	Level	8.58	8.65	+0.75
	Up	4.73	4.72	-0.14

Table 5-6 Battery SOC change

Driving cycle	Road gradient	Baseline controller [%]
NYCC	Down	1.98
	Level	-1.79
	Up	-4.25
LA-92	Down	19.63
	Level	5.3
	Up	-3.21
US-06	Down	15.7
	Level	-0.48
	Up	-7.03

Table 5-7 Engine efficiency

Driving cycle	Road gradient	Baseline controller [%]	Dynamic programming [%]	Improvement [%]
NYCC	Down	20.99	21.2	+0.21
	Level	23.42	24.13	+0.70
	Up	25.3	25.87	+0.57
LA-92	Down	21.99	18.94	-3.06
	Level	27.21	27.72	+0.51
	Up	29.15	29.39	+0.24
US-06	Down	23.49	22.45	-1.03
	Level	28.67	28.97	+0.30
	Up	29.34	29.65	+0.31

Table 5-8 Mechanical energy exchange in aggressive cycles

Driving cycle	Road gradient	Baseline controller [MJ] (to Engine [%])				DP [MJ] (to Engine [%])			
		Engine	EM			Engine	EM		
			Regenerative braking	Generating	Engine assist		Regenerative braking	Generating	Engine assist
NYCC	Down	1.517	-0.764 (-50.39)	-0.164 (-10.84)	0.067 (-4.44)	1.424	-0.773 (-54.32)	-0.295 (-20.69)	0.255 (-17.89)
	Level	2.073	-0.564 (-27.20)	-0.224 (-10.80)	0.089 (-4.29)	2.136	-0.57 (-26.70)	-0.442 (-20.68)	0.224 (-10.48)
	Up	2.867	-0.452 (-15.75)	-0.274 (-9.55)	0.122 (-4.24)	3.014	-0.457 (-15.17)	-0.542 (-18.00)	0.222 (-7.36)
LA-92	Down	5.247	-3.382 (-64.44)	-0.094 (-1.79)	0.479 (-9.13)	3.258	-5.355 (-164.35)	-0.002 (-0.07)	2.386 (-73.25)
	Level	14.903	-2.269 (-15.22)	-0.473 (-3.18)	0.433 (-2.91)	14.785	-2.286 (-15.46)	-1.066 (-7.21)	1.137 (-7.69)
	Up	29.912	-1.522 (-5.09)	-1.366 (-4.57)	0.792 (-2.65)	30.029	-1.533 (-5.11)	-1.952 (-6.50)	1.249 (-4.16)
US-06	Down	5.129	-2.327 (-45.37)	-0.082 (-1.61)	0.586 (-11.43)	4.149	-2.963 (-71.42)	-0.001 (-0.01)	1.495 (-36.03)
	Level	14.198	-1.315 (-9.27)	-0.45 (-3.17)	0.641 (-4.52)	14.241	-1.323 (-9.29)	-0.775 (-5.44)	0.922 (-6.47)
	Up	26.364	-0.861 (-3.26)	-1.058 (-4.01)	0.9 (-3.41)	26.678	-0.866 (-3.25)	-1.67 (-6.26)	1.194 (-4.48)

6 CONTROL WITH PREDICTIVE JOURNEY ESTIMATION

In the previous chapter, the baseline controller was compared with the DP to reveal the further improvement possibility. The result showed that there are still considerable margin, especially in case of the aggressive driving cycles in hilly terrain. It can be achieved by more appropriate battery energy management, which requires the information of the driving conditions ahead of current vehicle position.

In spite of the possibilities of a great fuel saving potential, the future journey prediction is not easy. As discussed in section 2.2.4, one of the solutions is the online prediction of the future state using navigation devices. This chapter introduces an online predictive controller for HEV. At first, the structure of the controller is presented, then detailed design procedure and simulation results are explained.

6.1 STRUCTURE OF CONTROLLER

Figure 6-1 depicts the structure of the predictive controller. The controller can be split into two parts. The first part is the electric energy management, and the second is torque distribution between the EM and the engine.

As shown in the previous chapter, battery SOC should be controlled according to the future driving conditions. It depends on driving cycle, which includes the vehicle speed, and road elevation. From the combination of these inputs, the controller can estimate required wheel torque. The other factor is current SOC because the final decision should be required EM power. Based on the current SOC level, the controller calculates required SOC change rate. Therefore, the control algorithm can be expressed as following two functions.

$$\Delta SOC_{req} = f_1\left(v_{VEH,predict}, T_{WHL,predict}, SOC\right) \tag{6-1}$$

$$T_{ENG,req} = T_{CRANK,req} - T_{EM,req} = T_{CRANK,req} - f_2\left(\Delta SOC_{req}\right) \tag{6-2}$$

The second function, torque distribution, is instantaneous decision making process and relatively easy to find the optimal. It is explained in the next section. The EM required torque is positive when the EM assist the engine. The first function, SOC control, is difficult to be derived as a simple explicit mathematical form. However, the controller

should be simple and intuitive for online calculation and calibration. For this purpose, fuzzy logic controller is designed, which is explained in section 6.3.

It is assumed that navigation system supplies vehicle speed and elevation data on forthcoming road. The infrastructure and interface providing this information is beyond this study. However, resolution of the data and the update interval are important factors to design the controller. In this study, update interval is assumed 1 second, which is typical update frequency of the GPS receivers in the market. Consequently, control loop time of SOC change request is 1 second. Control actions are based on timer, but the data from the navigation system is based on geographical position. Therefore, vehicle speed and road elevation data are the function of the distance from the current position. The control intends to predict the future driving conditions, so it does not require an instant sample but a kind of average information. On the purpose, supplied information is filtered by prediction window illustrated in Figure 6-2. Resolution of the data, window size and offset are design parameters of the controller.

6.2 TORQUE DISTRIBUTION

Optimal torque distribution of parallel HEV is depends not only on the driving conditions but also on the powertrain. There is no general solution but one of the methods is rule-based. To design a rule-based controller, the DP is used in order to extract optimal control actions in steady state load conditions.

6.2.1 STAGE 1 - CRUISING

As a first stage of investigation, optimal torque split is calculated in steady state cruising during 300 seconds. Five vehicle speed (10, 20, 30, 60, 90 km/h) and four road gradient (0, 3, 6, 9%) are selected. A negative gradient is not considered because in most cases the required torque level is below engine friction torque so the optimal solution is regenerative braking by EM. The boundary condition of battery SOC is 60%, same at the start and the end of the journey.

The result of the battery SOC and the torque level and occurrence are presented from Figure 6-3 to Figure 6-7. The graphes in the first row shows the optimal battery SOC trajectory in red. The green dashed lines represent the maximum SOC change limited by the available EM generating or motoring power. In the second and the third rows, the

optimal torque of the engine and EM torque along with the required torque at the crankshaft. Obviously, the required torque at crankshaft is sum of the engine and EM torque, and the torque level of each condition is different. However, there are only three cases of the shape of SOC trajectory.

The first case is that the battery SOC initially increases and then decreases to the given final condition, for example, in 10km/h level road. In this case, the engine supplies required torque for vehicle propulsion and generate electricity to charge the battery when the journey starts. From the middle of the journey, engine torque drops down and the EM assists the engine, which reduces battery SOC to meet 60% at the end. The histogram clearly shows that there are two operating points.

The second case is that the torque of the engine and the EM is constant during the journey, such as 10 km/h 3% gradient. The engine torque is slightly higher than the required torque at crankshaft because the EM need to supply electrical accessory load to maintain the SOC. As shown in the histogram, there is only one operating point for engine and EM each. The DP handles control and state variables as a quantised level, so the optimal solution frequently has small chattering between two values. This is the reason why the peak of the histogram is not at 100%.

The last case is 90km/h, 6% gradient, in which battery SOC goes up to 70%, stays for some time and then drops down to 60%. The torque level shows large chattering but the histogram tells the operating points are still only two. At the mechanical point of view, this is same as the first case, but the battery internal resistance is rapidly increased over 70% SOC as presented in Figure 4-2. Therefore, optimal solution is staying at this point rather than increasing more and then decreasing. This will be proved in the next sub-section starting from higher SOC.

Figure 6-8 and Figure 6-9 illustrate the EM and the engine operating points respectively. ‘o’ marks point out single operating point cases, and two ‘x’s connected by a line represent the cases which have two operating points. At the EM efficiency point of view, the operating points are not optimal and it is hard to find a rule intuitively. On the other hand, engine operating points show a trend. Two operating point cases switch the operating condition between two optimal efficiency lines, between the optimal efficiency line and the WOT line, or laid on the engine friction curve.

The preliminary conclusions from the first investigation are as follows,

- The optimal operation in steady state is staying in one condition or switching two operating points.
- The operating points are closely related to engine efficiency rather than EM efficiency.

In the next two sub-sections, those conclusions will be investigated and proved in different conditions.

6.2.2 STAGE 2 - EFFECT OF BOUNDARY CONDITIONS

In the stage 1, the boundary conditions of battery SOC are fixed as 60% at both ends. This is not always true in real driving situation. To see the effect of different boundary conditions, four operating points are investigated with different initial and final SOC level. The results are presented in Figure 6-10, Figure 6-11, Figure 6-12, and Figure 6-13. The trend is not different from the stage1. The engine and the EM are operated at a single point or switched between two points. These are illustrated in Figure 6-14 and Figure 6-15.

In the case of 10 km/h, 0% gradient shown in Figure 6-10, the engine drives the vehicle and charges the battery when the final SOC is higher than the initial. The engine torque is over 50Nm at which normalised engine efficiency is over 70%. On the contrary, the operating points are switching between the closed throttle line when the final SOC is equal to or less than the initial. In this case, the optimal control of engine is bang-bang because the average of the required engine torque is so small that the efficiency is very low. The EM drives the vehicle for some period and generates the electricity to supply the electrical accessory load in rest of the journey.

Next case is 20 km/h, 3% gradient which is in Figure 6-11. Regardless of the SOC profiles, the operating point is only one. Engine torque levels are between 60 and 120 Nm. As presented in Figure 6-15, the engine speed is idle and the normalised engine efficiency is 70 ~ 90%. This means that the engine should be used as a prime mover when the operating point is in the middle range of torque with high efficiency.

Figure 6-12 shows 30 km/h 9% gradient case. There are two operating points when EM is charging or maintaining SOC through the journey. In the charge depleting situation, the engine and the EM are working at a single point. The engine operating points are located in around 1500 rev/min in Figure 6-15. The single operating point is on the IOL, and the two operating points are positioned on the IOL and the WOT line. From this results, it is concluded that the IOL and the WOT line are a candidates of optimal operating points.

The final case is 60 km/h with 9% gradient. Required torque at crankshaft is highest among the four cases because of the high road load, but the behaviour of the controller is similar to the other cases. Regardless of the boundary conditions, there are two operating points as illustrated in Figure 6-13. In case of charge depleting, which requires less torque from engine, the engine is working on either of the IOLs. To charge the battery to increase the SOC, the operating points of the engine move up above the upper IOL, but not reach to the WOT. The reason of this is found in Figure 6-14. The real optimal operating point could be a point on the WOT line, but the EM maximum power limits the torque.

From the above investigation, the preliminary conclusions of the sub-section 6.2.1 can be refined as follows;

- The optimal operation in steady state is staying in one condition or switching two operating points, and independent from the boundary conditions.
- If the required torque is very low, which means the engine efficiency is very low, then the optimal engine control is bang-bang.
- If the required torque is medium which is below the lower IOL, then the optimal operating point has a single value.
- If the required torque is between the two IOLs, the engine runs on either of these two lines.
- If the required torque is over the upper IOL, then the engine operating point is on the IOL or WOT line. However, the higher torque point cannot be over the maximum EM generating torque plus the upper IOL torque.

6.2.3 STAGE 3 : JOURNEY DURATION

Journey time is another parameter which was not covered in previous sub-sections. If the journey duration is very short or long, then the optimal control action could be different because the SOC is a time dependent variable. To investigate this effect, simulation were performed with different journey duration, from 1 to 20 minutes. The results are depicted in Figure 6-16, Figure 6-17, Figure 6-18 and Figure 6-19. The operations are not different from the stage 1. The only difference by the duration change is the time portion of charging and depleting when there are two optimal operating points. This is clear in Figure 6-20 and Figure 6-21, too. The engine and the EM operating points are exactly same as the stage 1 and 2. Consequently, it is clear that the optimal control points are independent from the journey duration.

6.2.4 STAGE 4 : ENGINE OPERATING POINT

From the result of previous sub-sections, optimal torque distribution is a function of the required torque at crankshaft but independent from initial and final battery SOC and journey duration. Therefore, it is necessary to investigate the optimal solution directly at each engine operating point instead of the vehicle driving condition. By generating a grid of points on normalised engine efficiency map, it is found that the whole domain can be divided into 6 zones as follows;

- Zone 1 (in Figure 6-22 and Figure 6-23)

$$\begin{aligned} &\text{Condition}: && T_{ENG,CTT} < T_{ENG,req} \le -T_{EM,MOT} \\ &\text{Engine torque}: && T_{ENG} = T_{ENG,req} \end{aligned} \tag{6-3}$$

- Zone 2 (in Figure 6-24 and Figure 6-25)

$$\begin{aligned} &\text{Condition}: && \max\left(T_{ENG,CTT}, -T_{EM,MOT}\right) < T_{ENG,req} \le \min(-T_{EM,GEN}, 50) \\ &\text{Engine torque}: && T_{ENG} = \begin{cases} \max\left(T_{ENG,CTT}, -T_{EM,MOT}\right) & , \Delta SOC \le 0 \\ \min(-T_{EM,GEN}, 50) & , \Delta SOC > 0 \end{cases} \end{aligned} \tag{6-4}$$

- Zone 3 (in Figure 6-26 and Figure 6-27)

$$\begin{aligned} &\text{Condition}: && \min(-T_{EM,GEN}, 50) < T_{ENG,req} \le T_{IOL,LOW} \\ &\text{Engine torque}: && T_{ENG} = T_{ENG,req} \end{aligned} \tag{6-5}$$

- Zone 4 (in Figure 6-28 and Figure 6-29)

$$\begin{aligned} &\text{Condition}: && T_{IOL,LOW} < T_{ENG,req} \le T_{IOL,HIGH} \\ &\text{Engine torque}: && T_{ENG} = \begin{cases} T_{IOL,LOW} & ,\Delta SOC \le 0 \\ T_{IOL,HIGH} & ,\Delta SOC > 0 \end{cases} \end{aligned} \tag{6-6}$$

- Zone 5 (in Figure 6-30 and Figure 6-31)

$$\begin{aligned} &\text{Condition}: && T_{IOL,HIGH} < T_{ENG,req} \le \min\left(T_{IOL,HIGH} - T_{EM,GEN}, T_{ENG,WOT}\right) \\ &\text{Engine torque}: && T_{ENG} = \begin{cases} T_{IOL,HIGH} & ,\Delta SOC \le 0 \\ \min\left(T_{IOL,HIGH} - T_{EM,GEN}, T_{ENG,WOT}\right) & ,\Delta SOC > 0 \end{cases} \end{aligned} \tag{6-7}$$

- Zone 6 (in Figure 6-32 and Figure 6-33)

$$\begin{aligned} &\text{Condition}: && \min\left(T_{IOL,HIGH} - T_{EM,GEN}, T_{ENG,WOT}\right) < T_{ENG,req} \le T_{ENG,WOT} \\ &\text{Engine torque}: && T_{ENG} = T_{ENG,req} \end{aligned} \tag{6-8}$$

Zone 1 and 2 cover low torque area on the normalised engine efficiency map. Zone 2 is a low torque region in which the engine has poor efficiency. As tested through stage 1 ~ 3, the optimal control of the engine in this zone is bang-bang control. When the engine is off, the EM should provide the torque to spin the engine and drive vehicle. If target SOC is higher than the current value, the EM generates electricity at maximum power but less than 50Nm. This limit implies that direct driving by engine is more efficient than alternating charging and discharging battery above 50Nm at which the engine efficiency is better than 70%. Zone 1 is an extreme case of zone 2. Even though the engine efficiency is very low, the required torque is beyond the EM motoring capability. As a result, the engine should be fuelled and the EM works as an alternator.

Zone 3 represents the mid torque range and the powertrain works as a conventional vehicle like as zone 1. Basically, the engine has good efficiency in this region, so electric assist or battery charging is not necessary to improve the overall efficiency.

The high region is divided into zone 4, 5 and 6. The engine switches two operating points in zone 4 and 5. The borderlines of zone 4 are the lower and upper IOL, which are the most efficient points. According to the target and current SOC, the engine would be assisted by the EM or charge the battery. The working principle of zone 5 is similar to zone 4 because the WOT line is another optimal operating points from the efficiency point of view. Therefore the engine chooses either of the WOT line or the upper IOL as

an operating point. Zone 6 is the extreme case of zone 5, which is over the EM generating capacity. In this zone, the powertrain works same as in zone 1.

If the required torque of the engine is belonged to zone 2, 4, or 5, the controller set the command at this value. In the other zones, the controller chooses either low or high torque set point when the required SOC gradient is negative or positive respectively. The decision of the required SOC gradient comes from an adaptive-network-based fuzzy inference system (ANFIS), which will be explained in the next section.

6.3 BATTERY ENERGY MANAGEMENT

The battery energy management is the most important and difficult part of hybrid vehicle control, because a battery is a bi-directional energy storage device. An engine is a uni-directional powerplant, which generates mechanical energy by burning fuel in order to drive the vehicle but this process is not reversible. However, a battery can store or supply energy, so SOC is a time dependent variable. It means battery SOC is affected by past throughput energy and should be controlled considering future usage to get an optimal performance. It is difficult to describe this process mathematically because of so many unpredictable parameters such as driver's intension and traffic condition that are nonlinear, time-varying, and non-causal. Therefore, fuzzy logic is more preferable than model-based control systems. Fuzzy logic can describe complex system with non-linearity and uncertainty as a black-box using input-output relationship[177]. In the next sub-sections, design, optimisation and comparative study of the fuzzy controller will be explained.

6.3.1 CONTROLLER DESIGN

As described in Section 6.1 and Figure 6-1 and Figure 6-2, the inputs of the controller are estimated future vehicle speed and wheel torque and current SOC. The output of the controller is desired SOC change rate, which is positive if charging the battery is required and negative when engine assist is more preferable. Therefore, the fuzzy controller has 3-input 1-output structure.

There are two different structures of fuzzy inference system (FIS), Mamdani-type[178] and Sugeno-type [179]. These two types of inference systems vary somewhat in the way outputs are determined. Mamdani-type is more intuitive and easy to interpret input-

output relationship. On the other hand, Sugeno-type is better for mathematical implementation that fits to computer-based optimisation process, especially combined with the NN based optimisation algorithm. In this study, the ANFIS [180-182] is used in order to implement and optimise the controller. The ANFIS consists of a Sugeno-type FIS as a front-end and the NN to optimise parameters of the FIS. The ANFIS can be trained by the result from the DP, which provides the global optimal solution for a given condition.

Even though the ANFIS is a good tool to optimise parameters of the FIS, the structure of the FIS is a different matter. To build a FIS, the shape and the number of membership function should be determined. Widely used membership functions are Gaussian and triangular. Gaussian membership function requires more computation than triangular, but smoother transition phase between membership functions over the whole domain. The NN based automatic optimisation algorithm with triangular membership functions could be unstable because of the lack of the data in some parts of the domain. It gives discontinuity between domain and range or fails to find the optimised parameter set. Hence, Gaussian membership function is chosen in this study.

The very basic design of the FIS starts from small number of membership functions evenly spaced in the domain. However, this approach is not very efficient if there are huge amount of data is available for parameter optimisation. Furthermore, there is a trade-off between performance and computation time if the number of membership function is increased. Therefore, it is beneficial to start optimisation from a pre-conditioned initial structure including number of membership functions and centre position of each function. One of the approaches is fuzzy clustering, and this study uses subtractive clustering method [183], which is an improved algorithm from mountain clustering method [184].

The initial design parameters of the controller are listed in Table 6-1. Window resolution is directly related to infrastructure, which is not currently available for this kind of application. Rajagopalan, and Washington[105] demonstrate a predictive control strategy in time horizon with 5 data points in 150 seconds. However, actual infrastructure is not likely to provide the data in time based, because monitoring stations would be installed along the roads in fixed geographical locations and the navigation

system broadcast the data on the digital map. Considering the average vehicle speed of the NYCC, LA92 and US06 is 41.8 km/h, 30 seconds is equivalent to 348m. Deguchi et al [112] assume 150m information resolution for their study, which reflects recent technological advance in navigation system. In the initial design in this study, window resolution is setup as 200m. Controller can determine window offset and size and 5 and 10 points are used at the first respectively. Cluster radii are related to the input and output data clustering process. Large value gives less centre points which means less number of rules in the FIS.

To train the NN, the DP was performed in the NYCC, LA92 and US06 in level road. Three initial SOC, 40, 60, and 80% are chosen as boundary conditions and the final SOC is 60% in all cases. Therefore, total nine traces are used in order to optimise the controller parameters for combined case in Table 6-2. Optimised parameters by the NN show that the RMS error of the output is 18.05%, which is the difference of SOC change rate between the DP and the ANFIS output. Number of rules is only 3, mainly caused by the large cluster radius.

Another possibility of the predictive control is that the navigation system would be able to provide road classification such as urban, extra urban or motorway. In this case, individually tuned parameter set can be used in each driving cycle, and might improve the controller performance. To demonstrate the improvement by road classification, the FIS is trained in each cycle with three dataset that have different initial SOC, and the result compared in Table 6-2. In the NYCC and LA92, the RMS error is lower than the combined case even though the number of rules is same or less. US06 shows worse result, but this is the initial trial so can be improved by the optimisation presented in the next section.

6.3.2 PARAMETER OPTIMISATION

To optimise the controller, seven control variables should be determined to supply the training data for the NN. Three different levels of control variables are listed in Table 6-3. The variables related to the prediction window are increased and decreased from the initial design because there is no definite evidence to find the right direction. The cluster radii should be reduced because the initial result shows too small number of rules.

Finding an optimal combination of these variables is time-consuming computational work if full factorial test is involved, which requires 3^7 NN training for each driving cycles. Considering maximum 15 minutes in case of combined cycle training, this is not realistic practice. To reduce the optimisation trials, DOE is used in the process. DOE is a design tool to minimise the number of experiments to find the optimal combination of the controls where too many control variables are related each other. There are several type of design for this purpose, and this study uses Taguchi method [185] that adopts orthogonal array to navigate the control variable domain. Table 6-4 shows the L18 orthogonal array, which can cover up to eight variables and three levels. This method reduces number of experiments from 3^7 to 18 for each driving cycles, so the total 72 NN training process is required.

The DOE results listed in Table 6-4 too. It shows that the RMS error can be reduced significantly but the number of rules increases as well. The contribution of individual control variables is illustrated from Figure 6-34 to Figure 6-41. In all cases, the parameters related to the prediction window significantly affect the RMS error. If the windows resolution reduced to 100m, the error is not very affected or even worse in the case of LA92, because this reduces the prediction horizon. In the case of the NYCC, zero offset gives good result because the cycle has very short distance. On the other hand, LA92, which is the longest cycle, would be improved by long window size. In general, the small RMS error requires large number of rules. However, the cluster radii are more dominant factor to decide the number of rules, so there is an optimal compromise between the control performance and the complexity of the controller.

There are infinite number of solutions for compromised solution, so this study fix the maximum number of rules as 10 and find the combination of the control variables to minimise the error. The estimated values by linear programming (LP) from DOE and the final trained NN simulation are compared in Table 6-5. The LP estimated values are quite close to the trained NN. The error is considerably reduced and the number of rules is within the target value. Individually trained controllers show less error than combined case, but the US06 is the exceptional case. This is able to be explained from the figures of membership function, which is in Figure 6-42, Figure 6-43, Figure 6-44, and Figure 6-45. The axis are normalised from minimum to maximum of the data. The nominal

values of membership functions are well distributed over the vehicle speed and wheel torque. However, in the case of US06, most of the membership functions are located at each ends. As illustrated in Figure 5-3, the operating points of US06 is highly concentrated in high speed - low torque region or low speed – high torque region. The former case is high speed cruising, and the later case represents initial acceleration and final deceleration phase. Therefore, the NN cannot be trained properly to cover the whole domain more smoothly. In the NYCC, the membership functions of SOC is centralised at 0.5 which correspond to 60% SOC. Because of the short distance, the optimal control by the DP tends to control SOC to the final boundary condition.

Even though some cases mentioned above are exceptional, the general trends of the design result are well matched with the common sense, which is;

- If the predicted future vehicle speed is high and wheel torque is low then SOC should go down, because regenerative braking is expected.
- If the predicted future vehicle speed is low and wheel torque is high then SOC should go up, because engine assist for vehicle acceleration is expected.
- If the current SOC is high, then SOC should go down to avoid reaching battery SOC high limit.

6.3.3 SIMULATION RESULT

Using the controller designed in the previous sub-section, simulation is performed in three cycles with three different elevations. Table 6-6 shows the summary of fuel economy. The predictive control provides considerable amount of fuel saving from the baseline controller in the downhill cases. It was expected by the DP in the previous chapter because the baseline controller is not able to manage the battery SOC properly during continuous recuperation. The improvement on the level road is marginal, and the impact is negative in the case of uphill climbing. This result comes from the limited improvement margin by the mild hybridisation, as demonstrated by the DP in the previous chapter. The result shows that the predictive control is more effective for longer journey. As presented in the table, the LA-92 presents better improvement than the other cycles, and the NYCC is the worst case. The controller tuned by individual cycle delivers slightly more benefit than the case of single calibration, but still has a gap

to true optimal performance by the DP. This is caused by the limits of online control, which are the coarse resolution of future journey information and the receding horizon predictive window instead of the infinite horizon optimal solution.

The battery SOC trajectories and the difference between the initial and final points are depicted in Figure 6-46 and Table 6-7, compared with the result from baseline controller and the DP. In most cases, the predictive controller shows better performance than the baseline controller, and the result is close to the global optimal calculated by the DP. In addition, individually tuned controllers are better than the case trained by combined dataset. In downhill driving, the controller maintains SOC well below the high limit so saturation is not occurred during the cycles. In case of uphill, the predictive controller makes the final SOC closer to the initial value, which means SOC is well controlled by future journey information, even though there is a small amount of fuel economy penalty. In the level road, there is little difference between four controllers because the baseline controller works well as in the standard cycles.

6.4 SUMMARY OF PREDICTIVE CONTROL INVESTIGATION

In this chapter, the potential benefit of the predictive control has been investigated. The main tools of the controller design were the DP, the ANFIS with subtractive clustering and DOE. Using a quasi-static backward simulation model, the performance of the controller is compared with the result from the baseline control and the DP. The focus is fuel saving and SOC control at the end of journeys, especially in aggressive driving conditions and a hilly road. The structure of the controller consisted of two parts, which are the optimal torque split between the EM and the engine and the calculation of desired SOC. The tuning of the controller was carried out for the individual cycles to represent city, urban/extra urban, and motorway, as well as the combination of those.

Fuel economy improvement and SOC correction are close to the optimal solution by the DP, especially in long trip on steep road on which there was a large gap between the baseline controller and the DP. The controller tuned in individual cycles demonstrates better performance than the case when generally tuned. This implies the performance of the predictive control highly depends on the quality of future journey information. In overall, the future journey estimation gives a good potential to improve fuel economy

and tight SOC control in long journey and hilly terrain, even though the benefit is marginal in short trip and flat road.

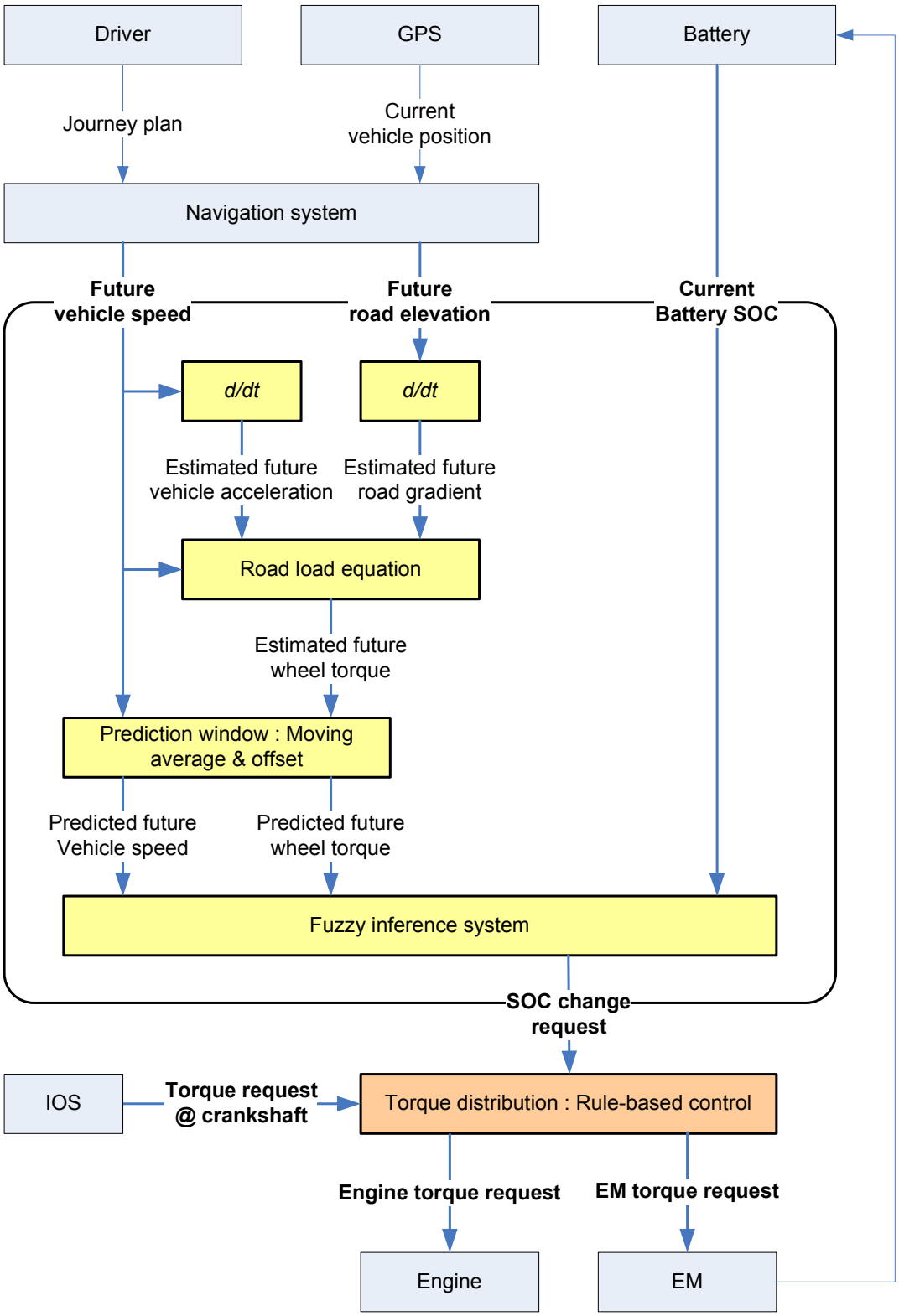

Figure 6-1 Structure of predictive controller

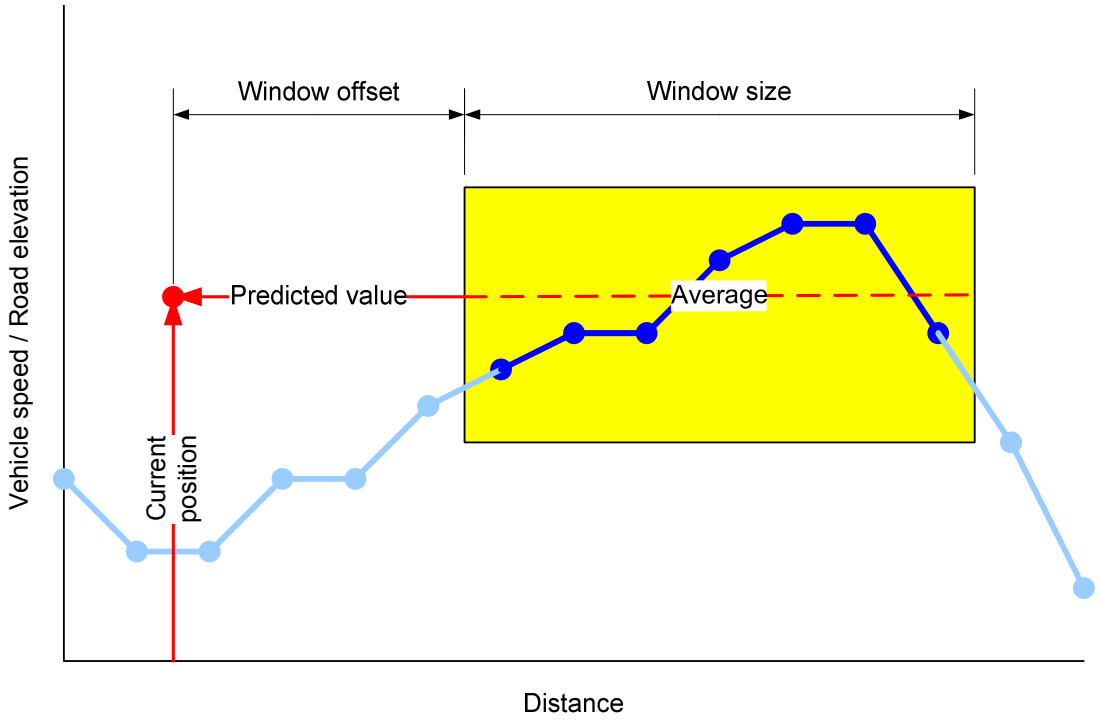

Figure 6-2 Prediction window

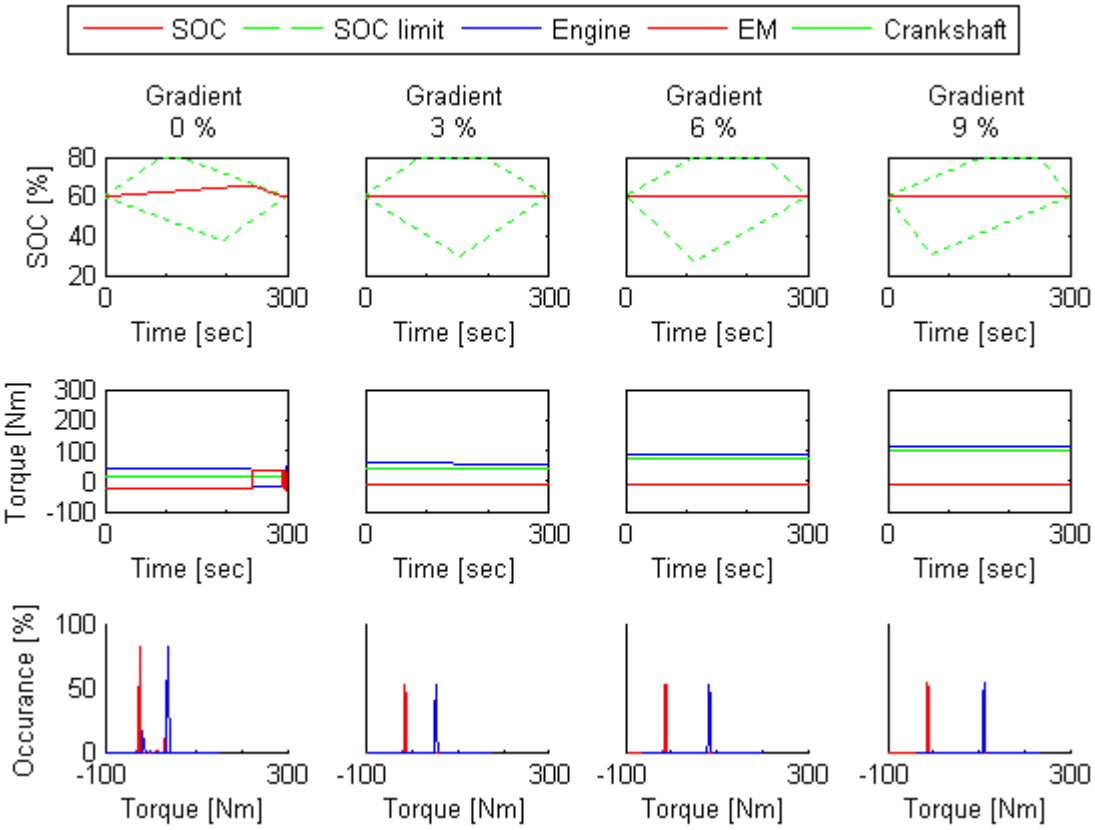

Figure 6-3 Stage 1 : 10 km/h

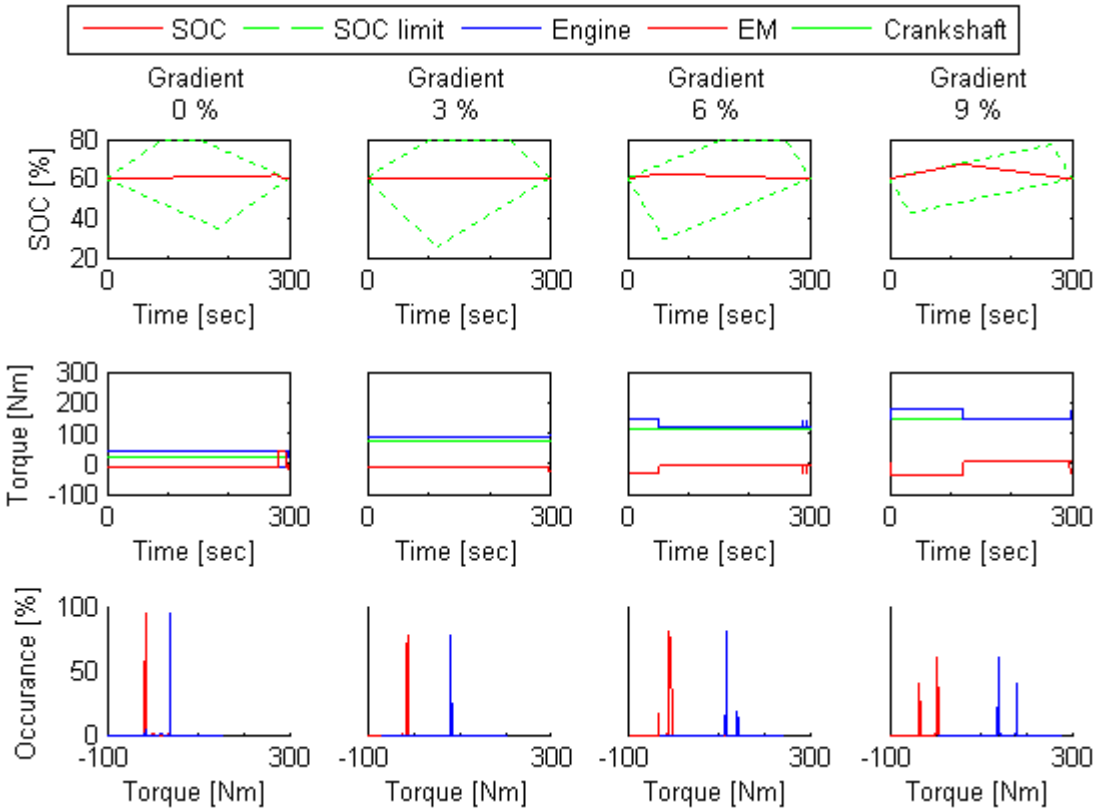

Figure 6-4 Stage 1 : 20 km/h

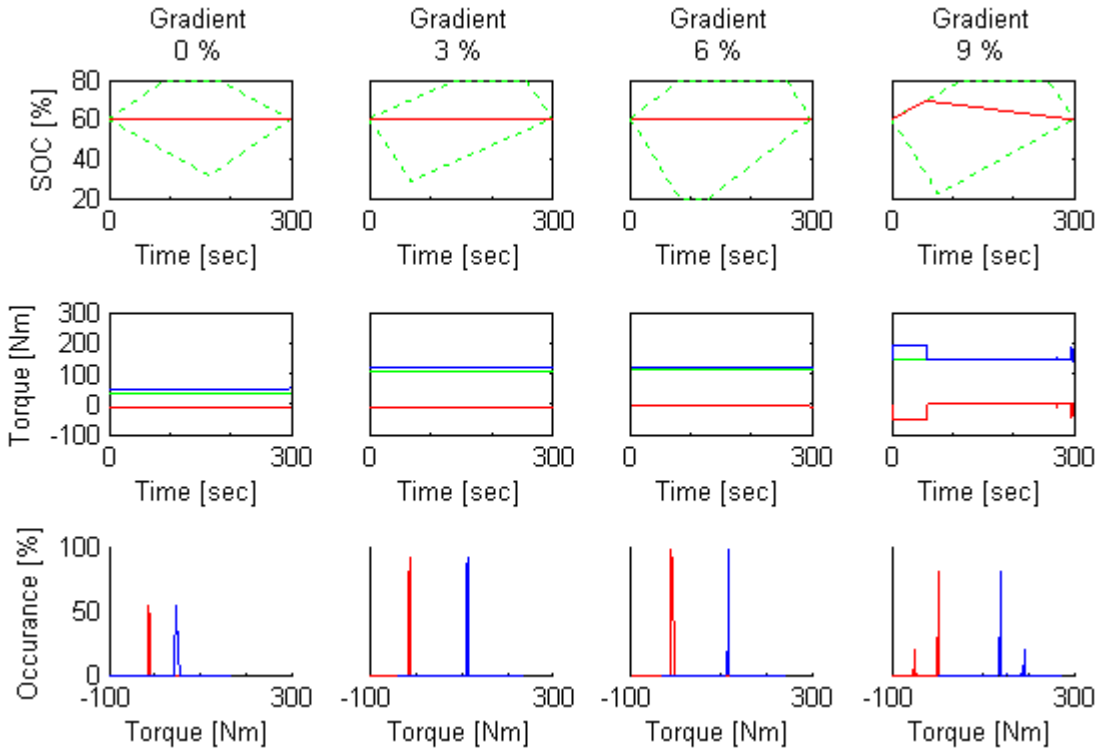

Figure 6-5 Stage 1: 30 km/h

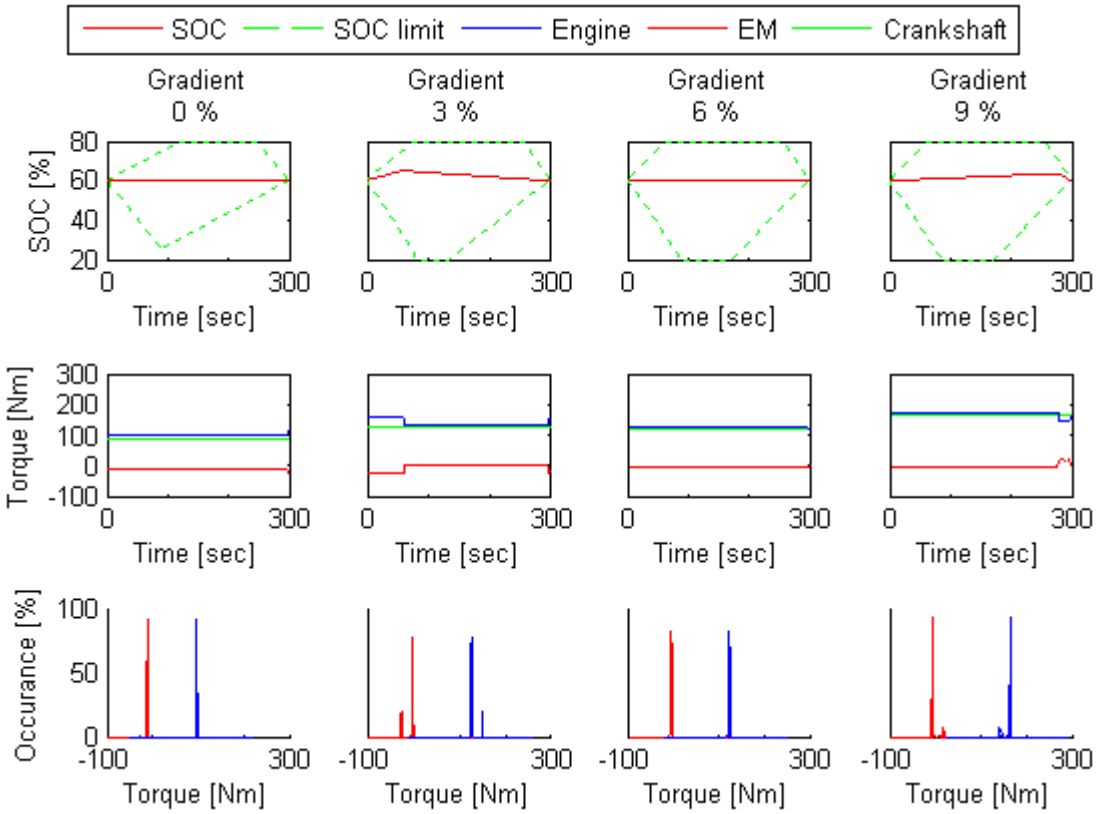

Figure 6-6 Stage 1: 60 km/h

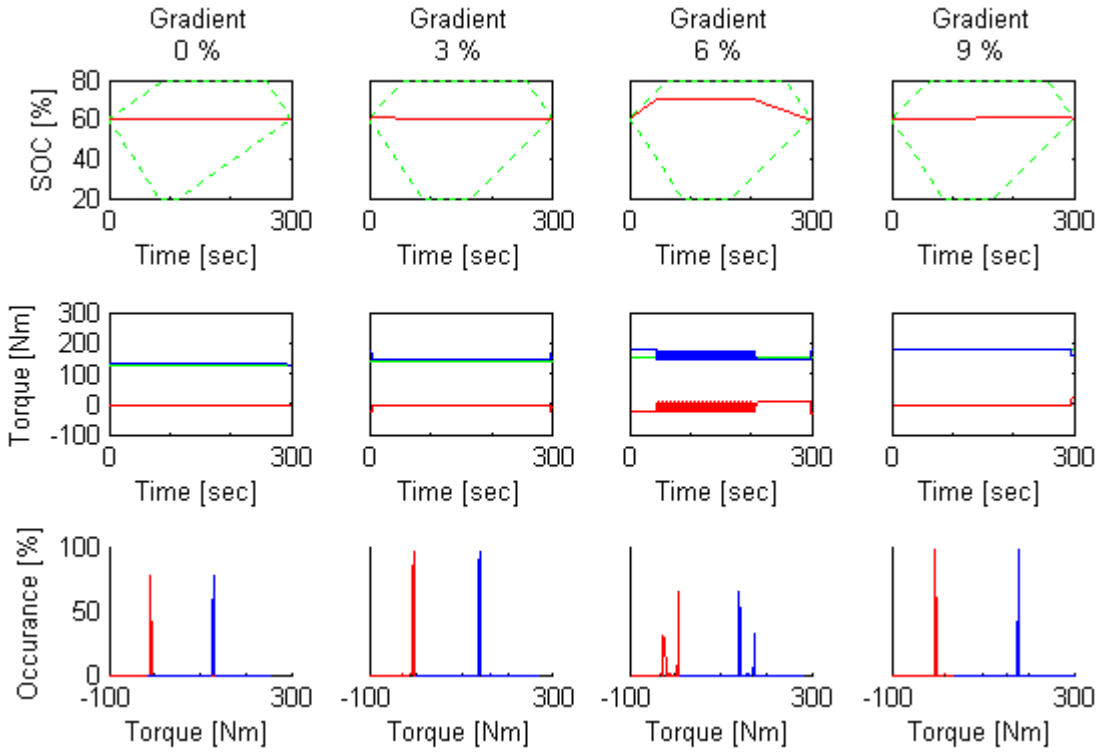

Figure 6-7 Stage 1 : 90km/h

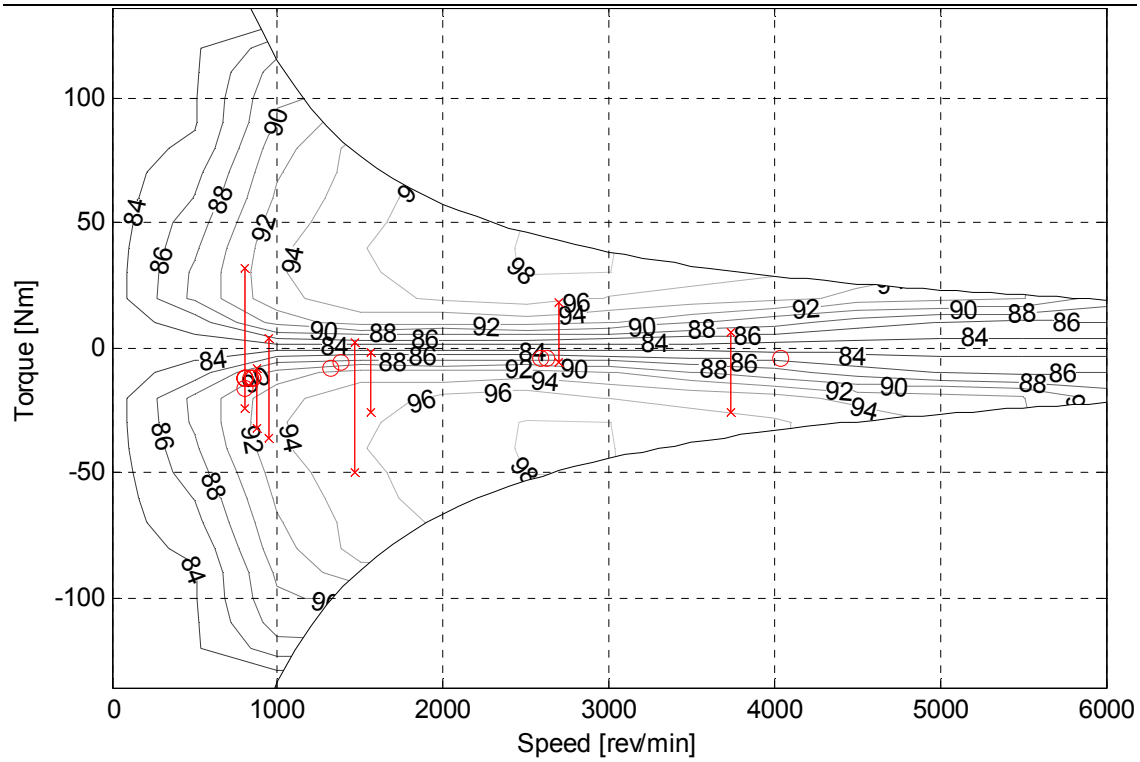

Figure 6-8 Stage 1 : EM operating points

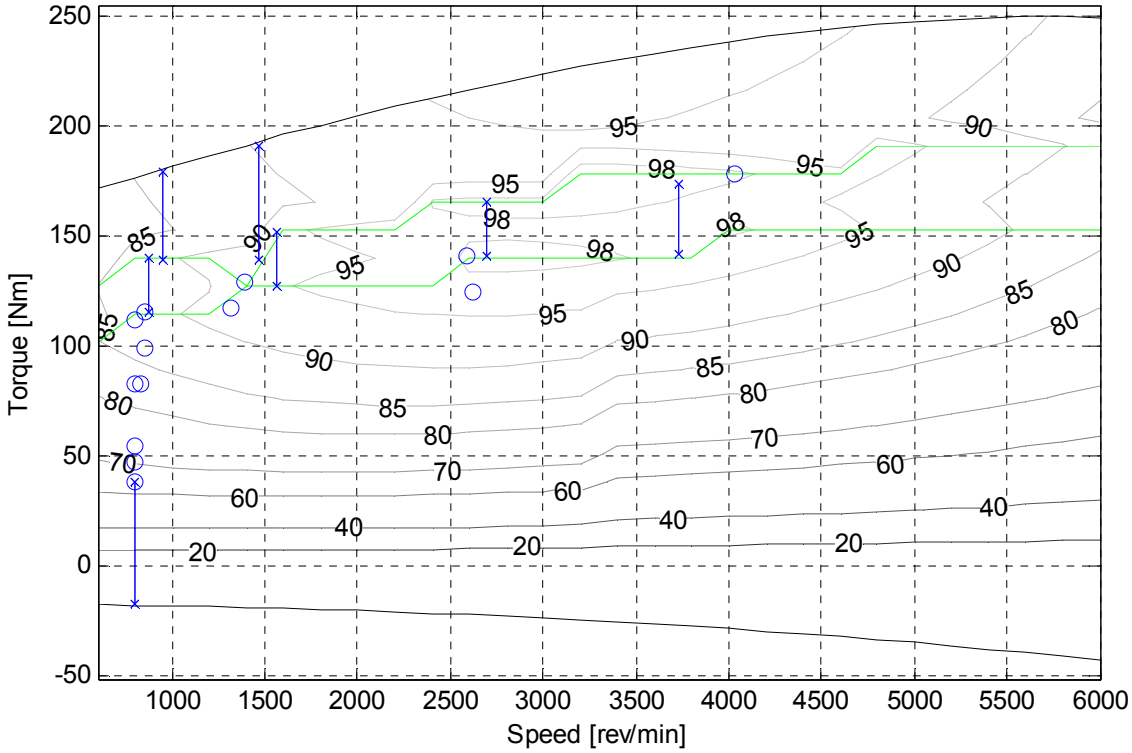

Figure 6-9 Stage 1: Engine operating points

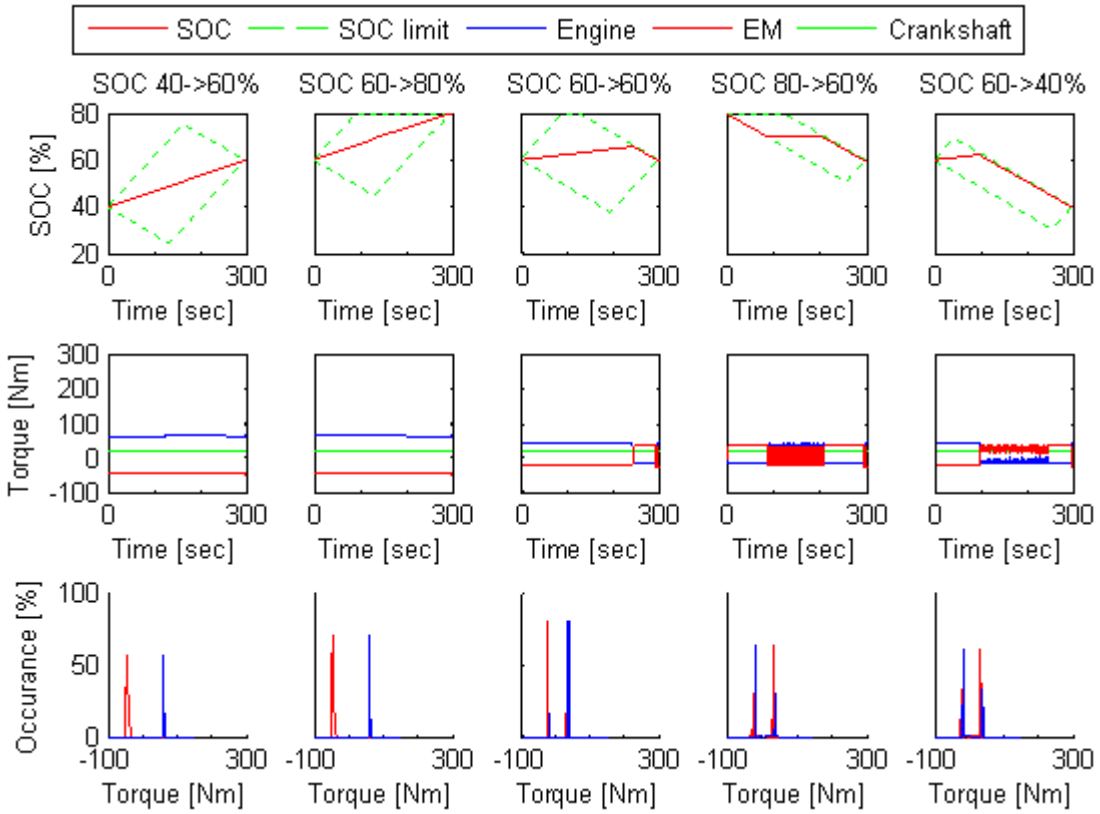

Figure 6-10 Stage 2: 10km/h, 0% gradient

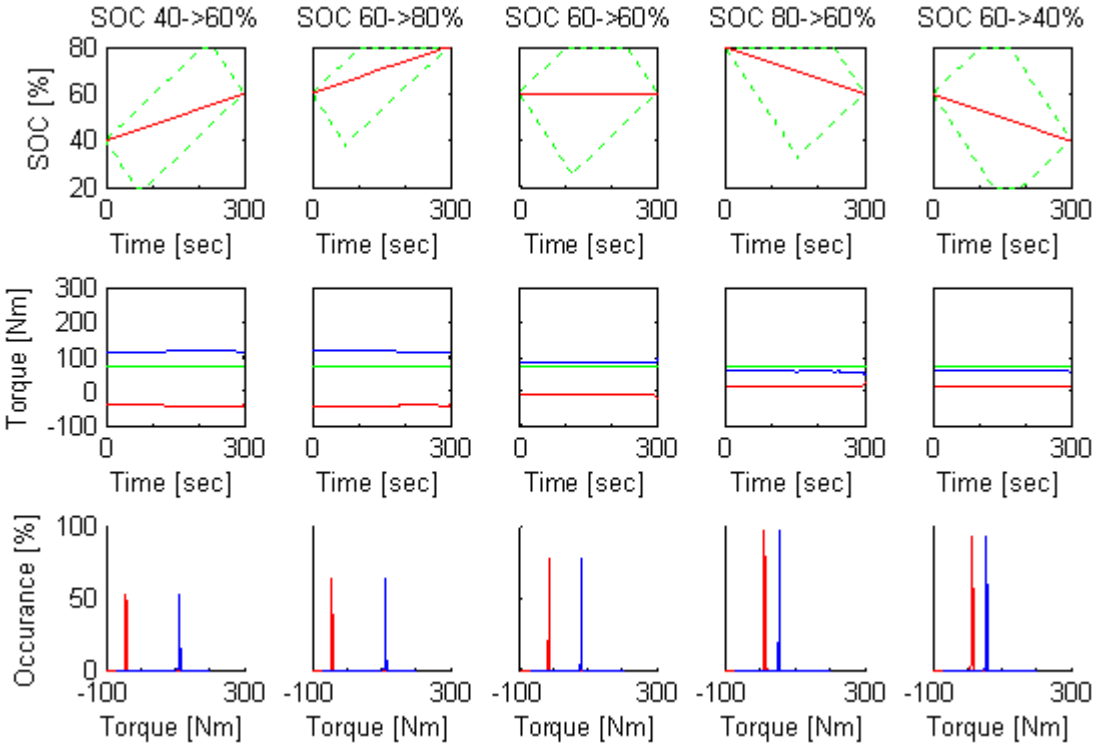

Figure 6-11 Stage 2: 20km/h, 3% gradient

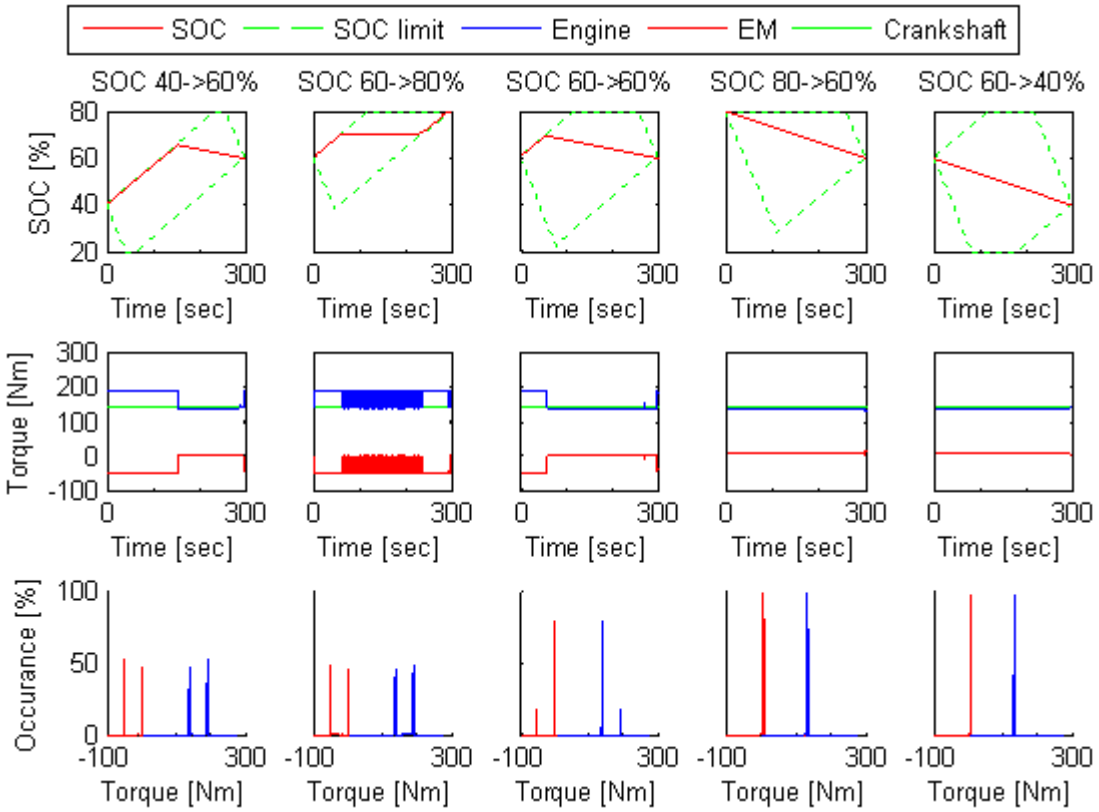

Figure 6-12 Stage 2: 30km/h, 9% gradient

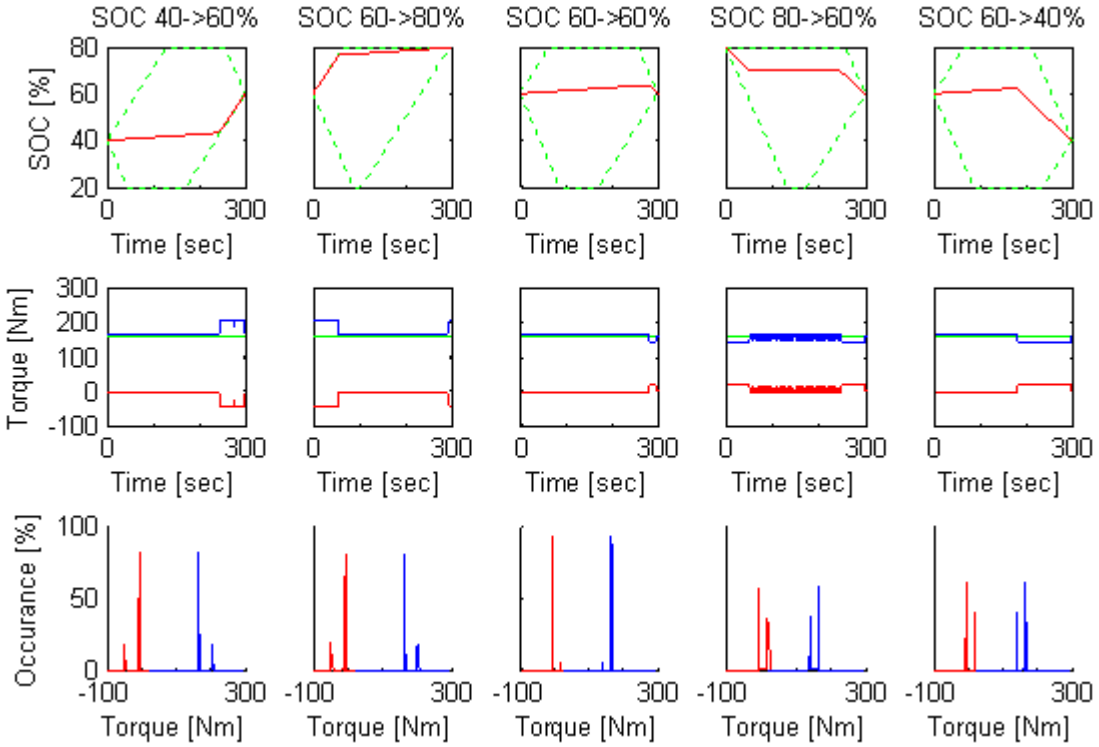

Figure 6-13 Stage 2: 60km/h, 9% gradient

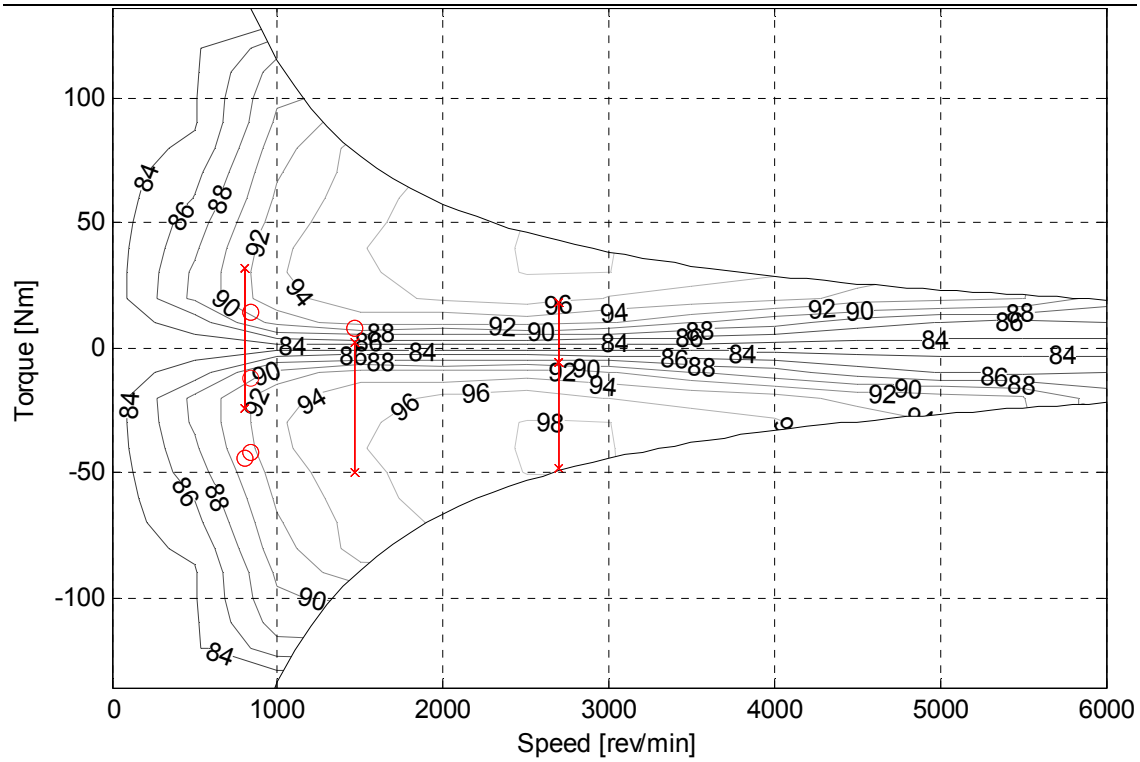

Figure 6-14 Stage 2: EM operating points

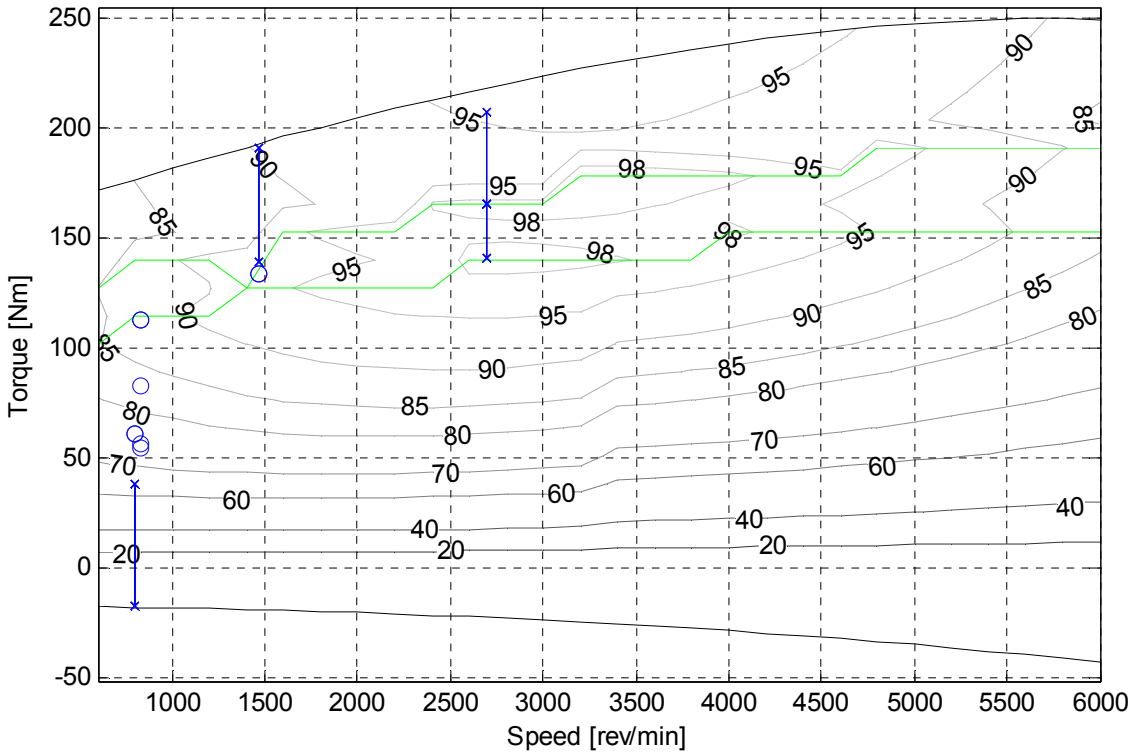

Figure 6-15 Stage 2: Engine operating points

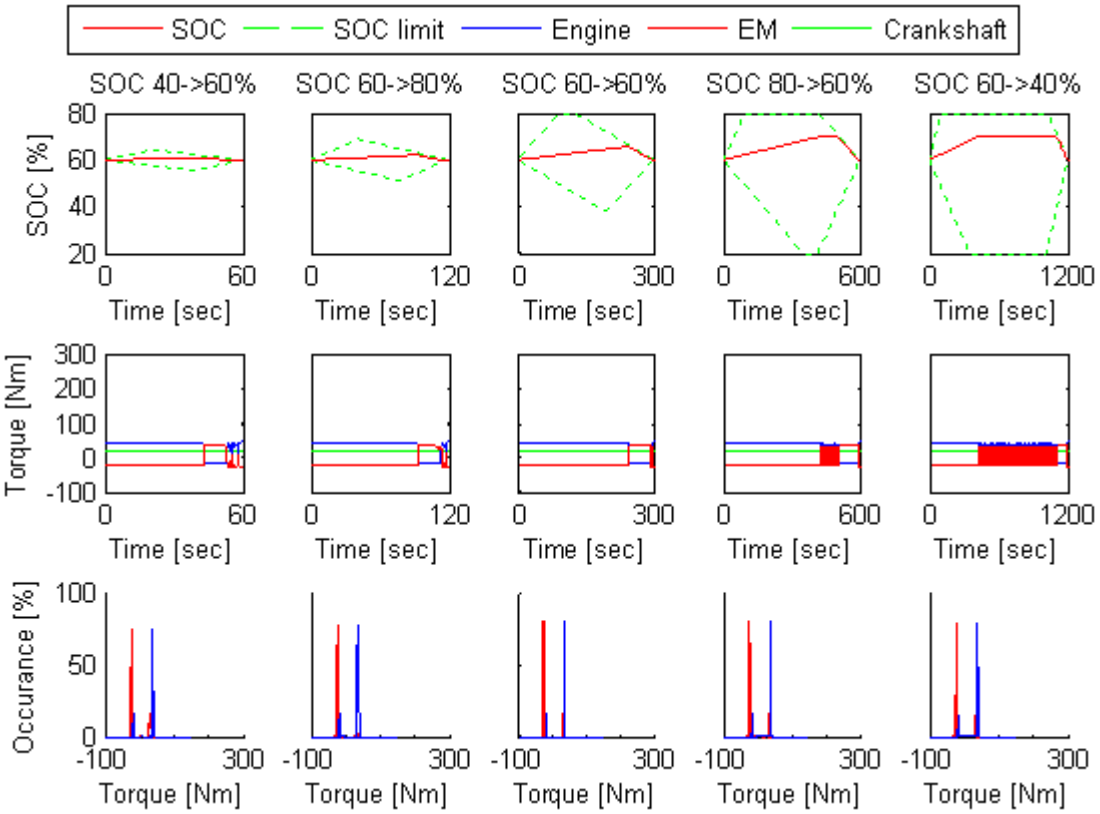

Figure 6-16 Stage 3: 10km/h, 0% gradient

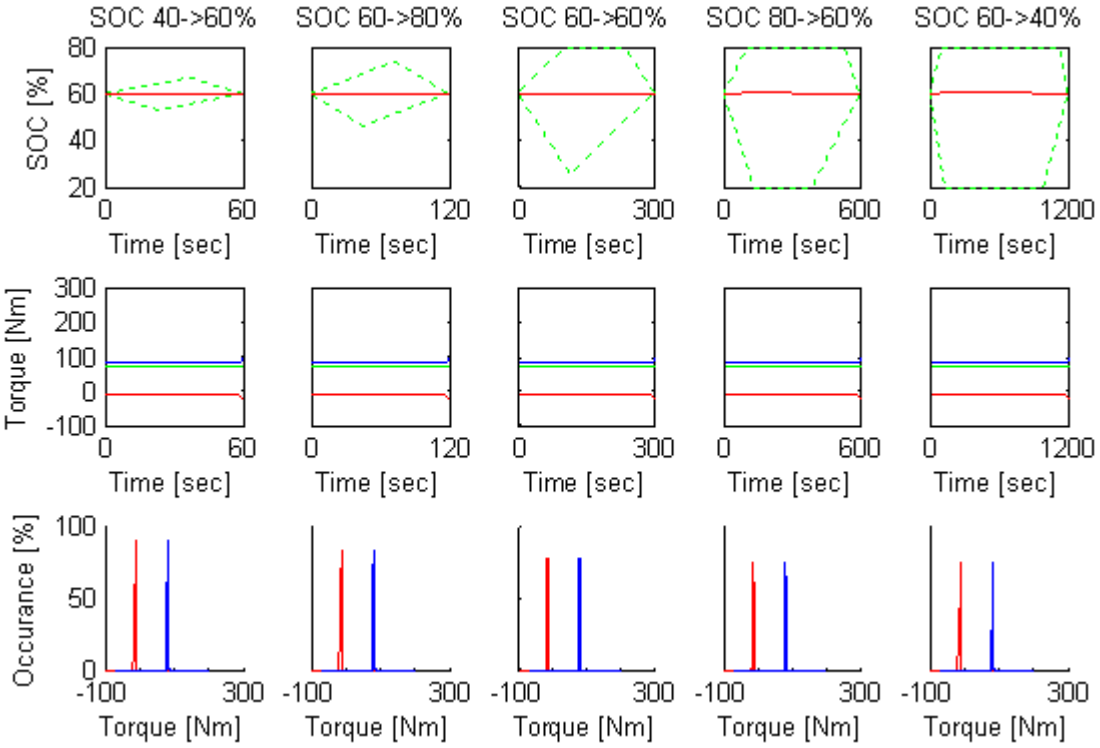

Figure 6-17 Stage 3 : 20km/h, 3% gradient

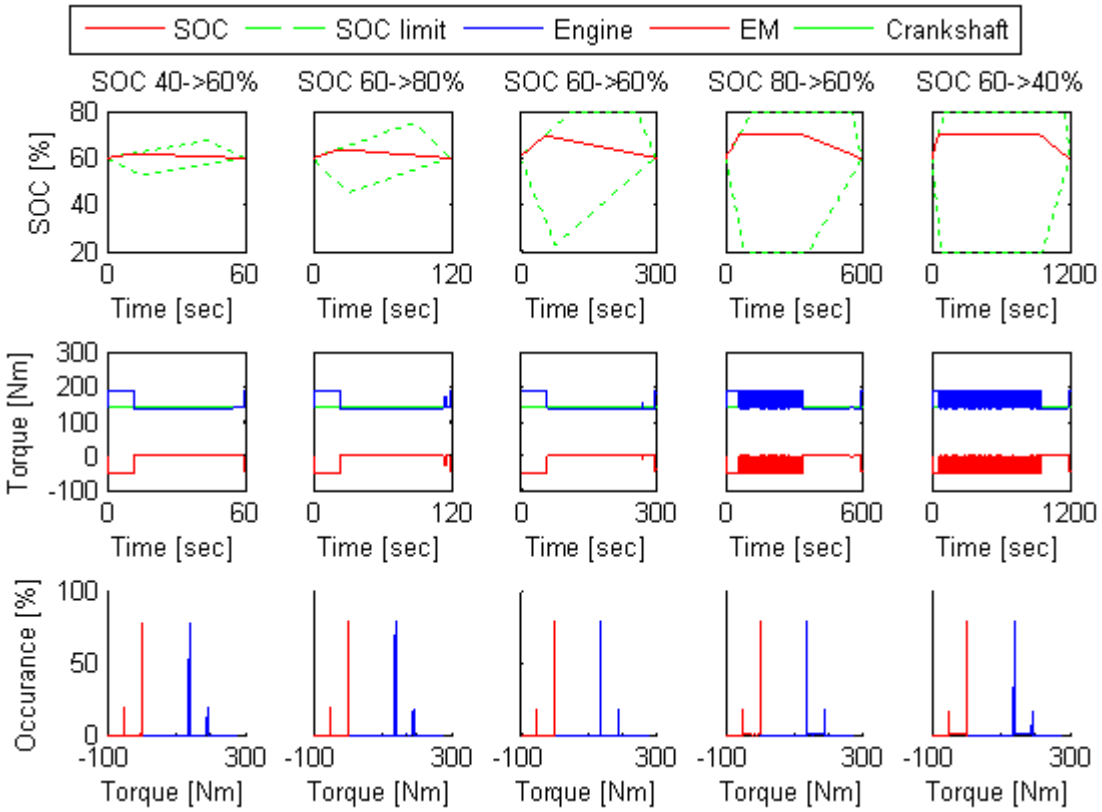

Figure 6-18 Stage 3: 30km/h, 9% gradient

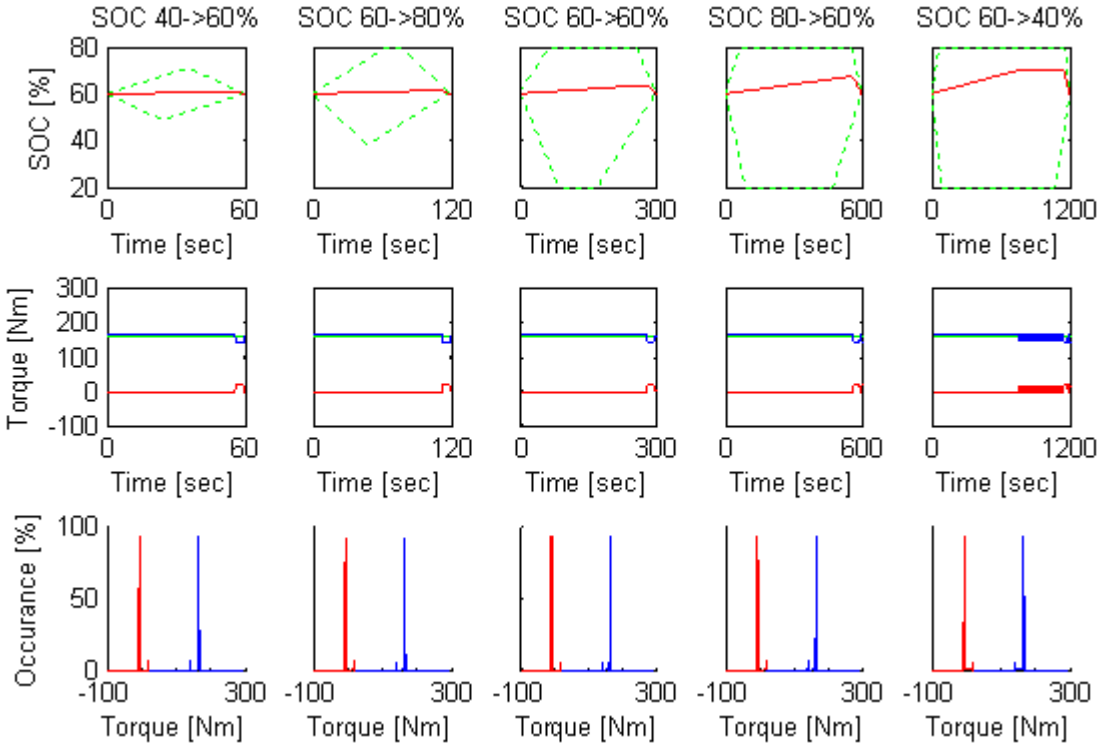

Figure 6-19 Stage 3: 60km/h, 9% gradient

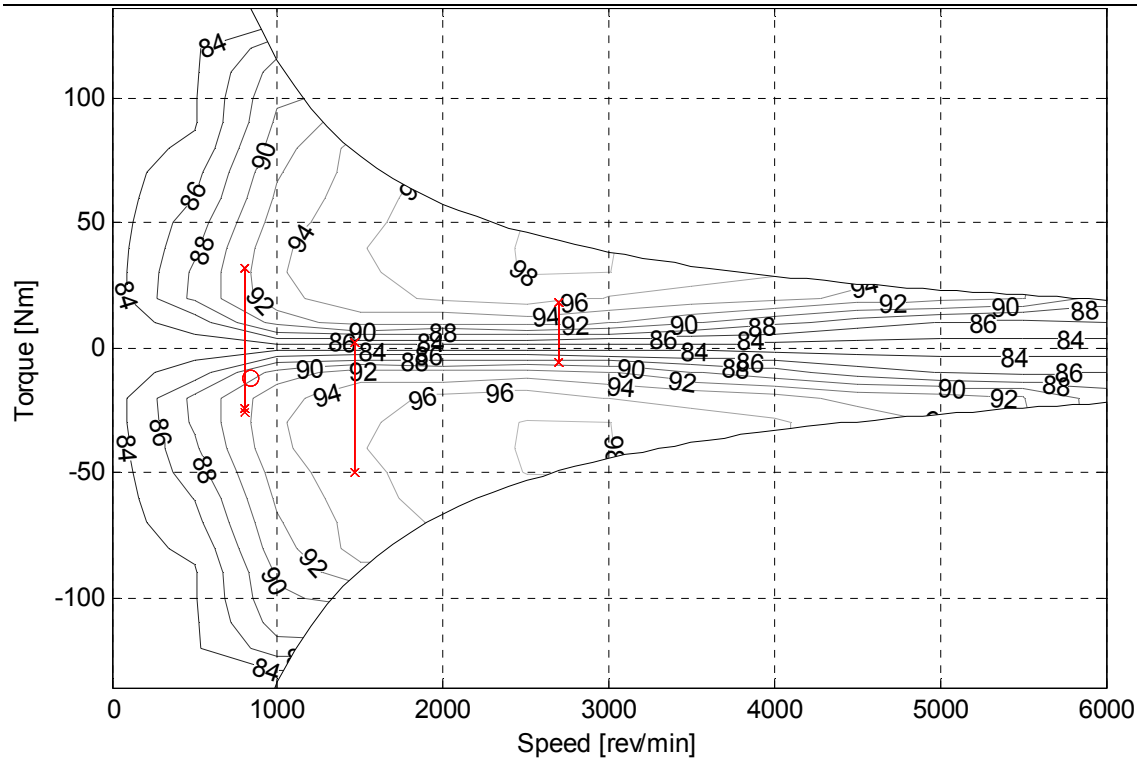

Figure 6-20 Stage 3 : EM operating points

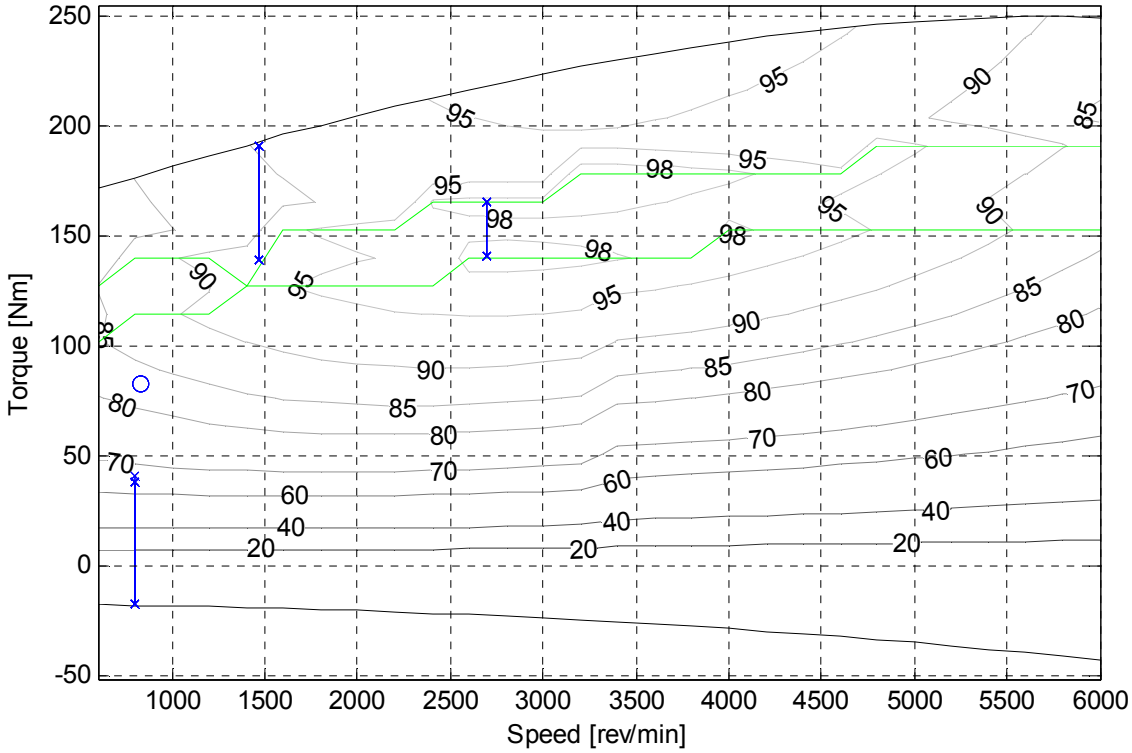

Figure 6-21 Stage 3: Engine operating points

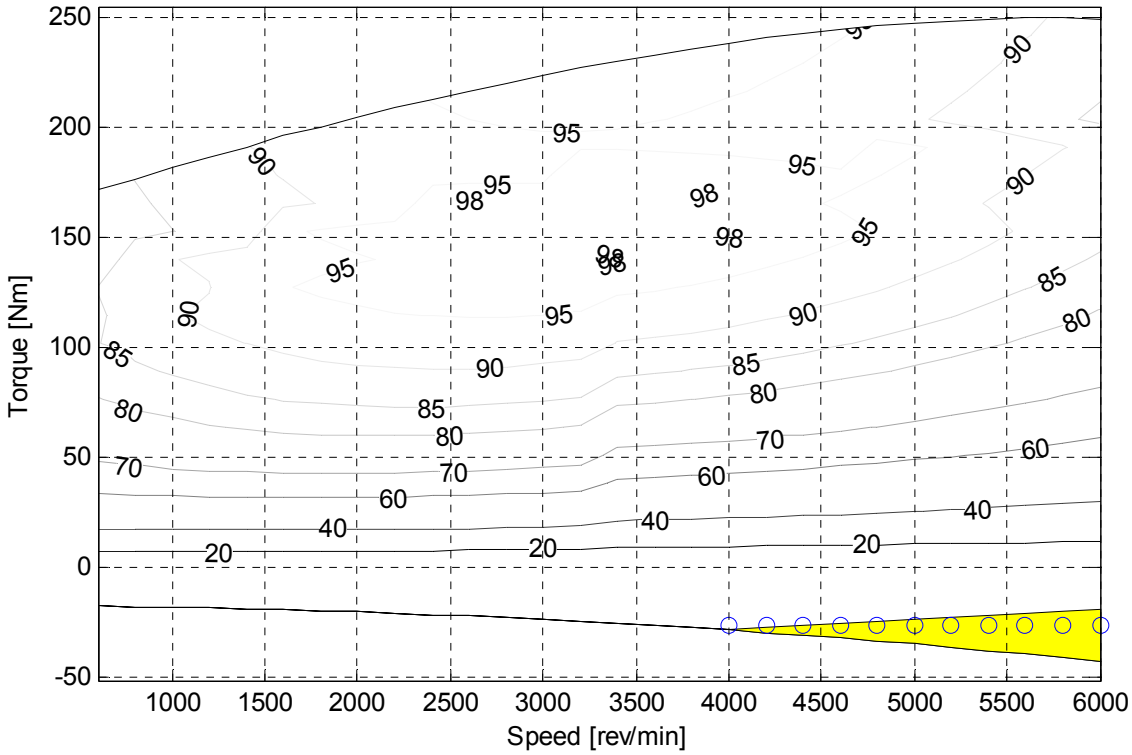

Figure 6-22 Stage 4: Engine operating points – Zone 1

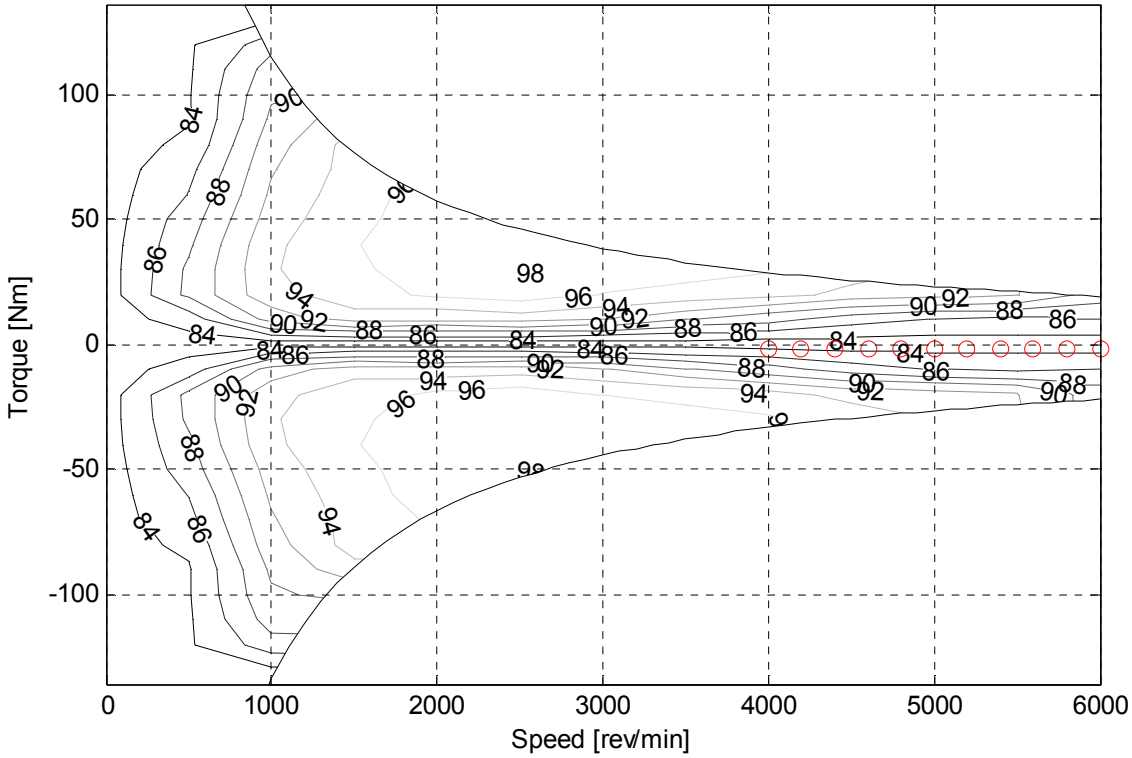

Figure 6-23 Stage 4: EM operating points – Zone 1

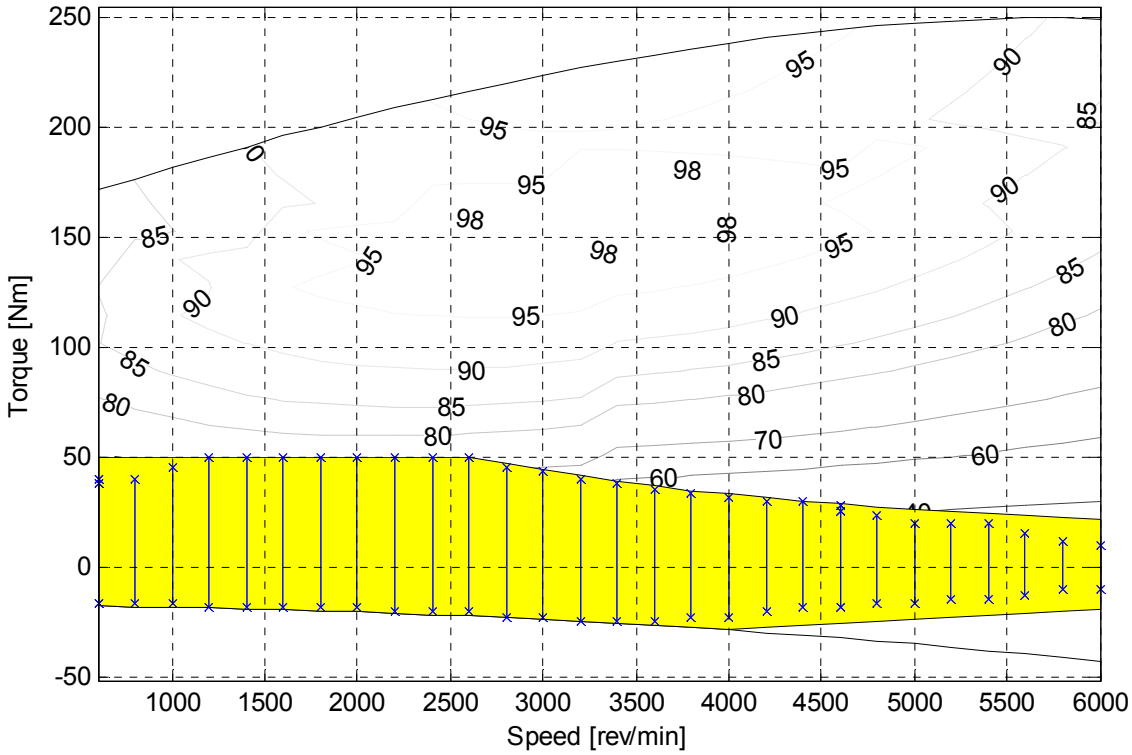

Figure 6-24 Stage 4: Engine operating points – Zone 2

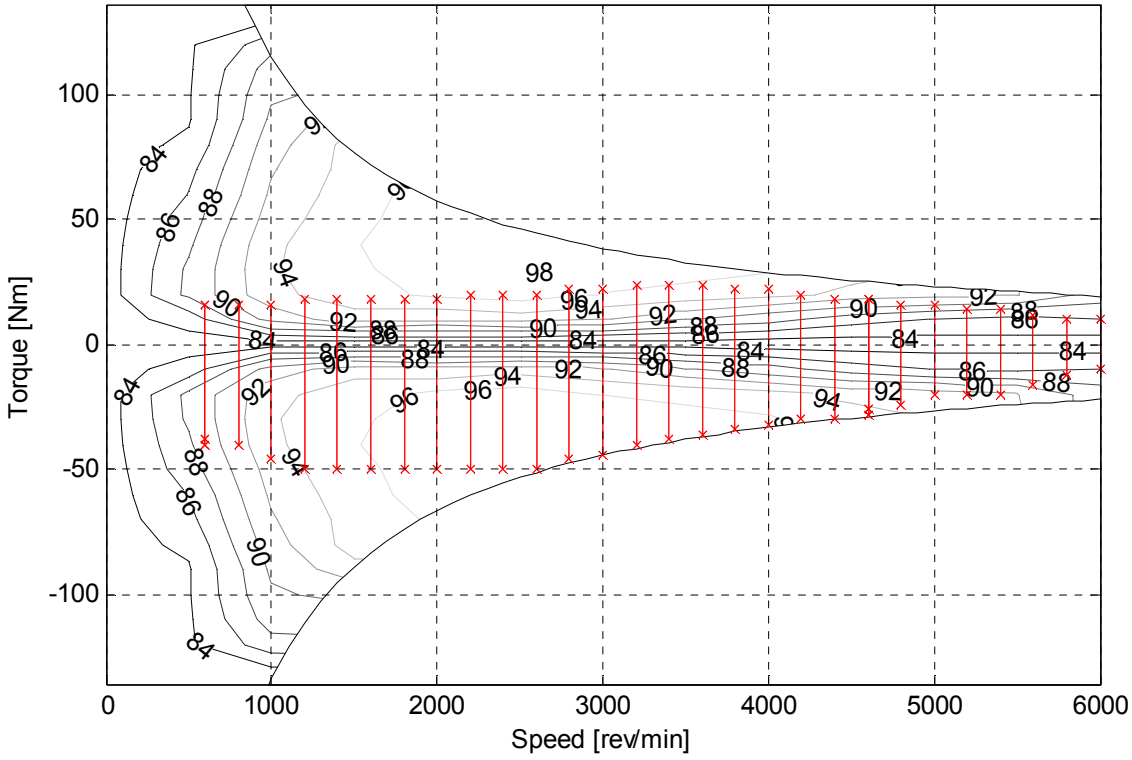

Figure 6-25 Stage 4: EM operating points – Zone 2

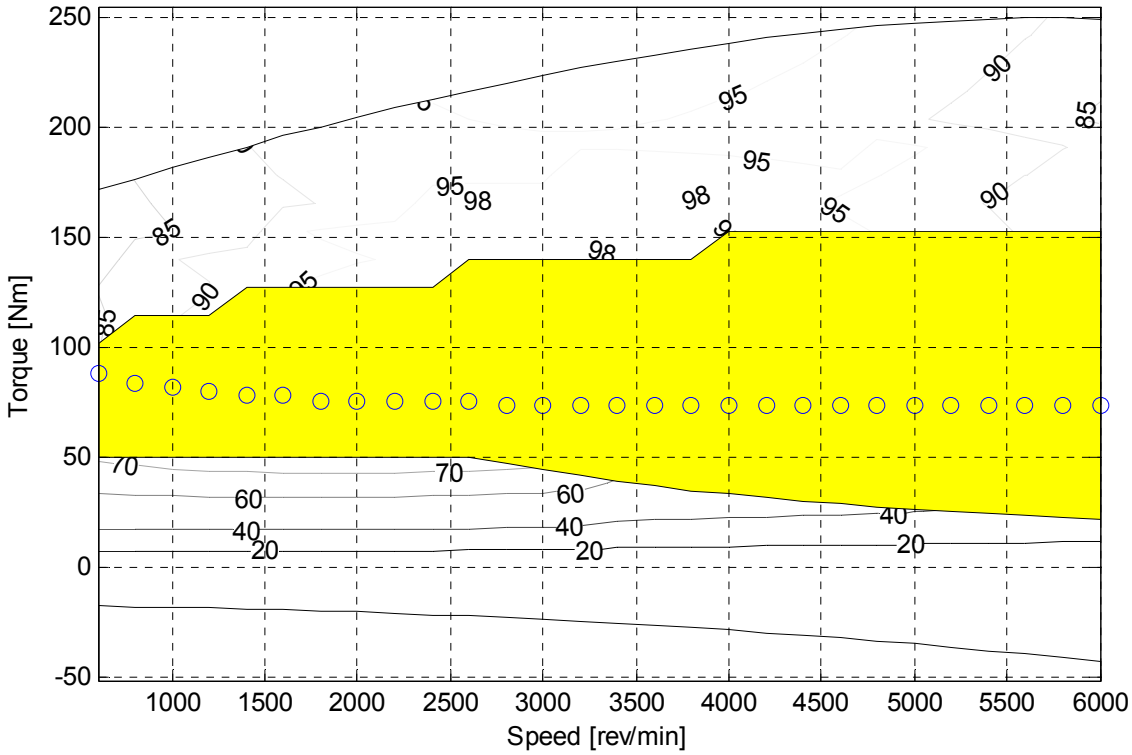

Figure 6-26 Stage 4: Engine operating points – Zone 3

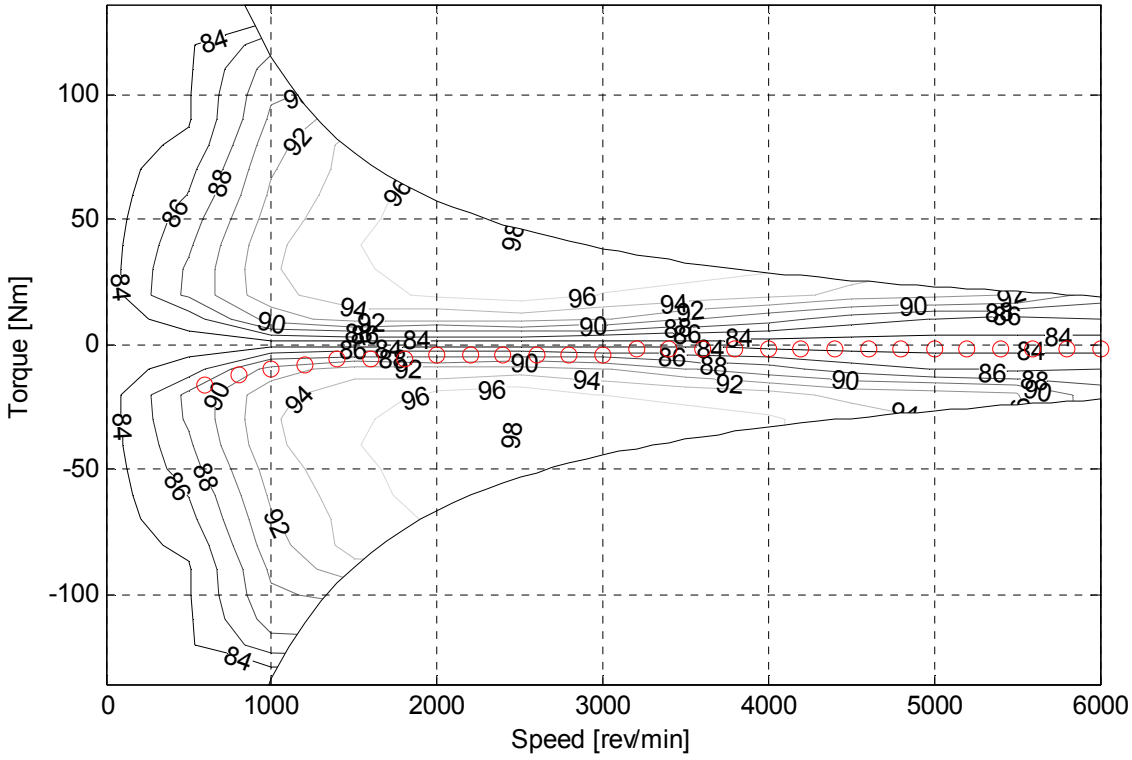

Figure 6-27 Stage 4: EM operating points – Zone 3

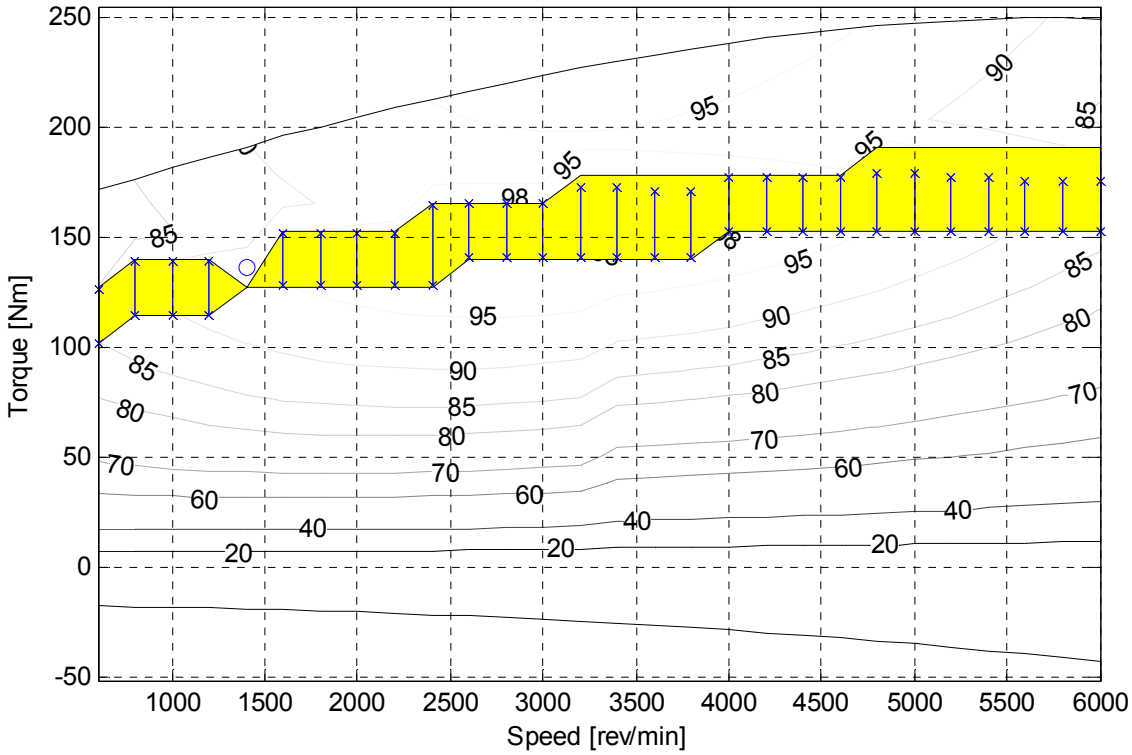

Figure 6-28 Stage 4: Engine operating points – Zone 4

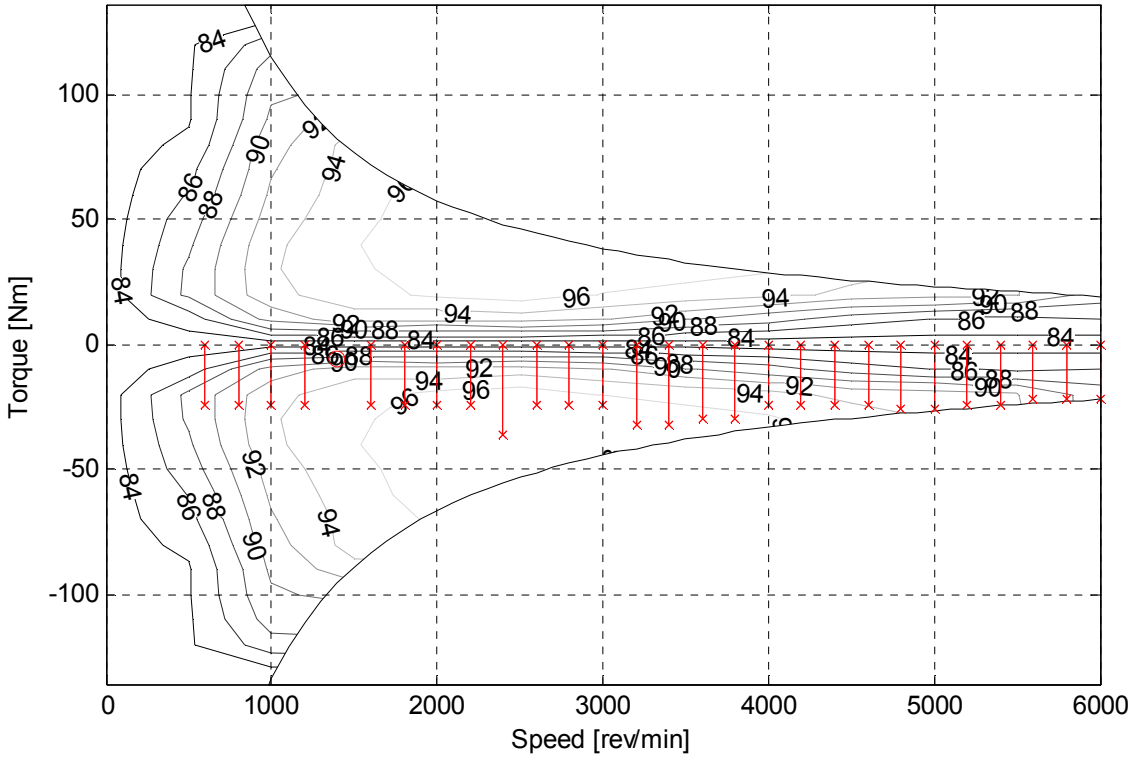

Figure 6-29 Stage 4: EM operating points – Zone 4

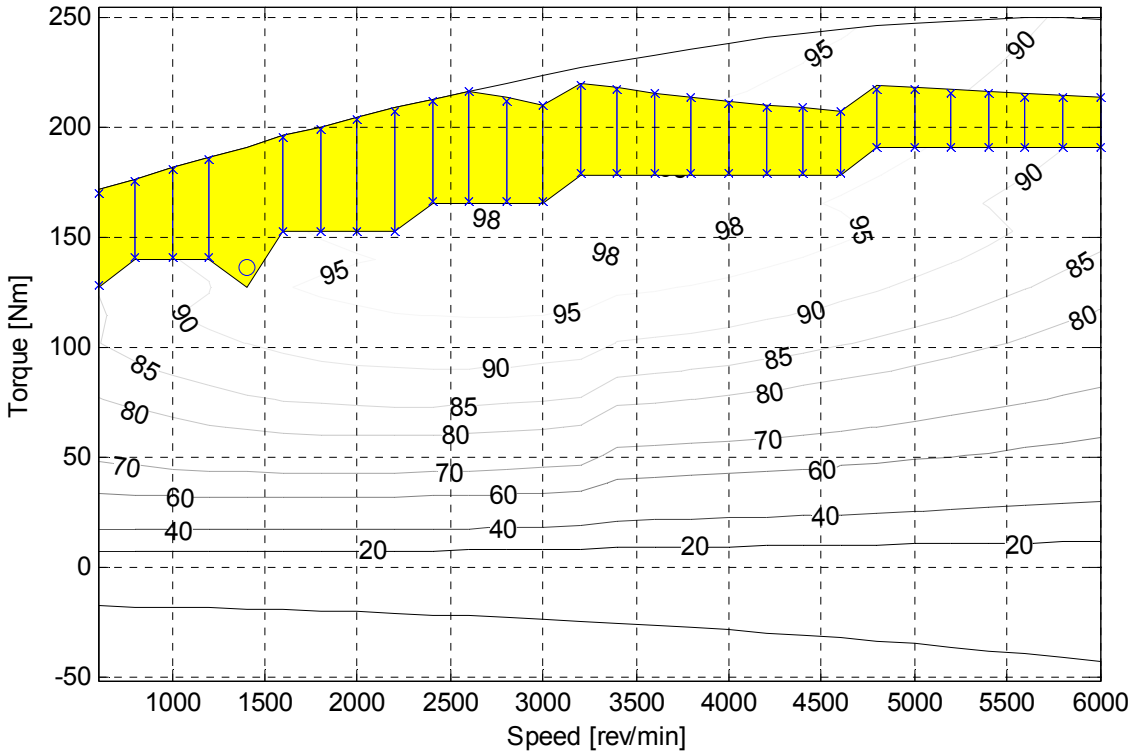

Figure 6-30 Stage 4: Engine operating points – Zone 5

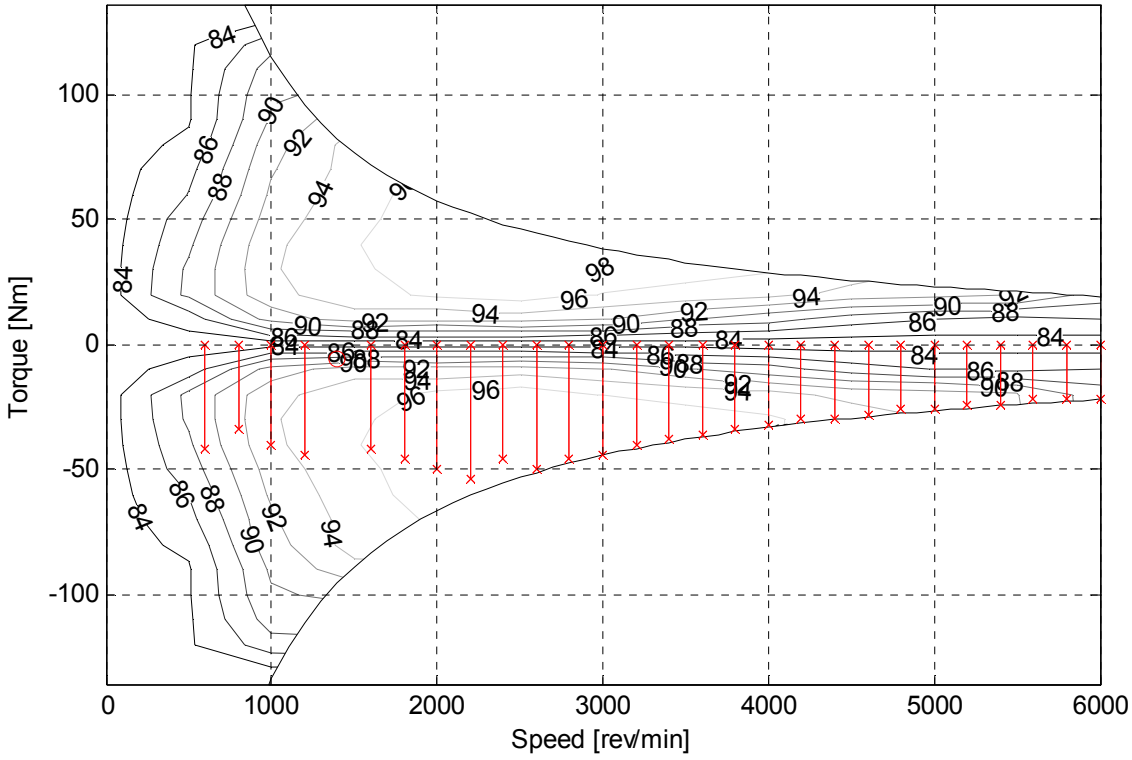

Figure 6-31 Stage 4: EM operating points – Zone 5

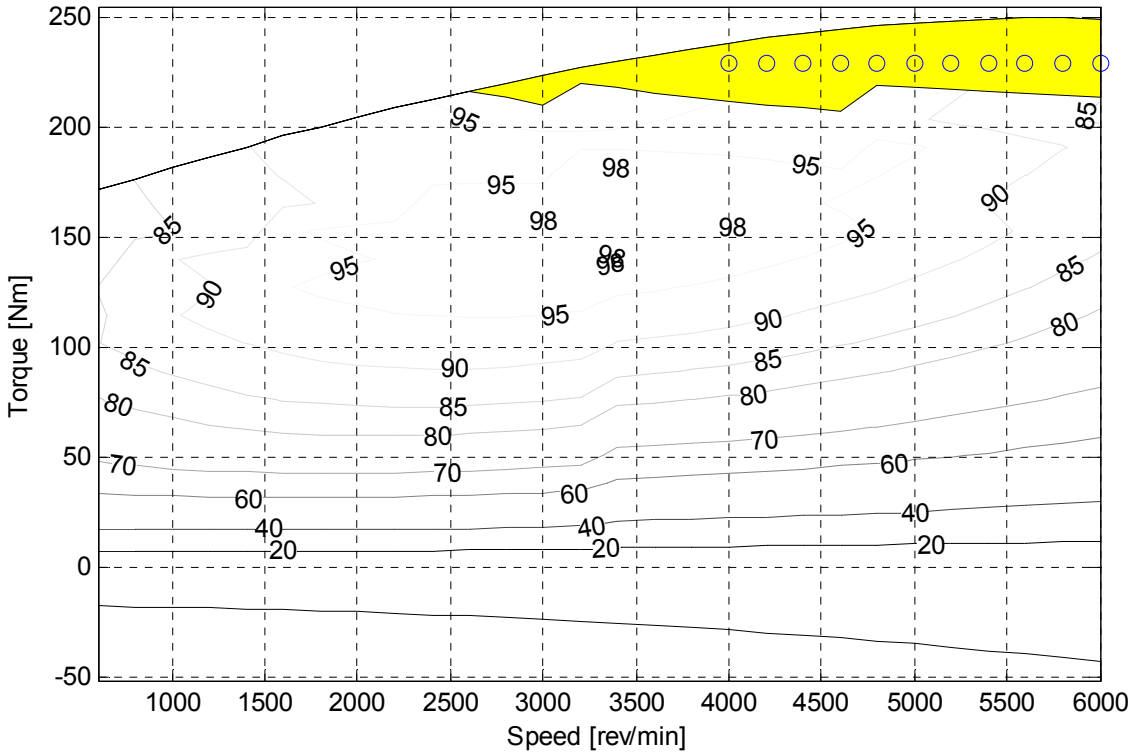

Figure 6-32 Stage 4: Engine operating points – Zone 6

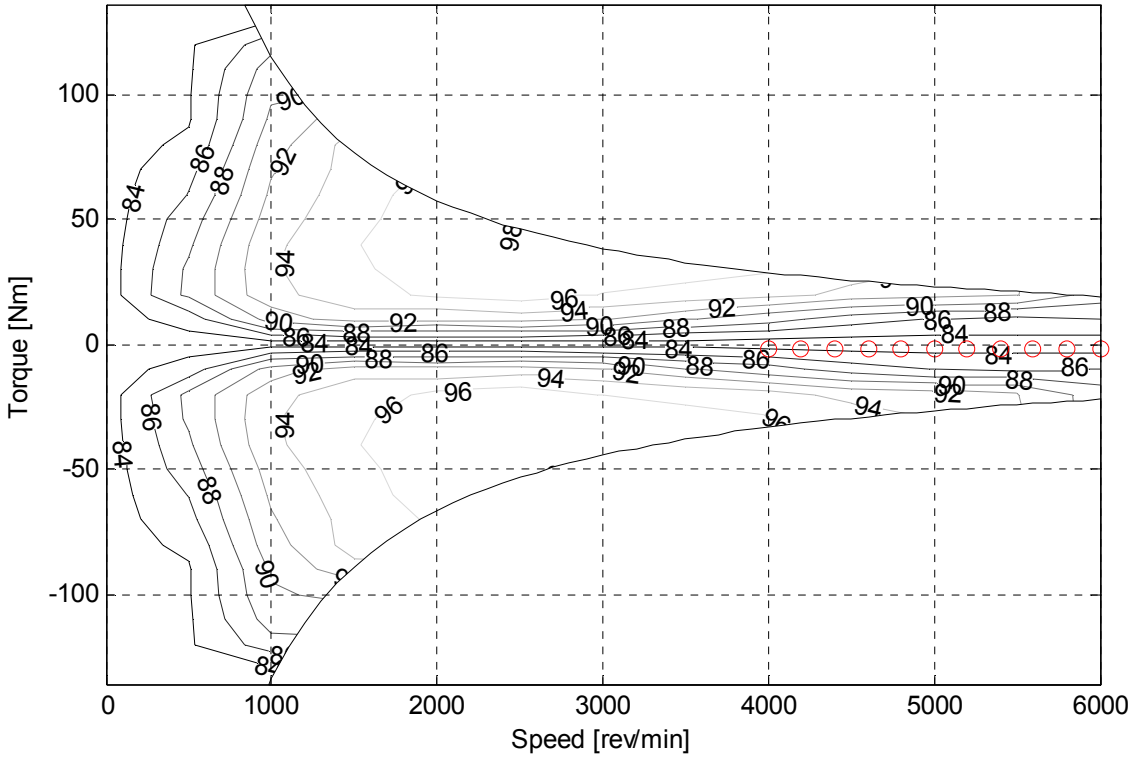

Figure 6-33 Stage 4: EM operating points – Zone 6

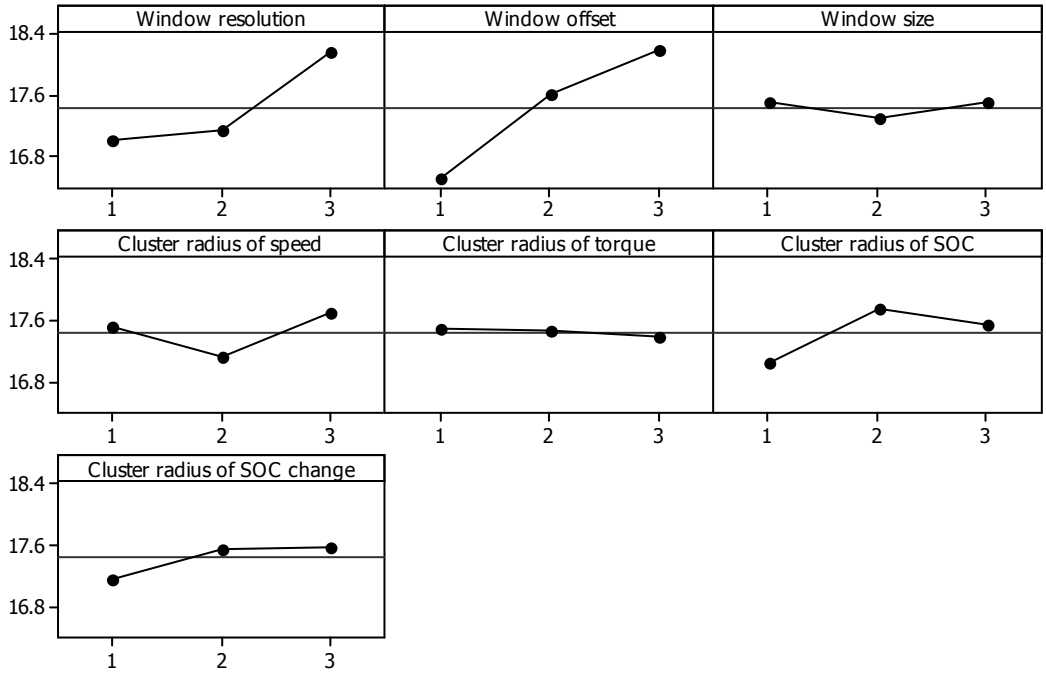

Figure 6-34 RMS error : combined cycle

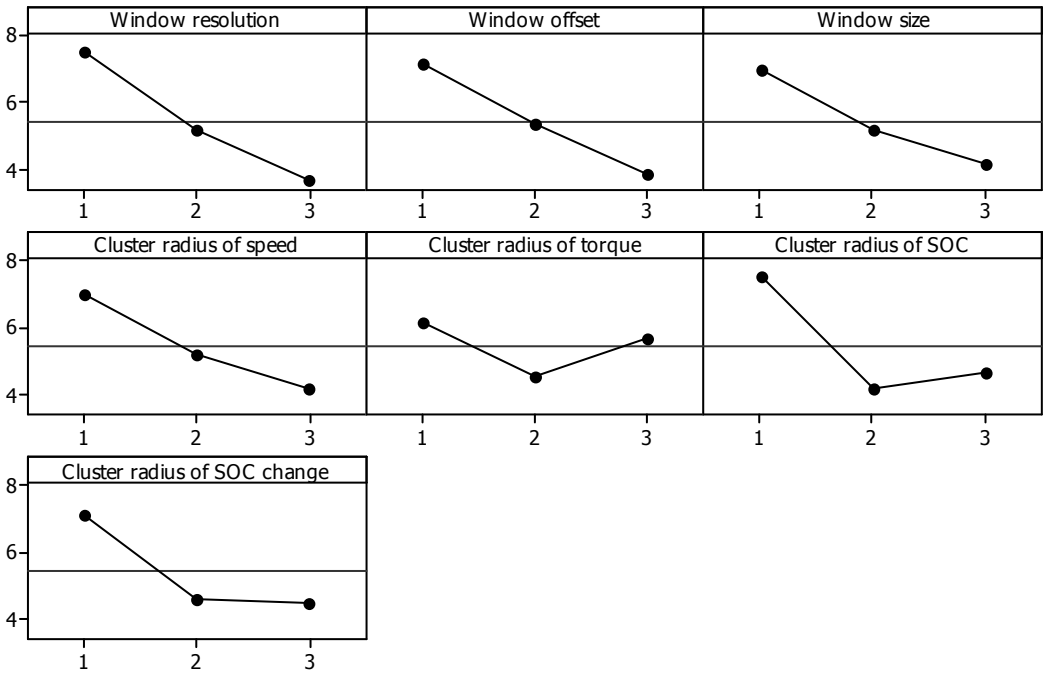

Figure 6-35 Number of rules : combined cycle

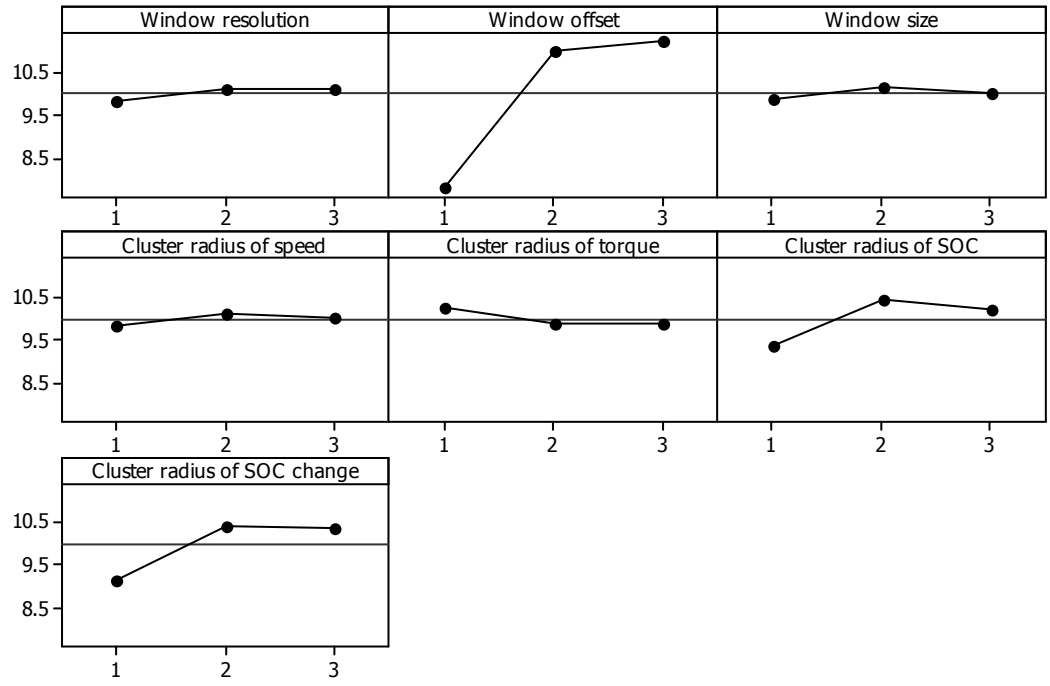

Figure 6-36 RMS error : NYCC

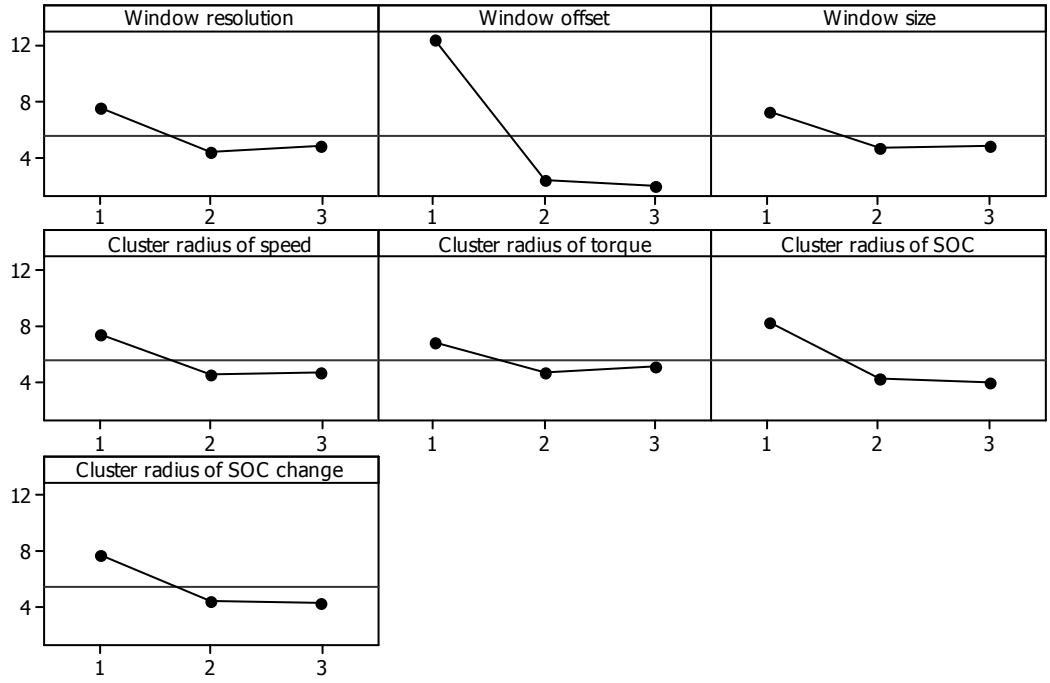

Figure 6-37 Number of rules : NYCC

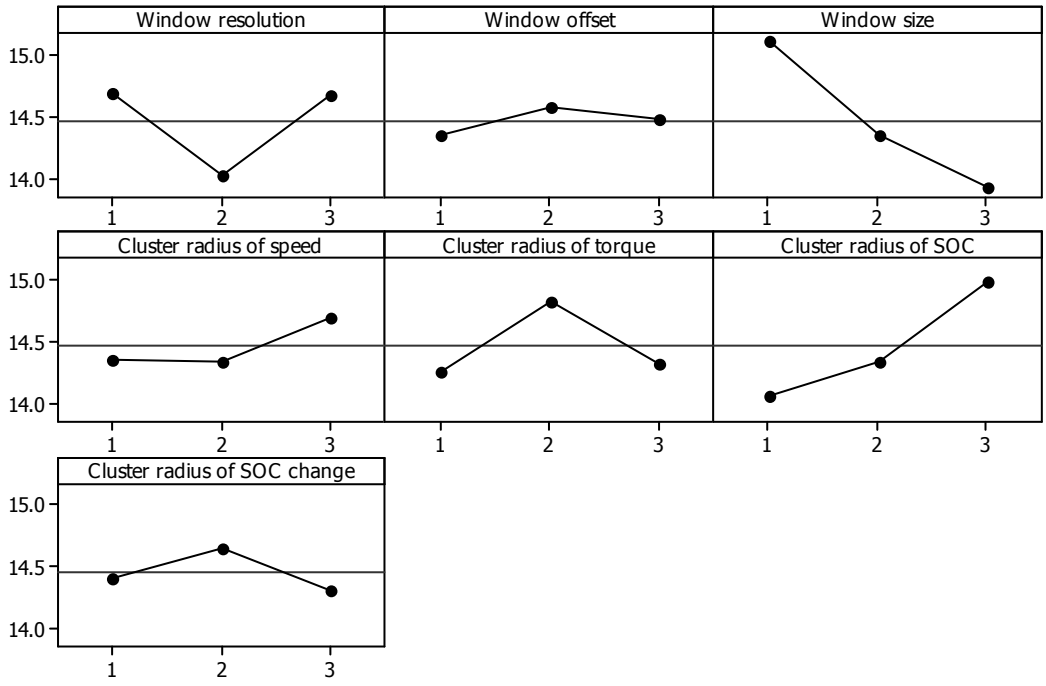

Figure 6-38 RMS error : LA92

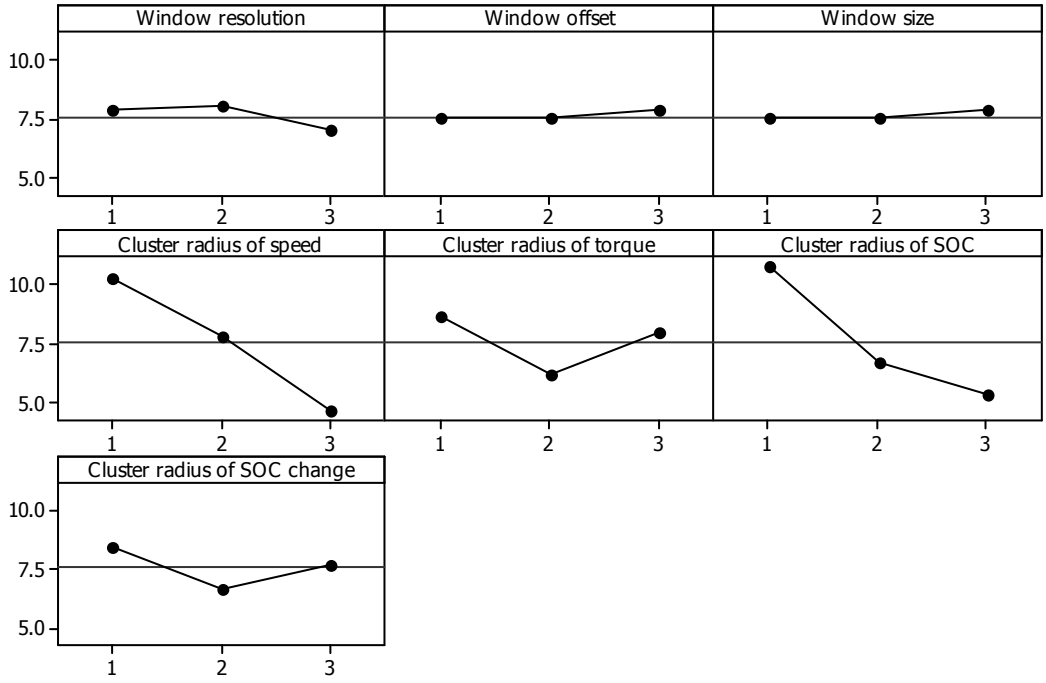

Figure 6-39 Number of rules : LA92

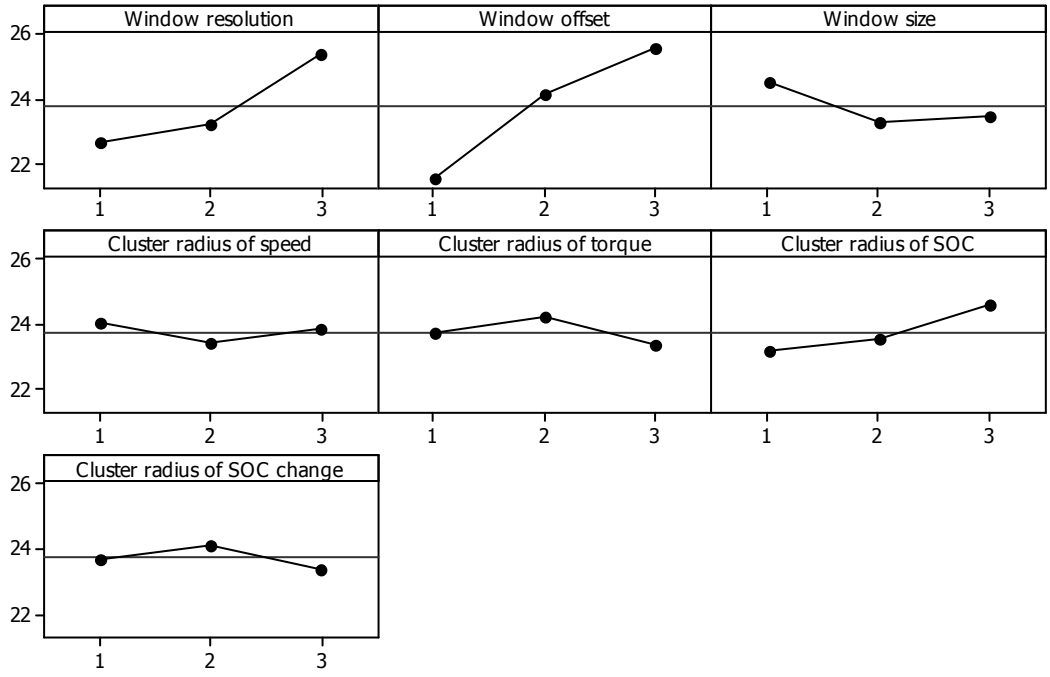

Figure 6-40 RMS error : US06

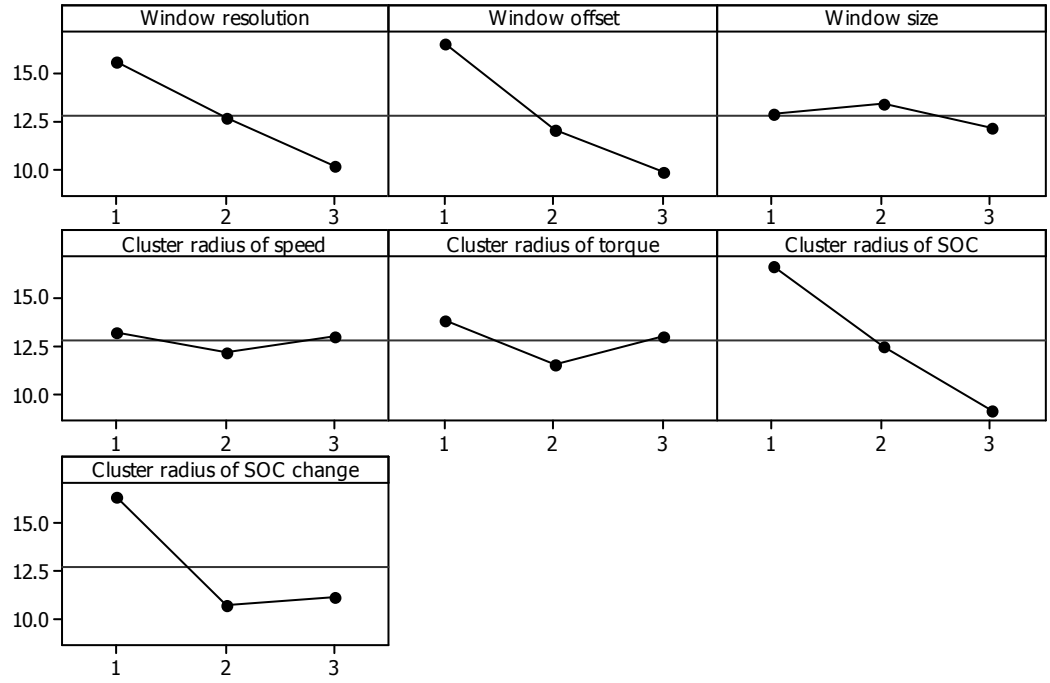

Figure 6-41 Number of rules : US06

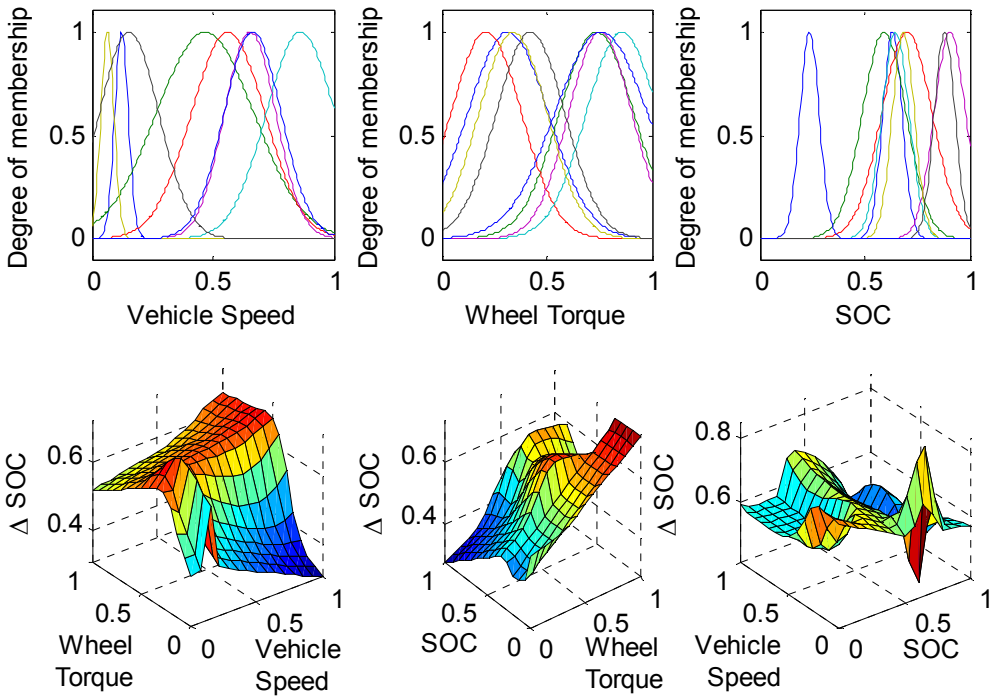

Figure 6-42 Fuzzy controller : combined cycle

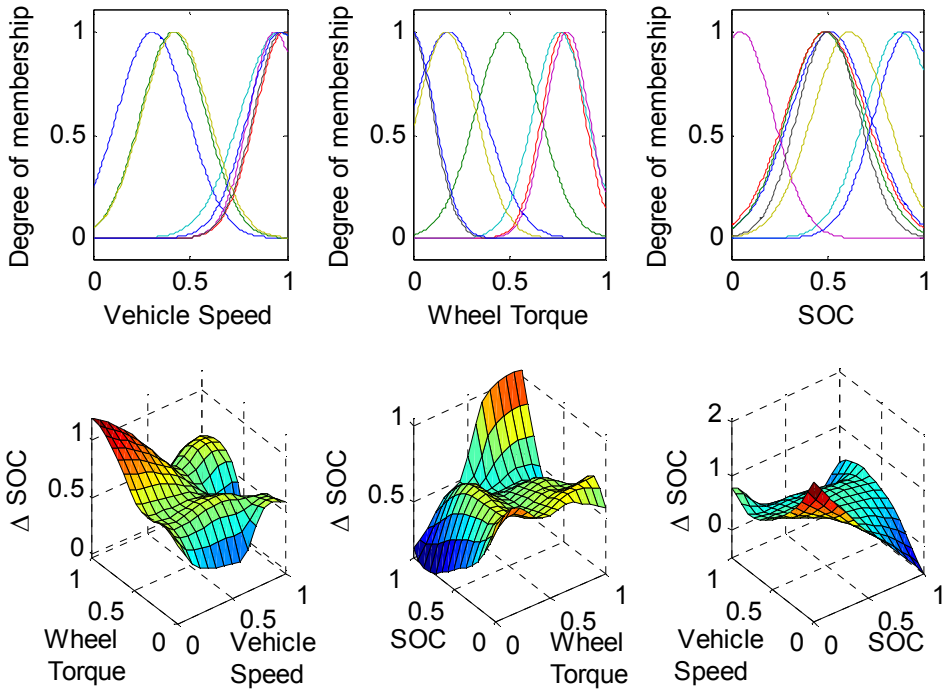

Figure 6-43 Fuzzy controller : NYCC

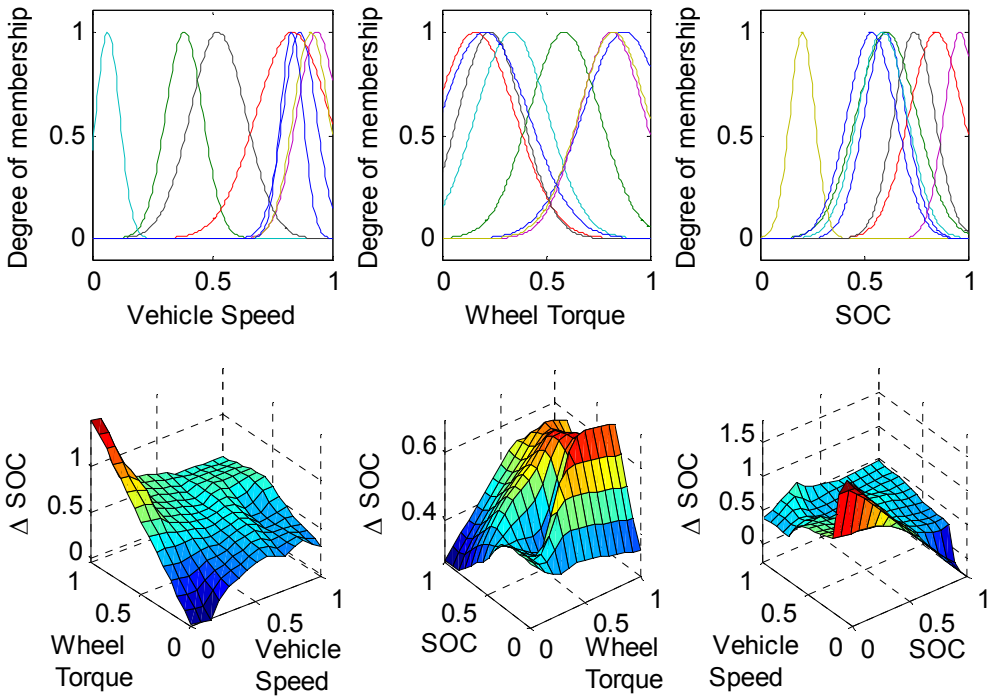

Figure 6-44 Fuzzy controller : LA-92

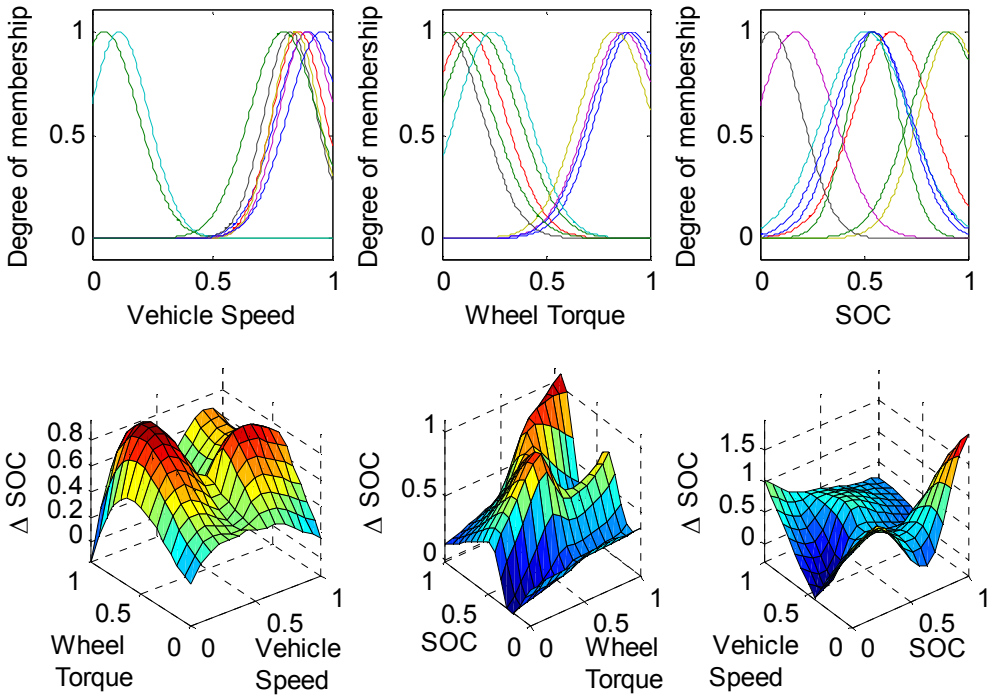

Figure 6-45 Fuzzy controller : US-06

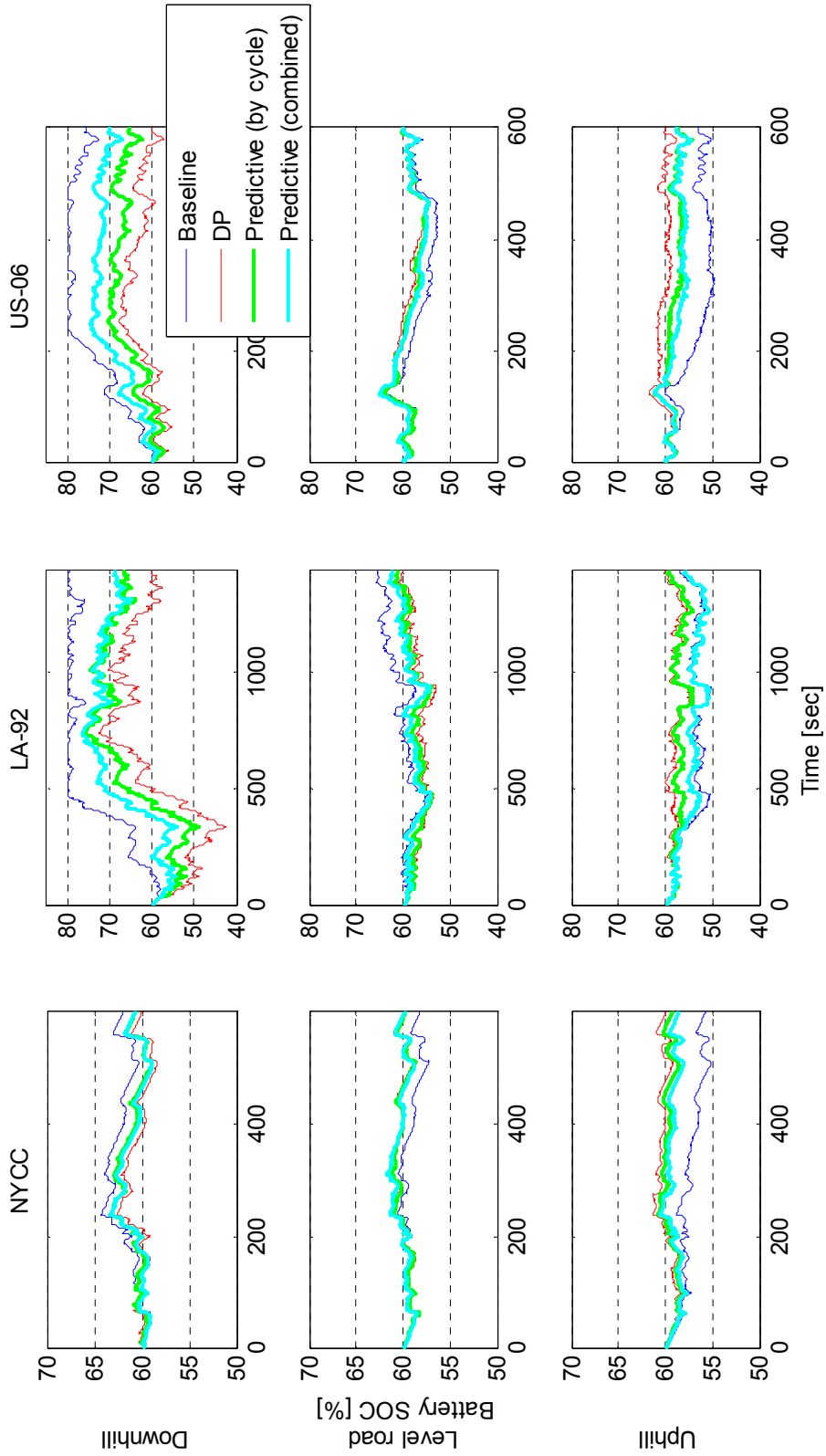

Figure 6-46 Battery SOC : Aggressive cycles

Table 6-1 Initial design of experiment

Prediction window			Cluster radius			
Resolution [m]	Offset [points]	Size [points]	Speed	Torque	SOC	ΔSOC
200	5	10	0.5	0.5	0.5	0.5

Table 6-2 Result of initial experiment

	Combined	NYCC	LA92	US06
RMS error [%]	18.05	12.34	14.84	23.75
No. of rules	3	1	3	9

Table 6-3 Level of control variables

Level	Prediction window			Cluster radius			
	Resolution [m]	Offset [points]	Size [points]	Speed	Torque	SOC	ΔSOC
1	100	0	5	0.2	0.2	0.2	0.2
2	200	5	10	0.35	0.35	0.35	0.35
3	500	10	20	0.5	0.5	0.5	0.5

Table 6-4 DoE result

	Level of control							Result							
	Prediction window			Cluster radius				Combined		NYCC		LA92		US06	
	Resolution	Offset	Size	Speed	Torque	SOC	ΔSOC	Error	Rules	Error	Rules	Error	Rules	Error	Rules
1	1	1	1	1	1	1	1	15.4	18	5.5	27	14.1	16	20.4	30
2	1	2	2	2	2	2	2	17.0	5	11.2	2	14.7	5	22.5	13
3	1	3	3	3	3	3	3	18.1	3	10.9	2	14.3	4	24.0	9
4	2	1	1	2	2	3	3	16.3	5	8.5	8	15.4	3	22.5	9
5	2	2	2	3	3	1	1	16.8	7	9.8	4	13.9	8	22.2	20
6	2	3	3	1	1	2	2	18.6	2	12.3	1	13.5	9	25.2	8
7	3	1	2	1	3	2	3	17.4	5	8.2	10	13.8	9	21.7	14
8	3	2	3	2	1	3	1	17.8	4	10.5	2	14.3	7	25.6	10
9	3	3	1	3	2	1	2	18.8	3	10.5	3	15.6	5	27.9	9
10	1	1	3	3	2	2	1	16.6	5	7.8	10	14.8	3	20.8	19
11	1	2	1	1	3	3	2	17.7	8	11.6	2	16.2	7	25.3	8
12	1	3	2	2	1	1	3	17.3	6	11.9	2	14.0	12	23.1	14
13	2	1	2	3	1	3	2	16.5	5	8.9	8	14.3	4	21.8	13
14	2	2	3	1	2	1	3	17.1	6	10.4	3	13.1	14	23.1	13
15	2	3	1	2	3	2	1	17.5	6	10.6	2	14.0	10	24.7	13
16	3	1	3	2	3	1	2	16.8	5	8.0	11	13.6	10	22.2	14
17	3	2	1	3	1	2	3	19.3	2	12.3	1	15.3	4	26.3	8
18	3	3	2	1	2	3	1	18.9	3	10.9	2	15.4	7	28.5	6

Table 6-5 Designed controller

Driving cycle	Level of control							Results			
	Prediction Window			Cluster radius				Prediction by DoE		Result from trained NN	
	Resolution	Offset	Size	Speed	Torque	SOC	ΔSOC	Error	Rules	Error	Rules
Combined	2	1	2	2	2	1	1	15.1	9.2	15.7	8
NYCC	2	1	3	3	2	3	1	7.2	9.3	6.8	8
LA92	2	1	3	2	3	2	3	12.8	7.8	13.0	8
US06	2	1	3	2	3	3	3	20.5	10.0	19.9	9

Table 6-6 Fuel economy

Driving cycle	Road gradient	Baseline Controller [km/L]	Predictive Control [km/L] (Improvement [%])	Predictive control by cycle [km/L] (Improvement [%])	Dynamic Programming [km/L] (Improvement [%])
NYCC	Down	8.67	9.10 (+4.98)	9.07 (+4.59)	9.33 (+7.61)
	Level	7.07	7.07 (0.00)	7.07 (0.00)	7.07 (0.00)
	Up	5.53	5.47 (-1.13)	5.42 (-1.96)	5.38 (-2.73)
LA-92	Down	21.85	28.22 (+29.14)	28.82 (+31.88)	30.3 (+38.69)
	Level	9.52	9.65 (+1.37)	9.71 (+1.98)	9.77 (+2.68)
	Up	5.08	5.09 (+0.24)	5.09 (+0.28)	5.1 (+0.43)
US-06	Down	19.47	21.86 (+12.26)	22.39 (+15.01)	23.01 (+18.19)
	Level	8.58	8.59 (+0.07)	8.63 (+0.62)	8.65 (+0.75)
	Up	4.73	4.72 (-0.13)	4.72 (-0.15)	4.72 (-0.14)

Table 6-7 Battery SOC change

Driving cycle	Road gradient	Baseline controller [%]	Predictive control [%]	Predictive control by cycle [%]
NYCC	Down	+1.98	+0.73	+0.69
	Level	-1.79	-0.12	-0.28
	Up	-4.25	-0.42	-0.72
LA-92	Down	+19.63	+8.74	+6.57
	Level	+5.30	+2.26	+1.08
	Up	-3.21	-4.25	-0.83
US-06	Down	+15.70	+10.15	+5.45
	Level	-0.48	-0.16	+0.05
	Up	-7.03	-2.48	-2.91

7 SOFTWARE-IN-THE-LOOP CO-SIMULATION

In Chapter 6, a predictive control algorithm using forthcoming journey information was developed, and a backward simulation model was used in order to demonstrate the performance of the controller. A quasi-static backward simulation is useful for initial design of the controller. However, detailed dynamics of the powertrain including sensors and actuators and a driver model were not included. Going toward the implementation stage, the controller should be verified in a more realistic simulation environment, which will be explained in this chapter.

7.1 SIMULATION MODEL

7.1.1 SOFTWARE-IN-THE-LOOP CO-SIMULATION

To verify the suitability of the controller for real implementation, a forward dynamic model developed in the SIL simulation environment using co-simulation techniques [186]. AMESim [187] and Simulink [188] were chosen as a programming environment. AMESim offers an intuitive and convenient physical modelling environment and a large number of pre-built libraries for the vehicle powertrain components. However, it is less efficient than Simulink to implement the logical algorithms generally required to design the controller. To combine the benefits from both, AMESim offers a co-simulation interface with Simulink. Powertrain and driver models are constructed in AMESim and control algorithms are implemented in Simulink. The supervisory algorithm converted into a SIL model of 32-bit Motorola MPC555 microcontroller, which is commonly used in automotive high-end embedded applications.

Figure 7-1 depicts the SIL co-simulation configuration. The physical model of the vehicle implemented in AMESim has continuous states, so a variable step solver is used in order to save simulation time and maintain numerical accuracy. All local controllers such as the engine control unit (ECU), motor control unit (MCU), transmission control unit (TCU) and brake control unit (BCU) are discrete-time models and communicate with the plant model by the co-simulation interface. There is no state variable exchange between the models, so AMESim and Simulink use their own solvers to increase the calculation efficiency. The supervisory control unit (SCU) is separately compiled by the

MPC555 compiler and emulated by a standard PC in the single precision floating point data type.

7.1.2 POWERTRAIN MODELLING

Figure 7-2 illustrates the forward-facing simulation model of the HEV implemented in AMESim. The engine is modelled as a simple torque source with inertia connected to a flywheel. A map based loss model with inertia and a clutch are used for the CVT because AMESim does not provide a full IVT model which loss is a function of torque, speed and transmission ratio. The vehicle model provides longitudinal 1-dimensional dynamics. A set of ready made models for an EM and a battery are in the AMESim library and included for the mild hybrid powertrain. All the controllers that appear as simple black boxes are Simulink co-simulation interfaces, which communicate data with the control algorithm implemented in Simulink during the simulation. The dynamics of all actuators including the throttle, the CVT ratio and the clutch, the brake, and the battery voltage are modelled as first order dynamics. The time constants used in the simulation are listed in Table 7-1. Even though the engine dynamics from the throttle pedal to the crankshaft is a function of the speed and the torque, it is assumed as a constant because it is not very different in normal driving cycle operating conditions. The CVT ratio and clutch lag by the hydraulic system is from the detailed IVT model. The default values of the library models are used as the time constants of the electrical components and mechanical brake.

7.1.3 CONTROLLER MODELLING

The top-level simulation diagram of the controllers is illustrated in Figure 7-3. The vehicle modelled in AMESim outputs all sensor signals to the SCU. The supervisory controller calculates the required control values including the engine torque, ratio of the transmission, engagement of the transmission clutch, and the brake torque. The local controllers translate the required values to the real control signal according to the scaling and the saturation of the actuators. Only the ECU and MCU among the local controllers receive the sensor signals directly because the idle controller requires the engine speed.

Each controller has independent control loop time. The ECU, MCU and BCU calculate the command signal at 1kHz rate, and the TCU is running on a 8ms time base. The timer of the SCU is set to the slowest local controller, so 8ms is also applied. To match the different running rate among the controllers and the vehicle, several rate transition blocks are inserted between them. The reference vehicle speed of driving cycles is supplied from the separate block.

Figure 7-4 shows the supervisory controller. The information from the vehicle model is fed to the mode selection block. Control strategies should be changed taking account of the vehicle status and the driver's request. In this study, 3 different control modes, the idling, braking, and propelling modes, are defined and determined by the supervisory controller. The control actions are different in each mode and the change criteria are summarised in Table 7-2. The default mode is idling in which the engine is turned off. When the accelerator pedal position is over a certain threshold level, the mode transition to the propelling mode occurs. In the propelling mode, the mode transition to the braking or the idling mode occurs depending on the vehicle speed. From the braking mode, pressing the accelerator pedal makes the transition to the propelling mode, or the mode is changed to the idling when the vehicle speed is reduced under a pre-defined low value. For each mode, the control actions of the local controllers are listed in Table 7-3.

The content of the SOC control is presented in Figure 7-5. The model represents the algorithm illustrated in Figure 6-1. Future vehicle speed and road elevation data are supplied from the driving cycle in every second, which represent a navigation device, and battery SOC is directly measured from the battery. The inputs of the ANFIS are pre-conditioned by road load calculation and prediction window. The ANFIS represents exactly the same algorithm designed in the previous chapter, and two different calibration sets are examined, which were tuned generally and by individual cycle.

7.2 SIMULATION

7.2.1 DRIVER MODEL TUNING

The forward simulation of the powertrain contains the driver model. In this work, the standard driver model in AMESim was adopted. This model consists of two PID

controllers, which are related to the accelerator and the brake pedal control. The gains should be tuned to maintain the vehicle speed error within given bounds. Furthermore, the standard model has an internal parameter to define the anticipation period, which introduced large under and overshoot of the vehicle speed at the sharp speed change in synthetic cycles such as the NEDC. Therefore, the parameter in C source code was slightly modified to satisfy the given speed error bound. From the default values, the gains are tuned intuitively in three standard cycles, which have allowable tolerance [189, 190], and the results are in Table 7-4. The anticipative or differential gain in braking is smaller than that in accelerating because the vehicle speed tends to be slowed down by the aerodynamic drag and the rolling resistance without any actions.

The speed error in the simulation over the driving cycles are summarised in Table 7-5. For the synthetic cycle, NEDC, the RMS error is only 0.2 km/h, which is relatively small because of the simple speed profile. The peak error value usually occurs at the vehicle launch. On the FTP-75 and HWFET, which are real world and dynamic driving schedules, the error is large but the peak values are still within the allowable tolerances. Therefore, it can be concluded that the driver model is properly tuned.

7.2.2 Comparison with backward simulation

The simulation was performed over the same cycles as used in the backward simulation. Fuel economy and the battery SOC level before and after the journey are summarised in Table 7-6 and Table 7-7 respectively.

In the case of the NYCC, there is no discernible difference between the backward and forward simulation. Fuel economy is not considerably different, and the difference of battery SOC changes less than 1%. As mentioned in chapter 6, the NYCC is a very short cycle and the vehicle is in idle stop state for a large portion of the driving time. Therefore, the total amount of consumed fuel or battery throughput current is hardly changed by the actuator dynamics and driver's pedal action.

LA92 and US06 show slightly more variation in case by case. Fuel economy is deteriorated in most cases. The maximum deviation is 0.5km/L in the case of US-06 downhill, which has long hard deceleration phase at the end of the cycle. The only exception is LA92 level road, but the improvement is only 0.01km/L, too small to have

much significance. These results imply that the controller designed in a quasi-static simulation environment might be worse in a real implementation stage. The driver's behaviour introducing speed overshoot or inconsistent braking could make the engine and EM run in less efficient regions and spend more energy than the ideal case demonstrated by a backward simulation.

This is also shown in the battery SOC change. In the downhill case, both LA92 and US06, SOC control look like showing better performance because the absolute values are reduced. The performance is degraded 2~3 % in most of the level or uphill situations. The worst case is the LA-92 uphill, individually tuned, which shows 4.33% reduced from the backward result. This is the longest and most dynamic cycle, so the impact of the driver and powertrain dynamics is largest. The final SOC of the battery is generally lower than the backward simulation regardless of the tuning and elevation conditions. This means the energy stored in the battery through prediction by forward simulation is smaller than the backward case even though the engine burns more fuel to drive the vehicle over the same journey. The speed overshoot caused by aggressive acceleration requires more engine assist from the EM. Also the speed undershoot overusing the mechanical brake is followed by either a coastdown or burning fuel to catch up the given speed trace which reduces the amount of recuperative energy available. In addition, the actuator delay prevents the engine and EM operating points staying at their optimal operating conditions. All of these effects contribute to deteriorate fuel economy and lower the battery SOC.

These effects might vary in the real-world from driver to driver and in different traffic conditions. However, the overall impact on the controller performance is considered to be not very significant, and the predictive controller shows more or less the same performance that was demonstrated in the backward quasi-static simulation model.

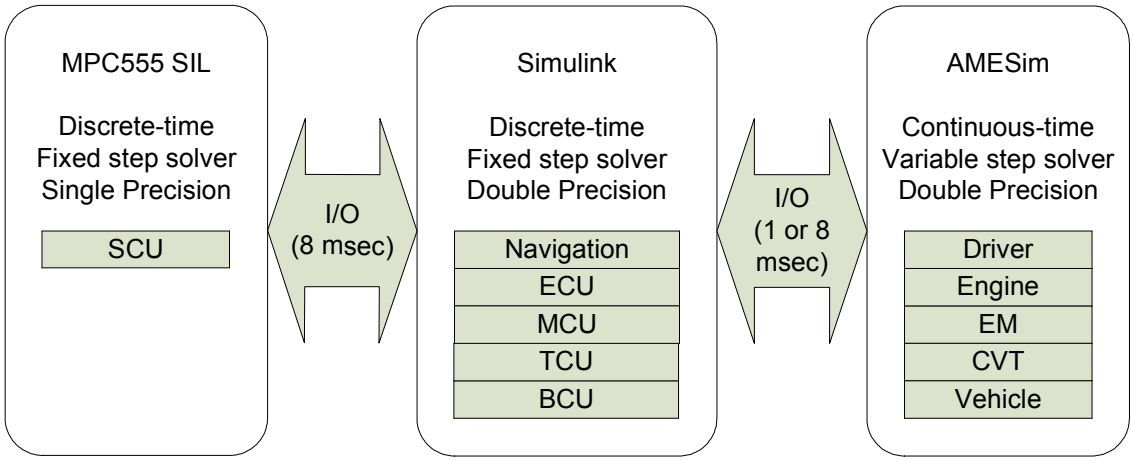

Figure 7-1 Concept of SIL co-simulation

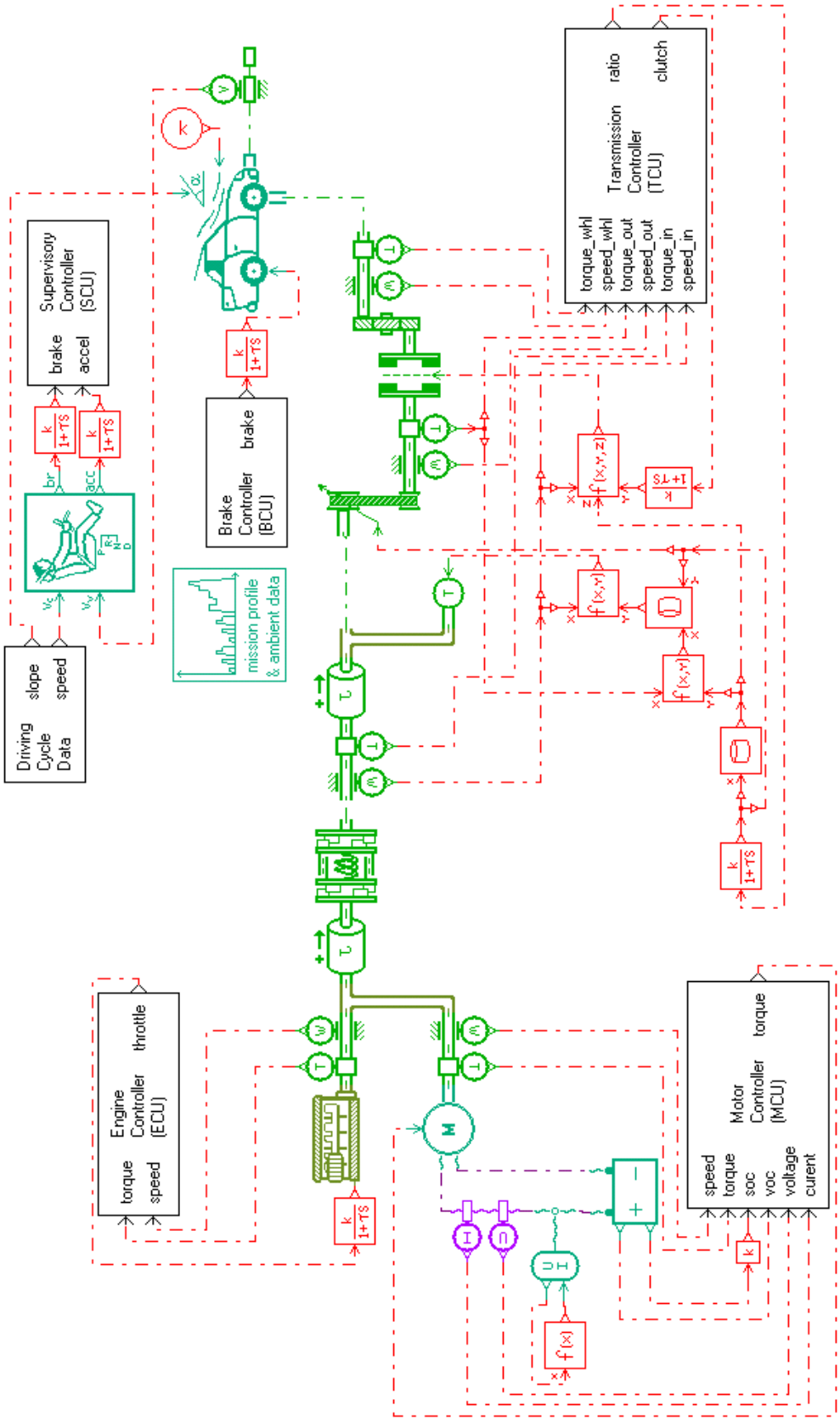

Figure 7-2 Simulation model of HEV

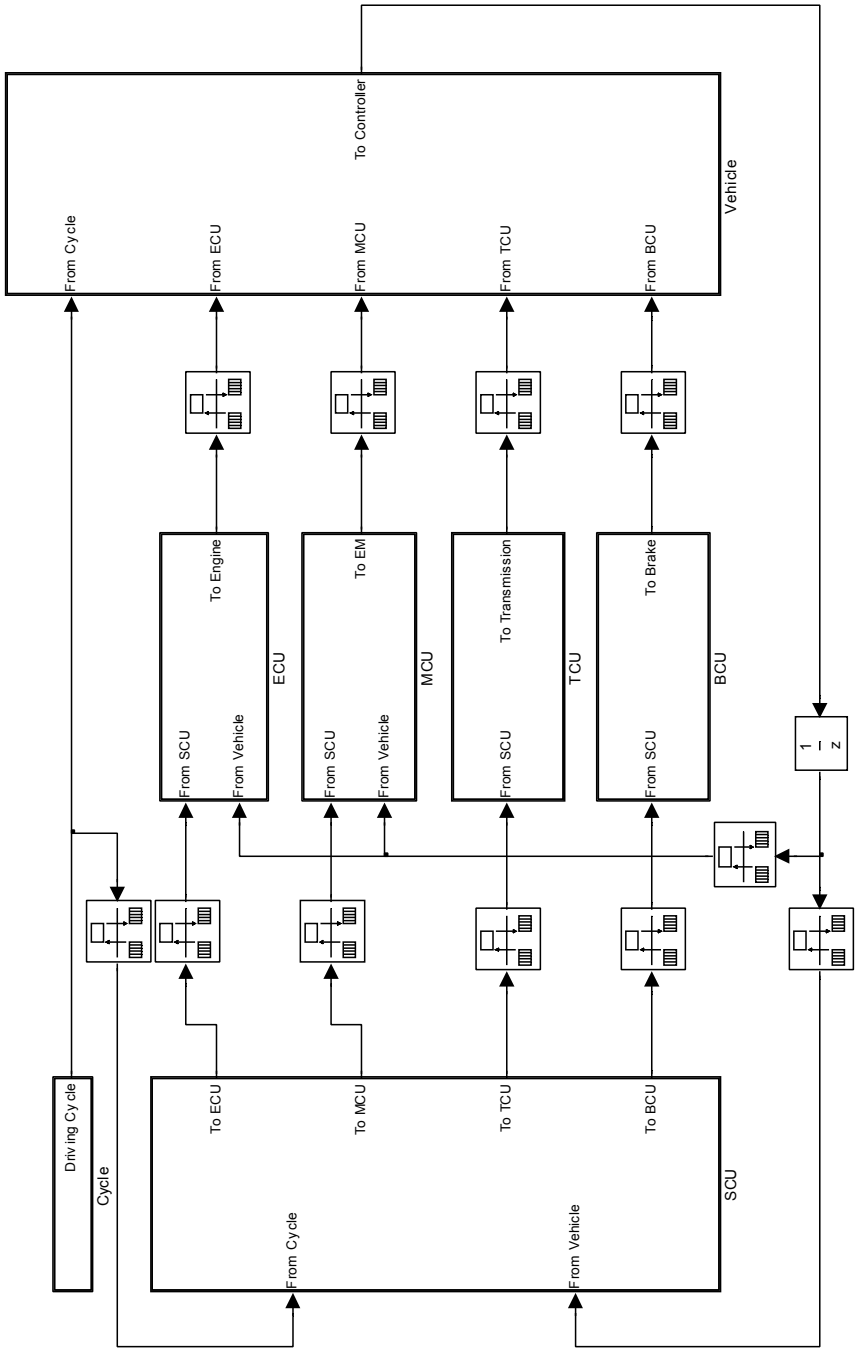

Figure 7-3 Structure of controller

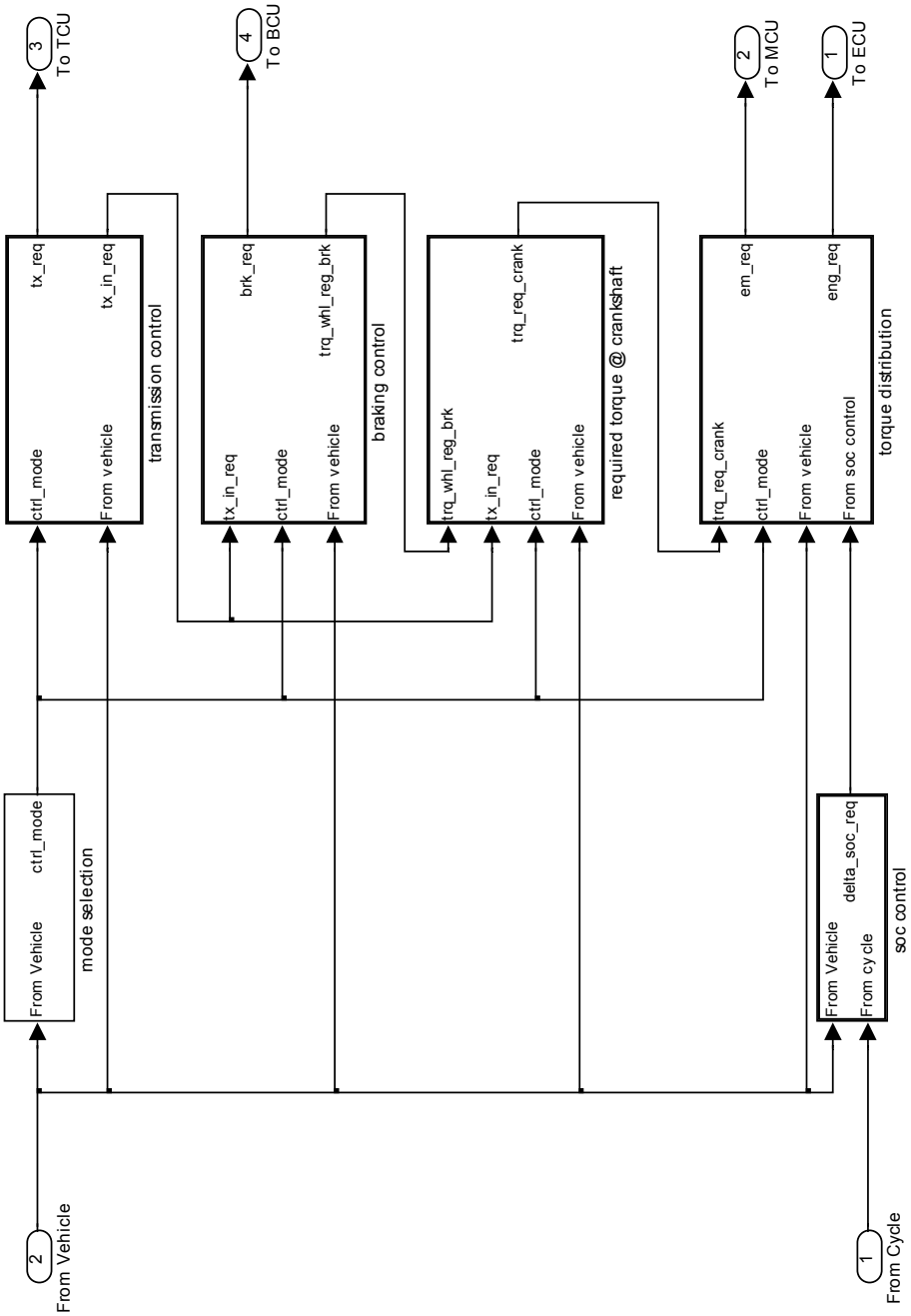

Figure 7-4 Supervisory controller

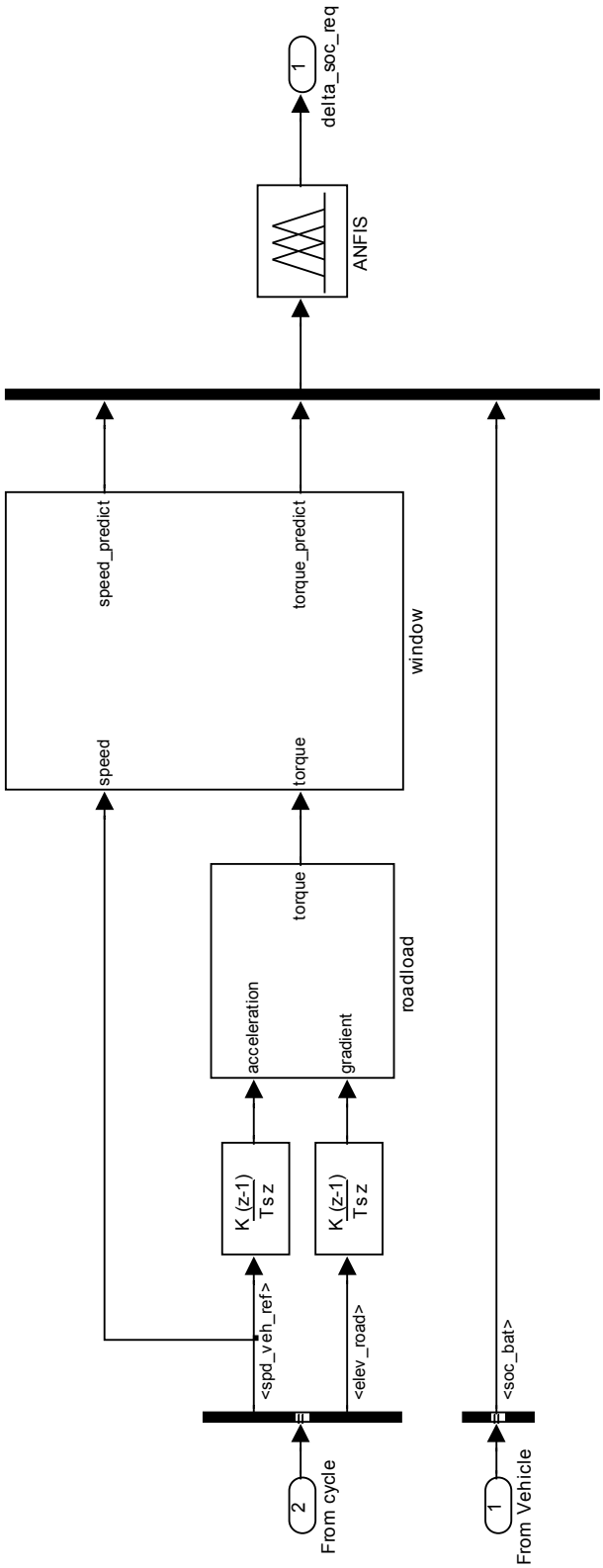

Figure 7-5 SOC control

Table 7-1 Actuator time constants

Actuator	Time constant [sec]	Actuator	Time constant [sec]
Engine throttle	0.10	EM torque	0.05
CVT ratio	0.10	Brake	0.05
CVT clutch	0.20	Battery voltage	0.10

Table 7-2 Control mode transition criteria

From \ To	Idling	Braking	Propelling
Idling	X	x	Throttle >1%
Braking	Vehicle speed< 0.5km/h	x	Throttle >1%
Propelling	Throttle>1% Vehicle speed<0.5km/h	Throttle>1% Vehicle speed>0.5km/h	X

Table 7-3 Control actions at each mode

Control parameter	Idling	Braking	Propelling
Engine torque	0	Controlled	Controlled
EM torque	0	Controlled	Controlled
CVT ratio	0	Controlled	Controlled
CVT clutch	Off	Controlled	On
Brake force	100%	Controlled	0%

Table 7-4 Gains of driver model

Gains	Accelerating	Braking
Proportional	0.20	0.20
Integral	0.02	0.02
Anticipative	0.35	0.15

Table 7-5 Speed error

Cycles	Allowable Tolerance [km/h]	Speed error [km/h]		
		Mean	RMS	Peak
NEDC	2.0	0.12	0.20	1.80
FTP-75	3.2	0.11	0.33	1.97
HWFET	3.2	0.45	0.49	1.84

Table 7-6 Fuel economy

Driving cycle	Road gradient	Predictive control [km/L]		Predictive control– by cycle [km/L]	
		Backward	Forward	Backward	Forward
NYCC	Down	9.10	9.11	9.07	9.00
	Level	7.07	7.11	7.07	7.20
	Up	5.47	5.23	5.42	5.39
LA-92	Down	28.22	28.09	28.82	28.66
	Level	9.65	9.66	9.71	9.67
	Up	5.09	4.94	5.09	4.97
US-06	Down	21.86	21.44	22.39	21.89
	Level	8.59	8.58	8.63	8.59
	Up	4.72	4.61	4.72	4.63

Table 7-7 Battery SOC change

Driving cycle	Road gradient	Predictive control [%]		Predictive control– by cycle [%]	
		Backward	Forward	Backward	Forward
NYCC	Down	0.73	0.08	0.69	1.09
	Level	-0.12	-1.21	-0.28	-1.21
	Up	-0.42	-0.41	-0.72	-0.42
LA-92	Down	8.74	6.76	6.57	3.34
	Level	2.26	-0.01	1.08	-2.04
	Up	-4.25	-5.16	-0.83	-5.16
US-06	Down	10.15	7.63	5.45	3.52
	Level	-0.16	-2.30	0.05	-1.11
	Up	-2.48	-2.28	-2.91	-3.98

8 CONCLUSIONS

This thesis presented a design process and evaluation of a control algorithm for a parallel HEV. The aim was to reveal the potential benefit of predictive journey information on fuel economy and battery SOC control. This enabled the controller to control the battery SOC level appropriately considering forthcoming regenerative braking possibilities and required engine assist at high power demand.

8.1 CONCLUSIONS

A SUV was chosen as a baseline vehicle because of the fuel saving potential by hybridisation. A generic powertrain was configured by the analysis of the relationship between engine power, size and vehicle kerb weight from SUVs currently available in the North American market. The baseline powertrain consisted of a 3.2L SIDI engine and a power split CVT. To control the CVT ratio, the IOS concept was introduced instead of the traditional IOL. The IOS showed more than a 5% improvement of powertrain efficiency in the low speed and mid to high torque region that is frequently used in order to accelerate the vehicle. A mathematical model of powertrain was derived to develop a quasi-static backward simulation model, and fuel economy simulation was carried out in four standard legislative driving cycles, which are the NEDC, FTP-75, and 10-15. The baseline vehicle showed 10.3 and 13.0 km/L in the FTP-75 and HWFET cycle respectively, which are much better than the reference vehicles' average fuel economy, 8.3 km/L for city and 10.6 km/L for highway. This demonstrated the ability of the optimised powertrain that consists of the stratified charge SIDI engine and the power split CVT.

Hybridisation of the baseline vehicle was proposed using the ISA with the capacity of the EM selected on the basis of the regenerative capability. A rule based control strategy was developed and tuned over the standard driving cycles, maximising fuel economy within an acceptable amount of the battery SOC change at the end of cycle. Fuel economy of the hybridised vehicle showed 1.3 ~ 26.8% improvement from the baseline conventional vehicle, depending on the characteristic of driving cycles such as the engine idling period and available regenerative braking energy. This confirms the

potential of the further fuel consumption reduction by a hybrid solution for the suggested baseline powertrain.

To investigate additional improvement potential by control strategy, the DP was used in order to find the global optimal solution in individual driving conditions. To accelerate computation, significant amount of calculation nodes was eliminated by the constraints such as boundary conditions of SOC and capability of the engine and EM. 50 ~ 75% of the overall calculation time was reduced by means of this node elimination.

Fuel economy benefits by global optimisation using the DP in the standard driving cycles were obtained between 0.13% and 2.21%. This further improvement is limited by the attributes of driving cycles, such as limited acceleration and the level gradient of the road. In addition, the baseline controller was already optimised over these cycles during the tuning process. To investigate the improvement potential of the hybridised powertrain, more practical and aggressive driving conditions, the LA-92, NYCC, and US-06 with different road elevation profiles were examined. In the downhill, the baseline controller was not able to control the battery energy effectively and the SOC was saturated to the upper hardware limit in long journey such as LA-02 and US-06. As a result, the final SOC controlled by the baseline controller was 1.98 ~ 19.63 % higher than the initial state, and there was 7.61 ~ 38.69% more room for fuel economy improvement. On the other hand, the baseline controller was tending to deplete the battery to assist the engine in uphill road, which resulted in 3.21 ~ 7.03 % battery SOC depletion.. On the level road, optimised energy management showed marginal potential of fuel economy as in the standard cycles. In general, the simulation using the DP demonstrated that there was still considerable gap between the global optimal solution and the baseline controller for fuel economy and battery energy management, especially in a long aggressive journey on hilly terrain.

Based upon the result by the DP, a predictive control algorithm using future journey information was developed. The structure of the controller consisted of two parts. The first part of the controller design was optimal torque split between the EM and the engine, which was a rule based algorithm. By intensive case studies instead of a traditional intuitive approach, engine operating conditions were divided into six zones according to the engine efficiency and the EM torque capacity. Another part of the

design process was the calculation of desired SOC using the ANFIS, which was the key part of the predictive control. From the moving average of vehicle speed and road gradient in the predictive window, required speed and torque at the wheel on the road ahead were estimated. This information and current SOC level were used as the inputs of the ANFIS, and the desired SOC gradient was calculated. The tuning process was carried out for the individual cycles to represent city, urban/extra urban and motorway, as well as the combination of those. The optimal solution obtained from the DP was used as a training dataset for the ANFIS. DOE and subtractive clustering were used as a tool to tune the controller. Seven parameters were involved in the design phase. Three of them were the prediction window size, resolution, and distance apart from the current vehicle position. The rest were the clustering radius of the inputs and the output of the FIS. Each parameter was tested in three different levels and DOE using an orthogonal array was able to decrease the tuning work from 3^7 to 18 trials. In case of the general tuning with all dataset from 3 different cycles, the optimised solution by DOE showed 15.7% RMS error, which was reduced from 18.05% of the initial design. The number of rules in the FIS was increased from three to eight. Tuning by individual cycle gave 1.8 ~ 5.5% performance improvement using less than ten rules. This number of rules is substantially smaller than the design suggested by Rajagopalan et al [191], which used 121 rules for two inputs.

Combined with the fuzzy system, the controller gave a good potential to improve fuel economy and tight SOC control. Fuel economy improvement and SOC correction were close to the optimal solution by the DP, especially in the long trip on steep road on which there was a large gap between the baseline controller and the DP. In case of downhill, the predictive control showed 5~30 % fuel economy improvement. This is comparable with the result presented by Deguchi et al. [112], in which they claim 7.8% improvement on 20km, 3% downhill route. The benefit of the predictive control on flat road is up to 1.98%, which is marginal as expected in the DP. On the uphill, the overall fuel economy was the same or slightly decreased but the final battery SOC is closer to the initial level in most cases. Considering common trip length and mild gradient of typical driving road, the predictive control did not provide a huge amount of fuel saving and still there was a gap to the true optimal performance. It was mainly caused by the limited future journey information such as the coarse resolution and the receding

horizon predictive window. The controller tuned in individual cycles demonstrated better performance than the case when generally tuned. This implies the performance of the predictive control highly depends on the quality of future journey information. Even though telematics technology is fast developing, the infrastructure to provide this information is not foreseeable in the short term. However, commuting vehicles such as city buses would be a good candidate because a number of vehicles run in the same route and can share the traffic information through vehicle-to-vehicle communication. In addition the implementation cost of the predictive control suggested in this study would be very small because it requires only the interface between the navigation and the supervisory controller. Considering the high cost of hybridisation or any other advanced powertrain technology, the predictive control is an attractive solution to improve fuel economy and energy management.

As a final step towards implementation, a fully dynamic forward simulation model was developed in the AMESim-Simulink co-simulation environment. Powertrain and driver models were implemented in AMESim, and the controller was redesigned in a Simulink SIL simulation based on the MPC555 microcontroller. The driver model was tuned in the standard driving cycles and the speed tracking error was within the allowable tolerance. The maximum deviation of fuel economy from the backward model was 0.5km/L and SOC control performance was degraded 2~3 % in most of the level or uphill situations. Therefore, it is concluded the controller proposed in this work would be practical for a real implementation and beneficial to reduce fuel consumption.

8.2 FUTURE WORK

This study assumed that the information of the forthcoming journey was supplied from virtual sources such as evenly spaced monitoring stations. In reality, it is difficult to setup the infrastructure to measure the vehicle driving information. If it were possible to access the real-time traffic information from a commercial service provider, the results would be able to reveal the real-world benefit.

It is possible that different sectors instead of small SUVs might have a higher potential for the predictive control and could be investigated. As mentioned in the previous section, route-commuting buses would be able to exchange the detailed road traffic information through the vehicle-to-vehicle communication, which is able to improve the

prediction performance. Another sector could be high performance vehicles that are generally driven more aggressively, hence the predictive control would give more benefit of fuel saving even though the vehicles may run over mild terrain.

Additonal potential of the predictive control on top of the fuel saving is optimising the battery size. The predictive control algorithm proposed in this work showed better fuel economy by optimising battery energy usage. Conversely, this would give an opportunity to downsize the battery, which is the most expensive part of the HEVs, without sacrificing fuel economy benefit. Series or plug-in hybrid vehicles that require large capacity battery would be a good place to investigate.

REFERENCES

1. UN, *Kyoto protocol to the united nations framework convention on climate change*. 1997, United Nations.
2. Botti, J.J. and C.E. Miller, *Powertrains of the future : Reducing the impact of transportation on the environment*, in *SAE International Congress and Exposition*. 1999: Detroit, Michigan, USA.
3. Jackson, N., *Futeure automotive powertrains - the end of the internal combustion engine?*, in *The 91st Thomas Hawksley Lecture*. 2003: London, UK. p. 1-11.
4. Ng, H.K., A.D. Vyas, and D.J. Santini, *The prospects for hybrid electric vehicles, 2005-2020 : Results of a Delphi study*, in *SAE Future Transportation Technology Conference and Exposition*. 1999: Costa Mesa, California, USA.
5. Conley, J. and S. Taylor, *Technological evaluation of fuel efficiency improvement concepts to meet future regulatory requirements in the north american market*, in *Powertrain and Fluid Systems Conference and Exhibition*. 2002: San Diego, California, USA.
6. Gott, P., J.-R. Linna, and J.P. Melco, *The evolution of powertrain technology 2008 and beyond - engines, hybrids, battery electric, fuel cells, transmissions*, in *Proceedings of the 2nd IMechE Automobile Division Southern Center Conference on Total Vehicle Technology*. 2002: Brighton, UK. p. 3-9.
7. Ronning, J.J. and G.L. Grant, *Global hybrid electric vehicle markets and missions*, in *SAE Future Transportation Technology Conference and Exposition*. 1999: Costa Mesa, California, USA.
8. West, J.G.W., *Propulsion systems for hybrid electric vehicles*, in *IEE Colloquium on Electrical Machine Design for All-Electric and Hybrid-Electric Vehicles*. 1999. p. 1-9.
9. Cuddy, M.R. and K.B. Wipke, *Analysis of the fuel economy benefit of drivetrain hybridization*, in *SAE International Congress and Exposition*. 1997: Detroit, Michigan, USA.
10. An, F., F. Stodolsky, and D. Santini, *Hybrid options for light-duty vehicles*, in *SAE Future Transportation Technology Conference and Exposition*. 1999: Costa Mesa, California, USA.
11. An, F., J. DeCicco, and M. Ross, *Assessing the fuel economy potential of light-duty vehicles*, in *SAE Future Transportation Technology Conference and Exposition*. 2001: Costa Mesa, California, USA.
12. Lukic, S.M. and A. Emadi, *Performance analysis of automotive power systems: effects of power electronic intensive loads and electrically-assisted propulsion systems*, in *IEEE 56th Vehicular Technology Conference*. 2002: Chicago, Illinois, USA. p. 1835-1839.

13. Louis, J.J.J., *Well-to-wheel Energy use and greenhouse gas emissions for various vehicle technologies*, in *SAE 2001 World Congress*. 2001: Detroit, Michigan, USA.

14. Ahman, M., *Primary energy efficiency of alternative powertrains in vehicles.* Energy, 2001. **26**(11): p. 973-989.

15. Moghbelli, H., et al., *A comparative review of fuel cell vehicles (FCVs) and hybrid electric vehicles (HEVs) part I: Performance and parameter characteristics, emissions, well-to-wheel efficiency and fuel economy, alternative fuels, hybridization of FCV, and batteries for*, in *Future Transportation Technology Conference*. 2003: Costa Mesa, California, USA.

16. Moghbelli, H., et al., *A comparative review of fuel cell vehicles (FCVs) and hybrid electric vehicles (HEVs) part II: Control strategies, powertrain, total cost, infrastructure, new developments, and manufacturing & commercialization*, in *Future Transportation Technology Conference*. 2003: Costa Mesa, California, USA.

17. Atwood, P., et al., *Degree of hybridization modeling of a fuel cell hybrid sport utility vehivle*, in *SAE 2001 World Congress*. 2001: Detroit, Michigan, USA.

18. Abolhassani, M., et al., *Impact of hybrid electric vehicles on the world's petroleum consumption and supply*, in *Future Transportation Technology Conference*. 2003: Costa Mesa, California, USA.

19. Anonymous, *Hybrid vehicles are worth it!*, in *IEEE Spectrum*. 2001. p. 79-84.

20. Lave, L.B. and H.L. Maclean, *Are hybrid vehicles worth it?*, in *IEEE Spectrum*. 2001. p. 47-50.

21. Kimura, A., T. Abe, and S. Sasaki, *Drive force control of a parallel-series hybrid system.* JSAE Review, 1999. **20**(3): p. 337-341.

22. DoE, *U. S. Department of Energy technology snapshot - Featuring the Toyota Prius*, D.o. Energy, Editor. 2001, Argonne National Laboratory.

23. Inoue, T., et al., *Improvement of a highly efficient hybrid vehicle and integrating super low emissions*, in *SAE International Fall Fuels and Lubricants Meeting and Exhibition*. 2000, Society of Automotive Engineers, Inc., Warrendale, Pennsylvania, USA: Baltimore, MD, USA.

24. Kuze, Y., et al., *Development of new generation hybrid system (THSII)*, in *SAE 2004 World Congress and Exhibition*. 2004: Detroit, Michigan, USA.

25. Muta, K., Y. Makoto, and J. Tokieda, *Development of new-generation hybrid system THS II~Drastic improvement of power performance and fuel economy*, in *SAE 2004 World Congress and Exhibition*. 2004: Detroit, Michigan, USA.

26. Itagaki, K., et al., *Development of the Toyota mild-hybrid system (THS-M)*, in *SAE 2002 World Congress*. 2002: Detroit, Michigan, USA.

27. Tomomatsu, H., et al., *Automatic transmission control system developed for toyota mild hybrid system (THS-M)*, in *SAE 2002 World Congress*. 2002: Detroit, Michigan, USA.

28. Teratani, T., et al. *Development of Toyota Mild Hybrid System (THS-M) with 42V PowerNet*. in *Electric Machines and Drives Conference, 2003. IEMDC'03. IEEE International* 2003.

29. Kojima, M., et al., *Highly efficient hybrid minivan with super low emissions*, in *SAE 2002 World Congress*. 2002: Detroit, Michigan, USA.

30. Kondo, K., S. Sekiguchi, and M. Tsuchida, *Development of an electrical 4WD system for hybrid vehicles*, in *SAE 2002 World Congress*. 2002: Detroit, Michigan, USA.

31. Oba, H., et al., *Development of a hybrid powertrain system using CVT in a minivan*, in *SAE 2002 World Congress*. 2002: Detroit, Michigan, USA.

32. Ozeki, T. and M. Umeyama, *Development of TOYOTA's transaxle for mini-van hybrid vehicles*, in *SAE 2002 World Congress*. 2002: Detroit, Michigan, USA.

33. Endo, H., M. Ito, and T. Ozeki, *Development of Toyota's transaxle for mini-van hybrid vehicles.* JSAE Review, 2003. **24**(1): p. 109-116.

34. Hata, H.K., Masahiro ;Watanabe, Hideto ;Mizutani, Tatsuhiko ;Kamiya, Munehiro ;Yanagida, Eiji ;Takizawa, Keiji *Development of a New Hybrid Transmission for FWD Sports Utility Vehicles*, in *SAE World Congress*. 2005, Society of Automotive Engineers, Inc.: Detroit, Michigan, USA.

35. Kimura, A.A., Ikuo ;Itagaki, Kenji *Development of Hybrid System for SUV*, in *SAE World Congress*. 2005, Society of Automotive Engineers, Inc.: Detroit, Michigan, USA.

36. Fukuo, K., et al., *Development of the ultra-low-fuel-consumption hybrid car - INSIGHT.* JSAE Review, 2001. **22**(1): p. 95-103.

37. DoE, *U. S. Department of Energy technology snapshot - Featuring the Honda Insight*, D.o. Energy, Editor. 2001, Argonne National Laboratory.

38. Duoba, M., H. Ng, and R. Larsen, *Characterization and comparison of two hybrid electric vehicles (HEVs) - Honda Insight and Toyota Prius*, in *SAE 2001 World Congress*. 2001: Detroit, Michigan, USA.

39. Ng, H.K., et al., *Engine start characteristics of two hybrid electric vehicles (HEVs) - Honda Insight and Toyota Prius*, in *SAE Future Transportation Technology Conference and Exposition*. 2001: Costa Mesa, California, USA.

40. Kelly, K.J., M. Mihalic, and M. Zolot, *Battery usage and thermal performance of the Toyota Prius and Honda Insight for various chassis dynamometer test procedures*. 2001, National Renewable Energy Laboratory: Long Beach, California, USA.

41. An, F., et al., *Evaluating commercial and prototype HEVs*, in *SAE 2001 World Congress*. 2001: Detroit, Michigan, USA.

42. Walters, J., H. Husted, and K. Rajashekara, *Comparative study of hybrid powertrain strategies*, in *SAE Future Transportation Technology Conference and Exposition*. 2001: Costa Mesa, California, USA.

43. Ogawa, H., M. Matsuki, and T. Eguchi, *Development of a power train for the hybrid automobile~The Civic Hybrid*, in *SAE 2003 World Congress*. 2003: Detroit, Michigan, USA.

44. Hanada, K.K., Masaaki ;Ishikawa, Susumu ;Imai, Toshitaka ;Matsuoka, Hideki ;Adachi, Hiromitsu *Development of a Hybrid System for the V6 Midsize Sedan*, in *SAE World Congress*. 2005, Society of Automotive Engineers, Inc.: Detroit, Michigan, USA.

45. Matsuo, I., T. Miyamoto, and H. Maeda, *The Nissan hybrid vehicle*, in *Future Car Congress*. 2000: Arlington, Virginia, USA.

46. Evans, D.G. and K.D.V. Maanen, *Electric machine powertrain integration for General Motors Corporation's hybrid full-size pickup truck*, in *SAE 2003 World Congress*. 2003, Society of Automotive Engineers, Inc., Warrendale, Pennsylvania, USA: Detroit, Michigan, USA.

47. Evans, D.G., et al., *Powertrain architecture and controls integration for General Motors Corporation's hybrid full-size pickup truck*, in *SAE 2003 World Congress*. 2003, Society of Automotive Engineers, Inc., Warrendale, Pennsylvania, USA: Detroit, Michigan, USA.

48. Holmes, A.G. and M.R. Schmidt, *Hybrid electric powertrain including a two-mode electrically variable transmission*. 2002, General Motors Corporation: USA.

49. Schmidt, M.R., *Two-mode, compound-plit electro-mechanical vehicular transmission*. 1999, General Motors Corporation: USA.

50. Conlon, B., *Comparative Analysis of Single and Combined Hybrid Electrically Variable Transmission Operating Modes*, in *SAE World Congress*. 2005, Society of Automotive Engineers, Inc.: Detroit, Michigan, USA.

51. Ai, X.A., Scott, *An Electro-Mechanical Infinitely Variable Transmission for Hybrid Electric Vehicles*, in *SAE World Congress*. 2005, Society of Automotive Engineers, Inc.: Detroit, Michigan, USA.

52. Hisada, H.T., Takao ;Tsukamoto, Kazumasa ;Yamaguchi, Kozo ;Suzuki, Kenji ;Iizuka, Matoi ;Mochizuki, Motoyasu ;Hirano, Yasuo *AISIN AW New Full Hybrid Transmission for FWD Vehicles*, in *SAE World Congress*. 2005, Society of Automotive Engineers, Inc.: Detroit, Michigan, USA.

53. Chau, K.T. and Y.S. Wong, *Overview of power management in hybrid electric vehicles.* Energy Conversion and Management, 2002. **43**(15): p. 1953-1968.

54. Phillips, A.M., M. Jankovic, and K.E. Bailey, *Vehicle system controller design for a hybrid electric vehicle*, in *Proceedings of the 2000 IEEE International Conference on Control Applications*. 2000: Anchorage, Alaska, USA. p. 297-302.

55. Phillips, A.M., *Functional decomposition in a vehicle control system*, in *Proceedings of the 2002 American Control Conference*. 2002: Anchorage, Alaska, USA. p. 3713-3718.

56. Laguitton, O., S. Streater, and R. Gordon, *Realizing the benefits of supervisory control - an essential approach for hybrid drivetrains*, in *Proceedings of the 2nd IMechE Automobile Division Southern Center Conference on Total Vehicle Technology*. 2002: Brighton, UK. p. 29-45.

57. Larsen, M., S. De La Salle, and D. Reuter, *A reusable control system architecture for hybrid powertrains*, in *Powertrain and Fluid Systems Conference and Exhibition*. 2002: San Diego, California, USA.

58. Bellman, R., *Dynamic programming*. 1957, Princeton, NJ, USA: Princeton University Press.

59. Kleimaier, A. and D. Schroder, *Optimization strategy for design and control of a hybrid vehicle*, in *6th International Workshop on Advanced Motion Control*. 2000: Nagoya, Japan. p. 459-464.

60. Kleimaier, A. and D. Schroder, *An approach for the online optimized control of a hybrid powertrain*, in *7th International Workshop on Advanced Motion Control*. 2002: Technische Univ. Munchen, Germany. p. 215-220.

61. Lin, C.-C., et al., *Energy management strategy for a parallel hybrid electric truck*, in *Proceedings of the 2001 American Control Conference*. 2001: Arlington, Virginia, USA. p. 2878-2883.

62. Lin, C.-C., et al., *Power management strategy for a parallel hybrid electric truck.* IEEE Transactions on Control Systems Technology, 2003. **11**(6): p. 839-849.

63. Paganelli, G., et al., *Simulation and assessment of power control strategies for a parallel hybrid car.* Proceedings of the Institution of Mechanical Engineers: Part D : Journal of automobile engineering, 2000. **214**(7): p. 705-717.

64. Paganelli, G., et al., *General supervisory control policy for the energy optimization of charge-sustaining hybrid electric vehicles.* JSAE Review, 2001. **22**(4): p. 511-518.

65. Paganelli, G., et al., *Equivalent consumption minimization strategy for parallel hybrid powertrains*, in *IEEE 55th Vehicular Technology Conference*. 2002. p. 2076-2081.

66. Paganelli, G., et al., *Control development for a hybrid-electric sport-utility vehicle: Strategy, implementation and field test results*, in *Proceedings of the 2001 American Control Conference*. 2001: Arlington, Virginia, USA. p. 5064-5069.

67. Delprat, S., et al., *Control strategy optimization for an hybrid parallel powertrain*, in *ProceediProceedings of the 2001 American Control Conference*. 2001: Arlington, Virginia, USA. p. 1315-1320.

68. Delprat, S., T.M. Guerra, and J. Rimaux, *Control strategies for hybrid vehicles : Optimal control*, in *IEEE 56th Vehicular Technology Conference*. 2002: Univ. de Valenciennes et du Hainaut Cambresis, France. p. 1681-1685.

69. Delprat, S., T.M. Guerra, and J. Rimaux, *Optimal control of a parallel powertrain: from global optimization to real time control strategy Optimal control of a parallel powertrain: from global optimization to real time control strategy*, in *IEEE 55th Vehicular Technology Conference*. 2002: Universitd de Valenciennes et du Hainaut Cambresis, France. p. 2082-2088.

70. Kirschbaum, F., M. Back, and M. Hart, *Determination of the fuel-optimal trajectory for a vehicle along a known route*, in *15th IFAC World Congress*. 2002: Barcelona, Spain.

71. Yoon, H.-J. and S.-J. Lee, *An optimization control strategy for parallel hybrid electric vehicle*, in *SAE 2003 World Congress*. 2003: Detroit, Michigan, USA.

72. Buntin, D.L. and J.W. Howze, *A switching logic controller for a hybrid electric/ICE vehicle*, in *Proceedings of the American Control Conference*. 1995: Seattle, Washington, USA. p. 1169-1175.

73. Bowles, P., H. Peng, and X. Zhang, *Energy management in a parallel electric hybrid vehicle with a continuously variable transmission*, in *Proceedings of the 2000 American Control Conference*. 2000: Chicago, Illinois, USA. p. 55-59.

74. Koo, E.-S., et al., *Torque control strategy for a parallel hybrid vehicle using fuzzy logic*, in *The 1998 IEEE Industry Applications Conference*. 1998: St. Louis, Missouri, USA. p. 1715-1720.

75. Lee, H.-D. and S.-K. Sul, *Fuzzy-logic-based torque control strategy for parallel-type hybrid electric vehicle.* IEEE Transactions on Industrial Electronics, 1998. **45**(4): p. 625-632.

76. Brahma, A., et al., *Modeling, performance analysis and control design of a hybrid sport-utility vehicle*, in *Proceedings of the 1999 IEEE International Conference on Control Applications*. 1999: Kohala Coast, Hawaii, USA. p. 448-453.

77. Baumann, B.M., et al., *Mechatronic design and control of hybrid electric vehicles.* IEEE/ASME Transactions on Mechatronics, 2000. **5**(1): p. 58-72.

78. Glenn, B., G. Washington, and G. Rizzoni, *Operation and control strategies for hybrid electric automobiles*, in *Future Car Congress*. 2000: Arlington, Virginia, USA.

79. Salman, M., N.J. Schouten, and N.A. Kheir, *Control strategies for parallel hybrid vehicles*, in *Proceedings of the 2000 American Control Conference*. 2000: Chicago, Illinois, USA. p. 524-528.

80. Schouten, N.J., M.A. Salman, and N.A. Kheir, *Fuzzy logic control for parallel hybrid vehicles.* IEEE Transactions on Control Systems Technology, 2002. **10**(3): p. 460-468.

81. Schouten, N.J., M.A. Salman, and N.A. Kheir, *Energy management strategies for parallel hybrid vehicles using fuzzy logic.* Control Engineering Practice, 2003. **11**(2): p. 171-177.

82. Kheir, N.A., M.A. Salman, and N.J. Schouten, *Emissions and fuel economy trade-off for hybrid vehicles using fuzzy logic.* Mathematics and Computers in Simulation, 2004. **66**(2-3): p. 155-172.

83. Piccolo, A., et al., *Optimisation of energy flow management in hybrid electric vehicles via genetic algorithms*, in *2001 IEEE/ASME International Conference on Advanced Intelligent Mechatronics*. 2001: Como, Italy. p. 434-439.

84. Quigley, C.P., et al., *Predicting journey parameters for the intelligent control of a hybrid electric vehicle*, in *Proceedings of the 1996 IEEE International Symposium on Intelligent Control*. 1996: Dearborn, Michigan, USA. p. 402-407.

85. Farrall, S.D. and R.P. Jones, *Energy management in an automotive electric/heat engine hybrid powertrain using fuzzy decision making*, in *Proceedings of the 1993 IEEE International Symposium on Intelligent Control*. 1993: Chicago, Illinois, USA. p. 463-468.

86. Won, J.-S. and R. Langari, *Fuzzy torque distribution control for a parallel-hybrid vehicle*, in *2001 Joint ADVISOR/PSAT Vehicle Systems Modeling User Conference*. 2001: Southfield, Michigan, USA. p. 106-111.

87. Langari, R. and J.-S. Won, *Intelligent energy management for hybrid vehicles via drive cycle pattern analysis and fuzzy logic torque distribution*, in *Proceedings of the 2003 IEEE International Symposium on Intelligent Control*. 2003: Houston, Texas, USA. p. 223-228.

88. Langari, R. and J.-S. Won, *Integrated drive cycle analysis for fuzzy logic based energy management in hybrid vehicles*, in *The 12th IEEE International Conference on Fuzzy Systems*. 2003. p. 290-295.

89. Langari, R. and J.-S. Won, *A driving situation awareness-based energy management strategy for parallel hybrid vehicles*, in *Future Transportation Technology Conference*. 2003: Costa Mesa, California, USA.

90. Won, J.-S. and R. Langari, *Intelligent energy management agent for a parallel hybrid vehicle*, in *Proceedings of the 2003 American Control Conference*. 2003: Denver, Colorado, USA. p. 2560-2565.

91. Jeon, S.-i., et al., *Multi-mode driving control of a parallel hybrid electric vehicle using driving pattern recognition.* Journal of Dynamic Systems, Measurement, and Control, 2002. **124**(1): p. 141-149.

92. Ippolito, L., V. Loia, and P. Siano, *Extended fuzzy c-means and genetic algorithms to optimize power flow management in hybrid electric vehicles*, in *Proceedings of 2003 IEEE Conference on Control Applications*. 2003. p. 115-119.

93. Ichikawa, S., et al., *Novel energy management system for hybrid electric vehicles utilizing car navigation over a commuting route*, in *2004 IEEE Intelligent Vehicles Symposium*. 2004: Parma, Italy. p. 161-166.

94. Jackson, N., *How far can hybrids take us?* 2003, Ricardo plc.

95. Owen, N. and R. Gordon, *"Carbon to hydrogen" roadmaps for passenger cars : Update of the study*. 2003, Ricardo Consulting Engineers: Shoreham-by-sea, UK.

96. Kawai, M., et al., *Development of a shift control system for automatic transmissions using information from a vehicle navigation system*, in *SAE International Congress and Exposition*. 1999: Detroit, Michigan, USA.

97. Inagawa, T., et al., *Shift control system development (NAVI.AI-SHIFT) for 5 speed automatic transmissions using information from the vehicle's navigation system*, in *SAE 2002 World Congress*. 2002: Detroit, Michigan, USA.

98. Bachmann, T. and S. Bujnoch, *Connecteddrive - driver assistance systems of the future*. 2002, BMW AG.

99. Venhovens, P.J.T., et al., *The application of advanced vehicle navigation in BMW driver assistance systems*, in *SAE International Congress and Exposition*. 1999: Detroit, Michigan, USA.

100. Reichart, G., et al., *Potential of BMW driver assistance to improve fuel economy*, in *1998 FISITA World Automotive Congress*. 1998: Paris, France.

101. Brandstaeter, M., W. Prestl, and G. Bauer, *Functional optimization of adaptive cruise control using navigation data*, in *SAE 2004 World Congress and Exhibition*. 2004: Detroit, Michigan, USA.

102. Terwen, S., M. Back, and V. Krebs, *Predictive Powertrain Control for Heavy-Duty Trucks*, in *IFAC Symposium on Advances in Automotive Control*. 2004, University of Salerno, Italy: Salerno, Italy.

103. Lutz, D., *Hybrid vehicle and process for operating a hybrid vehicle*. 2002, Mannesmann Sachs AG: USA.

104. Woestman, J.T., et al., *Strategy to use an on-board navigation system for electric and hybrid electric vehicle energy management*. 2002, Ford Global Technologies: USA.

105. Rajagopalan, A. and G. Washington, *Intelligent control of hybrid electric vehicles using GPS information*, in *Future Car Congress*. 2002: Arlington, Virginia, USA.

106. Back, M., et al., *Predictive control of drivetrains*, in *15th IFAC World Congress*. 2002: Barcelona, Spain.

107. Finkeldei, E. and M. Back, *Implementing an MPC algorithm in a vehicle with a hybrid powertrain using telematics as a sensor for powertrain control*, in *IFAC Advances in Automotive Control*. 2004, Elsevier Publications: Salerno, Italy.

108. Back, M., S. Terwen, and V. Krebs, *Predictive Powertrain Control for Hybrid Electric Vehicles*, in *IFAC Symposium on Advances in Automotive Control*. 2004, University of Salerno, Italy: Salerno, Italy.

109. Sciarretta, A., L. Guzzella, and M. Back, *A Real-Time Optimal Control Strategy for Parallel Hybrid Vehicles With On-Board Estimation of the Control*

Parameters, in *IFAC Symposium on Advances in Automotive Control*. 2004, University of Salerno, Italy: Salerno, Italy.

110. Sciarretta, A., M. Back, and L. Guzzella, *Optimal control of parallel hybrid electric vehicles.* Control Systems Technology, IEEE Transactions on, 2004. **12**(3): p. 352-363.

111. Jackson, N., P. Fussey, and R. Gordon, *The use of advanced optimization techniques to develop the supervisor control of a mild hybrid diesel vehicle*, in *JSAE Spring Conference*. 2003, Society of Automotive Engineers of Japan, Inc.: Yokohama, Japan.

112. Deguchi, Y., et al., *HEV Charge/Discharge Control System Based on Navigation Information*, in *Convergence 2004 Vehicle Electronics to Digital Mobility*. 2004: Detroit, Michigan, USA.

113. Johannesson, L., M. Asbogard, and B. Egardt, *Assessing the potential of predictive control for hybrid vehicle powertrains using stochastic dynamic programming*, in *Intelligent Transportation Systems, 2005. Proceedings. 2005 IEEE*. 2005. p. 366-371.

114. Kim, C., et al., *Fuel economy optimization for parallel hybrid vehicles with CVT*, in *SAE International Congress and Exposition*. 1999: Detroit, Michigan, USA.

115. Jeon, S.-I., et al., *Driving simulation of a parallel hybrid electric vehicle using receding horizon control*, in *IEEE International Symposium on Industrial Electronics*. 2001: Pusan, South Korea. p. 12-16.

116. Soltis, A. and X. Chen, *A new control strategy for hybrid electric vehicles*, in *Proceedings of the 2003 American Control Conference*. 2003: Denver, Colorado, USA. p. 1398-1403.

117. Pisu, P., et al., *A LMI-based supervisory robust control for hybrid vehicles*, in *Proceedings of the 2003 American Control Conference*. 2003: Denver, Colorado, USA. p. 4681-4686.

118. EPA. *New hybrid vehicles increase gas-saving options for consumers*. [website] 2005 [cited 8 Nov. 2005]; Available from: http://www.fueleconomy.gov/feg/hybrid_sbs.shtml.

119. Husted, H.L., *A comparative Study of the production applications of hybrid electric powertrains*, in *Future Transportation Technology Conference*. 2003: Costa Mesa, California, USA.

120. EPA, *Model year 2006 fuel economy guide*, U.S.D.o. Energy, Editor. 2005.

121. Birch, S., *Diesels and DCTs*, in *Automotive Engineering International*. 2003. p. 49-57.

122. Stobart, R. and J.-R. Linna, *Fuel economies of scale*, in *Engine Technology International*. 1999. p. 34-39.

123. Morita, K., *Automotive power source in 21st century.* JSAE Review, 2003. **24**(1): p. 3-7.

124. Salber, W., et al., *Synergies of variable valve actuation and direct injection*, in *SAE 2002 World Congress*. 2002: Detroit, Michigan, USA.

125. Shayler, P.J., G. Horn, and D. Eade, *Predictions of fuel economy for types of DISI and MPI spark ignition engines*, in *International Conference on Integrated Powertrain Systems for a Better Environment*. 1999: Birmingham, UK. p. 149-163.

126. Shayler, P.J., et al., *Characterisation of DISI emissions and fuel economy in homogeneous and stratified charge modes of operation*, in *SAE International Fall Fuels and Lubricants Meeting and Exhibition*. 2001: San Antonio, Texas, USA.

127. Shayler, P.J., et al., *DISI engine spark and fuel injection timings. Effects, compromise and robustness*, in *SAE International Fall Fuels and Lubricants Meeting and Exhibition*. 2001: San Antonio, Texas, USA.

128. Horn, G., *The prediction of fuel economy and pollutant emissions to assess the benefits of direct injection gasoline engines*. 2002, University of Nottingham: Nottingham, UK.

129. Matthes, B., *Dual Clutch Transmissions~Lessons Learned and Future Potential*, in *SAE World Congress*. 2005: Detroit, Michigan, USA.

130. Scherer, H., *ZF 6-speed automatic transmission for passenger cars*, in *SAE 2003 World Congress*. 2003: Detroit, Michigan, USA.

131. Lepelletier, P.A.G., *Multispeed automatic transmission for automobile vehicles*. 1992: USA.

132. Baran, J., J. Hendrickson, and M. Solt, *General Motors New Hydra-Matic RWD Six-Speed Automatic Transmission Family*, in *SAE 2006 World Congress*. 2006, SAE International, Warrendale, Pennsylvania, USA: Detroit, Michigan, USA.

133. Kusamoto, D., et al., *Toyota's New Six-Speed Automatic Transaxle U660E for FWD Vehicles*, in *SAE 2006 World Congress*. 2006, SAE International, Warrendale, Pennsylvania, USA: Detroit, Michigan, USA.

134. Greiner, J., et al., *The new 7G-TRONIC of Mercedes-Benz~Innovative transmission technology for better driving performance, comfort and fuel economy*, in *SAE 2004 World Congress and Exhibition*. 2004, Society of Automotive Engineers, Inc., Warrendale, Pennsylvania, USA: Detroit, Michigan, USA.

135. Kluger, M.A. and D.R. Fussner, *An overview of current CVT mechanisms, forces and efficiencies*, in *SAE International Congress and Exposition*. 1997: Detroit, Michigan, USA.

136. Wagner, G., *Application of transmission systems for differential driveline configurations in passenger cars*, in *SAE 2001 World Congress*. 2001: Detroit, Michigan, USA.

137. Kluger, M.A. and D.M. Long, *An overview of current automatic, manual and continuously variable transmission efficiencies and their projected future*

improvements, in *SAE International Congress and Exposition*. 1999: Detroit, Michigan, USA.

138. Abo, K., et al., *Development of new-generation belt CVTs with high torque capacity for front-drive car*, in *SAE 2003 World Congress*. 2003: Detroit, Michigan, USA.

139. Fussner, D. and Y. Singh, *Development of single stage input coupled split power transmission arrangements and their characteristics*, in *SAE 2002 World Congress*. 2002: Detroit, Michigan, USA.

140. Fussner, D. and Y. Singh, *Development of dual stage input coupled split power transmission arrangements and their characteristics*, in *SAE 2002 World Congress*. 2002: Detroit, Michigan, USA.

141. Nissan, *Extroid CVT for application to realr-wheeldrive cars powered by large engines; extroid cvt for application to realr-wheeldrive cars powered by large engines*. 1999, Nissan Motor Co.

142. Nakano, M., et al., *Development of a large torque capacity half-toroidal CVT*, in *SAE 2000 World Congress*. 2000: Detroit, Michigan, USA.

143. Machida, H. and Y. Murakami, *Development of the POWERTORUS unit half toroidal CVT.* Motion & Control, NSK Technical Journal, 2000. **9**: p. 15-26.

144. Imanishi, T. and H. Machida, *Development of POWERTORUS unit half toroidal CVT (2).* Motion & Control, NSK Technical Journal, 2001. **10**: p. 1-8.

145. Miyata, S. and H. Machida, *Development of POWERTORUS unit half toroidal CVT (3).* Motion & Control, NSK Technical Journal, 2001. **11**: p. 11-18.

146. Imanishi, T. and S. Miyata, *Development of the next-generation half-toroidal CVT.* Motion & Control, NSK Technical Journal, 2003. **14**: p. 20-24.

147. Vahabzadeh, H., J.P. Macey, and O. Dittrich, *A split-torque, geared-neutral infinitely variable transmission mechanism*, in *23rd FISITA Congress*. 1990: Torino, Italy.

148. Vahabzadeh, H. and S.M. Linzell, *Modeling, simulation, and control implementation for a split-torque, geared neutral, infinitely variable transmission*, in *SAE International Congress and Exposition*. 1991: Detroit, Michigan, USA.

149. Fellows, T.G. and C.J. Greenwood, *The design and development of an experimental traction drive cvt for a 2.0 liter fwd passenger car*, in *SAE International Congress and Exposition*. 1991: Detroit, Michigan, USA.

150. Brockbank, C. and H. Heumann, *Delivery of IVT for a 5 liter SUV: addressing the concerns of geared neutral*, in *Innovative Fahrzeun-Getriebe*. 2002.

151. Fuchs, R.D., Y. Hasuda, and I.B. James, *Full toroidal IVT variator dynamics*, in *SAE 2002 World Congress*. 2002, Society of Automotive Engineers: Detroit, Michigan, USA.

152. Hasuda, Y. and R. Fuchs, *Development of IVT variator dynamic model.* Koyo Engineering Journal English Edition, 2002(106E): p. 24-28.

153. Burke, M., et al., *Powertrain efficiency optimization of the torotrak infinitely variable transmission (IVT)*, in *SAE 2003 World Congress*. 2003: Detroit, Michigan, USA.

154. NREL, *ADVISOR*. 2002, National Renewable Energy Laboratory: Golden, Colorado, USA.

155. ANL, *PSAT*. 2002, Argonne National Laboratory.

156. Yasuoka, M., et al., *An integrated control algorithm for an SI eninge and a CVT*, in *SAE International Congress and Exposition*. 1999: Detroit, Michigan, USA.

157. Sakaguchi, S., E. Kimura, and K. Yamamoto, *Development of an engine-CVT integrated control system*, in *SAE International Congress and Exposition*. 1999: Detroit, Michigan, USA.

158. Kim, T. and H. Kim, *Performance of integrated engine–CVT control considering powertrain loss and CVT response lag.* Proceedings of IMechE Part D: J Automobile Engineering, 2002. **216**: p. 545-553.

159. Torotrak. *How it works?* [website] 2005 [cited 5 May 2005]; Available from: http://www.torotrak.com/howitworks.html.

160. CarsDirect. *New cars : specs & features*. [website] 2005 [cited 9 Nov. 2005]; Available from: http://www.carsdirect.com/research.

161. Malesh, T., *Integrated starter generator: The new centerpiece in automotive alternative power technology*, in *The Power Report*. 2001. p. 4-5.

162. Levin, M.B., et al., *Design and analysis of starter-alternator installation in a hybrid-electric vehicle*, in *SAE International Congress and Exposition*. 1999: Detroit, Michigan, USA.

163. Levin, M.B., et al., *Hybrid powertrain with an engine-disconnecting clutch*, in *SAE 2002 World Congress*. 2002: Detroit, Michigan, USA.

164. Sahin, F., A.M. Tuckey, and A.J.A. Vandenput, *Design, development and testing of a high-speed axial-flux permanent-magnetic machine*, in *Conference Record of the 2001 IEEE Industry Applications Conference*. 2001: Chicago, Illinois, USA. p. 1640-1647.

165. Kabasawa, A. and K. Takahashi, *Development of the IMA Motor for the V6 Hybrid Midsize Sedan*, in *SAE World Congress*. 2005, Society of Automotive Engineers, Inc.: Detroit, Michigan, USA.

166. Miller, J.M., *Propulsion systems for hybrid vehicles*. 2004, London, UK: The Institution of Electrical Engineers.

167. Yusaku, N.K., Hiroshi *Development of the Intelligent Power Unit for the V6 Hybrid Midsize Sedan*, in *SAE World Congress*. 2005, Society of Automotive Engineers, Inc.: Detroit, Michigan, USA.

168. Barnard, R.H. and C.M. Jefferson, *Criteria for sizing the prime mover and energy storage capacity in hybrid vehicles*, in *30th ISATA Conference on Electric and Hybrid Vehicles*. 1997: Florence, Italy. p. 363-370.

169. Cho, B. and N.D. Vaughan, *Dynamic Simulation Model of a Hybrid Powertrain and Controller using Co-simulation - Part II : Control strategy.* International Journal of Automotive Technology, 2006. **7**(7): p. 785-793.

170. Cacciatori, E., et al., *Regenerative Braking Strategies for A Parallel Hybrid Powertrain With Torque-Controlled IVT*, in *Powertrain and Fluid Systems Conference and Exhibition*. 2005, Society of Automotive Engineers, Inc., Warrendale, Pennsylvania, USA: San Antonio, Texas, USA.

171. SAE, *Recommended Practice for Measuring the Exhaust Emissions and Fuel Economy of Hybrid-Electric Vehicles*. 1999, Society of Automotive Engineers: Warrendale, Pennsylvania, USA.

172. MacBain, J.A., *Simulation influence in the design process of mild hybrid vehicles*, in *SAE 2002 World Congress*. 2002, Society of Automotive Engineers, Inc.: Detroit, Michigan, USA.

173. Simopoulos, G.N., et al., *Fuel economy improvements in an SUV equipped with an integrated starter generator*, in *SAE International Truck and Bus Meeting and Exposition*. 2001: Chicago, Illinois, USA.

174. Bellman, R.E. and S.E. Dreyfus, *Applied dynamic programming*. 1962, Princeton, NJ: Princeton University Press.

175. ANDRÉ, M., D. HASSEL, and F.-J. WEBER, *Development of short driving cycles*. 1998, Laboratoire Energie Nuisances.

176. Anonymous, *Design manual for roads and bridges - Volume 6. Load geometry*, T.H. Agency, et al., Editors. 2002.

177. Zadeh, L.A., *Fuzzy Sets.* Information and Control, 1966. **8**: p. 338-353.

178. Mamdani, E.H. and S. Assilian, *An Experiment in Linguistic Synthesis with a Fuzzy Logic Controller.* International Journal of Man-Machine Studies, 1975. **7**(1): p. 1-13.

179. Takagi, T. and M. Sugeno, *Fuzzy identification of systems and its applications to modeling and control.* IEEE Transactions on Systems, Man, and Cybernetics, 1985. **15**(1): p. 116-132.

180. Jang, J.-S.R., *Fuzzy Modeling Using Generalized Neural Networks and Kalman Filter Algorithm*, in *Proceedings of the Ninth National Conference on Artificial Intelligence*. 1991.

181. Jang, J.S.R., *ANFIS: adaptive-network-based fuzzy inference system.* Systems, Man and Cybernetics, IEEE Transactions on, 1993. **23**(3): p. 665-685.

182. Jang, J.S.R. and S. Chuen-Tsai, *Neuro-fuzzy modeling and control.* Proceedings of the IEEE, 1995. **83**(3): p. 378-406.

183. Chiu, S.L., *Fuzzy Model Identification Based on Cluster Estimation.* Journal of Intelligent and Fuzzy Systems, 1994. **2**(3): p. 267-278.

184. Yager, R.R. and D.P. Filev, *Generation of Fuzzy Rules by Mountain lustering.* Journal of Intelligent and Fuzzy Systems, 1994. **2**: p. 209-219.

185. Peace, G.S., *Taguchi methods: a hands-on approach*. 1993: Addison-Wesley Publishing Company.

186. Cho, B. and N.D. Vaughan, *Dynamic Simulation Model of a Hybrid Powertrain and Controller using Co-simulation - Part I : Powertrain Modelling.* International Journal of Automotive Technology, 2006. **7**(4): p. 459-468.

187. Imagine, *AMESim*. 2004, IMAGINE.

188. MathWorks, *Simulink*. 2005, The Mathworks Inc.: Natick, Massachusetts, USA.

189. EPA, *CFR Part 600 : Fuel Economy Regulations for 1977 and Later Model Year Automobiles*. 1975, US Environmental Protection Agency.

190. EC, *Council Directive 70/220/EEC : Measures to be taken against air pollution by emissions from motor vehicles*. 2004, Office for Official Publications of the European Communities.

191. Rajagopalan, A., et al., *Development of fuzzy logic and neural network control and advanced emissions modeling for parallel hybrid vehicles*. 2003, National Renewable Energy Laboratory: Golden, Colorado, USA.

192. Harbor, N., *The Development and Integration of Systems Models for the Simulation of V8 Engine Performance Attributes*. 2004, University of Nottingham: Nottingham, UK.

193. Sandoval, D. and J.B. Heywood, *An improved friction model for spark-ignition engines*, in *SAE 2003 World Congress*. 2003: Detroit, Michigan, USA.

194. Patton, K.J., R.G. Nitschke, and J.B. Heywood, *Development and evaluation of a friction mode for spark-ignition engines*, in *SAE International Congress and Exposition*. 1989: Detroit, Michigan, USA.

APPENDIX A

Gross indicated mean effective pressure (IMEP) is the sum of the brake work, pumping loss, friction loss, and accessory loss. The friction loss can be divided into four groups; the crankshaft, rubbing, rubbing by gas loading, and valvetrain. All of these except for the rubbing by gas loading and the accessory loss only depend on the engine speed and can be substituted by one term, the total mechanical friction loss. These relationships are expressed as follow;

$$\begin{aligned} imep_g &= bmep + pmep + fmep + amep \\ &= bmep + pmep + cfmep + rfmep + rfmep_{gas} + vfmep + amep \\ &= bmep + pmep + rfmep_{gas} + tmfmep \end{aligned} \quad \text{(A- 1)}$$

The gross IMEP calculated from the above equation is generally overestimated because the engine speed affects the efficiency. Therefore, a correction factor that is a function of the engine speed should be introduced. [192]

$$imep_g = C_1 imep_{g,ideal} \quad \text{(A- 2)}$$

$$C_1 = \text{-}8.1706\times10^{-7}\,\omega_{ENG}^2 + 7.6962\times10^{-4}\,\omega_{ENG} + 0.62055 \quad \text{(A- 3)}$$

In this study, a set of generic functions derived by Horn [128] is used in order to predict fuel consumption of a SIDI engine. All equations are shown as follow;

Ideal gross IMEP:

$$imep_{g,ideal} = \eta_c \eta_{th} \dot{m}_f Q_{LHV} \frac{4\pi}{V_s n \omega_{ENG}} \quad \text{(A- 4)}$$

$$V_s = \frac{\pi B^2}{4} S \quad \text{(A- 5)}$$

Thermal efficiency:

$$\eta_{th} = C_{th} \eta_{otto} \quad \text{(A- 6)}$$

$$C_{th} = \begin{cases} 0.86; & AFR < 18 \\ 0.92; & AFR >= 18, GFR < 25 \\ 0.95; & GFR >= 25 \end{cases} \quad \text{(A- 7)}$$

$$\eta_{otto} = 1 - \frac{1}{r_c^{\gamma - 1}} \quad \text{(A- 8)}$$

Gas-fuel ratio (GFR):

$$GFR = \frac{AFR + 1}{1 - x_b} \quad \text{(A- 9)}$$

$$x_b = x_r + \frac{(1 - x_r) AFR \cdot EGR}{AFR + 1 - EGR} \quad \text{(A- 10)}$$

$$x_r = \frac{1}{1 + 2\left(\frac{P_i}{P_e}\right)(r_c - 1)\eta_v \left(\frac{AFR + 1 - EGR}{AFR}\right)} \quad \text{(A- 11)}$$

Volumetric efficiency:

$$\eta_v = C_v \eta_{v,ideal} \quad \text{(A- 12)}$$

$$C_v = 5.6282 \times 10^{-7} \omega_{ENG}^2 + 1.8917 \times 10^{-4} \omega_{ENG} + 0.75 \quad \text{(A- 13)}$$

$$\eta_{v,ideal} = \frac{1 + \gamma(r_c - 1) - \frac{P_e}{P_i}}{\gamma(r_c - 1)} \quad \text{(A- 14)}$$

Pumping mean effective pressure (PMEP):

$$pmep = P_e - P_i + pmep_v \quad \text{(A- 15)}$$

$$pmep_v = 3.0 S_p^2 \left(\frac{P_i}{P_a}\right)^2 \left(\frac{1}{n_{iv}^2 r_i^4} + \frac{1}{n_{ev}^2 r_e^4}\right) \quad \text{(A- 16)}$$

$$S_p = S \frac{\omega_{ENG}}{\pi} \quad \text{(A- 17)}$$

Exhaust manifold pressure:

$$P_e = \frac{P_a}{2}\left(1+\sqrt{1+4c_{exh}RT_e\frac{\dot{m}_e}{P_a^2}}\right) \quad \text{(A- 18)}$$

$$c_{exh} = 1.5\times10^{6}\left(\frac{1.8\times10^{-3}}{V_s n}\right)^{\frac{4}{3}} \quad \text{(A- 19)}$$

Inlet manifold pressure:

$$P_i = \frac{4\pi\dot{m}_a RT_i}{(1-EGR)V_s n\eta_v\omega_{ENG}} \quad \text{(A- 20)}$$

$$\dot{m}_a = \dot{m}_f AFR \quad \text{(A- 21)}$$

Reciprocating friction mean effective pressure (FMEP) by gas loading:

$$rfmep_{gas} = 6.89\times10^{3}\frac{P_i}{P_a}\left(0.088r_c + 0.182r_c^{(1.33-2\times0.0238S_p)}\right): \quad \text{(A- 22)}$$

Total mechanical FMEP is a function of engine speed. Sandoval and Heywood [193] shows experimental data for a 3.0L MPI engine and the result of the second order curve fit is as follows;

$$tmfmep = 0.16871\omega_{ENG}^2 + 82.63\omega_{ENG} + 45524 \quad \text{(A- 23)}$$

To calculate the PMEP, ratio of the valve diameter to the cylinder bore are required. Patton et al.[194] suggest the following equations for the valve diameters from a given bore size.

$$r_i = \frac{6.11\times10^{-3} + 0.313B}{B} \quad \text{(A- 24)}$$

$$r_e = \frac{4.14\times10^{-3} + 0.286B}{B} \quad \text{(A- 25)}$$

Parameters and calibration values are listed in Table A-1 and Table A-2. The calculation procedure of the fuel mass flow rate and the WOT torque is explained in [128].

The closed throttle torque without fuelling is the sum of the total mechanical friction loss and the rubbing friction by the gas loading, assuming the full VVT is involved, which means the pumping loss can be negligible. In this case, the torque is only the

function of the engine speed. The experimental data in [193] for 3.0L engine is used for the model.

$$tmfmep + rfmep_{gas} = 0.25311\omega_{ENG}^2 - 1.4499\omega_{ENG} + 67019 \quad \text{(A- 26)}$$

Table A-1 Engine parameters

Symbol	Unit	Value	Symbol	Unit	Value
B	[m]	87.9×10^{-3}	r_c	-	12.5
n	-	6	S	[m]	87.9×10^{-3}
n_{ev}	-	2	T_e	[K]	1073.15
n_{iv}	-	2	T_i	[K]	293.15
P_a	[Pa]	1.0133×10^{5}	γ	-	1.3
Q_{LHV}	[J/kg]	44.0×10^{6}	η_c	-	0.98
R	[J/kg-K]	287.04			

Table A-2 Engine calibrations

Calibration	Unit	Stratified	Homogeneous
Operating speed	[rev/min]	≤ 3200	> 3200
Operating BMEP	[bar]	≤ 5.0	> 5.0
AFR	-	14.7 ~ 35	≥14.7
EGR	-	$\frac{1.5(AFR-14.7)}{100}$	0
GFR	-	≤ 60	≤ 25
Inlet manifold pressure	[bar]	≤ 0.95	≤ 0.95